Urban Wind Energy

Beller, Christina

Publication date:
2011

Document Version
Publisher's PDF, also known as Version of record

Risø DTU

Urban Wind Energy

Risø-PhD-Report

Beller, Christina
Risø-PhD-89(EN)
December 2011

Risø DTU
National Laboratory for Sustainable Energy

Author: Beller, Christina
Title: Urban Wind Energy
Division: Wind Energy Department

Risø-PhD-89(EN)
December 2011

Abstract (max. 2000 char.):
New trends e.g. in architecture and urban planning are to reduce energy needs. Several technologies are employed to achieve this, and one of the technologies, not new as such, is wind energy. Wind turbines are installed in cities, both by companies and private persons on both old and new buildings. However, an overview of the energy content of the wind in cities and how consequently turbines shall be designed for such wind climates is lacking. The objective of the present work is to deliver an objective and fundamental overview of the social, practical and physical conditions relevant for the installation of wind turbines in cities, with Copenhagen, DK, as example. Focus is taken on turbine with a swept area of maximum $5m^2$, since turbines of this size are relatively easy to be integrated in the urban space and are in the financial range for small companies as well as for private persons. Elements important for the implementation of wind energy conversion systems are the macro and micro wind climate, the siting within a micro wind climate and the choice of a wind turbine model most appropriate for the selected site. In the frame of this work, all these important elements are analyzed and a row of conclusions are found. Not as a surprise, it can be concluded, that the average wind velocities and with that the wind energy available in a city is somewhat lower than at a rural site outside the city. Furthermore, the wind climate in cities is very dependent on the buildings character and higher turbulences are expected. Therefore, methods are developed in this work to estimate the wind energy in cities depending on the built-up character, with both, simple and advanced calculation models. The energy produced by a wind turbine is also dependent on the turbine design, but especially on the rotor design. An analysis of which rotor type is most effective is carried out. A result of this analysis is, that turbines for the installation in cities need to be designed very differently than e.g. turbines for off-shore sites and that an optimization of the design can increase the energy production remarkably. Despite the lower wind energy in cities other factors foster the attractiveness of urban wind energy application, like the demand or wish to reduce CO2 emissions and the possibility to produce energy directly to ones household.

ISSN 0106-2840
ISBN 978-87-550-3953-7

Contract no.:

Group's own reg. no.:
(Føniks PSP-element)

Sponsorship:

Cover :

Pages: 167
Tables: 19
References: 83

Information Service Department
Risø National Laboratory for
Sustainable Energy
Technical University of Denmark
P.O.Box 49
DK-4000 Roskilde
Denmark
Telephone +45 46774005
bibl@risoe.dtu.dk
Fax +45 46774013
www.risoe.dtu.dk

Contents

Abstract

New trends e.g. in architecture and urban planning are to reduce energy needs, by isolation, use of daylight, public transportation accessibility and the like. At the same time decentralized technologies are introduced to provide a proportion of the inevitable energy. These two factors consequently reduce the energy procured from centralized power production. One of the technologies, not new as such, but utilized in a new context, constitutes wind energy in form of wind turbines. The objective of the present work is to deliver an objective fundamental overview of the social, practical and physical conditions relevant for Urban Wind Energy. Elements important for the implementation of wind energy conversion systems are the macro and micro wind climate, the siting within a micro wind climate and the choice of a wind turbine model most appropriate for the selected site.

In the frame of this work exemplary urban wind climates were analyzed in terms of e.g. Weibull distributions and mean wind velocity variability over a day. A method was proposed to determine the macro wind climate for a city district based on onsite wind measurements, a known macro wind climate outside but close by the city and a geometric description of the urban district. The micro wind climates in built-up areas were studied with a computational fluid dynamics (CFD) tool, which was developed to build and simulate typical urban district categories. With the tool general flow phenomena around obstacle, hence micro wind climates, could be concluded and with the help of these, discrepancies between energy production predictions based on wind measurements taken aside actual installed wind turbines and their actual measured energy productions explained. For the detection of wind energy potentials in a specific city district, meant to support siting of wind turbines in the urban micro wind climate, a scaling method was elaborated. Furthermore, the examination of manufacturer delivered power curves of existing small wind turbine models, designed for the operation in urban environments, were studied with respect to their load factors found in an exemplary urban wind climate. The maximum load factor was found to be 6% for one model, which was well designed for low wind velocities rather than for a broad wind speed range. This turbine model was installed at several sites within Copenhagen, DK. Load factors for the actually installed turbines were found to be about 2%. Following quality controlled power curve measurements showed tremendous differences between the data in the turbines technical specifications and the data collected at the Risø DTU test field. To design small-scale wind turbines, horizontal and vertical axis, parameter studies were conducted, and design directives and optimization strategies relevant for small wind turbines and low wind velocities delivered. One of the biggest design challenges for small-scale rotors was concluded to be the presence of low Reynolds numbers on the blade sections. An existing multiple streamtube model to calculate the aerodynamic performance of a Darrieus rotor with constant chord length distribution along the blade was modified and implemented in an existing optimization code. By implementing the modified aerodynamic model, it was possible to optimize the chord distribution along a Darrieus blade and with that a 13% efficiency enhancement in the design point of an exemplary layout achieved.

Generally, urban wind turbine cannot be compared to large offshore wind turbines. Theoretical concepts were found to reach load factors of 25% in an urban climate. Thereby was the ratio of rated power and swept area $28W/m^2$, indicating that future urban turbines might be equipped with small generators and airy rotors.

Resumé

Nye trends i arkitektonisk og bymæssig planlægning er at reducere energi behovet, ved at forbedre isolationen, bruge dagslys, forbedre tilgængeligheden af offentlig transport, etc. Samtidig introduceres decentrale teknologier til generering af energi. Disse to faktorer reducerer behovet for central energiproduktion. En af disse teknologier, som dog ikke er ny, men brugt i en ny kontekst er vindenergi, i form af vindmøller. Formålet med dette PhD-projekt er at give et objektivt og grundlæggende overblik over de sociale, praktiske og fysiske forhold, der er relevante for at installerer vindmøller i byerne. De vigtige elementer for implementering af vindenergisystemer er makro- og mikro-vindklima, positioneringen i mikro-vindklimaet og valget af den mest velegnede vindmølletype for den valgte positionering.

Indenfor rammen af dette arbejde blev udvalgte urbane vindklima analyseret med hensyn til for eksempel Weibull fordelingen og døgnets middelvindhastighedsvariation. En metode blev foreslået til at finde makro-vindklimaet for et byområde baseret på lokale vindmålinger, der kræver et kendt makro-vindklima udenfor men tæt på byen og en geometrisk beskrivelse af det byområde. Mikro-vindklima i bebyggede områder blev undersøgt med et computational fluid dynamics (CFD) værktøj, der blev udviklet til at bygge og simulere typiske byområdekategorier. Med dette værktøj kunne generelle strømningsfænomener omkring objekter og dermed mikro-vindklima konkluderes og ved hjælp af disse, uoverensstemmelser mellem forudsigelsen af energiproduktionen baseret på vindmålinger taget ved siden af installerede vindmøller og deres målte energiproduktion forklares. For lokaliseringen af vindenergipotentialer i et specifikt byområde, med hensyn til positionering a vindmøller i dette urbane mikro-vindklima, blev en skaleringsmetode udarbejdet. Undersøgelsen af effektkurver udleveret af leverandører af eksisterende små vindmøller, designet til drift i urbane omgivelser, blev desuden analyseret med hensyn til deres kapacitetsudnyttelsesfaktorer i et repræsentativt urbant vindklima. Den højeste kapacitetsudnyttelsesfaktor på 6%, blev fundet for en mølle designet til lave vindhastigheder og ikke til en bred vindhastighedsbåndbredde. Denne mølletype blev installeret i forskellige områder i København, Danmark. Kapacitetsudnyttelsesfaktorer for de installerede vindmøller var omkring 2%. Efterfølgende blev kvalitetskontrollerede effektkurvemålinger benyttet, og de viste betydelig divergens mellem vindmøllens tekniske specifikationsdata og data samlet på Risø DTU's prøvestation for små vindmøller. For at designe små vindmøller, både horisontal og vertikal akslede, blev parameterstudier gennemført, og designkriterier og optimeringsstrategier relevante for små vindmøller og lave vindhastigheder udarbejdet. Det blev konkluderet at en af de største designudfordringer for små vindmøller er de lave Reynolds-tal på vingerne. En eksisterende multiple streamtube model for at beregne den aerodynamiske ydeevne af en Darrieus rotor med konstant kordelængdefordeling langs bladet blev modificeret og implementeret i en eksisterende optimeringskode. Ved at implementere den modificerede aerodynamikmodel blev det muligt at optimere kordefordelingen langs et Darrieus blad og dermed opnå en 13% effektforøgelse i designpunktet.

Generelt kan urbane vindmøller ikke samelignes med store havvindmøller. Teoretiske koncepter blev fundet, som opnåede kapacitetsudnyttelsesfaktorer på 25% i et urbant klima. Forholdstallet af nominel effekt og rotorareal var $28 W/m^2$, hvilket tyder på at fremtidens urbane vindmøller kunne blive udstyret med små generatorer og lette rotorer.

Symbols

a	induction factor	[-]
A	Weibull scale parameter	[m/s]
A_d	total urban area	[m^2]
$A_{Darrieus}$	swept area of a Darrieus shaped rotor	[m^2]
A_f	sum of average building areas normal to the wind	[m^2]
A_H	swept area of an H shaped rotor	[m^2]
A_p	sum of all areas covered by buildings	[m^2]
A_{rotor}	swept area of a rotor	[m^2]
aa	site-independent constant within the geostrophic drag law	[-]
ac	acceleration coefficient	[-]
AEP	annual energy production	[Wh]
aoa	angle of attack	[^{0}]
aoa_{dsg}	design angle of attack	[^{0}]
AWP	annual wind energy potential	[Wh]
$\overline{B}$	buildings mean width	[m]
BAD	blade angle density	[-]
bb	site-independent constant within the geostrophic drag law	[-]
c	airfoil chord length	[m]
C_d	airfoil drag coefficient	[-]
C_E	wind potential dependent efficiency coefficient (=AEP/AWP)	[-]
C_l	airfoil lift coefficient	[-]
C_n	coefficient based on C_l and C_d	[-]
C_p	pressure coefficient	[-]
C_P	power coefficient	[-]
C_{Pdsg}	design power coefficient	[-]
C_{PinitH}	power coefficient of the initial H shaped rotor design	[-]
$C_{Pinitsin}$	power coefficient of the initial Darrieus shaped rotor design	[-]
C_{Plocal}	local power coefficient	[-]
C_{Pmax}	maximum power coefficient	[-]
C_{PoptH}	power coefficient of the optimized H shaped rotor design	[-]
$C_{Poptsin}$	power coefficient of the optimized Darrieus shaped rotor design	[-]
C_t	coefficient based on C_l and C_d	[-]
C_μ	Launder-Sharma coefficient as well as C_1, C_2 and C_3	[-]
d	displacement height	[m]
d	rotor diameter	[m]
D	distance between CFD domain inlet and first obstacle	[m]
dh	height a.r.l. where 3m/s is calculated with method I	[m]
f	Coriolis parameter	[1/s]
f_A	Coriolis parameter for a site outside the city	[1/s]
F_n	normal force	[N]
F_t	tangential force	[N]
F_x	streamwise force	[N]
F_x^*	non-dimensional streamwise force	[-]
$\overline{F_x}$	*average* streamwise force	[N]
G	geostrophic wind speed	[m/s]
G_A	geostrophic wind speed for a site outside the city	[m/s]
Δh	vertical height of a streamtube	[m]
h_c	cube height	[m]
H	rotor height	[m]
$\overline{H}$	buildings mean height	[m]
$\overline{H}_m$	model buildings mean height	[m]
$\overline{H}_o$	original buildings mean height	[m]

$\bar{H}_{o\ scale}$	scaled original buildings mean height	[m]
Je	Jensen number	[-]
k	Weibull shape parameter	[-]
$\bar{L}$	buildings mean length	[m]
m	constant to calculate the internal boundary layer height	[-]
n	number of blades	[-]
NT	number of angular sections per half rotation	[-]
NZH	number of horizontal sections per half rotor height	[-]
p_s	surface static pressure	[Pa]
p_δ	static pressure in the free stream at a height z=10h_c	[Pa]
P	power	[W]
P_{rated}	rated power	[W]
P_{shaft}	mechanical power on the shaft	[W]
r	local radius	[m]
rpm	rotational speed	[rpm]
rpm_{dsg}	design rotational speed	[rpm]
R	equatorial radius	[m]
$R_{Darrieus}$	equatorial radius of a Darrieus shaped rotor	[m]
R_H	equatorial radius of an H shaped rotor	[m]
Re	Reynolds number	[-]
Re_{ave}	average Reynolds number	[-]
Re_{dsg}	Reynolds number in the design point	[-]
Re_{local}	local Reynolds number	[-]
T	torque	[Nm]
tke	turbulence kinetic energy	[m^2/s^2]
u	wind speed	[m/s]
u_{ave}	average wind speed	[m/s]
u_{aveA}	average wind speed at a site outside the city	[m/s]
u_A	wind speed at a site outside the city	[m/s]
u_{dsg}	design wind speed	[m/s]
$u_{bicycle}$	bicycling speed	[m/s]
u_h	wind speed in the undisturbed flow at cube height	[m/s]
$u_{m\ scaled}$	scaled model wind profile	[m/s]
u_r	undisturbed wind speed at 10h_c	[m/s]
u_{tip}	tip speed	[m/s]
$u_{tip,dsg}$	design tip speed	[m/s]
$u_{II\ scaled}$	wind profile derived with method II and then scaled	[m/s]
u^*	friction velocity	[m/s]
u^*_A	friction velocity of a site outside the city	[m/s]
u^*_{scaled}	scaled friction velocity	[m/s]
U	wind speed in the rotor plane	[m/s]
U_{log}	wind speed in a logarithmic wind profile	[m/s]
U_R	relative speed of the fluid at the airfoil	[m/s]
U_∞	free stream velocity	[m/s]
W	width between two buildings	[m]
x	fetch downstream of a roughness change	[m]
Y	performance parameter	[-]
z	height where u is present	[m]
z_A	height where u_A is present	[m]
z_{ref}	reference height	[m]
z_0	roughness length	[m]
z_{0A}	roughness length at a site outside the city	[m]
$z_{0,o}$	original roughness length	[m]
$z_{0,o\ scaled}$	scaled original roughness length	[m]
Z	rotor height coordinate	[m]

Greek:

α	angle of attack	[^{0}]
β	blade slope	[^{0}]
δ	height of the internal boundary layer	[m]
$\Delta\theta$	azimuth angle segment contained in the discretized streamtube	[^{0}]
θ	azimuth position of an angle segment	[^{0}]
κ	Karman constant	[-]
λ	tip speed ratio	[-]
λ_{dsg}	design tip speed ratio	[-]
$\lambda_{equator}$	tip speed ratio referring to equatorial radius of a Darrieus rotor	[-]
λ_f	sum of building areas normal to wind/total urban area, (A_f/A_d)	[-]
λ_{max}	maximal tip speed ratio	[-]
λ_{min}	minimal tip speed ratio	[-]
λ_p	sum of all areas covered by buildings/total urban area, (A_p/A_d)	[-]
ν	kinematic viscosity	[m/s^2]
ρ	density of a medium	[kg/m^3]
σ	rotor solidity	[-]
σ_H	standard deviation of the building heights	[m]
φ	angle one blade spans over	[^{0}]
ϕ	local latitude	[^{0}]
Ω	angular speed of the earth	[1/s]

Abbreviations:

ADI	Âgencia De Inovação
AEP	Annual Energy Production
aoa	angle of attack
AWP	Annual Wind energy Potential
a.g.l.	above ground level
a.r.l.	above roof level
CFD	Computational Fluid Dynamics
conf	configuration
const	constant
DART	DARrieus Turbine
DK	Denmark
DTU	Danmarks Tekniske Universitet
ESDU	Engineering Sciences Data Unit
EWEC	European Wind Energy Conference
HAWT	Horizontal Axis Wind Turbine
HAWTopt	Horizontal Axis Wind Turbine optimization
HCØI	Hans Christian Ørsted Institut
LEED	Leadership in Energy and Environmental Design
MEK	Institut for Mekanisk Teknologi
QUICK	Quadratic Upstream Scheme
RANS	Reynolds Averaged Navier-Stokes
rpm	rotations per minute
rps	rotations per second
RPT	Rapid Prototyping
SIMPLE	Semi-Implicit Method for Pressure Linked Equations
TSR	Tip Speed Ratio
UCL	Urban Canopy Layer
UK	United Kingdom
VAWT	Vertical Axis Wind Turbine
VAWTopt	Vertical Axis Wind Turbine optimization
WAsP	Wind Atlas Analysis and Application Program

1 INTRODUCTION

In the urban environment, besides the industry and transport sector, a huge amount of energy is consumed. Housing was for a long time considered to merely shelter people, and the local energy needs were mostly covered and provided by centralized power plants, exploiting various energy sources and resources. New trends e.g. in architecture and urban planning are to reduce energy needs, by isolation, use of daylight, public transportation accessibility and the like. At the same time decentralized technologies are introduced to provide a proportion of the inevitable energy. These two factors consequently reduce the energy procured from centralized power production and path the way to sustainable cities. One of the technologies, not new as such, but utilized in a new context, constitutes urban wind energy in form of wind turbines. In the recent years, wind turbine models, available before and also especially designed for the use in the urban environment, were installed in the inhabited environment in various ways- in symbiosis with a new constructed building structure, attached to existing buildings, and free-standing close to buildings. In many cases the operational efficiencies are lower than anticipated and investment costs high, as for many technologies in the beginning of their development. Wind energy in the urban environment is a new area and a rather blank page concerning design criteria, aesthetics, concepts, minimizing costs etc. Even though the potential energy in the flow is much higher on the countryside or offshore, the erection of wind turbines in urban areas is carried out and also shows perspectives regarding e. g. direct use of the energy instead of redirecting the energy to the grid and reduction of transmission loss. Questions like, why should turbines be implemented in cities, what is their usage, where to position which configuration, how about the impact of the everyday life of the citizens, have to be answered.

Connected to the idea of wind energy inside inhabited areas are mostly small-scale wind turbines. Catalogues listing numerous small-scale wind turbines available on the market can be found [1]. They were usually commercially developed and not necessarily designed according to the conditions found in the urban areas. Although experiences with urban wind energy conversion are rare, research and technology reviews were carried out at different research institutes. Former investigations covered market analysis, for example in Sweden [2], intensive field trials [3], wind regime studies [4] with energy yield estimations and rotor designs.

One of the first more holistic works was done by Mertens [5], affiliated that time at TU Delft, Netherlands. In the frame of the activities at TU delft, a vertical axis wind turbine called Turby was developed especially for the operation in urban wind climates [6]. A big part of their rotor design investigations focused on flow conditions found on rooftops, where they expected a skewed flow [7], but also topics like dynamic stall behavior for a vertical axis wind turbine rotor was investigated [8]. Judging the progress over the last few years, a clear tendency towards small-scaled vertical axis wind turbines for the built environment could be observed.

Further academic investigations were done in UK at Loughborough University for example [9], mainly studying ducted wind turbines but also estimating the energy yield for wind turbines positioned on rooftops within building clusters. The University of Glasgow on the contrary published a work on the performance of different vertical axis wind turbine designs [10]. It can be said, that the UK was the most active player so far, when it comes to experimental set-ups. Their political conditions nourished the small wind turbine market, resulting among others in the commercially developed vertical axis wind turbine Q5, a rotor rated at 5kW, sculptured in such a way, that it could be seen as a piece of architecture. Lately,

quietrevolution, the company behind Q5 also started to collaborate with universities, publishing research work on their rotor [11]. Furthermore, the concept of integrating wind turbines into the building structure actually was realized in UK with the erection of the Strata Tower. Such or similar conceptual designs had been thought of by numerous architects, but hardly made the step from drawing board to construction site.

In general, the urban wind energy turbine theme "clashes" with the small wind turbine theme and both themes are relatively sparsely described. Therefore we need both to study the theme "small turbines" and the theme "urban wind energy". The present work is not meant to advocate the use or refusal of urban wind energy applications, but to deliver an objective and fundamental overview of the social, practical and physical conditions relevant for urban wind energy. Furthermore, the document is meant to analyze and assemble important issues for the installation of small wind turbines in the urban environment, while conclusions and summaries are addressed to a broad range of readers and therefore written in a manner easy to understand and at the same time maintaining a scientific level.

With the topics investigated in this work, an attempt is accomplished to deliver an insight into, and explanation of, the physical factors playing decisive rolls. Important elements for small-scale wind turbines sited in the urban environment are the macro and micro wind climate, the siting within a micro wind climate and the choice of a wind turbine model most appropriate for the selected site. This approach applies for common large wind turbines as well. Thereby, the micro wind climate at the common sites is not as complex and individual as in cities. For sites where large-scale wind turbines usually are erected, wind potential estimations tools are developed and already used for years. Consequently, well adapted wind turbines are designed and approved. To do the same for the urban environment, methods, tools and rotor designs are proposed in the framework of the PhD thesis on hand. In the present work an approach to the integration of wind energy into the built environment is carried out on the base of Copenhagen, DK.

On the way, ideas are created about the entry of wind energy into the inhabited area, since a known technology, but in a new context needs experience and not an immediate large implementation of heavy machinery. The inhabited area is a delicate ground and appropriate new technology has to evolve carefully step by step. Wind turbines in the beginning of their development were not installed in offshore parks either. Besides the clear defined physical challenges due to the wind conditions, factors less easy to be expressed in numbers or described with equations are present, like aesthetics and comfort.

To start with the physical challenges the urban wind climate is investigated on basis of an example site. The macro climate of the area is described in terms of roughness class and displacement height, determined with the help of the wind climate present at Kastrup Airport, DK, the specific city site composition and the punctual wind measurement taken at the city site. A few examples of existing wind turbine designs are analytically exposed to the wind conditions found at the specific site in the city of Copenhagen and their power curve characteristics are discussed in connection with their energy production in such a wind climate. Different from open land or open sea, the flow field in cities is complex and highly site-dependent. Usually, extensive wind measurements would be the most appropriate method to estimate the wind potential at a specific site. With that the micro climate would only be resolved punctual, though. Another method is to carry out computational fluid dynamics (CFD) simulations of the site of interest. Anyway, results from both methods would be site-dependent. In order to come up with more general rules, Reynolds Averaged

Navier-Stokes (RANS) solved CFD simulations of characteristic districts by means of built-up density, mean height and height variation are conducted to visualize general flow behavior and wind potential.

One task is to determine the wind potential and another task is to find an appropriate application to make use of it. By dints of a lift-driven vertical axis wind turbines (VAWT), important design parameters are explained and optimization strategies introduced. In combination with a given wind climate it was identified earlier, that the characteristics of the wind turbine power curve has a tremendous influence on the all-over efficiency. Besides the popular VAWT design, a micro-scale horizontal axis wind turbine (HAWT) is designed, to enter the urban space with a different strategy. In the end, the rather theoretical achievements are applied to real test cases, where small VAWTs were installed at various sites inside Copenhagen and its vicinity. The sites represent different macro climates and the wind turbines positioned within them were subjected to the site specific micro wind climates. Measurements of the onsite wind velocities, wind directions and data of their actual energy production are analyzed and with the help of the acquired tools and actual power curve measurements an attempt is made to explain the discrepancy of expected energy production and the measured production. Furthermore, the acquired tools and knowledge are combined to propose a siting method explained with the help of one of the test sites. At last, on the base of the all-over findings a concept study results in conclusions for VAWT designs, more advisable for the examined test sites.

But first of all, a brief overview is given about the background and state of the art conditions for wind turbines in the inhabited area.

1.1 History

In the course of time, the way energy was extracted from the wind, in which form the extracted energy was used and especially the location of the rotors has changed significantly. The graph in Fig. 1 tries to describe this evolution along with the importance wind energy conversion got assigned to in the corresponding time [12] [13] [14] [15].

Historically, the energy in the wind was first discovered and utilized to travel on the sea. With the knowledge of sails the oldest wind turbines were invented by the Persians. They used the energy contained in the wind to alleviate works, which were usually carried out with body effort. Mechanical energy was transformed into another form of mechanical energy to for example grind corns. Almost simultaneously, in China a more advanced model of turbine was developed. Independent of a wind direction and without additional buildings structure, they used the wind to pump water. Both concepts orientated the axis vertically. A bit later mechanical wind energy utilization started to emerge in Europe. The turbines were linked to a building, where the energy was used directly to ease the farmers work. In America the turbines were smaller and mainly used to pump water. At the same time as they were developed, the steam and combustion engine were invented and with that the popularity of wind mills decreased drastically, not to say made them dispensable.

At the beginning of the 20th century the Dane Poul La Cour came up with a turbine, generating electricity, instead of mechanical energy. This was a whole new way to think. But at the same time, there were much more efficient energy sources and so the research in the area of electricity generating turbines was only a small niche, investigated by Albert Betz, Sigurd Savonius, Georges Darrieus and Ulrich W. Hütter, to name the most influencing persons. On their way to make turbines more

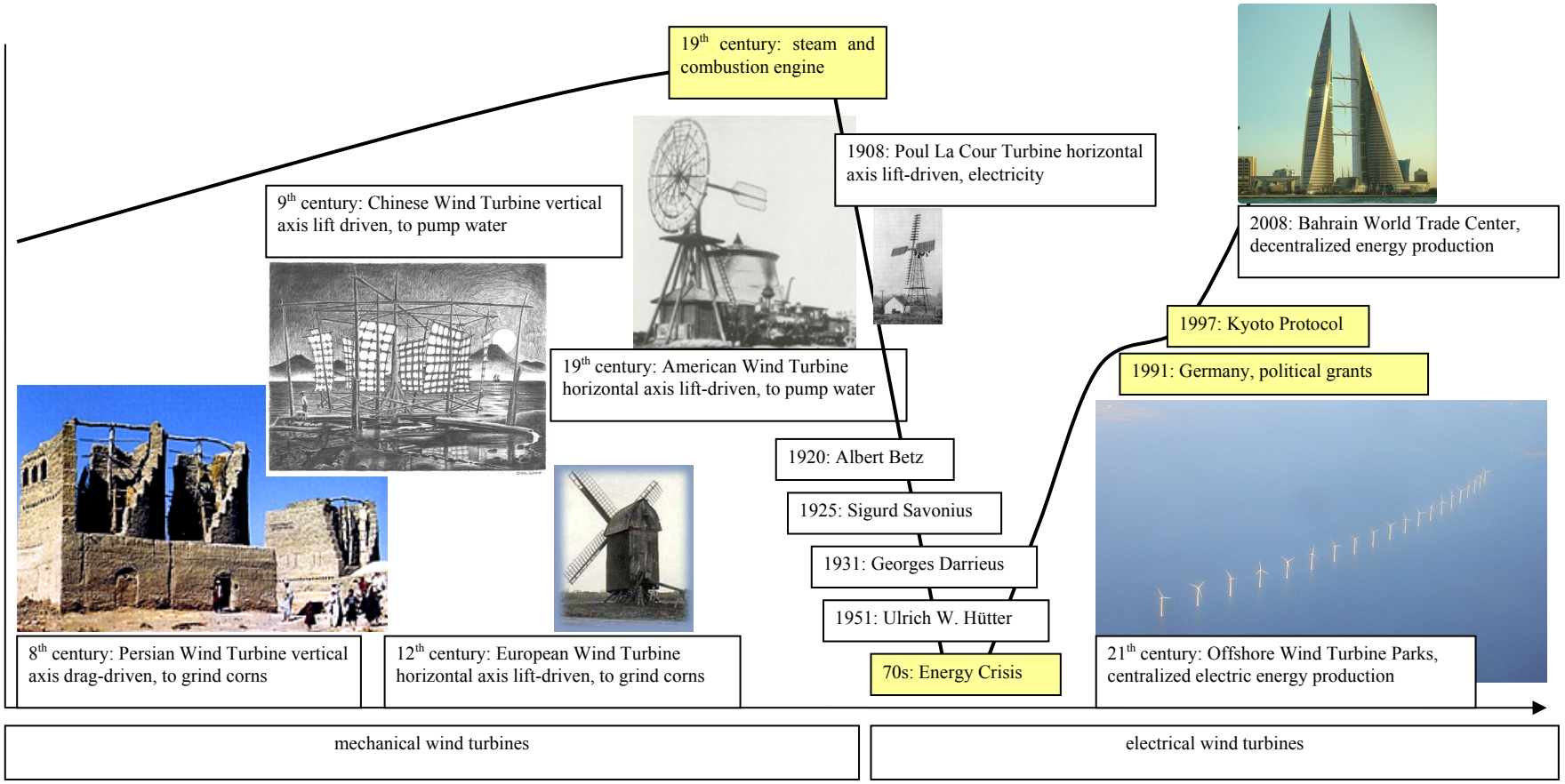

Fig. 1: Historical development of wind energy applications and their importance with example turbines

efficient and so competitive with for example oil, they had to face limits given by material, not fulfilling the load demands. Society and especially industry got hit by the oil crisis in the seventies. Prices for raw oil increased by 70% and alternative energy sources moved into the focus of interest. Wind energy experienced a great revival and astonishing enough, although the oil marked relaxed, ecological awareness maintained in the society. To keep the trend, in Germany for example wind energy received crucial political support in forms of for example feed-in grants. Due to the alarming global warming observations, the industrial countries passed the Kyoto Protocol in 1997. Since then wind turbines are built more efficient, bigger, higher, clustered in parks and whole wind power plants are installed, on- as offshore.

CO_2 emissions by combustion based energy sources are supposed to be replaced by renewable and clean solutions. This is only one part of the development- technology to use less energy were, and are, developed. In cities most of the energy is mainly used for heating and cooling, respectively. Architecture was always considered to host people, without respecting sustainable design. But now, in America for example, certificates such as LEED (Leadership in Energy and Environmental Design) are introduced. Buildings are using isolating materials, recycled materials, recyclable materials, natural light sources, solar panels and wind energy for natural ventilation. Until so far, only very few buildings were designed with respect to harvest wind energy onsite with the help of a wind turbine rotor. For now it is fancy to brand your design as green. But the more of them are introduced the more it will become habitual to design environmentally friendly.

Interesting is, that at the very beginning of the chronic line and the state of the art, it can be seen, that rotors had been integrated in building structures and are integrated in building structures again; 13 centuries later.

1.2 State of the Art Examples

In contrast to the well investigated large-scale wind turbines onshore and offshore, knowledge about designing, positioning and operating small-scale rotors was limited and is only slowly but surely acquired. Driven and due to the new field of wind energy application, private and scientific people sought for appropriate approaches of the eclectic challenge. That led to numerous solution projections with wind turbines integrated into buildings' structure, mounted on buildings' rooftops or positioned free-standing at public spaces. Also, the wind turbine designs were rethought. Almost forgotten configurations like the vertical axis wind turbine (VAWT) suddenly were removed from dust and reinvestigated in the new context.

Indeed, wind conversion systems have been sparsely implemented in cities at several places around the world, including for example Japan, Bahrain, America, UK, Holland, Portugal and DK. Among these test cases, a few intensive field trials were conducted, where the results were rather disappointing with regard to the energy output, but on the other hand delivered more experience, knowledge and with that a working surface [16] [17]. The expectations to the energy outcome are dependent on the local wind climate, the rotor positioning within this wind climate and the wind turbine design's capabilities to operate at this chosen position. In a state of the art 2009 report [18] the topic and its challenges are sketched. Some of the examples are shown here and arguments for and against the single integration methods are mentioned.

1.2.1 Wind turbines integrated in buildings

A number of examples of wind turbines in design of urban structures exist. It is a challenging mission to put it into reality though. Most of the designs never made their way from the drawing board to construction site. But the vision is the first step to mission. Integrated wind turbines are most reasonable for high rises, since their

height reaches into high wind velocity layers. The very first building, where wind turbines actually were integrated according to the buildings shape, or the other way around, was the Bahrain World Trade Center (BWTC). It was completed in the year 2008 (see Fig. 2 [19]).

Fig. 2: Bahrain World Trade Center

Three massive wind turbines, measuring 29 meter in diameter, are supported by bridges spanning between BWTC's two towers. Through its positioning and the aerodynamic design of the towers, the prevailing onshore Gulf breeze is funnelled into the path of the turbines, helping to create greater power generation efficiency. Once operational, the wind turbines will deliver approximately 11-15% of the BWTC tower's energy needs, eliminating around 55.000kg of carbon emissions every year.
Location: Manama, Bahrain, sea side facing (prevailing wind direction)
Height: 240m
Turbine: three HAWTs, 29m in diameter
Contact: www.bahrainwtc.com

Another way to combine wind turbines and the building's structure was carried out in London with the Strata skyscraper (see Fig. 3 [20]). Here the turbines are located in tunnels in the very top of the building. The idea is to make use of the so-called Venturi effect, capturing and directing the available wind towards the rotor.

Fig. 3: Strata Tower under construction

Three 9m wind turbines integrated into the top of the building are expected to generate sufficient power to drive the energy efficient lighting to the building. The turbines are encased by the structure, fixed in yaw and therefore aligned to the prevailing wind direction. Aerodynamic shaping of the casing shall enhance the power performance.
Location: South London, low built quarter
Height: 147m
Turbine: three HAWTs, 9m in diameter, encased, fixed yaw
Contact: www.stratalondon.com

At the same time the duct shields the wind turbine, which is a good thing in the inhabited area. In case of a blade loss the primary energy would be absorbed by the duct structure. Several investigations on turbines in ducts were made throughout the history. Specifically for this design, an investigation was made on the aerodynamic

design of the ducts and the influence of the turbines thrust in operation [21]. A disadvantage of such strict directionality is that the wind approaching from directions not to be captured by the duct are considerable, even for a site with a significant prevailing wind direction [22]. The Strata Tower was completed in 2010.

Arguments for Integrated Wind Turbines

- Lower energy demand, by covering a part with onsite generation is a sales argument
- Alternative to more and more expensive energy sources (oil, gas, electricity)
- Show environmental consciousness
- Get a certificate to stand out of the mass (e. g. LEED)
- Upwind generated by buildings facades increases wind velocities
- Buildings are reaching into high velocity layers, and with that no "useless" wind turbine tower is needed
- The structure can be used to encase turbines to enhance their performance, hide them visually and at the same time make them safer
- Aerodynamic building structure can direct and concentrate wind towards the turbine
- Long transmission lines for energy transportation, linked to significant losses, can be cancelled out

Arguments against Integrated Wind Turbines

- Natural ventilation and wind turbines for electricity production are depending on the wind and are therefore not reliable/ always available
- New surrounding buildings are changing the local wind conditions and must be part of the project as well
- Noise and vibrations close to buildings clash with the desire of more comfort
- Wind velocities in cities are lower and more turbulent than on rural sites
- "Empty space" = expensive volume where people could live in is used by implementing turbines
- The quantity of new buildings is low compared to the mass of already existing buildings

1.2.2 Small turbines on already existing buildings

Another option to implement wind turbines in built-up areas is to mount them on already existing buildings. Some manufacturers made big and incomplete promises to customers. Vibration transmission and with it fatigue breaks of buildings structure and also noise emission due to vibrations brought this market to a fast ending and at the same time they harmed the reputation of small-scale wind energy.

Manufacturers like Ampair are not recommending the installation on rooftops, because the turbines as well as the roof structure are not designed for this application. The group called WINEUR (Wind Energy Integration in the Urban Environment) carried out feasibility studies, including partners from France, the Netherlands and the UK. The results of their work can be downloaded for free [23].

Quietrevolution is probably the company, investing and investigating most intensively in this area, whereas many of their turbines are installed besides buildings as well. The Technical University of Delft, NL, has developed a vertical axis wind turbine appropriate for the installation on buildings. Both, the quietrevolution turbine and the Delft Turbine, Turby, have spiral blades (see Fig. 4 [24] [25]). In the course of this thesis, the characteristics of such blade shape are investigated. Another part of this work looks into the performance of vertical axis wind turbines mounted on flat rooftops in the city and vicinity of Copenhagen.

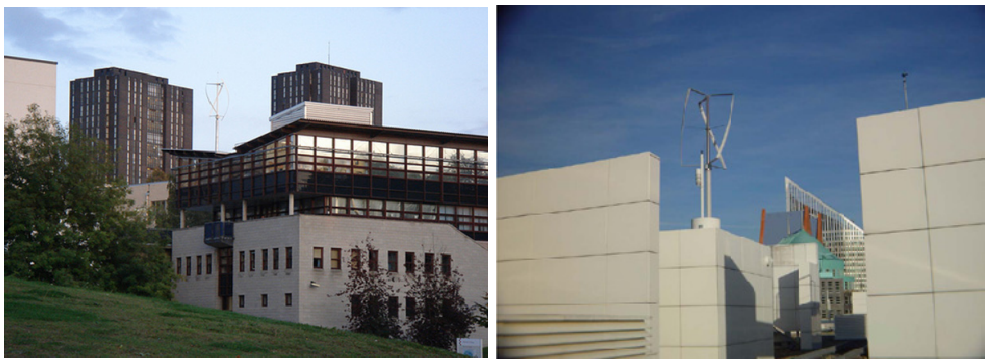

Fig. 4: Building mounted wind turbines. Left: quietrevolution rotor; right: Turby

Arguments for Small Wind Turbines mounted on Existing Buildings

- Less energy transportation loss
- Low wind velocities in cities are enhanced by the upwind by houses or other obstacles
- The background noise in cities is high and covers most of the turbines noise emissions
- Shorter towers are necessary
- Our energy need becomes visible
- Affordable for private persons and small companies
- Combined with solar energy, the whole weather spectrum is covered and the two systems can share the same hardware

Arguments against Small Wind Turbines mounted on Existing Buildings

- Every roof has its own material, construction and therefore characteristics and with that an universal solution is impractical
- Transmission of vibrations and noise is changing from case to case
- Lower noise emission limit, than on a free field
- High turbulences and fast changing wind velocity and direction
- High safety demands

1.2.3 Free-standing wind turbines

Different from the earlier mentioned ways of implementing wind turbines in the urban environment the free-standing wind turbine is mostly comparable to the rotors installed at the countryside. Surely, the wind conditions are very different. The energy use of such a turbine does not need to be connected to certain buildings, but could be thought of an energy source for an autarkic standing application.

In Japan for example, where earth quakes are a daily phenomena, plenty design for street lamps decoupled from the main grid can be found. In this way, even if the grid might breakdown, the lightening of the streets can be ensured. One example, where a drag-driven Savonius rotor is combined with a solar panel can be seen in Fig. 5, left.

In the same figure to the right an example of a downwind horizontal axis wind turbine is given [26]. The turbines were installed due to the laws imposed by the UK government, that a certain amount of energy consumption should be covered by renewable energy. With Blackpool's coastal location, the wind situation is appropriate to cover a fraction of their high energy consumption with onsite wind energy applications. In the next section examples for free-standing and autarkic wind turbines are presented for the city of Copenhagen, DK.

Fig. 5: Free-standing wind turbines. Left: Savonius type integrated in a light armature in Japan (picture taken by P. Friis). Right: Proven turbines erected in Blackpool, UK.

Arguments for Free-Standing Wind Turbines

- Autarkic energy systems can be created, e.g. street lamp
- No vibration transmission to building structure
- More freedom in positioning

Arguments against Free-Standing Wind Turbines

- Full length tower is needed, probably very high towers to reach up to sufficient wind velocities

1.3 Drivers

As the example given for the city of Blackpool, governments in several countries are imposing new laws with regard to renewable energy sources on the spot, where the energy consumption takes place. In Europe, the energy policies are passed by the European Union. New recommendations and laws within the energy sector, especially for the built environment, drive the development of new technologies and strategies. The current energy directive can be downloaded [27]. It defines the measurements that have to be taken in case of major renovation of old buildings and in case of planning new buildings. How the directives are employed in the single countries is depending on the governments. Besides the implementation of renewable energy technology in the inhabited area, the EU demands housings to be tagged with a label indicating their energy consumption. In America such labeling and certification of buildings has been done for some years now. The third party controlled program is called LEED (Leadership in Energy and Environmental Design). It is not a necessity to get a new building LEED certified, but it is a motivation to do so since the labeling contributes to a higher occupancy of such a building, compared to a building without it, and that the market demand for LEED certified buildings is higher than for not certified buildings [28]. It might be compared to the labeling of ecological food. Furthermore, it is known that wind velocities onshore are lower than offshore due to a higher surface roughness. With increasing roughness length the turbulence intensity is increasing as well. Going from an open land site into a densely built environment increases the roughness length, decreases the average wind velocity and increases the turbulence intensity remarkably. So, one might be eager to raise the question why wind energy applications are attempted to be installed in a wind climate, which is not optimal. Besides the earlier mentioned directives there are a few reasons. One reason is that transmission losses from centralized power plants are about 6% and could be eliminated with local energy production. The energy generated locally could then be used to drive a low voltage grid for example and with that reduce transformation losses. Another reason is that optimal sites, on- and offshore, are broadly used at which the field of offshore offers the possibility to go further out, but also deeper. Though, the transmission issue will temporally bench a physical limit. Urban wind energy is another niche, bearing the potential to complete the spectrum. State of the common art is 5MW turbines where development of 8 and 10MW turbines is in process right now aiming for the 20MW

machine. Such machinery is dependent on heavy investments and will rather be industrialized, than financed by private persons. The other end of the spectra is leading to small-scale wind turbines, machines with a 1 to 5kW generator connected to produce energy where it is consumed. A rain barrel can be seen as an allegory. The rain on your rooftop can be collected and stored to water your plants for example. Of course, it is good and necessary to have a reliable centralized water supply. Using the water onsite though means that parts of your needs can be covered by your own supply and at the same time it means that less water mass has to be transported.

1.3.1 Effect

Nowadays, the energy production is mostly decoupled from the user. New research shows that visualization of energy consumption can affect the user to reduce his/her consumption through awareness. This theory is referring to the so-called eco-visualization [29]. Another phenomenon can be triggered by the so-called eco-feedback [30]. A wide spread application of the eco-feedback can be found in cars, where the momentary fuel consumption rate is displayed to the driver. In this way the driver is informed about the consumption of the car in combination with the way of driving and can directly influence it by a more economical and ecological driving style.

The same effects could be evoked by energy systems connected immediate to the user. In Fig. 6 the progression of awareness is pictured. In the beginning the user is not aware of the source of energy. All, what is visible, is the plug and the knowledge, that whatever is plugged in will work. Once in a while an indication of consumption is given in form of a bill. Connecting a small wind turbine to the private household would first decrease the energy procured from the main grid. It can be thought of an independent 12V grid, since there are several items in a household running on lower voltage. In this way transformation losses will be reduced as well. In a vision it also could be purposed to use household tools as energy storage, instead of feeding the excessive energy into the main grid. Well, but by visualization of the energy production and with that the reduced energy purchase, the user might start to be more careful with energy usage in general and with that cutting down the amount of purchased energy. If this works for one person, the neighbor, colleague or relative might like to have the same system installed as well.

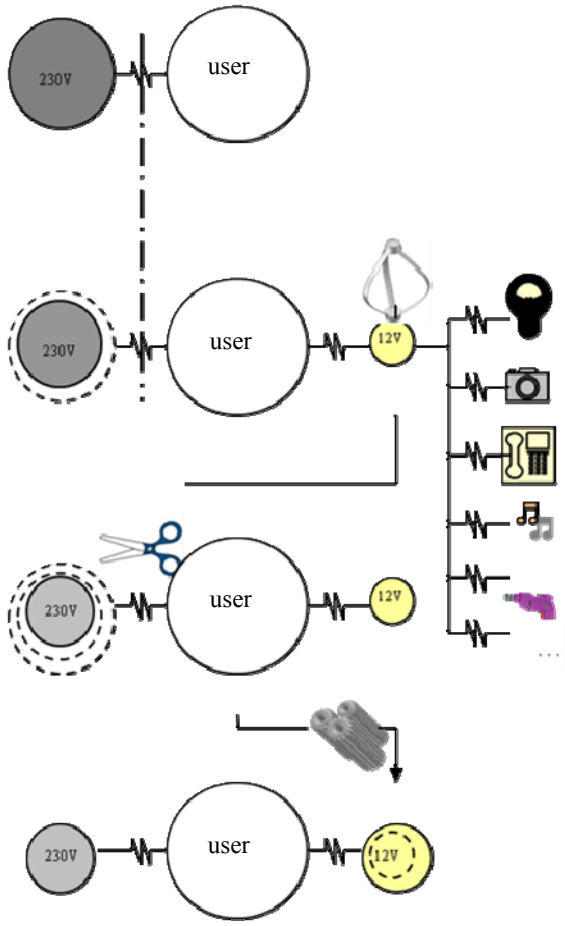

Fig. 6: Awareness progression with eco-visualization

1.3.2 Regulations in Denmark

Intensive regulations for private owned small wind turbines has been passed recently in Denmark and make it at least legally possible for the citizen to decide acquiring and installing a private wind conversion machine. Several issues are defined and put into limits and frames. The Danish Wind Turbine Association (in Danish: Danmarks Vindmølleforening) published for example fact sheets concerning the definition of what a household turbine is and where it can be set up [31] and they explain the regulations about noise [32] and flicker [33]. Wind turbines imported into Denmark or self-constructed have to be approved before installation. On forehand, several small wind turbines have been certified and been approved for the use in Denmark. On the homepage of the Danish Energy Agency (in Danish: Energi Styrelsen) [34] information about the different categories of certification for wind turbine, divided in type classes can be found and a list of approved wind turbines is accessible.

Especially interesting for the built environment are turbines with a rotor swept area up to $5m^2$. For this category of wind turbines, special rules apply. In Table 1 the currently approved turbines belonging to this type of class are listed. The market of small wind turbines in Denmark is growing fast with the supply side setting the agenda with doubling the number of certified or notified small wind turbines in one year (2010 to 2011), and with another doubling underway by the number of prototypes in testing and certification process at present.

Table 1: Wind turbines with a swept rotor area below $5m^2$, approved for the use in Denmark [35]

Manufacturer	Type	Power [kW]	Rotor [m]	Swept area [m^2]	Hub height [m]	Issuance date
Procure A/S	WG400	0.4	1.5	1.8	5.5	31-08-2009
Procure A/S	WG600	0.5	1.5	1.8	5.5	31-08-2009
Toria ApS og SJ Service	Futurenergy FE 1012/1024/1048	1	2.5	4.9	7.5	26-10-2009
Logik og Co ApS	Venco-Twister 1000-T ***	1	1.9 x 1.9	3.6	3	14-12-2009
Logik og Co ApS	Venco-Twister 1000-TL ***	1	1.9 x 1.9	3.6	3	14-12-2009
Build a Mill ApS	BAM 400	0.4	2.2	3.8	6.3	12-04-2010
Build a Mill ApS	BAM 600	0.6	2.4	4.5	6.3	12-04-2010
Carlo Gavazzi Handel A/S	Mistral 3K	3	2.49	4.9	6	25-05-2010
Zeteco Energy	ZEW03-6/ FD2.5-300	0.3	1.5	1.8	6	01-07-2010
Zeteco Energy	ZEW05-6/ FD2.7-300	0.5	2.5	4.9	4.9	01-07-2010

Besides the personal contribution to a more environmental friendly source of energy, the economy in such an investment is of interest for the user. A considerable role in the financial viability plays the way, how the energy is used, sold, bought and which kind of taxation applies. Information about this topic is summarized in a valuable presentation given by the Danish Energy Agency at the "Mini and Household Wind Turbine" workshop 2010 (in Danish: Mini- og Husstandsmølle Temadag 2010) [36].

1.4 Demands

Some of the demands for wind turbines and their installation at a rural open land site apply for wind turbines and their installation in the urban area as well, but might be

stricter. In addition, demands unbeknown to former applications have to be taken into account. In the section with the state of the art examples a few challenges were already mentioned in form of advantages and disadvantages. A summary and completion of the conditions which have to be considered is shown in Table 2. The demands are numerous and probably not even complete. Since there are plenty of challenges, not all of them are covered in the present work. Mostly it was focused on the wind conditions, the performance and design of wind turbines (*). Most of the issues connected to comfort and installation conditions are not part of the investigations. Some of them are shortly discussed in the course of the work (**).

Table 2: Overview of the conditions relevant for the implementation of wind energy applications into the urban space

wind conditions	
low wind velocities	(*)
high roughness length and with that high turbulence intensity	(*)
frequently changing wind direction	(*)
wind profile displacement height	(*)
wind climates are complex and site specific and are not as predictable as for a simple site	(*)
positioning within micro climate	(*)
comfort conditions	
flicker	
noise emission	(**)
increased safety	(**)
visual impact	(**)
installation conditions	
vibration transmission to building structure	(**)
losses in transformer and inverter	(**)
installation and maintenance costs	
usage of the produced energy and taxation laws	
vegetation and neighboring buildings can change	
sharing components with other energy conversion systems	(**)
demolition threats (by intention, animals, branches or other objects hitting the rotor)	

1.5 Entering the Urban Space/ Design Examples for Copenhagen

Besides the lower wind velocities and higher turbulence intensity, the residential area is a delicate ground. In terms of safety, comfort and aesthetics, materials and concepts have to be chosen thoughtfully to meet a high standard. In general, the introduction of a technology new to an environment can be done in various ways. Installing common wind turbines in a range of 200kW on a large scale is one scenario. But this bears the potential to feel like an invasion, followed by absolute refusal of acceptance. Yet, common wind turbines are neither designed for the physical conditions nor the psychological conditions present in the residential area. Another, more deliberated approach is, to start with very small-scaled rotors in the size of 5W to give an understanding of the technology to the inhabitant, working like seeds in a fertile ground. In this manner, the acceptance as well as the technology can be developed and grow. Similar to this strategy is the implementation of intermediate wind turbines with a rated effect up to 5kW, but at only a few selected sites, serving as examples to gain experience on both sides, on the side of the user and the supplier.

In this section a rough scan of the conditions and opportunities in the city of Copenhagen is carried out and forms the point of origin for most of the following

recessed work. The following presented design, usage and implementation examples are own ideas mixed with two designs, accomplished by others. Theirs are referred to in particular to distinguish between proposition and inspiration.

1.5.1 Pre-considerations

First of all, the city environment is looked at as a neutral space on the example of Copenhagen and scanned for sites, more destined for wind energy applications than others. In the contemplations the usage of the produced energy is included as well. On top of its coastal location, Copenhagen's most known characteristics are its bridges, channels, broad streets, lakes, towers and bicycles. Such a silhouette offers ground for design principles.

1.5.1.1 Energy usage

Before the locations are discussed, the question 'who is going to use the energy and how ', is reviewed. In the future, private households shall be able to produce and use their own energy. In this section, though, the possible entries into the urban space are sketched to start with. To circumvent the possibility of a neighbor being bothered by a turbine, without gaining anything from the turbine, a solution to attain acceptance is to use turbines for public needs first. They are not necessarily connected to a building, but to an advantage of all citizens. This could for example be done in form of street lamps, drawing energy from a close by wind turbine or wind turbines can be integrated directly in the street lamp.

Another application idea is the charging of electronic city bikes, while care has to be taken not to invent new electronic items raising the energy needs. To achieve sustainable urban living, a combination of two trends is inevitable. One of them is to reduce energy needs by increased awareness, more efficient technologies and strategies and the other is the supply from renewable energy sources. A strategy drawn from this philosophy is to use the energy where it is produced, that means the onsite produced energy shall not vanish anonymously into the grid.

To go back to ancient times, another idea is to convert the mechanical energy from the rotor directly into another form of mechanical energy like a water pump for example. In this way, the loss due to transformation from one energy form into another can be minimized. These mechanical application options are inspiring, but in a modern society rather limited, though. Thinking further in terms of minimized transformation losses, electrical wind turbine systems can be combined with other local technologies, like photovoltaic panels. Connecting them to common hardware, decreases financial and energetic costs. Instead of transforming the direct current into alternating current, the energy can be stored in a battery or drive a low voltage grid, since many items in a household are running on a voltage lower than 230V. Fig. 7 shows a simplified set-up. In a further perspective, household items can be equipped with batteries, serving as storage, similar to an electric car within a smart grid.

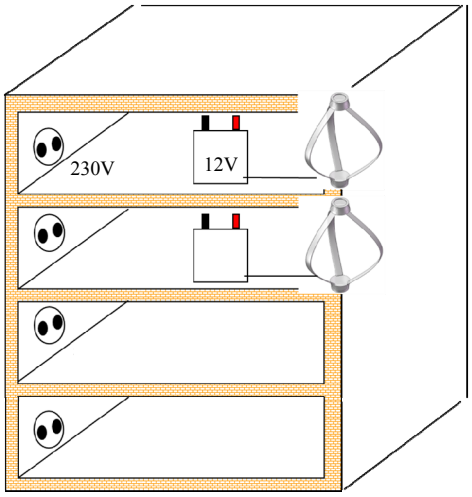

Fig. 7: Private housing with small wind turbines supporting 12V source

1.5.1.2 Water and street canyons

Within a city, buildings constitute obstacles to the wind. They provoke lower wind velocities, increase the turbulence intensity and in certain districts the wind is skimming over the rooftops with only a small portion of wind movements in the lower regions between the buildings. Other areas with wide open spaces are found to be windy. Higher wind speeds are generally experienced on bridges, on crossroads, in parks, in outskirts, close to the coast and water channels. This is explained by and dependent on the macro and micro wind climates. A special phenomenon is the funneling effect of a so-called street canyon, where the wind is caught between two long stretched mostly impermeable construction complexes. Such an effect is for example typical for broader main roads and also for water channels, framed with buildings (see Fig. 8). Wind is like water following the path of lower resistance.

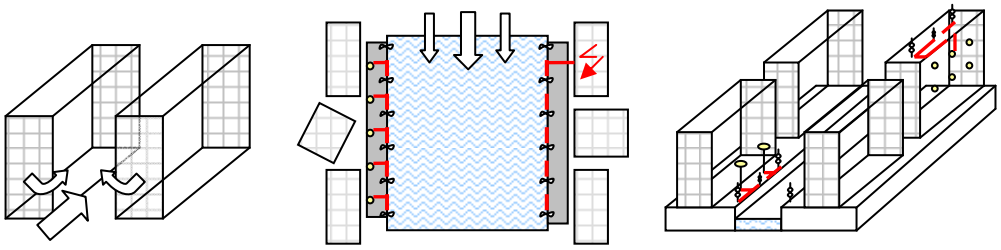

Fig. 8: Sketch of different conceivable street canyon situations in Copenhagen with ideas of rotor positioning and energy usage

1.5.1.3 Various applications

A rotationally symmetrical structure like the pavilion in Fælledparken, Copenhagen, (see Fig. 9, left [37]) offers the opportunity to install a unidirectional turbine on the top. The flow will be concentrated and accelerated towards the top and with the gained energy lights or something more symbolic, like an ice machine, could be driven.

Fig. 9: Possible wind turbine positioning. Left: Pavilion in Fælledparken; right: Tycho Brahe planetarium

However, as can be seen at the photo the trees in this specific case will decrease the wind speed to a level, which probably will make a wind turbine installation at the top of the building too inefficient. A building like the Tycho Brahe Planetarium, Copenhagen, (see Fig. 9, right [38]) is not independent from the wind direction. Its orientation towards the water is advantageous if the wind comes from the lake side, because of the low roughness of the water surface.

Turbines in cities could be installed “offshore” as well. Especially in parks, where people go to relax, having a picnic and play e. g. football, a turbine in the middle of the field is limiting the freedom upwards. A football, a boomerang or other flying

devices are exposed to the risk of being hit by the rotating turbine blades. The same applies for the turbine, but vice versa. By erecting turbines in the middle of a small lake (without boat traffic), a natural distance is kept between the citizen and turbine. Also, a low roughness surface is surrounding the turbine, of course depending on the amount of trees in the park and their distance. As for offshore wind turbines, more complex and expensive components have to be used in matters of waterproof housings, under water cables, etc. and installation and maintenance is more time and money intense.

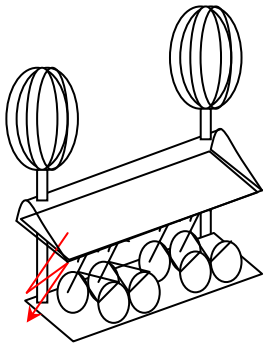

Besides the bridges, towers and lakes, the city bikes are characteristic for Copenhagen. Turbines could be erected at the bike stations. It would couple the green thought of cycling to the green thought of wind energy. At the same time, the stations would be easy to find. The energy could be used, for example, to charge electric bikes. Energetic people could even produce energy by cycling and support charging the electric bikes (see Fig. 10).

Fig. 10: Wind turbines charging electric city bikes

Wind turbines in public could be coupled to an indicator, meaning that the power should not vanish in the grid. The production should be coupled directly to the usage like the Netherland wind mills milling grain and create an autonomous circuit. Autonomous circuits are operating when it is windy weather. Which application could be attractive in windy weather? High wind velocities are mostly coupled to cold and unpleasant weather. But wind turbines can be used to cheer up people with light fragile and moving structures as for example the idea "Wind to Light", by Jason Bruges Studio (see Fig. 11 [39]). At the same time they should stick to a simple design, otherwise the design could become "out of fashion" fast.

Fig. 11: "Wind to Light", by Jason Bruges Studio

1.5.2 Individual site design

Instead of installing series products similar to parabolic antennas, a strategy is to design wind turbine sculptures embedded into individual sites. Such a site for Copenhagen could be at the lakes. Because the water is only slowly mixing, it could have advantage of an artificial ventilation system. Vertical axis wind turbines could be arranged as shown in Fig. 12. The idea is that the captured wind energy is directly converted into a fountain or other visible water movement. When a set maximum is reached, lights could start to illuminate the spot.

Individual site design is a method to enter an urban space, but does not lead to a vast mass of urban wind energy.

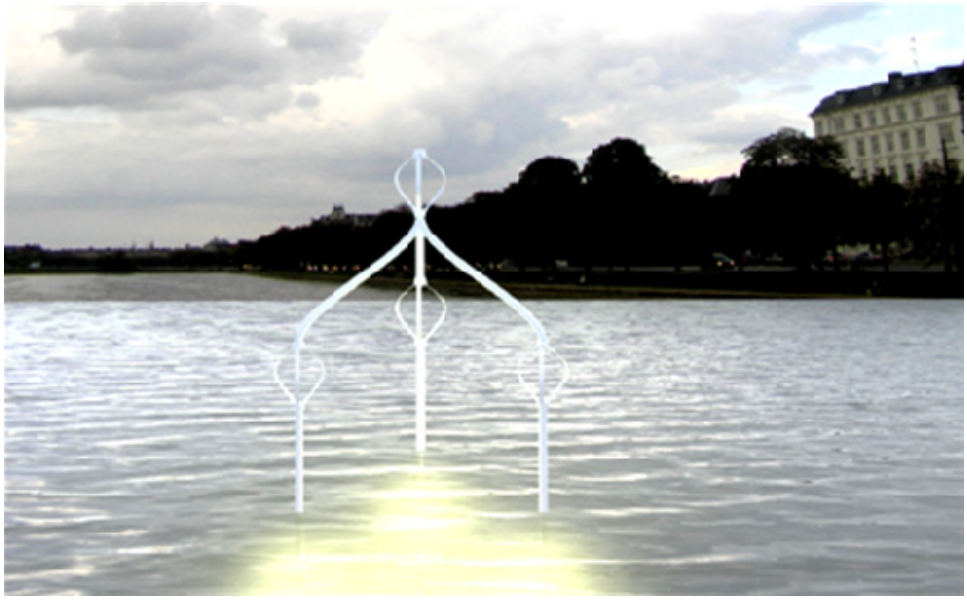

Fig. 12: Offshore turbines in city lakes, e.g. Peblinger Sø, Copenhagen, by C. Beller

Quietrevolution has found a design which looks individual and at the same time is a serial product. Several of their example cases show a well functioning integration into the residential area. Although these are not areas within Copenhagen, three of them are shown in Fig. 13 [[24]] to illustrate an exemplary way of siting at a beach site, left, along a water channel, middle, and mounted on the side of a medium high building, right.

Fig. 13: Individual siting by quietrevolution, on a beach site (left), along a water channel (middle), attached to a building (right)

As it is shown later, the power curve of a wind turbine has to fulfill certain characteristics for a reasonable performance in the urban wind climate. Beforehand, low wind velocities are rather frequent in the residential area and the mean velocity is low. A crucial part for the power curve is therefore a low cut-in wind speed. In the technical specifications given by the manufacturer of the quietrevolution turbine, they announce their cut-in wind speed to be 4.5m/s. Later in this work it is shown that the cut-in wind speed in e.g. Copenhagen should be somewhat lower.

1.5.3 BellAIR- an autarkic energy system

Another design idea to enter the inhabited area is a small autarkic energy system. It is directly coupled to the user in several ways. Instead of installing a wind turbine at

a fixed location, a rotor with a very small diameter is thought of being mounted on the handle bar of a bicycle for example, similar to an external rear-view mirror. Whenever the owner is bicycling, wind is created in the order of the cycling speed and consequently energy can be produced.

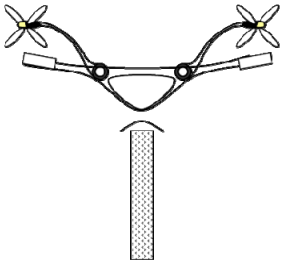

Fig. 14: Small rotors attached to a bicycle handle bar charging personal electrical items, by C. Beller

A common dynamo actually is more efficient and as known from a dynamo, the cyclist has to work more to move forward and deliver momentum to the dynamo at the same time. The same applies for rotors mounted on a bike. Electricity can be produced on the cost of raised drag. Unlike a dynamo though, a rotor can produce energy while the bicycle is parked, given that the wind is blowing. The energy can be stored in a battery and charge private mobile items like MP3 players, telephones, photo cameras. Thus, the bicyclist has a direct connection to his/her energy needs and forms a feeling for what it takes to power a convenience gimmick and for the advantage and freedom of being independent from a grid. In the chapter "Rotor Design", the design process of such a rotor is followed, as described also in [40].

2 URBAN WIND CLIMATE

The city is a lively space. Each city is individually built up, so for each city the wind climate is individual as well. First of all, it plays a role, where a city is located. The European Wind Atlas [41] for example determines the wind climate in a country, based on several wind measurements and topologic descriptions. In Fig. 15 [41] the European Wind Atlas is shown for onshore sites. It indicates the local wind resource at 50m a.g.l. (above ground level) for different types of topographic conditions.

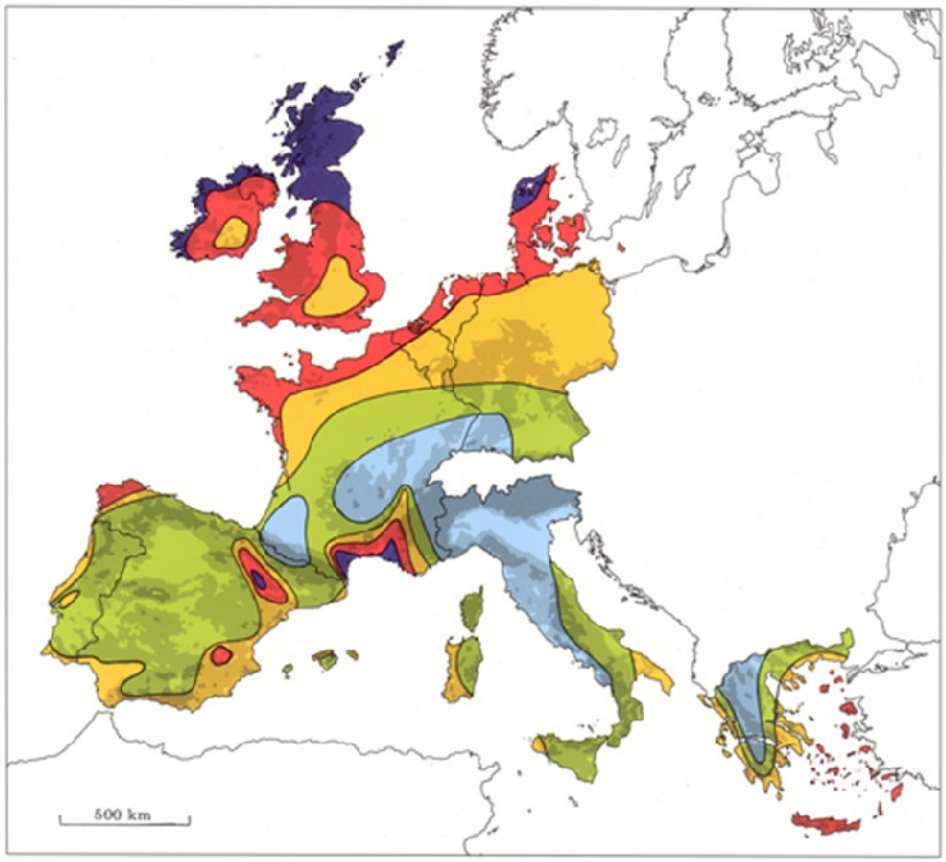

Wind resources[1] at 50 metres above ground level for five different topographic conditions

	Sheltered terrain[2]		Open plain[3]		At a sea coast[4]		Open sea[5]		Hills and ridges[5]	
	$m\,s^{-1}$	Wm^{-2}	$m\,s^{-1}$	Wm^{-2}	$m\,s^{-1}$	Wm^{-2}	$m\,s^{-1}$	Wm^{-2}	$m\,s^{-1}$	Wm^{-2}
	> 6.0	> 250	> 7.5	> 500	> 8.5	> 700	> 9.0	> 800	> 11.5	> 1800
	5.0-6.0	150-250	6.5-7.5	300-500	7.0-8.5	400-700	8.0-9.0	600-800	10.0-11.5	1200-1800
	4.5-5.0	100-150	5.5-6.5	200-300	6.0-7.0	250-400	7.0-8.0	400-600	8.5-10.0	700-1200
	3.5-4.5	50-100	4.5-5.5	100-200	5.0-6.0	150-250	5.5-7.0	200-400	7.0- 8.5	400- 700
	< 3.5	< 50	< 4.5	< 100	< 5.0	< 150	< 5.5	< 200	< 7.0	< 400

Fig. 15: Wind resources for Europe at 50m above ground level

To estimate the wind conditions at a specific onshore site, tools like WAsP- Wind Atlas Analysis and Application Program [42] can be used. So far, these tools are working well for simple landscapes. Forests or hills are considered to be complex terrain. Similar to a forest a city can be described in terms of a canopy, seen by the wind as a single roughness. Sites located close by, not to talk about sites lying within, cannot be described accurately with such macro wind climate tools. Anyway, the location of a city within a macro wind climate has an influence on the micro wind climate of a city. The micro climate is very complex and influenced by many kinds of parameters.

One method to determine the wind conditions at a certain urban location is to take intensive wind measurements on the spot. This method is very accurate, but does not resolve the flow pattern in a city district. Taking measurements at a spot in several heights can help to reconstruct the in-situ wind profile though. Another method, besides wind tunnel measurements, is the computational simulation of the wind field. So far most investigations of the urban micro wind climate were carried out within the research field of dispersion problems, wind loads on buildings and pedestrian wind comfort [43] [44] [45]. But more and more attempts are made to describe complex wind climates analytically. Among them is the work of Badde and Plate [46], forming the base for investigations in the next chapter "Flow Around Obstacles".

Here, a specific spot in the center of Copenhagen serves as an example for a case, where wind measurements are taken 8m above a flat rooftop. Based on the in-situ measurements, description of the surrounding and a relation to measurements taken at the Airport of Copenhagen, an urban wind profile is analytically derived and shown. Detailed analysis of the onsite wind conditions follow and finally the performances of existing wind turbines exposed to the found wind regime are estimated and discussed.

2.1 Site and Measurements

On the rooftop of the H.C. Ørsted Institute building, situated at Nørre Allé close to the very center of Copenhagen, measurement devices are installed. Fig. 16 [47] shows the location within Copenhagen and a three dimensional built-up of the institute.

Fig. 16: H. C. Ørsted Institute's location. Left: Copenhagen's coastal position; middle: Institute's surrounding; right: three dimensional model of the surrounding with measurement location indication (triangle)

Hourly averaged data are published on the internet [48] where e.g. wind direction and wind velocity were collected in a period over three years. However, the data are not

quality controlled. Furthermore, it must be mentioned, that the data of a whole year need to be analyzed, in order to include seasonal variations. The measurements are taken on the Institute building, which lies furthest towards south. Fig. 17, top, shows the building's rooftop. Where the triangle can be seen a mast is located. A sonic anemometer on a boom is attached to the mast at a height of 8m. This figure and more detailed information about the measurements can be found in a report [49].

According to Badde and Plate [46] a site can be described in matters of built-up density, λ_P, buildings mean height, $\overline{H}$, the standard deviation of the building heights, σ_H, the roughness length, z_0, and a few more parameters. For the method used in the next section λ_P and $\overline{H}$ are of interest. The surrounding of the Institute can be described with λ_P=0.15 and $\overline{H}$=15m (see Fig. 17, bottom [47]). The building itself is 20m high.

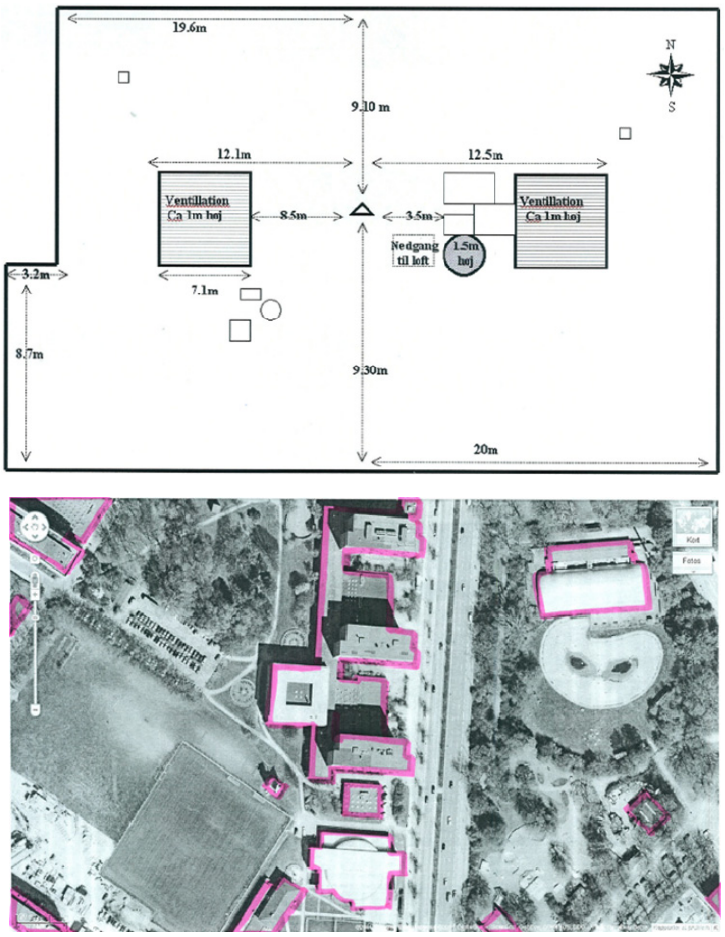

Fig. 17: Top: sketch of H. C. Ørsted Institute rooftop; bottom: surrounding plot with build-up areas indication (hand drawn pink lines)

Former works use Theurer's [50] description of an urban area in form of coefficient λ_P and λ_f with the definition

λ_P = sum of all areas covered by buildings/total urban area, (A_p/A_d),

λ_f = sum of average building areas normal to the wind/total urban area, (A_f/A_d).

In Fig. 18 their definition is pictured.

In order to obtain the roughness length, z_0, and displacement height, d, of a logarithmic wind speed profile present in such set-ups, Theurer declares a relation in the following way,

$z_0(\lambda_f)$, dependent on the wind direction, and

$d(\lambda_P)$, independent of the wind direction.

The shape of the urban wind profile representative for the H.C. Ørsted plot is derived in the next section. It has to be mentioned, that such profiles constitute the wind velocities averaged over the whole area A_d.

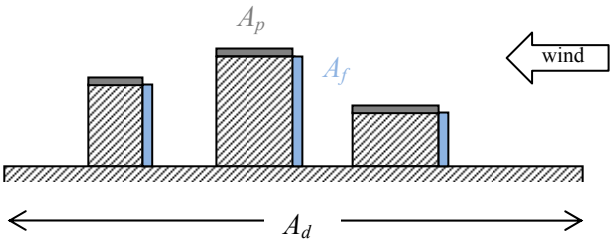

Fig. 18: Sketch to explain urban built-up parameter definitions

2.2 Wind Velocity Profile

Wind velocities onshore are lower than offshore due to a higher surface roughness. With increasing roughness length the turbulence intensity is increasing as well [51]. Going from an open land site into a densely built environment increases the roughness length, decreases the average wind velocity and increases the turbulence intensity remarkably. Referring to the Davenport roughness classification [52], open sea corresponds to roughness *class one* (z_0=0.0002m), open land with only isolated obstacles and low vegetation to roughness *class two* (z_0=0.005m) and cities to roughness class seven or eight, depending on the buildings density and variation in buildings height (z_0=1.0m/z_0≥2.0m). In roughness *class five* and beyond a so-called displacement height has to be considered, which means that the logarithmic wind profile starts at a height somewhere above the ground level. A list of the Davenport roughness classification is attached in Appendix A.

2.2.1 Roughness step (method I)

Bade and Plate categorize different urban sites with the help of various parameter [46]. One of the parameters is the ratio, λ_p, of the building's plan area, A_p, to plot area the buildings sit on, A_d. Dependent on this ratio is according to Theurer et al [50] the so-called wind profile displacement height, d. The displacement height, d, can be determined by taking measurements at a specific site at two heights. Such measurements in the center of Copenhagen do not exist at the moment. However, a few distributed measurements of different quality and set-up are available. Among them is the measurement station 8m above the rooftop of the H. C. Ørsted Institute.

In case of available wind measurements outside a city, an average wind profile can be determined for a city, if certain characteristics of the city are known. If for example wind measurements are taken at an airport in the vicinity of a city, these wind conditions will change, when entering the city, due to the roughness step and the propagation above the obstacle spiked run. Using the H.C. Ørsted Institute onsite data in combination with the wind climate found at the airport Kastrup, DK, located about 10km south to the city center of Copenhagen, an analytical approach is

conducted to reconstruct the urban logarithmic wind speed profile based on neutral conditions. The measurements at the airport are taken at 10m a.g.l..

In general, the logarithmic wind profile is defined as in Eq. 1,

$$u(z) = \frac{u^*}{\kappa} ln\left(\frac{z-d}{z_0}\right) \qquad \text{(Eq. 1)}$$

with u^*as friction velocity, κ=0.4 as Karman constant, z as height were velocity $u(z)$ is found. Mertens [53] uses in his investigations an equation to describe the change of the wind profile after a roughness step. His definition is as shown in Eq. 2.

$$u(z) = u_A \frac{ln\left(\frac{z-d}{z_0}\right)}{ln\left(\frac{\delta-d}{z_0}\right)} \frac{ln\left(\frac{\delta}{z_{0A}}\right)}{ln\left(\frac{z_A}{z_{0A}}\right)} \qquad \text{(Eq. 2)}$$

Here, u_A is the velocity at height z_A in the area before the roughness step and z_{0A} the roughness of this area. It is assumed, that the area before the roughness step does belong to a class below roughness *class five*. δ is the height of the internal boundary layer, which develops after the roughness step. In the paper by Heath et al [54] they refer to Taylor and Lee [55] to determine the internal boundary layer height with Eq. 3,

$$\delta = mz_0 \left(\frac{x}{z_0}\right)^{0.8}, \qquad \text{(Eq. 3)}$$

where x is the fetch downstream of the roughness change and m is a constant which Mertens [5] sets to m=0.28, which is applicable for roughness changes from smooth to rough and vice versa up to a height $z<0.2\delta$. Heath et al [54] base their work on the approach Taylor and Lee choose [55]. They set m=0. 75.

Mertens [5] explains that the boundary of the investigated area A_d should be approximately two kilometers upwind from the point where z_0 is estimated in order to provide an average value for the roughness across which the boundary layer is developed. Furthermore, Mertens refers to the displacement height definition given by ESDU [56] with Eq.4,

$$d = \bar{H} - 4.3z_0(1 - \lambda_P) \qquad \text{for} \quad 0.2 \le \lambda_P \le 0.8, \qquad \text{(Eq. 4)}$$

where $\bar{H}$ is the mean height of the obstacles. According to Mertens [5] typically 42% of the total area of a city is occupied with buildings, λ_P=0.42.

These equations with m=0.75 are used in conjunction with the measurements taken at the H. C. Ørsted Institute (HCØI), the definition of its surrounding and the description of the airport site (see Table 3).

Table 3: Site describing parameters

	$\bar{H}$	λ_P	k	A	$u_{ave}(z_{ref})$	z_{ref}	z_{0A}	x
HCØI	15m	0.15	2.4	4.4m/s	4.0m/s	28m	-	12460m
Airport	-	-	2.3	7.1m/s	6.3m/s	10m	0.01m	-

A and k are the so-called Weibull parameters. Based on onsite measurements and the probability density function, Eq. 5, the parameters A and k can be derived.

$$f(u) = k\frac{u^{k-1}}{A^k} exp\left[-\left(\frac{u}{A}\right)^k\right] \qquad \text{(Eq. 5)}$$

A special case of the Weibull distribution is the Rayleigh distribution, with k=2, which is a typical value for many locations. A higher value of k, such as 2.5 or 3, indicates a site where the variation of hourly mean wind speed about the annual mean is small. A lower value of k indicates greater variability about the mean wind speeds.

Based on the measured data at the Institute, best fit is obtained with k=2.4 and A=4.4m/s (see Fig. 19). This Weibull distribution is representing the wind velocities at the site, not taking into account where the wind comes from. In comparison, at the Kastrup Airport, DK, the Weibull parameters at 10m height are k=2.32 and A=7.1m/s. The site of the airport is characterized in the European Wind Atlas [41] with z_{0A}=0.01m, z_A=10m and an average wind velocity of u_A=6.3m/s.

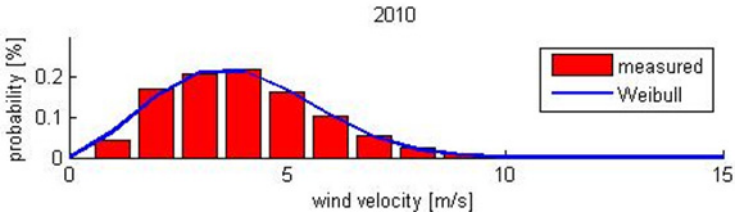

Fig. 19: Measured and fitted Weibull distribution for H. C. Ørsted Institute

With the information of the mean velocity at a known height at a roughness length determined site close to the city, the knowledge about the distance between the outer site and urban site, description of the urban site in manners of mean building height, plane city occupation and a punctual mean velocity at a known height within this district, the roughness length and the wind profile displacement height for this district can be obtained and with that the logarithmic profile.

Results with such an approach are subjected to some assumptions and limitations. To start with, the downstream fetch shall not exceed the range of 500m≤x≤5000m as Mertens says referring to Simiu and Scanlan [57]. Furthermore he says, the urban district's boundaries shall lie about two kilometers upwind the point of roughness length determination, since the resulting logarithmic wind profile is representing an average wind profile. With that we also shall be aware of, that the wind profile obtained with this method does not represent the wind profile directly above a building for example. It is more a representation of wind profile, the building of interest was exposed to. Surely, using a punctual measurement taken on top of a building as input to derive an average profile seems to be contradictory, but at that moment they were the only input available. Another limitation inherited by the use of Eq. 4 is, that it only is valid for $0.2 \leq \lambda_p \leq 0.8$.

Considering the airport site as area before the roughness step and assuming that the roughness length from the change up to the H.C. Ørsted area is the same, a displacement height of d=10m and a roughness length of z_0=1.4m is found in an iterative process using Eq. 2, Eq. 3 and Eq. 4. Usually, the fetch is too large and the built-up density too low in order to give accurate results with the employed equations. But due to the lack of more and sufficient data, this method is applied anyway. Later on, the same method is applied to further urban set-ups.

Although some of the parameters are out of the applicable range, the values found here are in an acceptable range. The building mean height is said to be 15m, whereas the building itself is 20m high. That results in the ratio $d/\overline{H}$=0.62, which seems to be reasonable. Also, the found roughness length is in an order, which is rather typical for such district category (see Appendix B).

2.2.2 Geostrophic drag law (method II)

Since the reference measurement in the roughness step method is given at the rooftop, the urban wind profile is forced to go through this point. Especially above a rooftop however the local wind profile varies significantly from the average profile, due to the influence of the building. Another method to derive a wind profile by referring to another known wind climate close by is the method of the geostrophic drag law. It needs the input of z_0 and d at the area of interest though. Here the geostrophic drag law is used to see the difference between the two methods. First, the geostrophic wind speed, G_A, is calculated based on the known wind climate and topography. It is defined as in Eq. 6,

$$G_A = \frac{u_A^*}{\kappa}\sqrt{\left[ln\left(\frac{u_A^*}{f_A z_{oA}}\right) - aa\right]^2 + bb^2}\ , \qquad \text{(Eq. 6)}$$

with aa=1.8 and bb=4.5 as site-independent constants. f_A is the Coriolis parameter, depending on the position on the globe. It is defined as in Eq. 7,

$$f_A = 2\Omega sin\phi_A \qquad \text{(Eq. 7)}$$

where Ω is the angular speed of the earth, Ω=7.29*10^{-5}s^{-1}, and ϕ_A is the local latitude and for Copenhagen 55°40'N. Since the two sites, Institute and airport, are close to each other f_A=f is valid. The geostophic drag law says, that G_A=G. Using z_0 found with the help of the first method, in an iterative process u^* for the urban district is found to be 0.52m/s. With that and the displacement height derived with method I, another urban profile can be drawn. In Fig. 20 the logarithmic profile at the airport and the logarithmic profile in the urban district found with method I and method II are plotted.

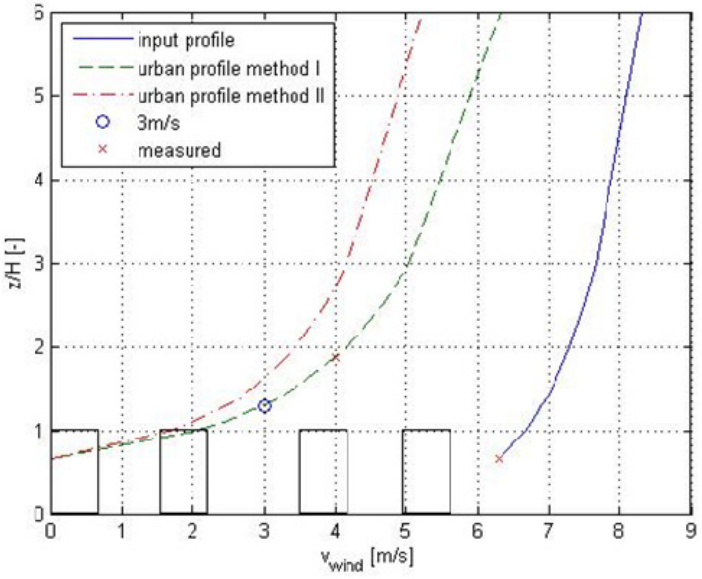

Fig. 20: Wind speed profiles derived with method I and II

In Fig. 21 profiles derived with method II are shown. It shall clarify the difference between open land and inner city and depict that the macro wind potential in urban

areas is significantly lower than in areas, where wind turbines usually are installed. That means that the design of a wind turbine system has to be adapted to this condition.

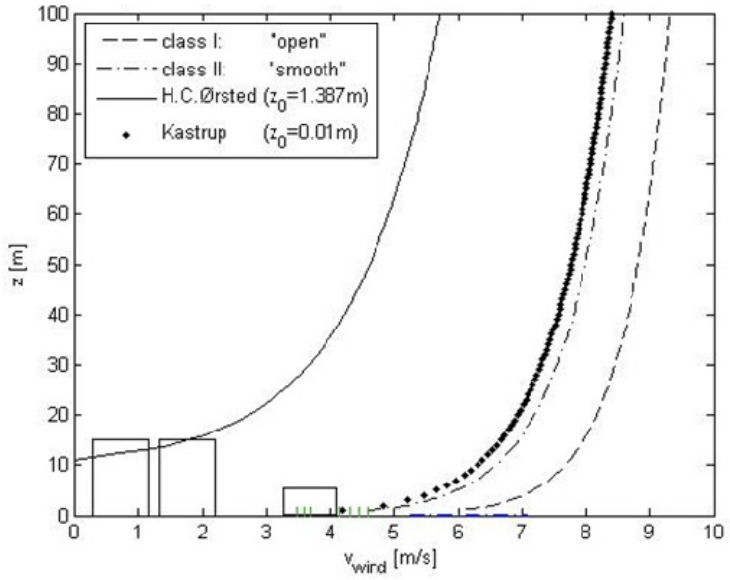

Fig. 21: Wind speed profiles for different roughness classes

It has to be mentioned, that the urban profile is representing the averaged mean wind velocity and describes only, what lies above the displacement height. That means, going to a specific site within the district would show a site-dependent variance above the displacement height and what lies below is only zero for the case of a building. These profiles are useful for the macro climate and are appropriate as inflow condition for CFD simulations. In "Installation Cases & Siting" they help to obtain a scaling factor for micro climate flow fields.

2.3 Seasonality and Directionality

After clarifying the average wind profile in the surrounding of the measurement position, in this section a closer look on the in-situ wind conditions is taken. Similar to the conditions outside a city the variability of the average wind speed during a day is observed. In night times wind speeds use to decrease and with increasing temperature in the course of a day, wind speeds are increasing as well, driven by pressure differences and thermal convection. That was not necessarily expected, since the thermal household of a city is influenced by the cooling and heating of buildings, streets and a like, not present on a rural site to such an extent. In Fig. 22 the monthly averaged wind velocities over a day are plotted for the year 2008, 2009 and 2010. Most complemented is the dataset collected in 2010. Therefore it is used for further analysis. Besides that, even though the data from the prior years are not consistent, the Weibull distributions are surprisingly alike to 2010, indicating a rather stable and predictable wind climate.

Averaging over the whole year 2010, a clear curve is found for the daytime dependent characteristic (see Fig. 23, top). This can be helpful to decide on a complementing technology or strategy to use wind energy. Solar energy follows a connatural curve for example, whereas energy consumption in a private household might peak in the morning and the evening hours. In office working spaces the energy load might be peaking in the afternoon, depending on heating or cooling the space and so on. Talking about complementing technologies like solar energy, the

variability over a year is more relevant. In Fig. 23, bottom, the average velocity per month is plotted over a year. Again, the tendencies inside the city coincide with rural sites. In autumn it is windier than during the summer, but data from more years would be necessary to draw a smooth trend line. So, solar energy is mostly available in the warm periods and wind energy mostly in the cold periods, but both at the same daytime.

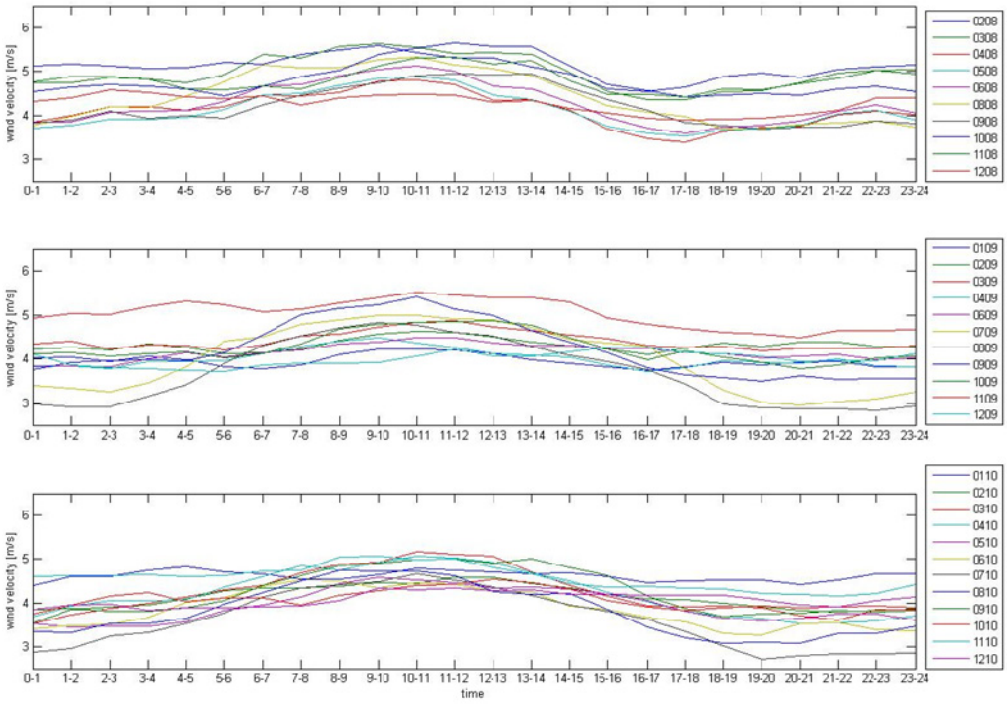

Fig. 22: Curves representing monthly averaged wind velocities in the course of a day at H. C. Ørsted Institute (2008-2010); top-bottom

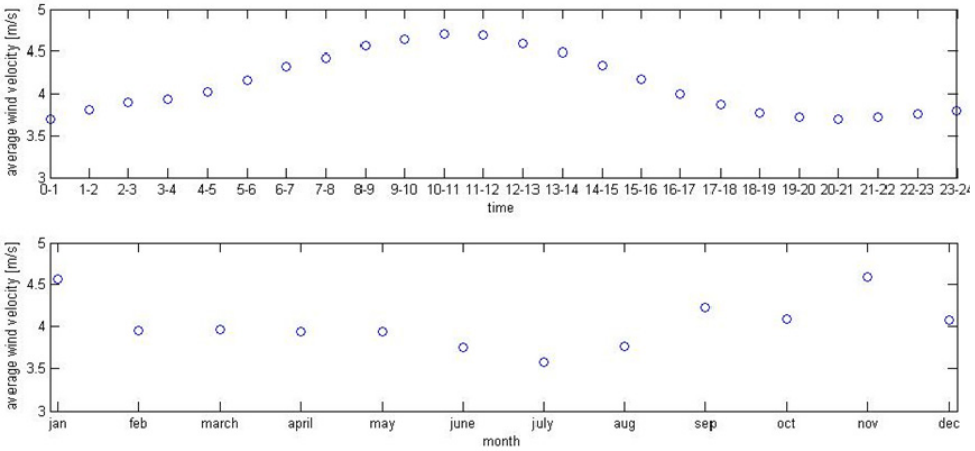

Fig. 23: H. C. Ørsted Institute. Top: daily wind speed course averaged for 2010. Bottom: Monthly Average wind speeds in the course of the year 2010.

For some wind conversion applications the wind direction is of importance. As introduced in the first chapter, wind turbines can be integrated into the buildings structure. To make such implementation yielding, a prevailing wind direction has to be present or at least the inlet should be orientated towards the direction promising

the highest energy content. An investigation for a ducted wind turbine exposed to this site is carried out in another work [22]. In Fig. 24 the frequencies of wind direction incidences for 2010 are plotted in a rose and to the right a satellite pictures shows the measurement site [47] with a triangle marking the measurement spot.

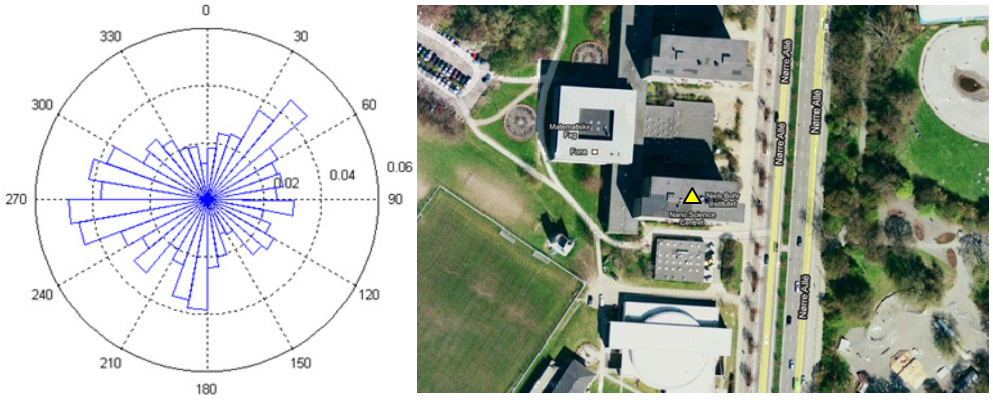

Fig. 24: Wind direction incidence rose in the year 2010 (left) present at the rooftop of the H. C. Ørsted Institute (right)

Examining the directionality in conjunction with the building's positioning, agitates the guess, the free fields to the west and east or the neighboring buildings to the north and south respectively having an impact on the wind accessibility to the rooftop. Another considerable factor for wind conversion systems fixed in yaw is the seasonal directionality. Possibly an integrated solution would only perform in certain periods of the year. Actually, the roses in Fig. 25 reveal prevailing wind from north-east in the winter months, western winds for spring and during summer wind mainly from south and west. Some installations on the rooftop are present (see) and e.g. season depending ventilation can be influencing the local directionality as well.

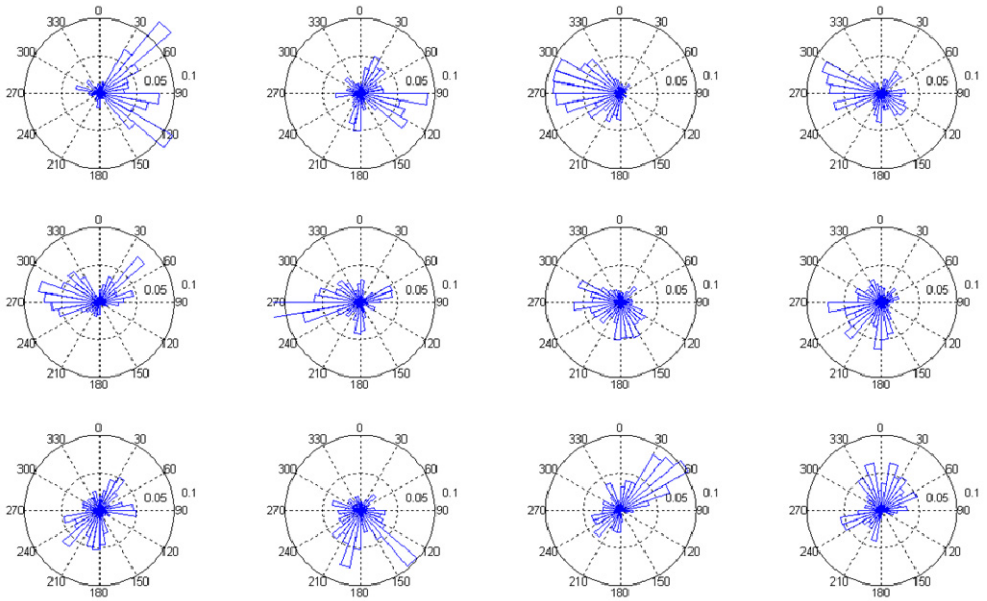

Fig. 25: Monthly wind direction incidence roses at H. C. Ørsted. Left to right and top to bottom: January to December 2010

Surely, the directionality does not say anything about the energy contained in the wind. If for example the wind speeds are frequent but very low from one direction, a

dedicated orientation towards it would not be recommendable. In the following, the local energy content is calculated and the performance of three small-scale wind turbines exposed to the measured data estimated.

2.4 Energy Production Estimation

There are numerous small wind turbines on the market. Some are installed in an urban context and are also said to be designed for these conditions. In this section, the power curves from three commercially available wind turbines are used to estimate their annual energy production (AEP) in the wind conditions present in 2010 at the H.C. Ørsted Institute rooftop. Thereby, the hourly averaged wind speeds, u, are taken into account when calculating the power, P, as in Eq. 8,

$$P = \tfrac{1}{2}\rho u^3 A_{rotor} C_P(u) \ . \qquad \text{(Eq. 8)}$$

C_P is the power coefficient, derived from the power curves published by the manufacturer, ρ is the density of air with ρ=1.225kg/m^3 at normal conditions (15°C and 1013hPa) and A_{rotor} is the swept area of the rotor. The swept area for a wind turbine is the projected rotor area seen by the wind. For a horizontal axis wind turbine (HAWT) the area has the shape of a circle, and for a vertical axis wind turbine (VAWT), where more degrees of freedom exist compared to a HAWT, the shape depends on the shape of the rotor. The power coefficient for a wind turbine differs depending on the design of each blade section (the profiles), the blade design, the regulation concept, size and tip speed ratio, which is the ratio between the tip speed and the wind speed. C_P=0.35 states the approximate maximum for a small, free-standing, lift-driven VAWT. In comparison to that, large HAWTs reach values of around C_P=0.48.

Among the example rotors are two vertical axis wind turbines with twisted blades forming a rectangular swept area and a horizontal axis wind turbine, all shown in Fig. 26 [58] [59]. They are introduced briefly in the following.

Fig. 26: Left: Turby; middle: full scale model of T. Urban (photo by C. Beller); right: VENCO

2.4.1 T. Urban

T. Urban is a small wind turbine, especially designed for the urban environment. The project T. Urban is coordinated by INETI (Instituto Nacional de Engenharia, Tecnologia e Inovacão), Portugal, and co-sponsored by ADI, the Portuguese Innovation Agency under program DEMTEC. At the European Wind Energy Conference (EWEC) 2008 the model was presented. Until this date one turbine was installed. It was located in Lisbon, while the site was not optimum for its operation. It should have been commercially available in 2009, they claimed. Its technical key figures are listed in Table 4.

Table 4: T. Urban; technical information

Model:	**T. Urban**	Rotor Type:	HAWT, upwind
Rated power [kW]:	2.5	No. of Blades:	3
Cut In [m/s]:	3.5	Blade Material:	n/a
Cut Out [m/s]:	25	Rotor Diameter [m]:	2.3
Survival [m/s]:	n/a	Generator Type:	Synchronous
Rated [m/s]:	13.5		permanent magnet

2.4.2 Turby

Different from the Darrieus shape, the designer of the VAWT Turby fixed the blade distance to the shaft. In this way experiences the whole blade the same wind and tip speed. To reduce the inevitable vibrations due to the change of the angle of attack between +20° and -20° resulting in a change of the mechanical stress in the blades two times per revolution, Turby's developers chose an odd number of blades of a helical shape, making all changes pass off gradually. On the homepage some examples of installations in urban environment can be found. Some key numbers are summarized in Table 5.

Table 5: Turby; technical information

Model:	**Turby**	Blade Material:	composite
Rated power [kW]:	2.5	Rotor Diameter [m]:	2.0 (and 2.65m high)
Cut In [m/s]:	4.0	Generator Type:	synchronous
Cut Out [m/s]:	14		permanent magnet
Survival [m/s]:	55	Rated rpm:	120-400
Rated [m/s]:	14	Head Weight [kg]:	136.0
Rotor Type:	VAWT	Brakes:	electrical, short circuiting
No. of Blades:	3	Noise [4m/s-10m/s]:	n/a

2.4.3 VENCO

Similar to the Turby layout the VENCO rotor is a VAWT design with three twisted blades. On their homepage they describe their product as designed to start rotating at 1.5 m/s wind speed and to begin to produce power at a wind speed of 3.5 m/s. Due to the special design, they say, the VENCO-Twister-1000-T is operating virtually quiet. The robust construction is without wearing parts. Furthermore they claim, it is maintenance free and works reliable even under extreme conditions. See Table 6 for VENCOs key figures.

Table 6: VENCO; technical information

Model:	**VENCO**	Blade Material:	epoxi glass resin
Rated power [kW]:	1.2	Rotor Diameter [m]:	1.9 (and 1.9m high)
Cut In [m/s]:	3.5	Generator Type:	permanent magnet
Cut Out [m/s]:	20		shrunk-on-disk rotor
Survival [m/s]:	50	Tip speed ratio:	2.3
Rated [m/s]:	14	Head Weight [kg]:	150kg incl. mini pole
Rotor Type:	VAWT	Brakes:	eddy current brake and short circuit
No. of Blades:	3	Noise [4m/s-10m/s]:	n/a

Especially this turbine model is looked at carefully later on. It is installed and monitored at various places around Copenhagen, among others at the test field at Risø DTU, Roskilde, Denmark.

2.4.4 Annual energy production (AEP)

The power curves, as they are found on the manufacturer data sheets are applied to the wind climate at the H. C. Ørsted Institute. An international standard for small wind turbines is about to be approved, to make sure that power curves and other technical facts are published in a common manner. Until now, it is uncertain what the power curves actually depicted. It could be that they are based on theoretical calculations, wind tunnel measurements, where the power refers to the mechanical power on the shaft or the power is the value measured at the point where the electricity is fed into the grid. Without knowing this rather fundamental information, the results have to be relished with caution. However, in the end the characteristics of the power curves as they are, lead to conclusions helping the understanding for a well designed rotor for such climate. The results are listed in Table 7.

Table 7: Estimated annual rotor performances for three turbines exposed to the H. C. Ørsted Institute wind climate

turbine	**rotor type**	P_{rated}	A_{rotor}	**AEP/m²**	**load factor**	**AWP/m²**	C_E
		[kW]	[m²]	[kWh/m²]	[-]	[kWh/m²]	[-]
T.Urban	HAWT	2.5	4.2	**219.4**	0.042	571.86	**0.38**
TURBY	VAWT	2.5	5.3	133.9	0.032		0.23
VENCO	VAWT	1.2	3.6	194.2	**0.067**		0.34

That means the HAWT rotor with an AEP of 220kWh/m² performs best out of the three designs in terms of energy production per swept area. The so-called load factor which is defined as in Eq. 9,

$$load\ factor = \frac{AEP}{24h*365d*P_{rated}} \quad , \qquad \text{(Eq. 9)}$$

is a measure of the generators capacity utilization. For large offshore wind turbines a value of 0.3 to 0.4 is common. In a field trial in UK [17], they found load factors for most of the small wind turbines mounted on buildings to be about 0.03. One single wind turbine, rated at 1.5kW reached a load factor of 0.074, which was a maximum. Besides the load factor another coefficient is defined here, C_E. It sets the AEP into relation with the local annual wind energy potential (AWP) and with that characterizes how efficient the rotor is performing in the given climate, see Eq. 10.

$$C_E = \frac{AEP}{AWP} \qquad \text{(Eq. 10)}$$

In terms of load factor VENCOs generator is dimensioned best. With regard to the coefficient C_E T. Urban is capable to convert the greatest fraction of the energy contained in the present wind. In Fig. 27 the applied power curves and their corresponding C_P values vs wind speed are plotted.

Comparing the annual energy production per square meter, showed that the VENCO turbine performs distinctively better than the TURBY turbine for the given wind climate. Crucial for the given wind conditions is a rotor well designed for low wind velocities (see dashed ellipse in Fig. 27), rather than for a broad bandwidth of wind velocities up to 14m/s. The AEP of the T. Urban rotor is the highest, but inspecting the C_P curve shows that values of 0.5 are reached, which seems to be unrealistic for turbines of this size. The theoretical optimum is C_P=0.59. Considering Gipe's factor of 5/9 for small wind turbines [60] a maximum of C_P=0.33 could be expected.

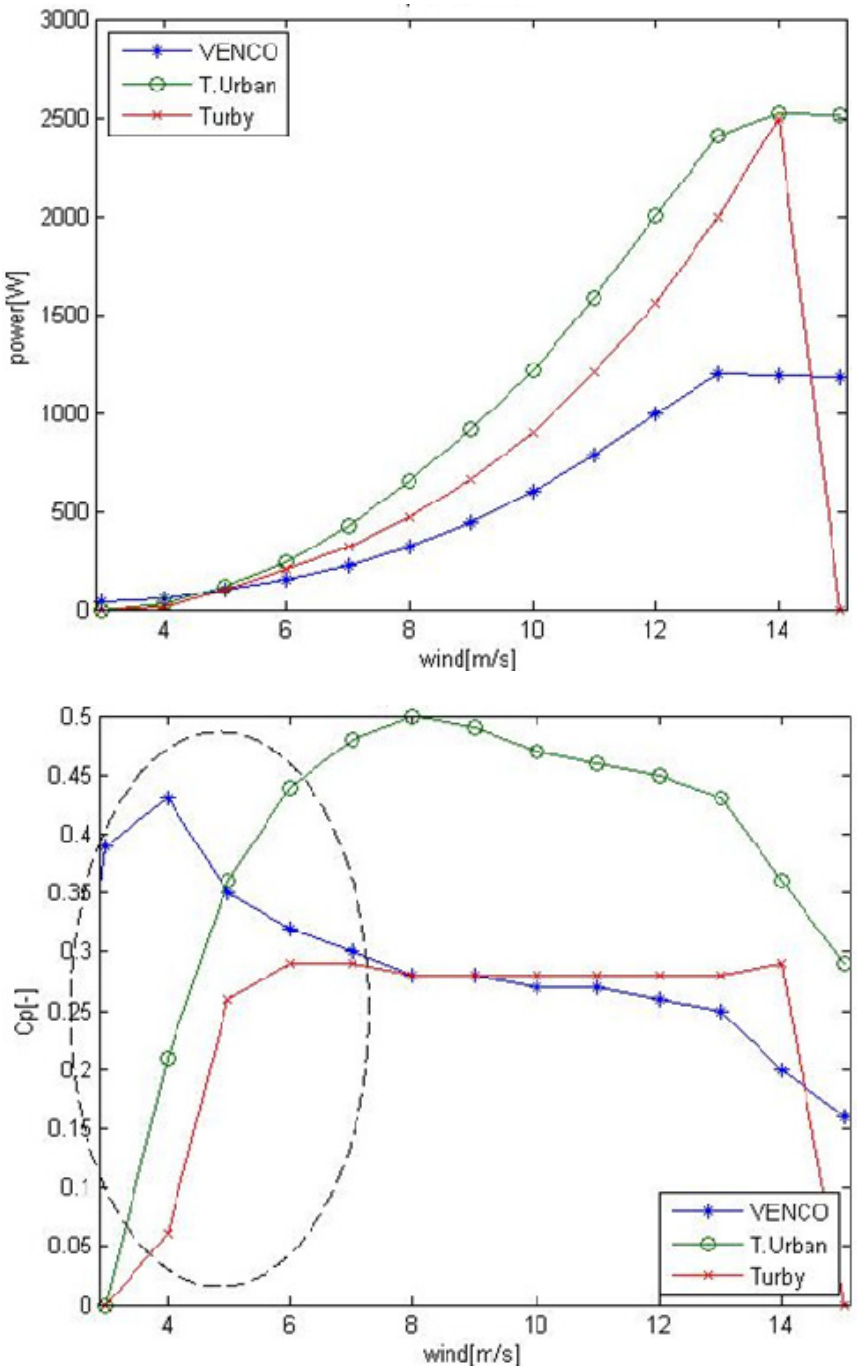

Fig. 27: Top: Power curves drawn on base of the power curves published by the manufacturers. Bottom: C_P vs wind speeds corresponding to the power curves. The dashed ellipse stresses the part of the C_P curves most important for a successful performance in the urban wind climate

2.5 Summary and Conclusion

The content of this chapter is summarized below and the concluded findings, as well as facts, known on beforehand and found to be important, are imbedded as bullets into the continuous text.

Extensive wind measurements in cities to determine the macro wind climate in urban districts are generally rare.

- With the roughness step method (method I as described in the chapter) a way is found to ascertain a roughness length and a displacement height for a representative average logarithmic wind speed profile.

To apply the method it needs wind measurements at a known height outside, but close to the city, the roughness length of this area and from there the distance between the city boundary and the inner city district of interest. Inside the city the built-up density and buildings mean height of the district and wind measurements at a known height within this district are necessary to know. With this method a roughness length of z_0=1.4m and a displacement height to buildings mean height ratio of $d/\bar{H}$=0.67 are found for the H. C. Ørsted Institute example site. Thereby the resulting logarithmic wind profile is forced to contain the inner city measurement.

- The used inner city measurements are taken at a rooftop and with that at a spot where local wind profiles vary significantly from the district's averaged wind profile due to the influence of the building.

This fact motivates the application of the geostrophic drag law method (method II as described in the chapter) using z_0 and d as input, obtained with method I, resulting in a friction velocity for the district. With that the profile is not forced to be fitted to the point of measurement any longer.

- It is indicated that the geostrophic drag law method (method II) delivers a more general wind profile.

No validation of methods is carried out, though. They are found and developed according to the available information and the results seem to be in a reasonable range.

- Profiles found with method II are representative for macro climates and are appropriate as inflow condition for CFD simulations and are useful for a scaling method for micro climate flow fields.

Averaged wind profile for inner cities are significantly different from averaged wind profiles for offshore sites or open and smooth land sites. Wind profiles representative for sites outside a city are characterized with a low roughness length and no displacement height. Common wind turbines are designed for these conditions.

- The design of wind turbines for the use in the urban environment has to be adapted to the urban wind climate.

Based on the measurements at the H. C. Ørsted Institute in Copenhagen, some conditions outside and inside the city are observed to be akin to each other.

- Variability of the average wind speed during a day in the city is similar to outer city sites.
- Weibull distributions found for the example site over three years are surprisingly alike to each other, indicating a rather stable and predictable urban wind climate.

The average wind speed variability over a day and over a year can be helpful in terms of planning parallel technologies as solar energy.

- Based on the measurements from Copenhagen, it appears that solar energy is mostly available in the warm periods and wind energy mostly in the cold periods, but both at the same daytime.

If a wind conversion system is planned to be oriented towards a prevailing wind direction care has to be taken.

- From the measurements in Copenhagen directionality is observed to be seasonal.

An evaluation of the performance of three small-scale wind turbines virtually exposed to all wind directions found at an example site is conducted. The power curves for small wind turbines are not subjected to standards yet.

- Power curves for small wind turbines can be based on theoretical calculations or wind tunnel measurements. Furthermore, the power can refer to either the mechanical power on the shaft or the electrical power thus including generator and transformer losses.

The results of the turbine performances are expressed in manners of load factor and a new defined parameter, setting the annual energy production into relation with the onsite wind energy potential.

- In a wind climate where low wind velocities are dominant and velocities of 10m/s are barely seen, a rotor shall be well designed for low wind velocities, rather than for a broad bandwidth of wind velocities above 10m/s.

3 FLOW AROUND OBSTACLES

After studying the more general wind conditions in the residential area in chapter "Urban Wind Climate" by means of average wind speed profiles in different roughness classes and a more detailed look at a certain spot within the local flow field, in this chapter the flow field around obstacles is investigated. The macro wind climate renders the wind energy potential of a district in general and is dominated by its surroundings. In urban areas, the logarithmic profile is displaced and the city is seen as a canopy, with the wind skimming slightly beyond the skyline, depending on the built-up density (see Fig. 28 [61]) and variation of building heights. For domains with huge gaps in between, the buildings are experienced as remarkable roughness objects, resulting in high roughness length and low displacement height. The closer the buildings are arranged to each other, the higher the logarithmic wind profile is displaced and seeing only the tips of the buildings as roughness objects, so a low roughness length but great displacement height characterizes districts as in Fig. 28 (c).

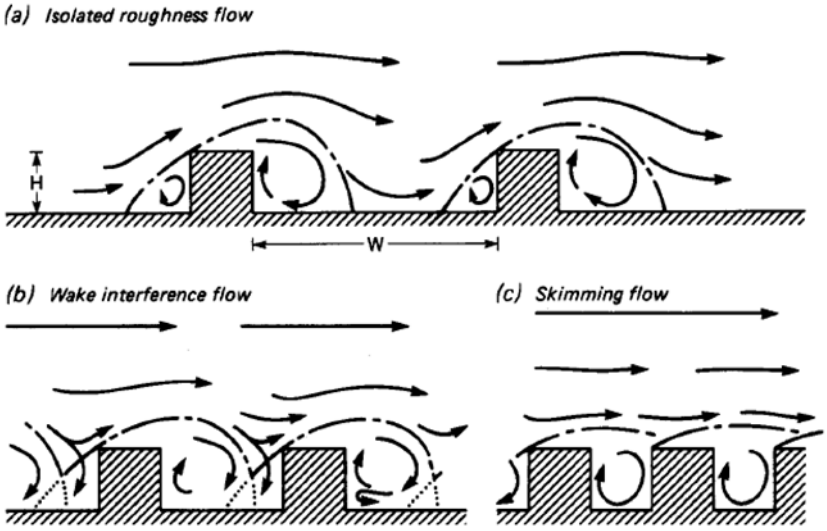

Fig. 28: Flow regimes associated with flow over building arrays of increasing H/W

What happens in the urban canopy layer (UCL) and slightly above when picking an individual site in a district, is looked into with the help of computational fluid dynamics (CFD). For this purpose the CFD tool EllipSys [62] [63] [64], developed at Risø DTU and DTU, MEK, Denmark, is used in conjunction with a Reynolds Averaged Navier-Stokes (RANS) solver.

This chapter starts with a case to validate the settings of the code and the design of the computational domain, whereupon a basic law for bluff bodies is proven true. With the validated CFD set-up, several typical building configurations, orientated on Badde and Plate's work [46] are emulated in a simplified manner. Simulations are carried out with wind approaching the building arrays from four directions (0°, 90°, 180° and 270°). On the basis of one of the configurations general flow phenomena are visualized and discussed. The chosen configuration represents a city center area including parks, high rise buildings and public facilities, similar to the H. C. Ørsted Institute (see Fig. 24). Among others, the flow field around flat roof edges is shortly discussed, since several innovation ideas are motivated by the upwind effect, with the prospect of accelerated wind on the ridge.

3.1 PlayBox

A simulation tool called PlayBox was developed and presented also in [40]. The idea is to be able to rebuild typical building configurations within a CFD simulation environment. In a domain, consisting of 8x14x4 cubes of the same size, single cubes can be set to solid and thus simulate a building. In this way the tool is flexible, but at the cost of a detailed representation of the buildings. A roughness length of z_0=0.2m applied to the buildings surface accounts for the neglect of balconies, blinds, oriels or roof rails etc. The physical dimensions of a single cube are 12.5m x 12.5m x 12.5m. With that a district can be rebuilt with building heights of 12.5m, 25m, 37.5m and 50m.

3.1.1 Computational domain

Three dimensional CFD is based on finite-volume discretization. That means that the continuous fluid medium, here it is air, is subdivided into small cells, forming a grid. The applied computational code is then solving the governing equations at the center of every single cell. In areas with large gradients of e.g. velocity, a finer resolution is needed than in areas where the flow is undisturbed and homogeneous. But since computational time increases with increasing numbers of cells, a satisfying trade-off between accuracy and computational time has to be found. The domain of the tool designed here consists of 1024 blocks. Each of the blocks contains 24^3cells, which makes approximately $15x10^6$ cells in total. In Fig. 29 a) the round ground plate of the whole domain is shown, where the lines are showing the arrangement of the blocks. The circular shape is chosen to use the same domain for different inflow angles.

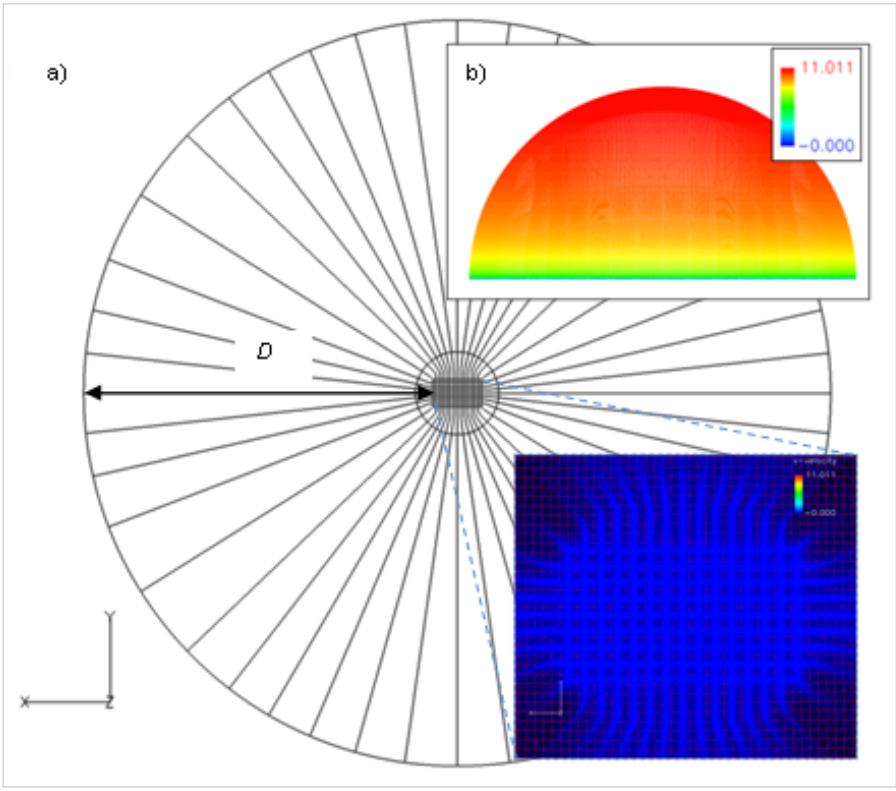

Fig. 29: Hemispherical computational domain a) top-view with block outlines and detail-view of the center-located block arrangement and in b) side-view with colored legend, indicating the applied logarithmical velocity distribution on domain surface.

In the center, an area is located consisting of 8x14x4 equally sized cubes, which can be set to solid obstacles, representing buildings. The distance between inlet and this

area, D, is around 25 times the height of the tallest building possible to be built. In this way the wake provoked by the obstacles is expected to be fully developed within the domain. In order to reduce the block number and to keep cells as less skewed as possible, the domain is built up as a hemisphere. Fig. 29 b) shows the side-view of the domain, where no cubes are set to solid and an inflow boundary condition of a logarithmic inflow profile in y-direction is applied. The colors show the velocity distribution. The height of the first cell above any possible solid object is set to 0.16m in order to capture a roughness length of 0.20m and higher.

3.1.2 Simulation settings

A RANS solver in combination with a k-ε turbulence model is applied. The code is set-up as in [65], where a SIMPLE algorithm of [66] is used to enforce the pressure/velocity coupling and the convective terms are discretized using a third order QUICK upwind scheme, implemented using the deferred correction approach first suggested by Khosla and Rubin [67].

Parameters are set as:

Launder-Sharma coefficients: C_μ=0.09; C_1=1.44; C_2=1.92; C_3=0

Medium density: ρ=1.225kg/m^3

Kinematic viscosity: ν=1.5x10^{-5}m/s^2

Inflow friction velocity in x, y and z direction: u^*=0.0m/s; v^*=0.5m/s, w^*=0.0m/s

Roughness length: z_0=0.2m

The boundaries of the computational domain are defined as:

WALL: No-slip condition
-on the ground plate and the block surfaces, if they are set to solid

INLET: Atmospheric boundary layer conditions
-on hemisphere surface depending on inflow direction

OUTLET: Fully developed flow assumption
-on hemisphere surface, changing according to inflow direction

The shape of the inflow profile defined at the inflow boundary is set to logarithmical and forms a wind profile as described in Eq.1. No displacement height is applied.

3.1.3 Validation

To verify the CFD settings within the flow solver, eight cubes are set to solid, forming one single cube in the middle of the domain. With that the cube height is h_C=25m. The results from the simulation are compared with results found for a cube mounted on a plate in a wind tunnel experiment [68].

Three different simulation cases are conducted, where the roughness length is varied with z_0=0.2m, 0.5m, 0.825m. The wind tunnel experiment settings are z_0/h_C=0.02, which corresponds to a roughness length of z_0=0.5m for the CFD set-up. Fig. 30, top, shows plots of the velocity profiles found on top of the cube center, half cube height behind the cube and one and a half cube height behind the cube. For comparison reasons the velocities are normalized with a reference velocity, u_r, defined as free-stream velocity at z=10h_C.

In Fig. 30, bottom, the pressure coefficient, C_p, found along the cube sides is plotted. The pressure coefficient is defined as in Eq. 11,

$$C_p = \frac{(p_s - p_\delta)}{\frac{1}{2}\rho u_h^2}, \qquad \text{(Eq. 11)}$$

where p_s is the surface static pressure, p_δ is the static pressure in the free stream at a height of z=10h_C and u_h is the velocity in the undisturbed flow at cube height, h_c. The validation of the tool shows good agreement.

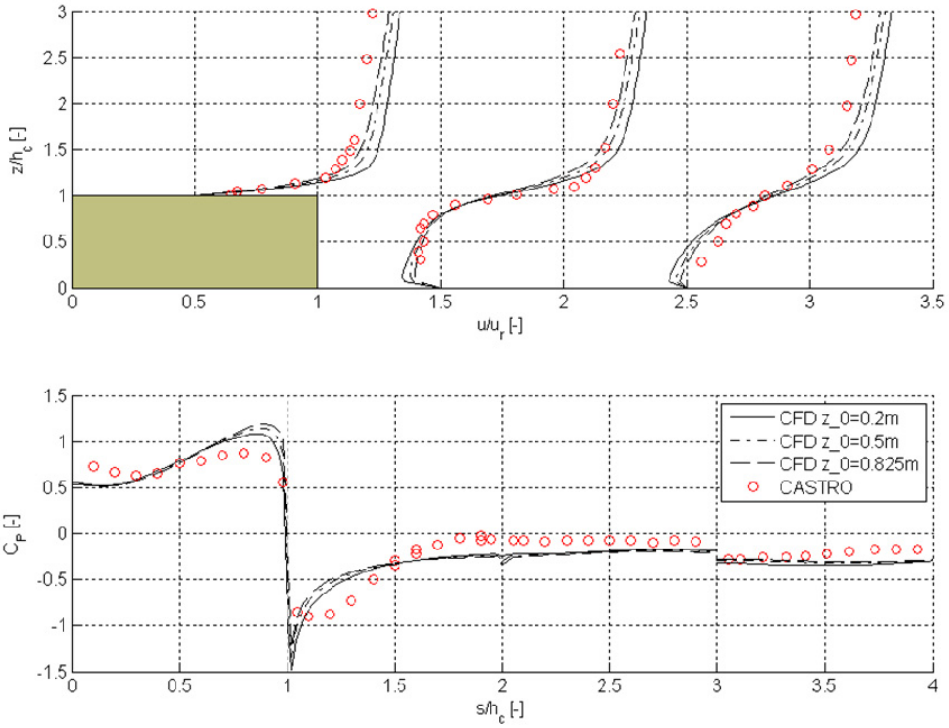

Fig. 30: Comparison of results from experiment conducted by Castro and Robins with results from CFD simulations (z_0=0.200m; 0.500m; 0.825m). Top: velocity profiles plotted on top of the cube center, $h_c/2$ behind the cube and at $3h_c/2$ behind the cube. Bottom: C_p found along cube sides, starting with the front side $C_p(x=0; y=-h_c/2; z=0$ to $h_c)=C_p(s/h_c=0$ to 1), continuing over the roof $C_p(x=0; y=-h_c/2$ to $h_c/2; z=h_c)=C_p(s/h_c=1$ to 2), moving downwards on the rear side $C_p(x=0; y=h_c/2; z=h_c$ to $0)=C_p(s/h_c=2$ to 3) and finally upwards along a side wall $C_p(x=h_c/2; y=0; z=0$ to $h_c)=C_p(s/h_c=3$ to 4).

Earlier simulations in a test domain show a Reynolds number independency (see Appendix C), which arises from the aerodynamic behavior of bluff bodies as soon as a critical Reynolds number is exceeded. Castro and Robins state for their set-up a Reynolds number independency for Reynolds numbers beyond *Re*=4'000 [68]. The Reynolds number in this case is based on the free-stream velocity at cube height and the cube height as characteristic length. Such independency means on one hand that for a certain building set-up, areas of high and low wind velocities respectively will be at the same location independent of the incoming wind velocity. On the other hand it means that the cube size is scalable, as long as the roughness length is scaled correspondingly to the Jensen number, *Je*, which has to be kept constant. It is defined as in Eq. 12,

$$Je = \frac{h_c}{z_0}, \qquad \text{(Eq. 12)}$$

with h_c as height of the bluff body geometry, here the cube height. The Jensen number is only applicable in fully turbulent flow though.

3.1.4 Show cases

Typical building configurations as commercial and industrial areas, city center areas including parks, high-rise buildings and public facilities were parameterized in the work by Badde and Plate in 1994 [46]. They define 10 different configurations in terms of mean building height, $\overline{H}$, relative standard deviation of the building heights, σ_H, mean length to mean width ratio $\overline{L}/\overline{B}$, mean length to mean height ratio $\overline{L}/\overline{H}$ and two more coefficients; λ_p=sum of all areas covered by building/total urban area; λ_f=sum of average building areas normal to the wind/total urban area. Four configurations are rebuilt following these parameters and are shown in Fig. 31. In the following they are referred to as *CASE1* (Fig. 31 a)), representing areas with one-family buildings one to two stories high, *CASE2* (Fig. 31 b)), demonstrating residential blocks regularly aligned three to five stories high, *CASE3* (Fig. 31 c)), forming city center areas including parks, high-rise buildings and public facilities and *CASE4* (Fig. 31 d)), describing commercial and industrial areas two to five stories high. In Appendix B, the table of building arrangements as defined by Badde and Plate can be seen. The roughness lengths announced in the figure legend are values for the influence of the buildings themselves. That means that they could be removed and be replaced by a roughness length of that value.

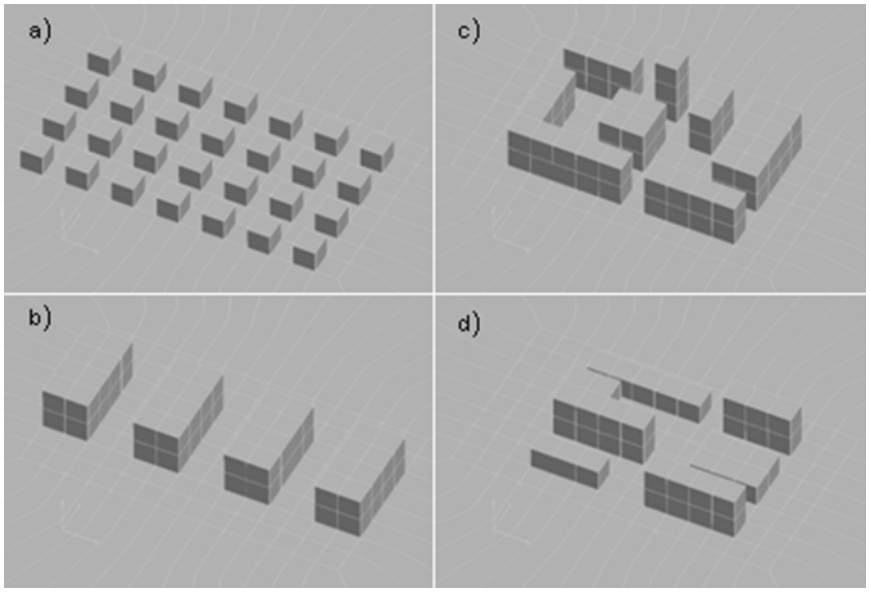

Fig. 31: Picture of chosen building configurations oriented on parameters defined by Badde & Plate. In a) CASE1: one family buildings 1-2 stories; z_0=1.3m. In b) CASE2: residential blocks regularly aligned 3-5 stories; z_0=1.5m. In c) CASE3: city center areas including parks, high rise buildings and public facilities; z_0>2m. In d) CASE4: commercial and industrial area 2-5 stories; z_0=0.6m

To respect the neglect of balconies, blinds and the like a roughness length of z_0=0.2m is applied on the surface of the blocks, but also for the incoming wind. In this way the configurations are placed in a cultivated or natural area with high crops or crops of varying height and scattered obstacles at relative distances of 12 to 15 obstacles heights for porous objects (e.g. shelterbelts) or eight to 12 obstacles heights for low solid objects (buildings), following the Davenport classification of effective terrain roughness [52]. That is not representing real conditions, since city centers are very unlikely to be positioned in such an environment, but for an initial study a regular roughness length is chosen.

3.1.5 Evaluation

In order to evaluate the wind conditions found around and within the building arrangements with respect to wind energy applications, the velocities and turbulence kinetic energy, *tke*, are studied. In the results figures are shown where the acceleration coefficient, *ac*, is plotted. It is defined as in Eq. 13,

$$ac = U(x,y,z)/U_{log}(z)\ , \qquad \text{(Eq. 13)}$$

where $U_{log}(z)$ is the inflow profile and calculated corresponding to Eq. 1. $U(x,y,z)$ is the local speed including all velocity components (Eq. 14), that means that

$$U(x,y,z) = \sqrt{u(x,y,z)^2 + v(x,y,z)^2 + w(x,y,z)^2} \qquad \text{(Eq. 14)}$$

does not include information about directions, but is more a measure of energy. In areas where $ac>1$, the buildings presence causes an acceleration, whereas in areas of $ac<1$, the buildings cause a deceleration compared to the free-stream profile. The other variable of importance is *tke*, Eq. 15, characterized by measured variances of the velocity components.

$$tke = ½\ (\langle u' \rangle^2 + \langle v' \rangle^2 + \langle w' \rangle^2) \qquad \text{(Eq. 15)}$$

The obstruction of the flow by the buildings provokes an increase in turbulence, which would have an impact on the performance of wind turbines and their fatigue loads.

3.1.6 Results

For the implementation of wind turbines, areas as rooftops, house corners and location beside or in between buildings are interesting. Fig. 32 shows *ac* for *CASE1* and *CASE2* at the physical height of z=5m, with the wind approaching from the south direction. In Fig. 33 a) the same but for *CASE4* can be seen. Due to the huge amount of visual information, the illustration of the method is limited to one example, *CASE4* (see Fig. 33 b)-d)), where further *ac* cuts are chosen at 13.5m, which corresponds to 1m above the first roof-level and 8% of cubes height respectively, at 28m, corresponding to 3m above second roof-level and 12% of two cubes height respectively and at 32m, which is 7m above second roof-level height and with that 28% of two cubes height.

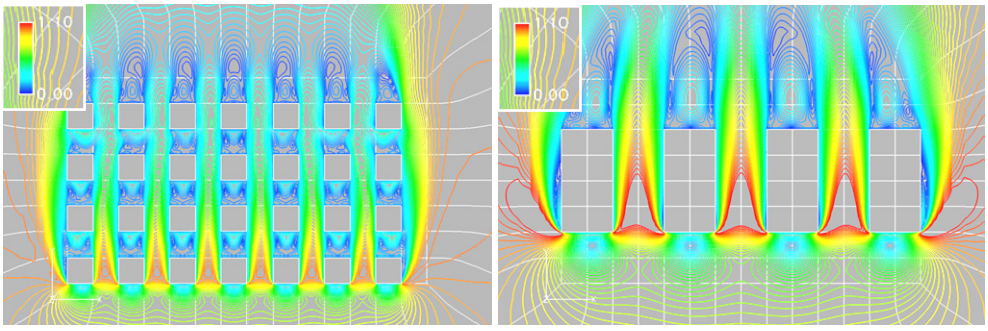

Fig. 32: Parameter ac=0.0-1.1 plotted at z=5m; left: CASE1 and right: CASE2

Especially in low regions high *ac* values are present. The plots do not show the actual velocity, but regions with velocities higher than 3m/s at 5m are found for an inflow velocity of $U_{log}(z$=10m)=4.9m/s. 3m/s is a threshold value for many wind turbines to start electricity production. It is interesting to see in Fig. 33 c) and d) how the region of high *ac* values broadens with increasing height. That might support the

decision making of the wind turbine size. On the rooftop edge a horizontally orientated vertical axis wind turbine (VAWT) could be mounted, close to the rooftop with a smaller diameter than further away, where a bigger diameter might be chosen.

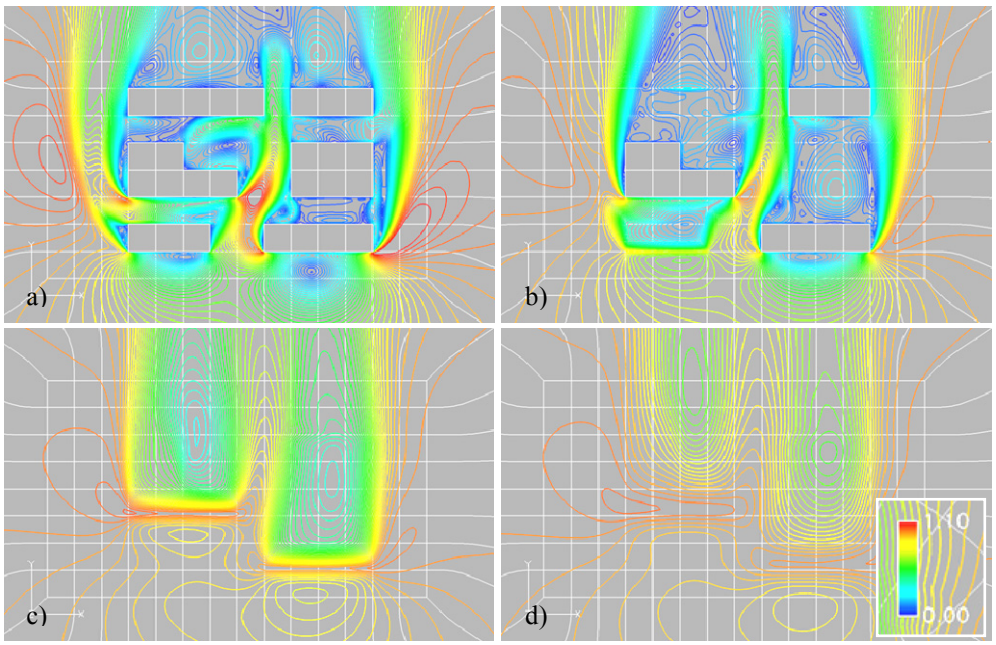

Fig. 33: CASE4; a)-d) ac=0.0-1.1 plotted at z=5m, 13.5m, 28m and 32m

Besides velocity, turbulence is a driver for a successful implementation of wind turbines. Fig. 34 b)- d) depicts *tke* iso-surfaces. The highest *tke* values appear at areas where high pressure gradients are present. See Fig. 34 a) for pressure distribution on the block surfaces.

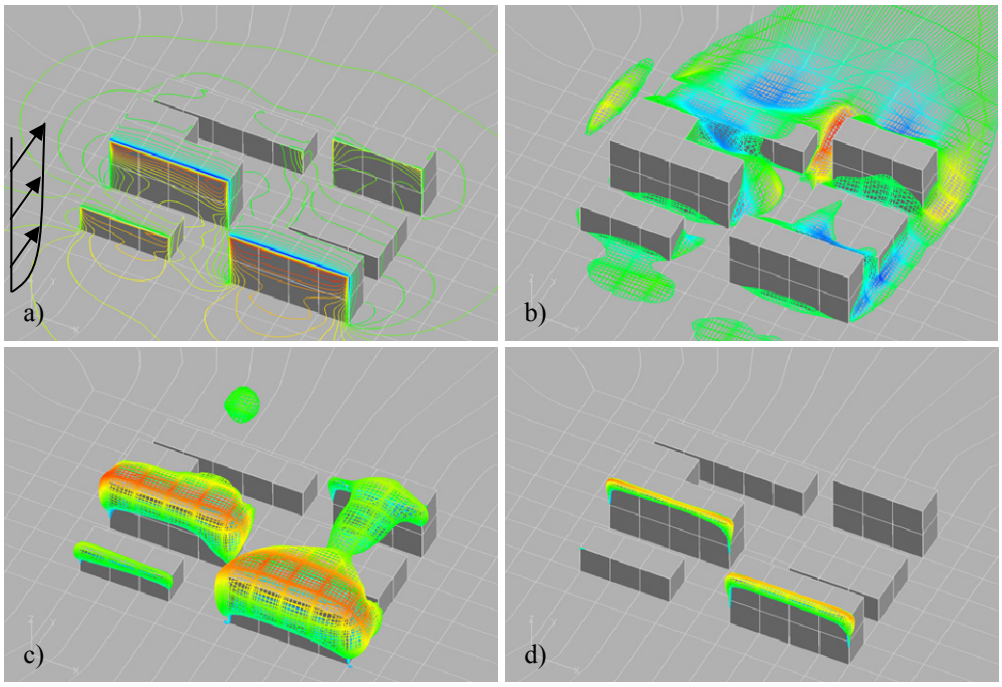

Fig. 34: CASE4: a) static pressure distribution; b)-d) tke iso-surfaces (tke=0.5; 3; 6m^2/s^2) with velocity component v distribution

3.1.7 Discussion

The tool is very useful to get an overview of the wind situation for certain building arrangements. Quantitative conclusions can be obtained by exploring the areas of interest. General statements can be made like increased turbulence is present at areas of high pressure gradients, buildings higher than the mean height of an area bear the potential of higher wind velocities and upwind acceleration is present on the front edge as for first row obstacles, where buildings located in the wake of another building of the same height or below are facing increased turbulence and lowered wind velocities. The fact that the clusters are exposed to an undisturbed wind profile has to be kept in mind. If other buildings surround the quarter, a higher roughness length and a displacement height have to be considered for the inflow conditions. Furthermore, the results are representing the situation for only one wind direction. To predict the most favorable placing of a wind turbine, all directions have to be taken into account. The Reynolds number independency is not verified for the showcases and therefore has to be assumed, but carefully.

3.1.8 Conclusion

Comparing the simulations of a single cube using the CFD tool with wind tunnel tests shows very good agreement. An important conclusion from this study is the independency of Reynolds numbers on flow patterns around buildings. This means that despite of changing wind speeds the flow patterns are maintained. Using the tool for a certain configuration of buildings illustrates the methodology to analyze the wind energy potential at different positions on buildings to identify the most appropriate positions in terms of both wind energy potential and low fluctuations in the wind, i.e. low turbulence kinetic energy. With this information, future mounting of wind turbines in urban districts can be based on quantitative potentials rather than on qualitative estimations. The perspective for further development is to apply the local wind rose as inflow boundary conditions to obtain a more complement picture of the local average wind energy potential.

3.2 Flow Phenomena

After introducing the tool PlayBox in the previous section, here some general flow behavior is visualized with the help of *CASE3*, constituting city centers. The inflow conditions and boundary settings are the same as explained in the foregoing section. First examined are the streamlines emerging in the flow, approaching the set-up from only one direction. Another visualization method is applied afterwards to give a more complete picture of the flow field, followed by an example where the influence of an applied wind rose is shown.

3.2.1 Streamlines

Streamlines are instantaneously tangent to the velocity vector of the flow. They show the direction a fluid element will travel in at any point in time. The results from the simulations are averaged and steady, so that the streamlines are constant and do not change in time. That does not reflect reality. Information gained with this approach is used to explain the flow conditions in a built-up area, since wind in the everyday life is not visible. In Fig. 35, left, the investigated buildings array can be seen and in Fig. 35, right, the same picture, but with the surface pressure distribution is shown.

Typical for a cube exposed to an undisturbed free flow is the upwind effect experienced on the front face, resulting in great pressure differences where the front face and the top face meet, indicated in the mentioned figure by the color red, high pressure, and the color blue, low pressure. As known, wind is driven by pressure differences, proceeding from high pressure to low pressure. In such areas higher wind velocities are expected to occur. The high pressure on the front face is due to the sudden deceleration of the flow, where dynamic pressure turns into static pressure. In the following streamline plots, the colors indicate the speed along the

visualized paths. Examining Fig. 36, right, the front row is the first obstacle the incoming logarithmic wind profile experiences. Here the upwind effect is present. At the downwind buildings this effect is absent both for buildings close by or double the distance. That is true for buildings with the same height. The part of a tower looming above the building mean height of a district with low mean height variation can be considered as a first row obstacle. A study of increasing the distance between the obstacles was not carried out.

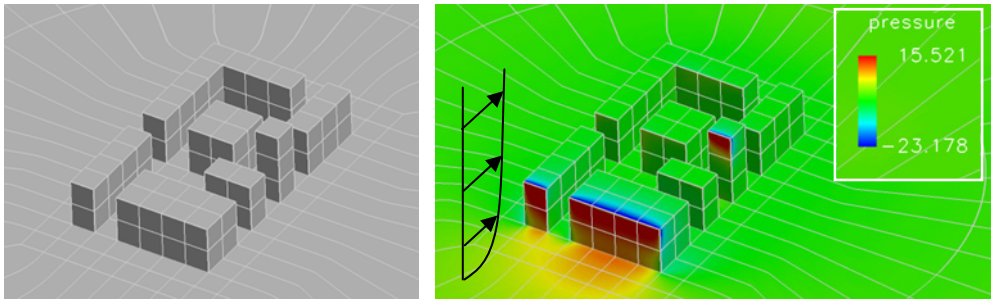

Fig. 35: CASE3; left: plain building arrangement; right: pressure distribution and indication of the inflow direction

Earlier the street canyon effect was mentioned briefly. This is the effect of a street for example, where buildings to both sides are bordering a street, funneling the wind. In Fig. 36 top, the incoming flow is first redirected because of the building, blocking the way of the wind. The flow circumvents the obstacle in the lower regions to the right and to the left, depending on the width to height ratio of the resistant object. A portion is then proceeding through the opening of the first row, where it is accelerated similar to the flow through a nozzle. This acceleration does not continue throughout the district. The medium is lifted and exits the array over the rooftop of the last row, gaining in speed. Going back to Fig. 32, right, it can be seen, that even though the canyon is continuous, the acceleration effect does decrease. Different from a nozzle, the flow can disperse through the open top and does therefore loose in speed. The highest acceleration effect is found close to the ground, where however the absolute speeds are low and probably not worth harvesting.

Proceeding to Fig. 36, bottom, shows the streamlines approaching the array a bit further to the right in relation to the ones seen in Fig. 36, top. Again, a part of the flow is redirected into the canyon, whereas the higher parts are taking the course over the first obstacle's roof edge. A strong acceleration does take place there, where the flow bends from vertical to horizontal, continuing with an almost constant speed and height striating over the rooftops and gaps. Reminding the drawings in Fig. 28, the flow is skimming over the buildings and the gaps are filled with recirculation bubbles of low speed, as they also can be seen in Fig. 36, bottom.

In Fig. 37 streamlines at a higher position heading for the tower are illustrated. At the top, the conditions can be seen, similar to the first row phenomena. Streamlines are swerving to the right, the left and over the rooftop. The maximum speed in the legend was set to 5m/s. That is why the acceleration effect around the edges cannot be seen distinctively. The figure at the bottom depicts, that a part different from the first row case, is redirected downwards. It clearly shows the sharp and sudden deceleration due to the resistant imposed by the tower's presence. Furthermore, the shadow effect of the tower can be seen, where low speeds are found behind it, slowly recovering in speed downstream.

The last streamline illustration, Fig. 38, shows the flow over in-line obstacles of constant height. Most of the flow remains undisturbed in this course, but is slightly lifted in height gradually and the lower parts indicate lower speed. An explanation for this circumstance is the portions of flow from the lower regions redirected over the rooftop and displacing the visible streamlines. Another factor is that the streamtubes decelerated by the no-slip condition on the solid roof surface are expanding in volume, according to the mass conservation law in conjunction with the Bernoulli principle.

These flow phenomena introduced and visualized with the help of streamlines on hand *CASE4* are general rules, which are applicable to similar set-ups as well, for sure only to some extent.

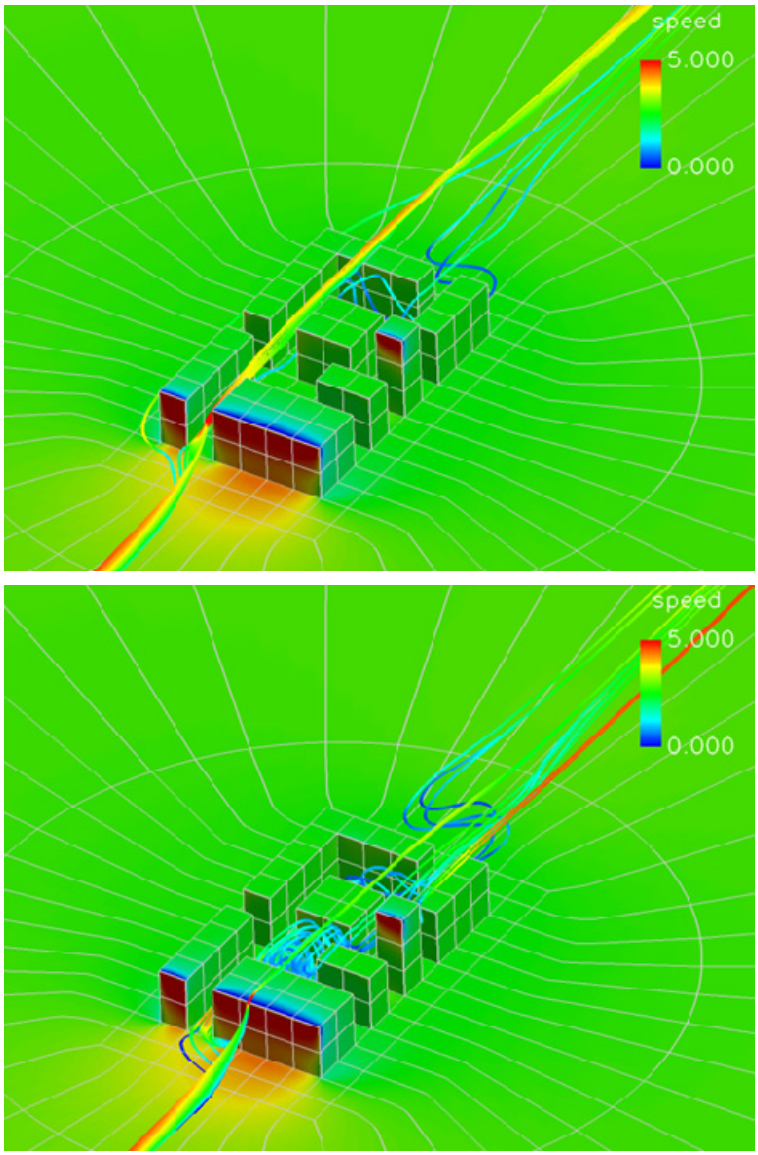

Fig. 36: CASE3; top: redirected streamlines accelerated through a street canyon; bottom: decelerated streamlines at first row obstacle with upwind effect and acceleration at first row roof-edge, partly entering street canyon, caught in ground recirculation zones

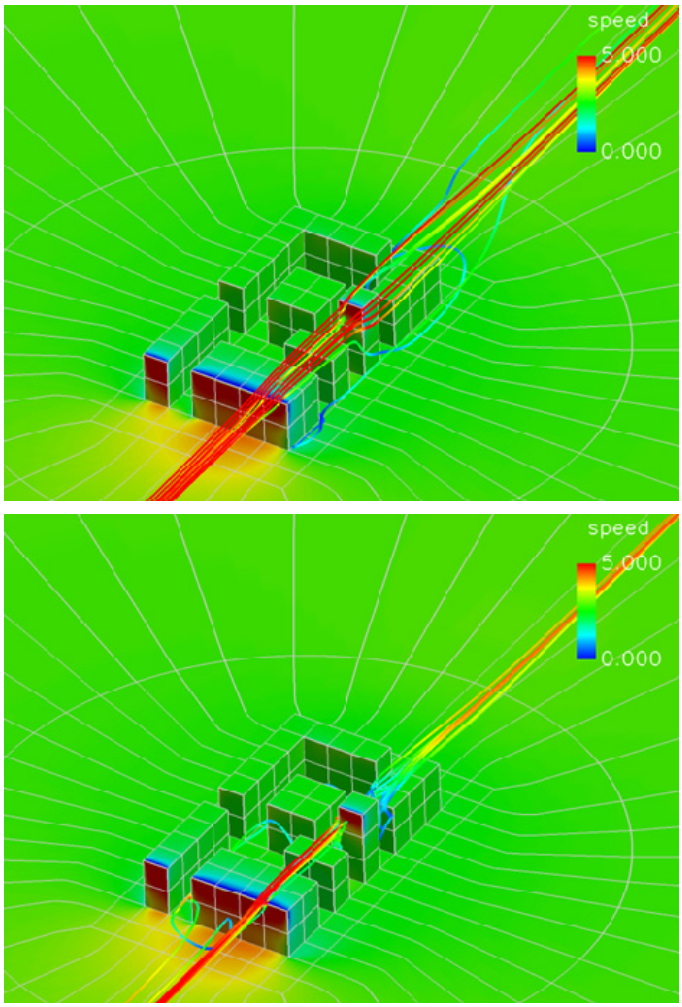

Fig. 37: CASE3; top: streamlines surrounding tower top, similar to first row obstacle; bottom: streamlines directed downwards at tower tip front side and streamlines in the tower tip wake

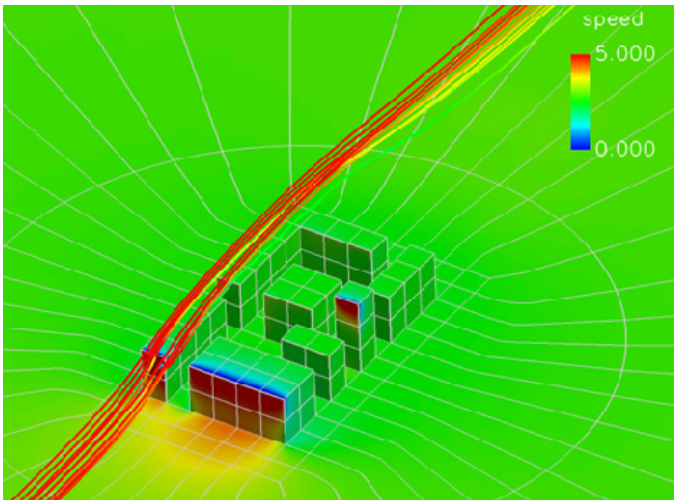

Fig. 38: CASE3; streamline propagation over in-line obstacles of constant height

3.2.2 Grid planes

In the previous section, the flow behavior was visualized with streamlines and the speed along their paths. To resolve the flow field more extensively, wind speeds on concrete grid planes are exemplified. In Fig. 39, left, the grid planes at the first row front face are visible. The wind speed is about 5m/s or beyond almost throughout the whole area. Interesting is the asymmetry in the spacing between the two building blocks. Because the broader building is blocking out a larger proportion of wind mass, a larger amount is entering the canyon from its side forming the asymmetry.

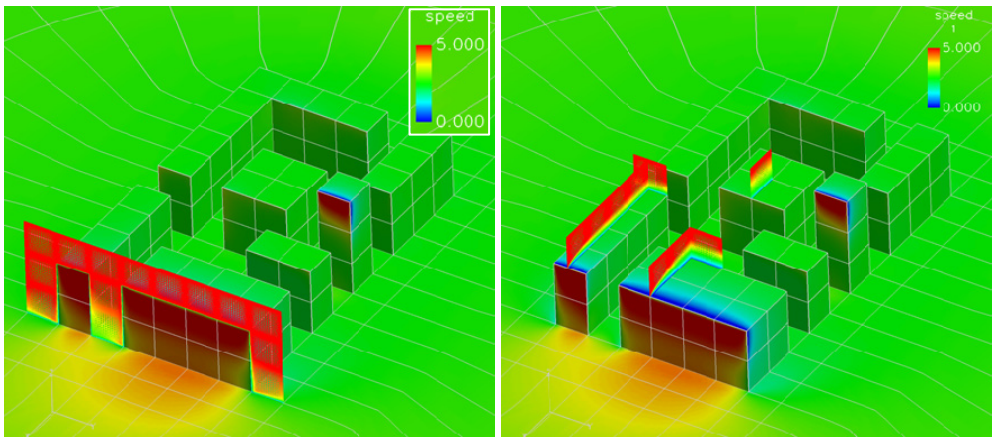

Fig. 39: CASE3; left: speed distribution on first row grid planes perpendicular to inflow direction; right: grid planes along the free stream direction picturing speed profiles on first row rooftops and second row rooftop

Grid planes along the middle of some of the rooftops in Fig. 39, right, confirm what was already seen with the streamline visualization. At the first row façade the undisturbed flow is deflected strongly, forming a speed profile on the rooftop's front edge. High velocities are found close to the edge, evolving into a rather constant speed distribution. Buildings inside the array and of the same height as their upstream buildings experience homogeneous speed distributions along the rooftop, without any upwind effect. Studying Fig. 40, left, the skimming effect is clearly revealed. The speed distribution in the internal field where no buildings are present is surprisingly akin to the distributions found at the rear edge of the upstream building and the front edge of the building further downstream. In Fig. 40, left, the fact that the array is not surrounded by other buildings can be seen by the generally downwards bowed wind speed distributions. The grid planes to the right and left of the tower's front face in Fig. 40, right, are so different from each other, because the flow, not entering the array is almost undisturbed and not decelerated or displaced. In contrast to the more or less continuous asymmetry due to the position of the array in an open field, the speed distribution evoked by the tower's wake in combination with the downstream roof influence does barely show any asymmetry.

In Appendix D, a plot can be found where the discussed phenomena are summarized in one figure. Further general phenomena can be detected and studied with a tool like the introduced PlayBox. Its simplicity is on the one hand neglecting a lot of details, but on the other hand, it helps to study very basic rules. If chimneys, trees or the like would be included, it would be rather difficult to tell, which obstacle causes what. The single influences would be blended together and the result associated with increasing numerical inaccuracy tends to give blurry information. Until so far, the simulation results were shown only for one wind velocity profile approaching from one direction. Increasing or decreasing the incoming wind velocities would not

change the flow pattern, based on the Reynolds number independency assumption. In real conditions, the flow is not approaching from only one direction, but from various directions with certain probabilities and Weibull distributions, forming a wind rose. The next section examines onsite wind profiles and the importance of the local wind rose.

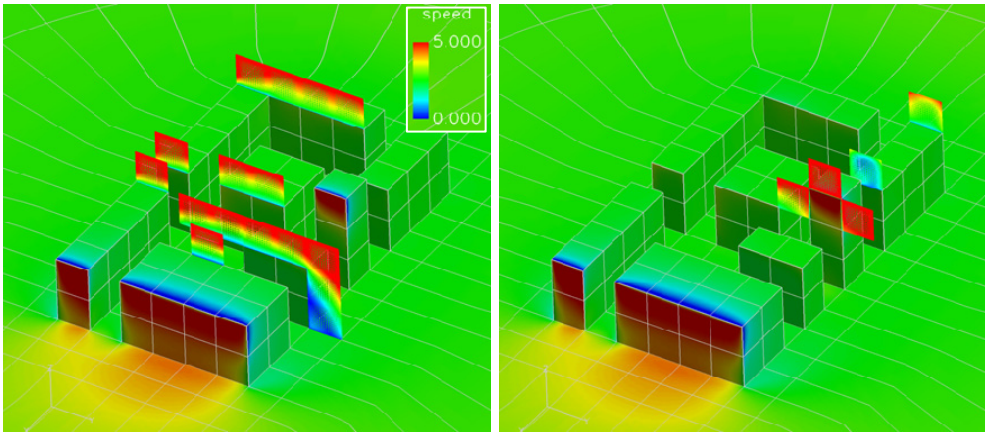

Fig. 40: CASE3; grid planes perpendicular to inflow direction; left: mainly at rooftop front and rear edges visualizing skimming flow; right: on tower top front side and in the tower wake

3.2.3 Wind roses

A wind rose is a graphic tool to give an instant overview of for example the distribution of occurring wind directions at a certain location. Such a wind rose can be divided in several direction sectors. Earlier in chapter "Urban Wind Climate", the wind rose found at the H.C. Ørsted Institute was plotted in 10° steps. Simulations within the PlayBox domain are carried out for only four inflow directions, 0°, 90°, 180° and 270°. The more sectors are simulated, the more detailed the conditions can be resolved. For now, 90° steps are sufficient to demonstrate the influence of the wind direction probability on the local wind profiles.

One more time, *CASE3* is used to serve as an exemplar demonstration. Similar to met masts, wind speed data are extracted at three vertical lines on three rooftops of the building array. These met masts are named pole1, pole2 and pole3. How they are positioned and the way the inflow direction is declared can be seen in Fig. 41.

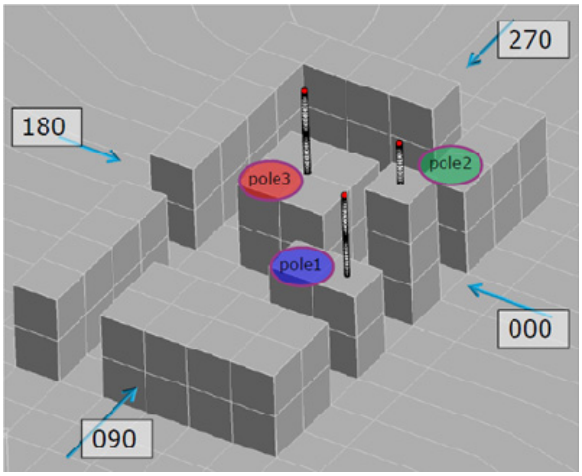

Fig. 41: Pole positioning and indication of wind direction and pole designation

The inflow conditions are as in the cases before, only the inflow direction is changed. Wind profiles found at the indicated positions are plotted in terms of total wind speed. It is not looked into the actual local directionality, which in terms of wind turbine installation could be interesting.

The speed profiles present at the three poles for the single inflow directions are plotted in Fig. 42. Besides that the inflow profile is plotted as well, starting at the height of the corresponding rooftops. In this way the difference of a turbine positioned on a rooftop and of a free-standing wind turbine with the same tower height is shown. A blue dashed line is indicating a wind speed of 3m/s, the cut-in wind speed for many small wind turbines. Taking a closer look at the profiles, the ones at pole2 are almost the same despite the changing incoming wind direction.

Pole1 shows high speeds in case of the wind coming in from the 000 direction. This can be explained with the fact that the building is standing in the first row. Surprising is the similarity for the direction 090 and 180. Although the tower is decelerating the flow from 090 as could be seen in one of the streamline figures, it looks like its influence does not reach the upstream position of pole1, at least not significantly. In opposition to that, the influence of the tower on pole1, when the wind is entering from 270 is enormous. Continuing the observations, the profiles found at pole3 are very similar to each other. With its position in the middle of the array and the formerly detected skimming flow this was somewhat anticipated. For the case where the wind approaches from the 000 direction, pole3 is located in the wake area of the tower. It is interesting to see, that the influence of the wake is weaker, since pole3 is not located directly in-line with the tower as pole1 and also the distance is slightly bigger.

Combining the extracted results from the single wind directions forms the speed profiles in Fig. 43. Three wind roses can be seen, showing the probability distribution which is used to calculate the corresponding wind rose dependent local speed profiles.

For the first incoming wind rose an equal distribution is chosen, $p(000)=0.25$, $p(090)=0.25$, $p(180)=0.25$ and $p(270)=0.25$. The wake deficiency seen for pole3 is almost compensated by the contribution from the three other directions. If the wind is predominately coming from direction 000, which is simulated in the second plot with $p(000)=0.50$, $p(090)=0.25$, $p(180)=0.20$ and $p(270)=0.05$, the wake influence at pole3 is maintained. For pole1 where a strong wake deficiency was seen, the second scenario is favorable. Scenario three shows the profiles resulting from a wind rose with the settings $p(000)=0.10$, $p(090)=0.15$, $p(180)=0.30$ and $p(270)=0.45$.

For all the three direction probability roses, the incoming wind profiles are the same. In reality the wind direction incidence is site-dependent, but also the mean wind speed and wind speed distribution in form of a Weibull distribution in each section is site-depending. An investigation of these factors could be part of future work on the topic.

There are many more possibilities to examine the flow around obstacles and only a few methods were illustrated here. Tools like the one used here are very helpful to conduct case studies to acquire understanding for the conditions in complex terrain. To define general rules in form of equations was desirable, but concluded to be infeasible in this context.

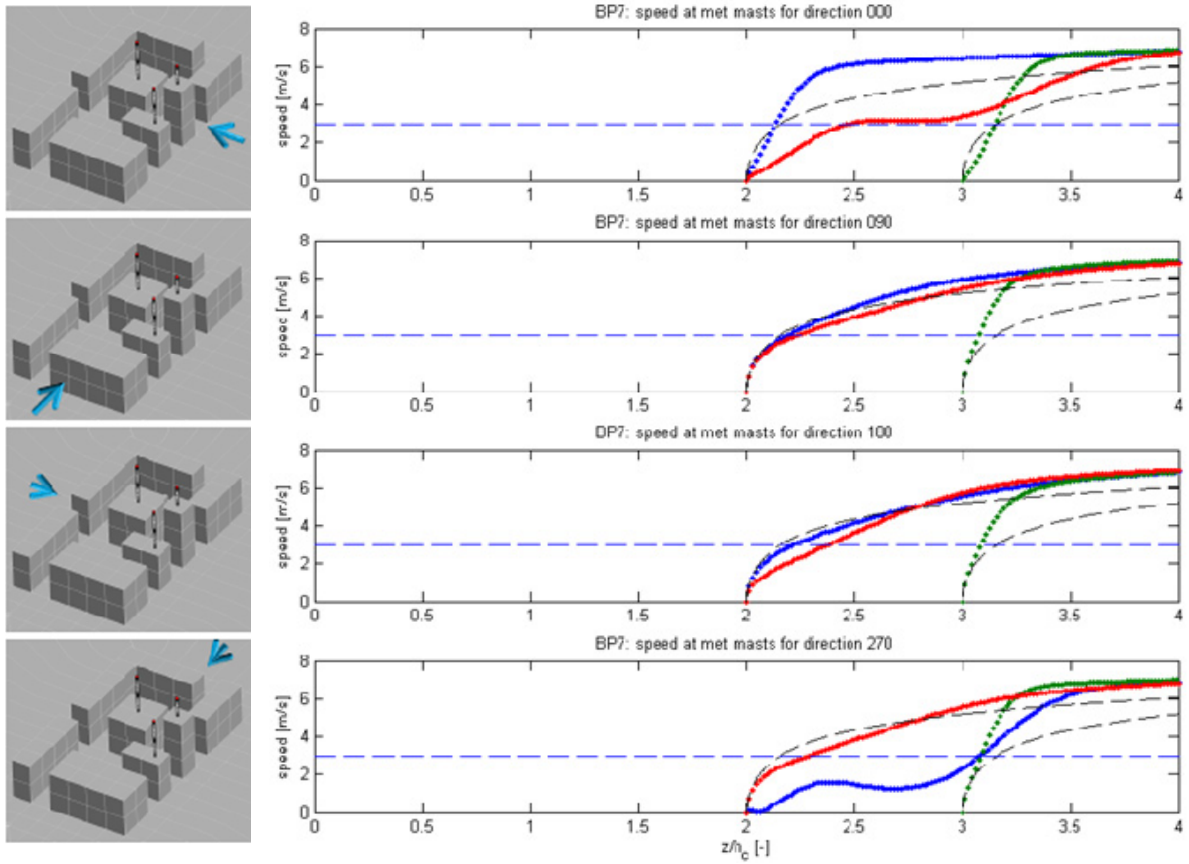

Fig. 42: Speed profiles present at the three poles for the single inflow directions (pole1: blue; pole2: green, pole3: red). Black dashed line is the inflow profile, starting at the height of the corresponding rooftop. Blue dashed line indicates 3m/s speed.

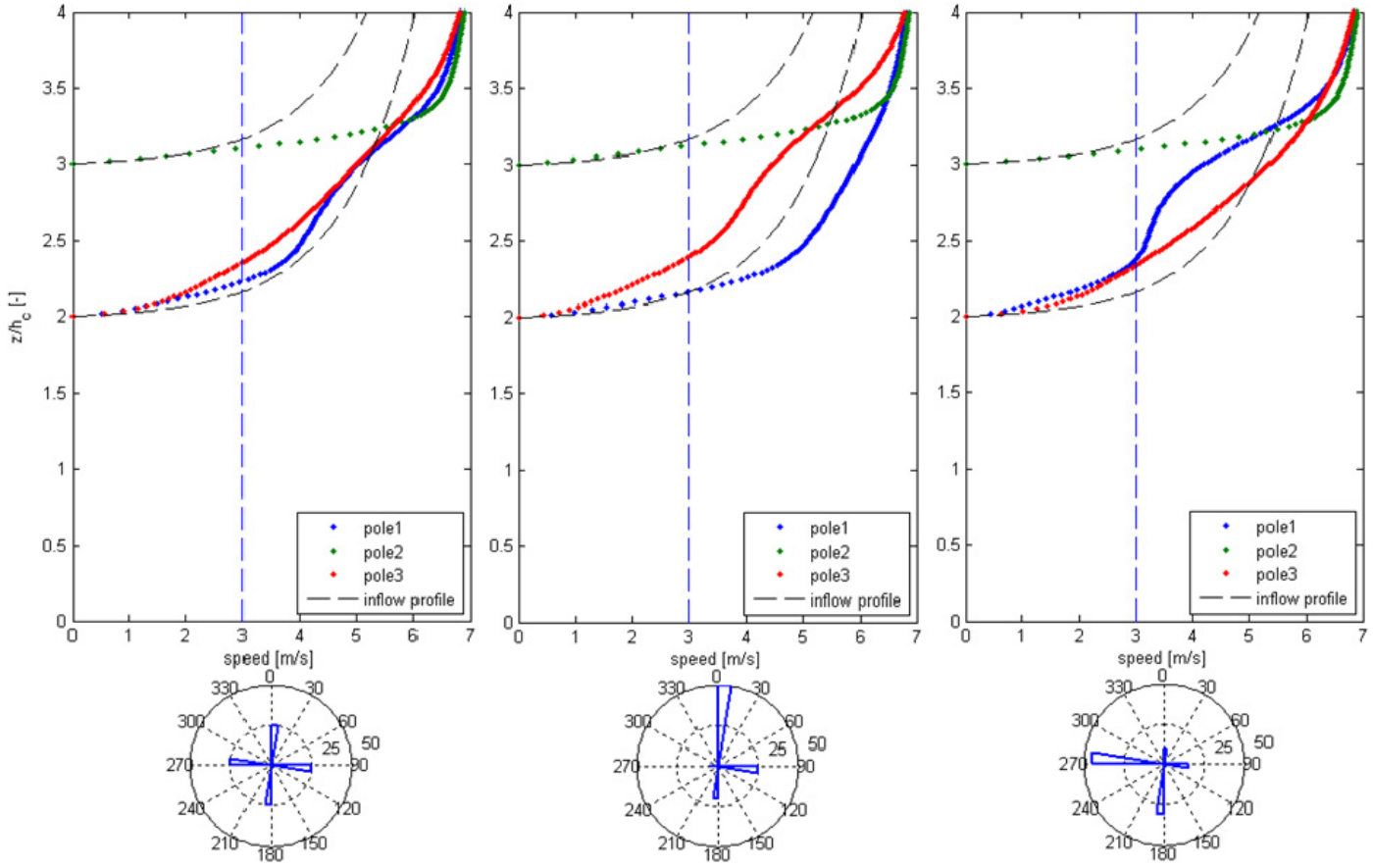

Fig. 43: Wind speed profiles present at the three poles for three different wind rose incidents

3.3 Summary and Conclusions

The content of this chapter is summarized below and the concluded findings, as well as facts, known on beforehand and found to be important, are imbedded as bullets into the continuous text.

The micro wind climate in cities is very complex and highly site-dependent. A CFD tool, Playbox, is developed to build simplified cluster arrangements to investigate general flow behavior with respect to successful implementations of wind conversion systems. Some observations and general rules are derived with only a few information extractions and many more can be found with help of the tool.

- A circular shape is chosen for the computational domain ground plate to use the same domain for different inflow directions.
- In order to reduce the block number and to keep cells as less skewed as possible, the computational domain is built up as a hemisphere.

Cubes representing buildings are bluff bodies and with that the aerodynamics are different from streamline shaped bodies.

- CFD simulations where flow behavior is calculated around bluff bodies, can capture Reynolds number independencies as long as the Jensen number is maintained.

That means on one hand that for a certain building set-up, areas of high and low wind velocities respectively are at the same location independent of the incoming wind speed. On the other hand it means that the buildings are scalable, as long as the roughness length is scaled correspondingly to the Jensen number.
Comparing the wind speeds of the incoming flow with the wind speeds present around the buildings and evoked by them as well was defined as an acceleration parameter.

- Especially in low regions of the building arrangements, high values for the acceleration parameter are present. The absolute wind speeds might be too low to harvest though.
- At the front rooftop edges of first row obstacle and the front rooftop edges of buildings higher than the mean height of the urban district, areas of high acceleration are present.

Besides wind speed, turbulence kinetic energy is another important parameter for the implementation of wind turbines.

- The highest turbulence kinetic energy values appear at areas where high pressure gradients occur, as for example at roof edges.

One popular topic is the so-called upwind effect, where high velocities are expected to occur on roof edges.

- In an area with a typical urban built-up density skimming flow is a matter of fact, and therefore upwind accelerations of flow over the roof edges are low.

That means, that the upwind effect is absent for most of the buildings within a common urban set-up.

- Upwind effect is mostly present for first row obstacles and buildings higher than the mean height.

More general rules apply.

- Buildings higher than the mean height reach up into high velocity layers.
- Buildings in the wake of a higher building and buildings below the mean height are facing increased turbulence and lowered wind speeds.

The most known flow phenomena between two buildings, if the wind approaches from a certain direction is the so-called street canyon effect.

- The flow entering a street canyon is accelerated similar to the flow through a nozzle, while the acceleration effect decreases along the canyon.

That is because different from the flow in a nozzle the flow in a street canyon can disperse through the open top and does therefore loose in speed. The speed distribution in the entrance of a street canyon is dependent on the buildings forming the entrance.

- The height to width ratio of buildings at a street canyon entrance influences the speed distribution at the canyon entrance, most probably forming an asymmetric distribution.
- Wind perpendicular to a street canyon causes recirculation structures and no acceleration as such.

A clear disadvantage of the developed tool, PlayBox, is that the buildings cluster is positioned in a free field, where in reality an urban district is surrounded by other built-up neighborhoods. The flow field on the cluster boundaries is affected by the absence of neighboring buildings. Despite that effect, the flow field found in the wake of a tower seems to be unaffected by this.

Investigating the wind speed profiles at certain spots within the cluster for different inflow directions reveals a row of rules.

- At the center of a tower rooftop the wind profiles are almost the same, despite the changing incoming wind direction.
- On the rooftop of a reasonable high building, higher than the buildings mean height of the urban district, and on rooftops of first row buildings, velocities comparable to the countryside and higher can be reached with a tower of the same height or even shorter towers than necessary for a free-standing turbine in the countryside.
- Tower wakes evoke speed deficiencies in the downwind region at heights even above tower height.
- The wake influence decreases with increasing downwind distance to the wake provoking obstacle.
- Deceleration in front of a higher obstacle takes place very close to its front façade and does not affect the upwind flow fields significantly.

The probability of inflow direction incidences is site-dependent. An average wind speed profile at a certain spot is a composition of the local effects present for the single wind directions. The weight of the single effects' contribution is thereby dependent on the wind direction probability and also on the Weibull distribution

representative for the single wind direction sectors. Simple exemplary wind direction probability distributions lead to basic conclusions.

- Depending on the local wind rose, tower wake deficiencies can be compensated considerably.
- Positioning on a first row obstacle does not need to be of advantage, if e.g. a higher building is located close by.
- Locations above the buildings mean height of an urban district and in reasonable distance to higher buildings are mostly independent of wind directionality in a typically dense built-up district.

4 ROTOR DESIGN

In the last two chapters the wind climate in cities was clarified. For one scenario the annual energy production of three different small-scale wind turbines was estimated, showing that the power curve characteristic has a tremendous influence on the all-over performance. It was concluded, that in wind climates where wind velocities beyond 9m/s are barely seen and most of the wind incidences occur at around 4m/s, a rotor has to be optimized according to such conditions. In this chapter focus is taken on rotor design. First, an overview is given of the different main groups of wind turbine configurations. All of them have their eligibility to coexist. A certain design might be more appropriate for a certain application, where another is more advantageous under other circumstances.

For the application of building mounted small-scale wind turbines VAWTs (Vertical Axis Wind Turbine) are an option. The layout of such a rotor is studied in detail, starting with a row of case studies. The relevance of various design parameters is illustrated with the help of calculations based on a multiple streamtube code called DART, developed at SANDIA in 1975 by Strickland [69]. In a second step, design optimization methods are shown, which are derived with a modified DART code implemented into the optimization tool developed at Risø DTU, by Fuglsang in 2001 [70]. A short description of the DART code and its modification are given. A detailed report about the way the code was further modified and implemented in HAWtopt is available too [71].

Another strategy to enter the urban space was mentioned in the chapter "Introduction", where an idea for a small autarkic energy system was introduced. In the end of the present chapter the design process of such a system is presented, where the original HAWTopt code was used to find a HAWT rotor layout.

4.1 General Configurations

Several small turbines are on the market, while some are more successful and some less. One big drawback is definitely the lower efficiency compared to large scale turbines. Furthermore, large wind turbines, depending on the chosen site, are paying back on the energy level within only a few months (~three month [72]). In contrast, some small turbines need several years until they have produced the amount of energy, which was necessary to produce and operate them [73]. Paul Gipe discusses small turbines with a critical eye. He states that large wind turbines produce ~9/5 more energy than small turbines per swept area [74]. The dominant concept with a Horizontal Axis Wind Turbine (HAWT) using three blades upstream of the tower has shown to be reliable and cost effective. However, this concept is developed for MW sized turbines at sites with relatively low turbulence intensity. Considering wind turbines in an urban context and determining appropriate concepts needs an open-minded approach, where the weight on different design drivers has been changed to put new emphasize on noise, aesthetics, fast varying flow directions and a high fraction of manpower cost per kWh. Therefore, new concepts compared to the current dominating concept should be considered such as Vertical Axis Wind Turbines (VAWT) and other types of HAWTs.

4.1.1 HAWT vs VAWT

VAWTs specifically designed for an urban environment offer a complementary strategy for power generation to conventional wind farms. Sizes in rotor diameter can range from 1-20m and power output from 100W-100kW. To gain public acceptance, much thought has to be put into an aesthetic and reliable design. The principal advantage of modern vertical axis wind machines over their conventional

counterparts is that VAWTs are omnidirectional- they accept the wind from any direction. Furthermore, the vertical axis of rotation permits mounting the generator and gear at around ground level, which is of advantage with regard to dynamic behavior, but also for maintenance reasons. In terms of applications in the residential environment, the wind turbine shall be unintrusive and well integrated into the face of the city, be considered as a part of architecture. A VAWT in operation describes a volume constant in its shape. In contrast to that, an operating HAWT free to yaw follows the wind direction- seen from a fixed point forming a disk for one moment and a line for another. High turbulence in the built environment is coupled to frequently changing wind directions. A HAWT following the changing wind directions is suspected to implement visual disturbance and to perform less efficient, because of intensive redirecting activity and misalignment.

4.1.2 Lift- and drag-driven

VAWTs like HAWTs can be divided into two major groups- those driven by aerodynamic drag to extract power from the wind, e. g. the Savonius type, and those driven by the aerodynamic lift from an airfoil. Further, most known VAWTs from the 70's using airfoils subdivide into those with straight blades, e. g. the H-rotor type, and those with curved blades, e. g. Darrieus type (see Fig. 44 [75]).

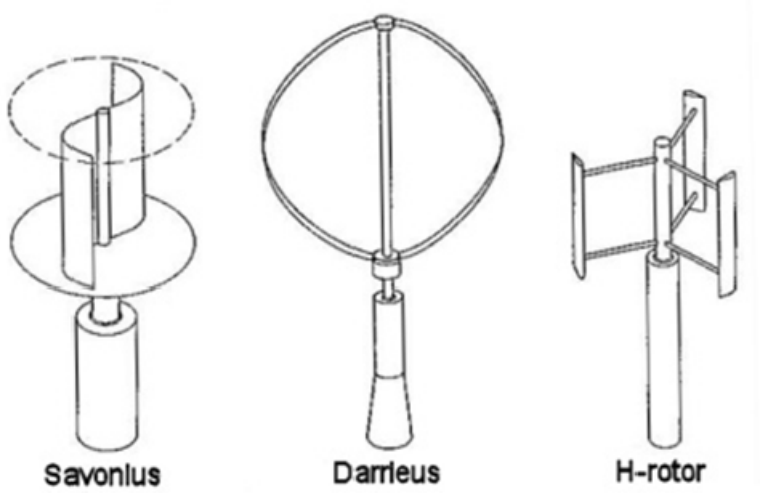

Fig. 44: VAWT concepts (left to right): Savonius, Darrieus and H-rotor type

Nowadays, where VAWT designs are reinvestigated for the use in an urban context, many of the layouts seen on the market are H-rotors with three twisted blades. In the following case study section, a short look is taken on the properties of such twisted blades. The simplest configuration uses two or more straight blades attached to the ends of a horizontal cross arm. The drawback is that this configuration permits centrifugal forces to induce severe bending stresses in the blades at their point of attachment. D. G. M. Darrieus invented in the 20's a rotor that cleverly dealt with this limitation. Instead of using straight blades he attached curved blades to the rotor. When the turbine was operating the curved blades would take the form of a spinning rope held at both ends. In this way the centrifugal forces are directed through the blade's length towards the points of attachment, thus creating tension in the blades rather than bending. Because materials are stronger in tension than in bending, the blades could be lighter for the same overall strength and operate at higher speeds than straight blades. A significant drawback of Darrieus turbines is that they were never reliably self-starting. Their fixed-pitch blades cannot drive the rotor up to operation speed from standstill unless the blades are parked in just the right position relative to the wind. H-rotors with straight blades can vary the blade pitch as the

blades orbit around the rotor axis and with that operate more efficient. On the other hand more movable parts are added, more control is needed and with that costs are increasing.

Anyhow, the H-rotor has one important advantage over the Darrieus design. It captures more wind. The swept area of an H-rotor is a rectangle. For the same height and diameter an H-rotor sweeps more area than an ellipse does [74]. On the other hand, the supporting structure necessary to keep the shorter blades of the H-rotor in place and shape implies additional eminent drag.

As mentioned above the VAWTs are omnidirectional. The HAWTs, however, have to align with the wind direction in order to be most efficient. This horizontal alignment is commonly called yawing.

4.1.3 Yawing

Various yawing concepts exist to align with the wind direction, passive and active. The conventional HAWT concept in MW size is equipped with an active yawing system, which can e. g. consist of a wind measurement device detecting the current wind direction, and a motor to adjust the rotor to the new wind direction. Small-scale wind turbines are usually designed with a passive yaw system. One of the oldest passive yaw systems is the wind vane, which can be seen in Fig. 45 in the middle. The vane has to have an appropriate area and arm, so that in case of changing wind direction a pressure force is imposed on the vane face and generates a moment great enough to align the rotor. Another passive yaw system is included in a less frequent wind turbine concept, the downwind concept.

4.1.4 Upwind and downwind

In general HAWTs can be divided in upwind and downwind concepts. A wind turbine design is called upwind concept when the position of the rotor relatively to the tower lies upwind. That means, that the wind first passes the rotor plane and then the wind passes the tower (see Fig. 45 [76] (a) and (b)). A wind turbine design is called a downwind concept when the position of the rotor relative to the tower lies downwind. That means that the wind passes the tower first and then the rotor (see Fig. 45 (c)).

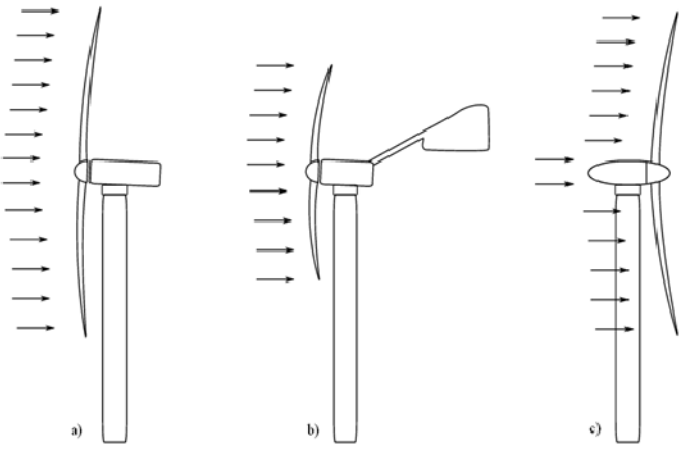

Fig. 45: HAWT concepts (left to right): upwind with active yaw; upwind with passive yaw; downwind with passive yaw

With the downwind concept the rotor aligns with the wind direction without any additional construction or sensors, but noticeable noise emission was experienced with this concept, originating from the blades crossing the tower wake.

4.1.5 Advantages and disadvantages

Summarizing the comparison between HAWTs and VAWTs, the advantages of vertical turbines are

- independent of wind direction
- generator can be located on the ground (structural advantage and maintenance accessibility)
- less noise (Darrieus type has no tip vortex)
- withstands high turbulences
- symmetric and aesthetic

While the disadvantages are

- not self-starting
- changing angle of attack over one rotation
- fixation of the upper end of the axis is needed (for big turbines)
- low C_P (see Fig. 46 [77])

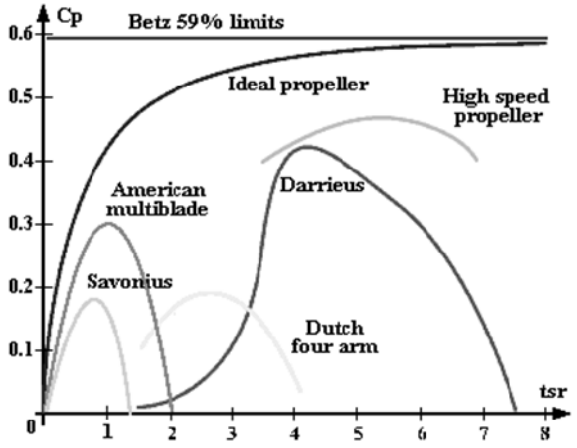

Fig. 46: Typical C_P vs λ curves for various rotor types

The graph above is drawn for rather large rotors exposed to rather constant wind conditions, especially in wind direction. With small rotors a maximum power coefficient of C_P=0.35 is expected for VAWTs. Although the C_P values are said to be lower for VAWTs than for HAWTs, the max C_P for a small-scale HAWT in a climate with frequently changing wind directions is expected to be lower than for one exposed to constant winds. So, this disadvantage for VAWTs diminishes and might even turn into an advantage. Motivated by the argument of a quiet geometry and the omnidirectionality for a vertical axis rotor, its design parameters and layout is elaborated and presented in the following section.

4.2 VAWT Parameter Study

In order to conduct parameter studies for VAWT rotors, several methods are available. To name the four most common methods to model the aerodynamics of a VAWT rotor with

- Single Streamtube Model [78]
- Multiple Streamtube Model [69]
- Actuator Cylinder Model [79]
- Vortex Model [80].

The simplicity of the multiple streamtube model and its similarities to the HAWT aerodynamic BEM model leads to the decision to use the so-called DART model for a parameter study. With a simple change in the code, it is possible to calculate H-rotor geometries as well. Afterwards the original code written in Fortran is translated into C and with further modifications implemented as aerodynamic model for VAWT designs into the HAWT optimization tool HAWTopt.
A short introduction of the used model is given, followed by the design directives drawn from the conducted case studies. The design directives are basically also valid for HAWT layouts.

4.2.1 DART

The DART (DARrieus Turbine) code was developed by Strickland in 1975 [69]. Since it is a simple model, some effects are not taken into account. Following assumptions and issues have to be considered, when using the basis code:

- Quasi-steady flow through the rotor
- Constant streamwise velocity is a function of streamwise position, and flow velocities normal to the freestream direction are neglected
- Blades are lightly loaded (for small and moderate tip speed ratio)
- Near-wake structure is missing (important for positioning WT to each other)
- Dynamic stall effects are ignored (important for small tip speed ratio, $\lambda_{equator} \leq 4$)
- Inadequate in describing distortions and interactions. Most serious deficiency is, under conditions of large solidity and high λ, the simple momentum considerations inherent in the model break down
- No tip-losses considered
- No supporting structure included
- Only symmetric profiles without pitch and only with constant chord distribution along the blade
- Blades are considered to be in a plane containing the rotor axis, no twist
- Horizontal symmetry plane in the rotor equator
- Rotor geometry is limited to Darrieus shapes, described by a sinus function

It seems as if the code comes with a lot of restrictions, none the less, the results give a variety of possibilities to conduct interesting parameter studies. First, the background theory of the DART model is sketched and the design directives concluded on hand of the conducted parameter study follow.

4.2.2 Theory

Strickland's multiple streamtube model is based on Glauert's blade element theory. As it is explained in the paper [69], the theory uses the streamwise momentum equation, where the streamwise forces on the airfoil blades are equated with the change in fluid momentum through the rotor plane. Different from the single streamtube model, the model here divides the rotor plane in several streamtubes for a more detailed local velocity distribution. Because momentum is extracted in the rotor plane, the velocity there, U, is lower than the incoming free flow, U_∞. Together with the Bernoulli equation, these velocities and streamwise force can be related to each other in the following way, Eq. 16,

$$\bar{F_x} = 2\rho A_S U(U_\infty - U)\ \bar{F_x} = 2\rho A_{rotor} U(U_\infty - U) \qquad \text{(Eq. 16)}$$

Here, ρ is the fluid density and A_{rotor} is the cross-sectional areas of the streamtube given by Eq. 17,

$$A_{rotor} = \Delta h r \Delta\theta sin\theta \ , \qquad \text{(Eq. 17)}$$

with Δh as the vertical height of the streamtube, r is the local radius, $\Delta\theta$ is the azimuth angle segment contained in the discretized streamtube and θ is the azimuth position of the angle segment. The average force in the streamtube can be related to the force extracted by the individual blade element, F_x, when it passes through the certain streamtube. Each of the n blades' elements spends $\Delta\theta/\pi$ percent of the time in this particular streamtube. The average force is therefore composed of Eq. 18.

$$\bar{F}_x = nF_x \frac{\Delta\theta}{\pi} \qquad \text{(Eq. 18)}$$

The streamwise force on the individual blade element is then split into a force normal and tangential to the airfoil, Eq. 19.

$$F_x = -(F_n sin\beta sin\theta + F_t cos\theta) \qquad \text{(Eq. 19)}$$

In this equation the blade slope, β, appears for the first time. It is explained in detail later on. The normal force, F_n, and tangential force, F_t, are defined as Eq. 20 and Eq. 21.

$$F_t = ½ C_t \rho \frac{\Delta h c}{sin\,\beta} U_R^2 \qquad \text{and} \qquad \text{(Eq. 20)}$$

$$F_n = -½ C_n \rho \frac{\Delta h c}{sin\beta} U_R^2 \ , \qquad \text{(Eq. 21)}$$

where c is the airfoil chord length and U_R the relative velocity of the fluid at the airfoil. The coefficients C_t and C_n are based on the airfoil lift and drag coefficients, C_l and C_d, Eq. 22 and Eq. 23,

$$C_t = C_l sin\alpha - C_d cos\alpha \ , \qquad \text{(Eq. 22)}$$

$$C_n = C_l cos\alpha + C_d sin\alpha \ , \qquad \text{(Eq. 23)}$$

which are dependent on the angle of attack, called *aoa* or α, the angle between U_R and the airfoil chord line.

Equating Eq. 16 and Eq. 18 leads to Eq. 24.

$$\frac{nF_x}{2\rho A_S U_\infty^2} = \frac{U}{U_\infty}\left(1 - \frac{U}{U_\infty}\right) \qquad \text{(Eq. 24)}$$

The term on the right hand side is shortened to F_x^*, the non-dimensional streamwise force. With inserting Eq. 17, Eq. 19, Eq. 20 and Eq. 21 into Eq. 24 the expression, Eq. 25,

$$F_x^* = \frac{nc}{4\pi r}\left(\frac{U_R}{U_\infty}\right)^2 \left(C_n - C_t \frac{cos\theta}{sin\theta sin\beta}\right), \qquad \text{(Eq. 25)}$$

can be derived. In an iterative process the streamtube momentum equation, Eq. 26,

$$a = F_x^* + a^2 \qquad \text{(Eq. 26)}$$

is solved with the implicit induction factor a, Eq. 27,

$$a \equiv 1 - \frac{U}{U_\infty} \, . \qquad \text{(Eq. 27)}$$

Strickland explains in his paper the complete procedure. Here only the most important equations are mentioned and the theory is roughly sketched. More background information including Fig. 47 can be found in the original paper.

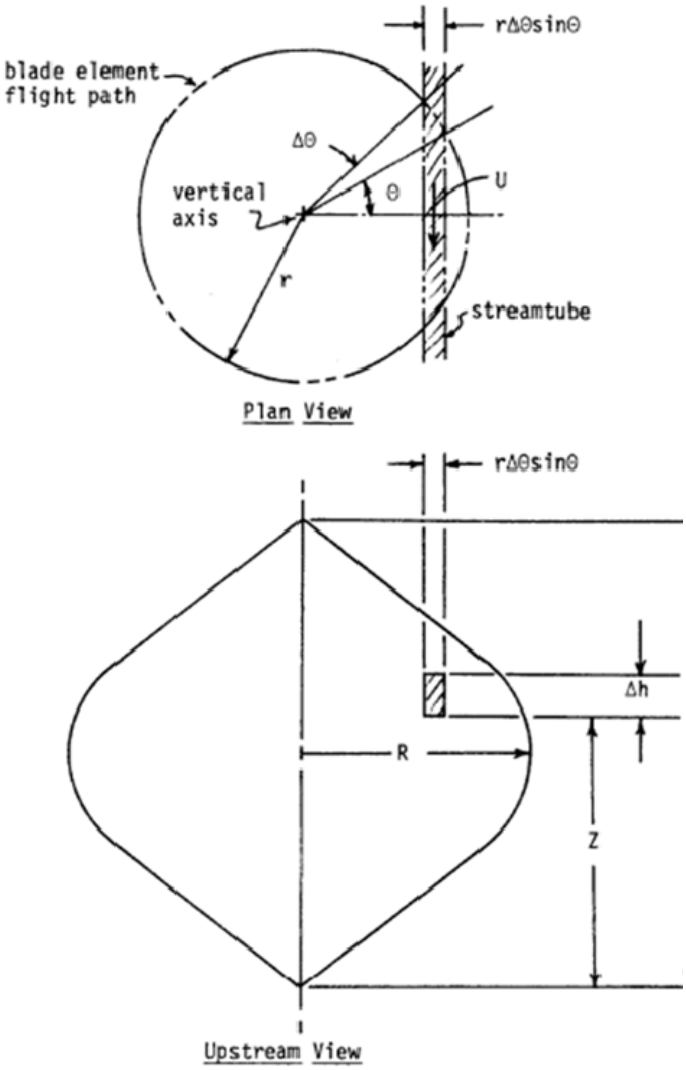

Fig. 47: Sketches explaining the streamtube method

4.2.3 Geometry

As input for the original DART code and so parameters which can be investigated are:

- H/R Ratio (*HR*)
- Solidity (σ)
- Profile Data
- Tip Speed Ratio (λ)

Another parameter is the rotor shape. Foremost, the code is designed for troposkien shaped vertical axis wind turbines, where the geometry is approximated with a sinus function, Eq. 28 (see Fig. 48).

$$r(Z) = Rsin\left(\pi \frac{Z}{H}\right) \qquad \text{(Eq. 28)}$$

The blade slope, β, is then given by Eq. 29 to 31.

$$r'(Z) = m = R\frac{\pi}{H}cos\left(\pi\frac{Z}{H}\right) \quad \text{(Eq. 29)}$$

$$\tan(\beta) = \frac{1}{m} \quad \text{(Eq. 30)}$$

$$\beta = \arctan\left[\frac{H}{R\pi cos\left(\pi\frac{Z}{H}\right)}\right] \quad \text{(Eq. 31)}$$

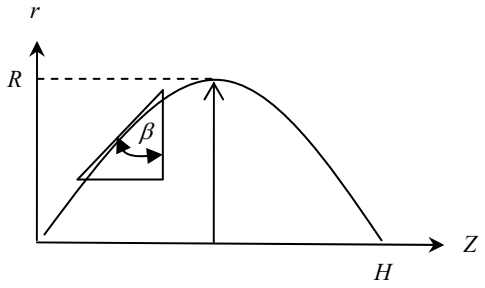

Fig. 48: Darrieus rotor geometry definition within DART code

The geometry of an H-rotor is implemented with

$$r(Z) = const. = R \qquad \text{and} \qquad \beta = \frac{\pi}{2}.$$

An inaccuracy is introduced by this manipulation. With an H-rotor tip-losses occur, different from the Darrieus configuration. For the Darrieus geometry the *H/R* ratio is a parameter of importance, since the slope is a function of it, whereas the *H/R* ratio in the H-rotor case does not have any meaning without any tip-loss correction.

Another important parameter within rotor design is the so-called solidity, σ, dependent on the number of blades, *n*, the chord and the equatorial radius, *R*, Eq. 32.

$$\sigma = \frac{nc}{R} \quad \text{(Eq. 32)}$$

The original code is assuming a constant chord for the whole blade. That means that if the radius is not constant over the rotor height, e.g. Darrieus rotor, the local solidity over the rotor height is neither. The local solidity is given by Eq. 33.

$$\sigma(Z) = \frac{nc}{r(Z)} \quad \text{(Eq. 33)}$$

In the manipulated version implemented in HAWTopt the chord length *c* is dependent on *Z* as well.

4.2.4 Rotor discretization

In the used multiple streamtube model, the rotor volume can be seen as if it was stretched to a flat plane, perpendicular to the inflow. Such an analogy is used, because the model does not distinguish between upstream or downstream rotor parts. That is also why only symmetrical profiles can be used. In the model it is assumed, that throughout a streamtube the same induced velocity is present and the streamtube deflection is neglected. In this way the profile at e.g. θ=5° and at θ=355° (see convention Fig. 49, left) are treated in the same way. Furthermore, each streamtube has virtually the same width in the plane analogy.

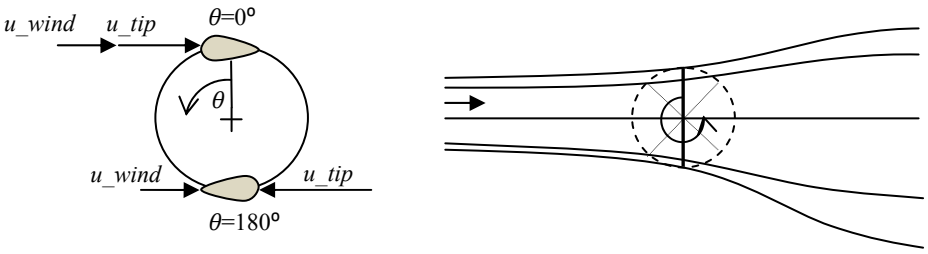

Fig. 49: Azimuth angle convention (left); plate analogy and streamtubes (right)

So, the rotor is divided into angular pieces of the same size, but it is also divided into horizontal slices of the same height (see Fig. 50). In the original code the angular section amount is defined by the parameter *NT* and the horizontal section amount by the parameter *NZH*. *NT* is dividing half of the rotation and *NZH* is dividing half the rotor height. For more details, study the basic code in [69].

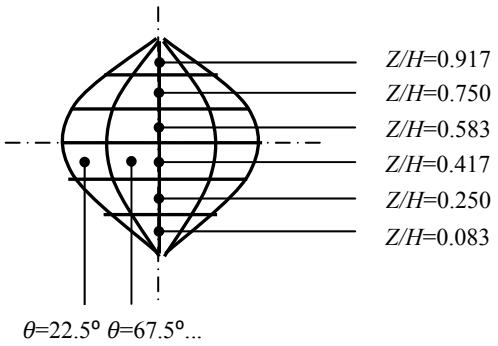

Fig. 50: Rotor sectioning in height (slices) and azimuth

For each of these elements the angle of attack, *aoa*, normal force, F_n, tangential force, F_t, induction factor, a, and local power coefficient, C_{Plocal}, are calculated. By summing up the elements with respect to their relative contribution, an average power coefficient, C_P, of the rotor is derived for different λs. The local λ is defined as

$$\lambda(Z) = \frac{2\pi r(Z) rps}{U_\infty} . \qquad \text{(Eq. 34)}$$

4.2.5 Design directives

There are some general design rules for vertical axis wind turbines, which of course depend on the purpose of the wind turbine. And most of the rules are applicable for horizontal axis wind turbines as well. Based on parameter studies conducted with the help of the original DART code with a small modification to make it applicable to H-rotor geometries, design directives can be drawn and are summarized in this section.

Some extractions of the case study accompany the design directives. The airfoil data for NACA0018, which are mainly used for the test cases, can be found in Appendix E. The graphs along the directives are results from whether an H-rotor, indicated with H on top of the graphs or a Darrieus rotor, indicated with SIN above the graphs. Both rotor geometries are considered to have a radius of R=0.83m. Generally spoken, the design process is an iterative process and requires user's insight to a certain extend.

4.2.5.1 Tip speed ratio

Without any specific investigations, some general rules about the tip speed ratio can be given. The tip speed ratio sets the speed of the blade tip in relation with the incoming wind speed and is thereby a parameter for the resulting wind speed vector. But besides aerodynamic issues it is also of importance in noise emission and safety issues. Mertens states [5], the noise emission of a turbine is dependent on the tip speed ratio as

$$\lambda^5 \sim noise.$$

Especially in the urban area it might be advisable to design turbines with a rather low tip speed ratio. Furthermore, high tip speed ratios for small wind turbines are connected to high rotational speeds. A possible blade loss or even only small parts of it at high rotational speeds do not conform to a high safety demand.

4.2.5.2 Profile variation

The results for the performance of a rotor are highly depending on the airfoil data. That means that if a slightly different set of C_l–C_d is used for the same profile, the results can be quite different from each other. Especially for low Reynolds numbers the differences might be rather big. Applying a multiple streamtube model to a VAWT limits the use of profiles to symmetrical ones. Examining the performance of a rotor using various NACA00XX profiles at *Re*=360'000 shows that the C_{Pmax} values are very close to each other, whereas the tip speed ratio where they occur spreads a little bit (see Fig. 51).

The choice of profile does not seem to be the most important design parameter, when using the code together with symmetrical airfoils. More important is a reliable set of data. In the initial phase of a design process trying a couple of profiles would be advisable though.

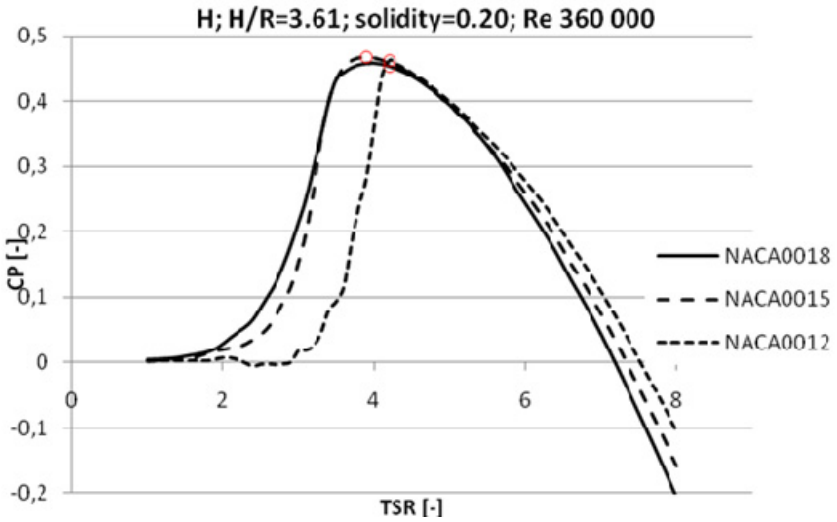

Fig. 51: C_P vs λ plot; profile variation for an H-rotor; NACA0012, NACA0015, NACA0018, all at Re 360'000. C_{pmax} indicated with red circles

4.2.5.3 Reynolds number variation

For small-scale wind turbines the Reynolds numbers on the blade sections are likely to be low. High Reynolds numbers are essential in order to reach reasonable C_P

values. The Reynolds number sets the inertial effects into relation with the viscous effects of the flow and for example an airfoil as in Eq. 35,

$$Re = \frac{uc}{\nu}, \qquad \text{(Eq. 35)}$$

with u as a characteristic velocity, c as the airfoils chord length and ν as kinematic viscosity of the fluid, mostly air. Low Reynolds numbers flow is dominated by viscous effects and effects of increasing boundary layer thickness become more pronounced. The low flow velocity field adjacent to the airfoil is rather vast and the effective airfoil geometry is significantly altered, resulting in high drag and low lift coefficient. Furthermore, at very low Reynolds numbers the whole boundary layer or most of it is laminar. Such boundary layer is less capable of handling an adverse pressure gradient without separation. Laminar separation bubbles do appear, because of the flow's inability to make a transition to turbulent flow in the attached boundary layer on the airfoils surface. The resulting pressure drag over the region of the laminar separation bubble is responsible for the relatively high airfoil drag. Low lift and high drag coefficients lead to low C_P values.

The case studies shows that increasing the Reynolds number increases the C_{Pmax} value significantly, where mainly Reynolds numbers between Re=40'000 to 360'000 are examined (see Fig. 52). For higher Reynolds numbers the changes in C_{Pmax} (red circles in the figure) become very small compared to the lower Reynolds numbers. For the lower numbers the $\lambda(C_{Pmax})$ decreases noticeable with increasing Reynolds number followed by a slightly reversed trend until $\lambda(C_{Pmax})$ stays more or less constant for Re>1'000'000. A matter of interest could also be that with increasing Reynolds number the λ range of operation broadens towards lower λ values as well as towards higher λ values. That is of great importance for the operational wind speed range.

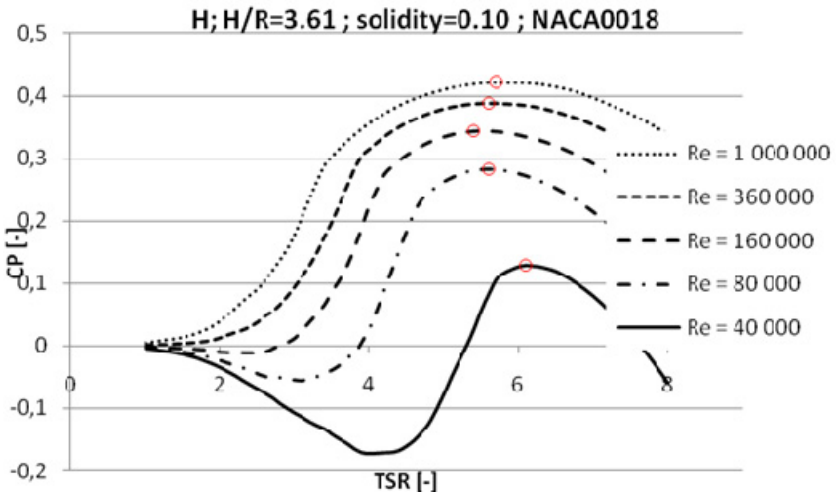

Fig. 52: C_P vs λ plot; Reynolds number variation for an H-rotor with NACA0018; Re=40'000-1'000'000. C_{pmax} indicated with red circles

The Reynolds number is a function of the local relative velocity at the blade element, the elements chord length and the viscosity of the fluid.

$$Re_{local} \sim c \qquad\qquad Re_{local} \sim U_R$$

The designer has influence on the chord length and number of blades, which are in combination with the rotor shape directly connected to the solidity. The local relative velocity at the blade is composed of the reduced wind velocity in the rotor plane and the blade element velocity, depending on the rotational speed and radius.

4.2.5.4 Solidity variation

The solidity is defined as in Eq. 32. With change in the rotor solidity the C_{Pmax} value as well as the $\lambda(C_{Pmax})$ value varies considerably (see Fig. 53). $\lambda(C_{Pmax})$ decreases with increasing solidity. An intermediate value for the solidity bears the highest C_{Pmax} value.

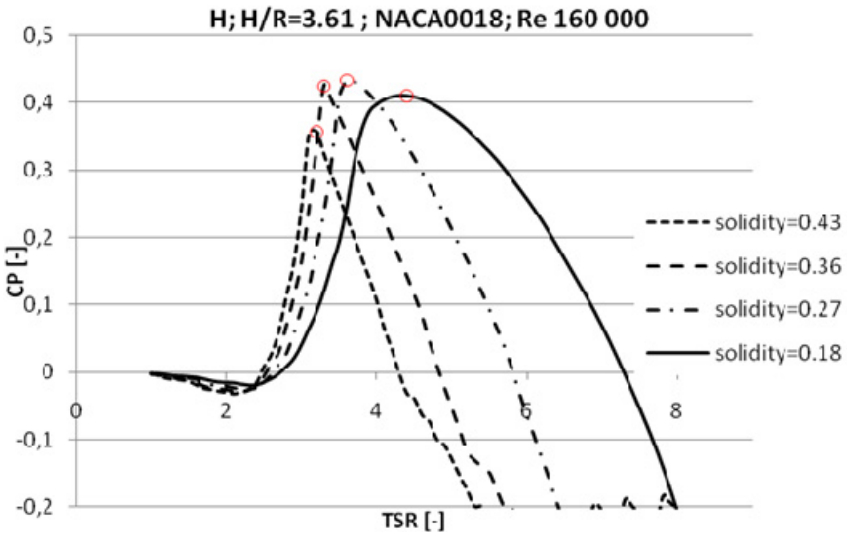

Fig. 53: C_P vs λ plot; solidity variation for an H-rotor with NACA0018 at Re=160'000; σ= 0.18-0.43. C_{pmax} indicated with red circles

The lower the solidity gets, the higher the λ_{max} and broader the operational λ range becomes. λ_{min} does not vary too much. So, in case of a desired low cut-in wind speed a low solidity design is proposed. Surely, a sufficient Reynolds number still has to be reached with the shorter chord connected to a lower solidity. A rotor configuration with fewer blades could be considered as well in such a case, which means that for the same solidity a larger chord per blade can be employed.

4.2.5.5 Rotational speed

Choosing and controlling the rotational speed influences λ directly (Eq. 34). λ is the ratio of the velocity of the blade element due to the rotor rotation over the undisturbed wind velocity. This ratio is influencing the *aoa*. The higher the rotational speed is chosen in relation to the wind speed, meaning a higher tip speed ratio, the more stable is the *aoa* over one rotor revolution, meaning consequently the torque over one revolution as well, which is shown later on.

Furthermore, the rotational speed is linked to the relative velocity at the blade, which again is directly connected to the Reynolds number. The relationship between rotational speed, λ and wind speed is important for the system design. Since the tip speed ratio is decisive for the *aoa* and with that more or less the rotor C_P at that ratio, choosing a constant rotational speed does decide at which wind speed this C_P occurs. That also means, that for each wind speed an optimal rotational speed exist. Low rotational speed means low cut-in wind speeds, but at the same time the actual Reynolds number decreases (see Fig. 54).

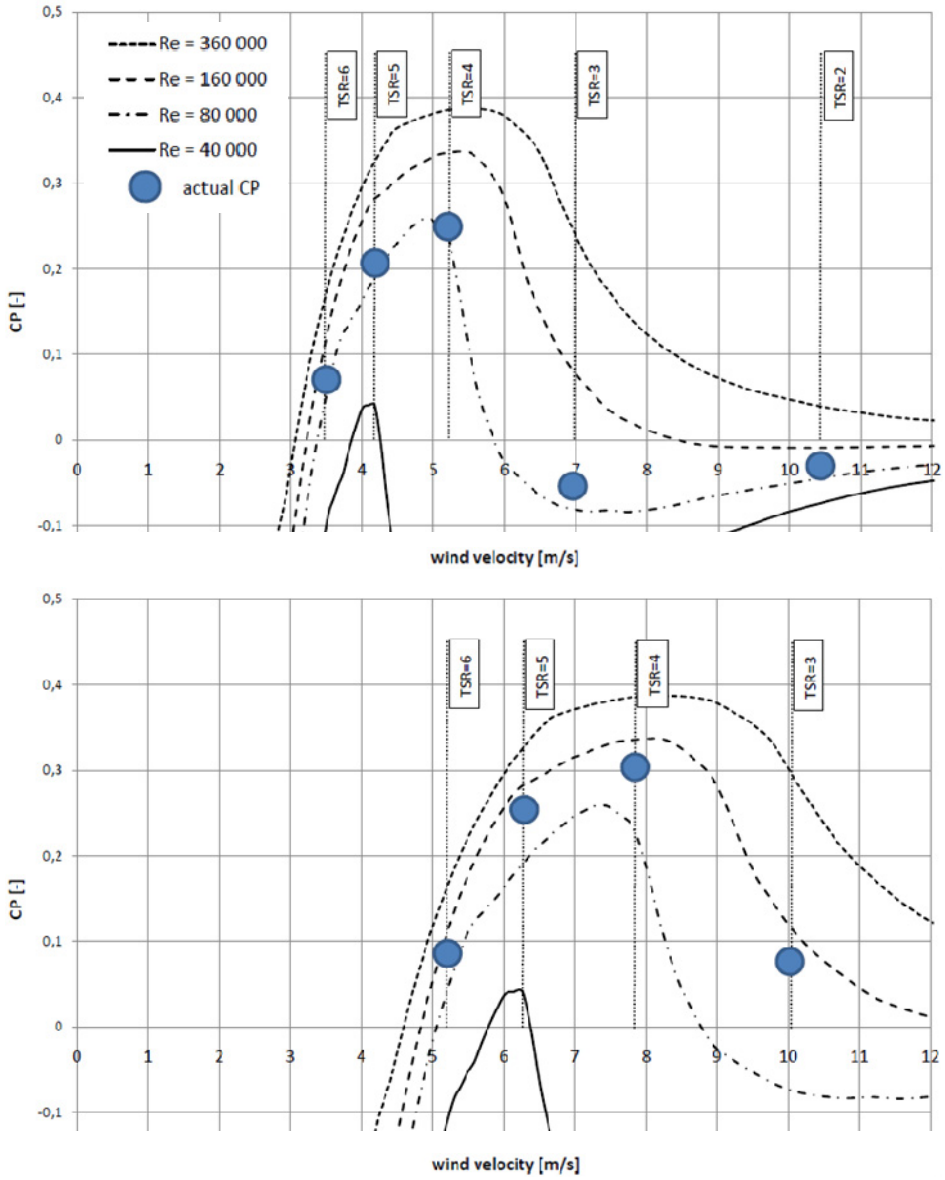

Fig. 54: Actual C_P determination for a three bladed Darrieus rotor (σ=0.27; NACA0018; H/R=2.0 and R=0.83m) operating at 4Hz (top) and 6Hz (bottom)

4.2.5.6 Blade shape and twist

The fact, that with the DART code for each discretized blade element an angle of attack, *aoa*, normal force, F_n, tangential force, F_t, induction factor, a, and a local power coefficient, C_{Plocal} is calculated and these values are direct or indirect output for each element per azimuth position, make it possible to conduct one more parameter study on the base of an H-rotor.

For this examination it is important to divide the H-rotor into a sufficient number of horizontal slices. Outside the DART program an excel sheet is prepared to examine the blade twist's influence on the rotor torque by summing up the equivalent elements per rotational step (see Fig. 55, left). The smallest rotational step size is equal to the angular element size. Depending on the blade number and assuming they are equally distributed around the center the rotor torque per rotational step can be calculated (see Fig. 55, right).

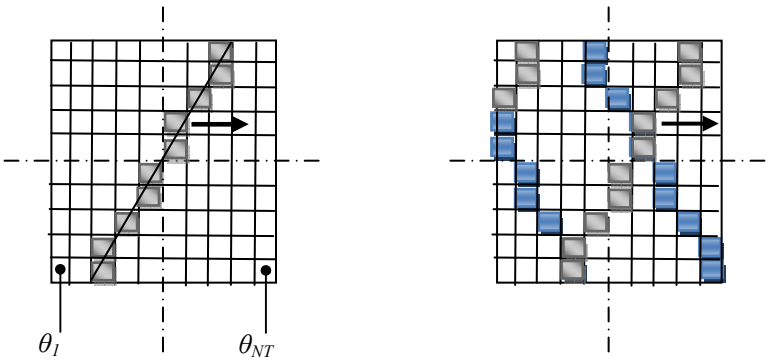

Fig. 55: Element summation to determine forces at a certain azimuthal position found for one blade (left) or more (right), where the blue elements represent blade elements on the downwind side of the rotor and grey elements the ones on the upwind side

With that, the last parameter study is about the blade angle density, *BAD*, which is defined as in Eq. 36,

$$BAD = \frac{n\varphi}{360°} \ , \qquad \text{(Eq. 36)}$$

where n is again the number of blades and φ is the angle one blade spans over (see Fig. 56, left). To start with, the C_P *vs* λ curves for a Darrieus and the H-rotor, investigated in the following, with the same *H/R* ratio are plotted in Fig. 56, right.

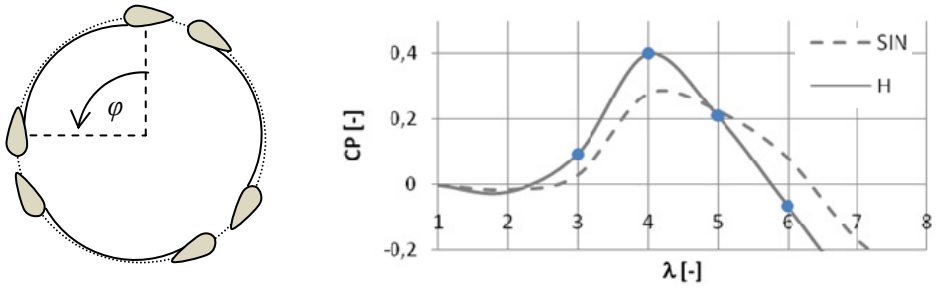

Fig. 56: Left: illustration of the span angle for the view from top on the rotor; right: C_P vs λ for H-rotor and Darrieus rotor, both with the same H/R radius and same Reynolds number

In general, the C_P vs λ characteristics for an H-rotor in comparison to a Darrieus rotor are reaching up to higher C_P values, have a more narrow λ band width and a sharper shape around the C_{Pmax}. This can be explained by the fact, that an H-rotor with a constant chord has the same solidity over the rotor height, since all blade elements have the same distance to the axis, whereas a Darrieus rotor with constant chord has a changing solidity over the rotor height. That means that only a part of the bended blade actually is operating at an optimal σ-λ-ratio. Both designs though, H and Darrieus, follow the behavior that the lower σ gets, the greater is the λ where the corresponding C_{Pmax} occurs. Furthermore, with decreasing σ the λ range broadens and the curves become more flat around the maximum C_P. Depending on the design frame, high λ can be advantageous to start the energy production at low wind velocities. Besides the energy production, another design issue is how the torque from the blades is transmitted to the tower over one rotation. In the following the *BAD* parameter and its influence on the torque contribution over one rotation is examined for λ=3.0; 4.0; 5.0. The used settings for the rotor geometry, profile and constant rotational speed are listed in Table 8.

Table 8: Geometric and operational input for BAD investigation

geometry	H	
H	4.0	[m]
R	0.83	[m]
H/R	4.8	[-]
n	3	[-]
c	0.10	[m]
$\sigma=nc/R$	0.27	[-]
profile	NACA0018	
BAD	0.0; 0.75; 1.50	[-]
Re	160 000	[-]
rotational speed	350	[rpm]

Fig. 57 shows the results for the torque delivered to the tower by the single blades and the total torque it experiences, depending on the azimuth position of the single blades.

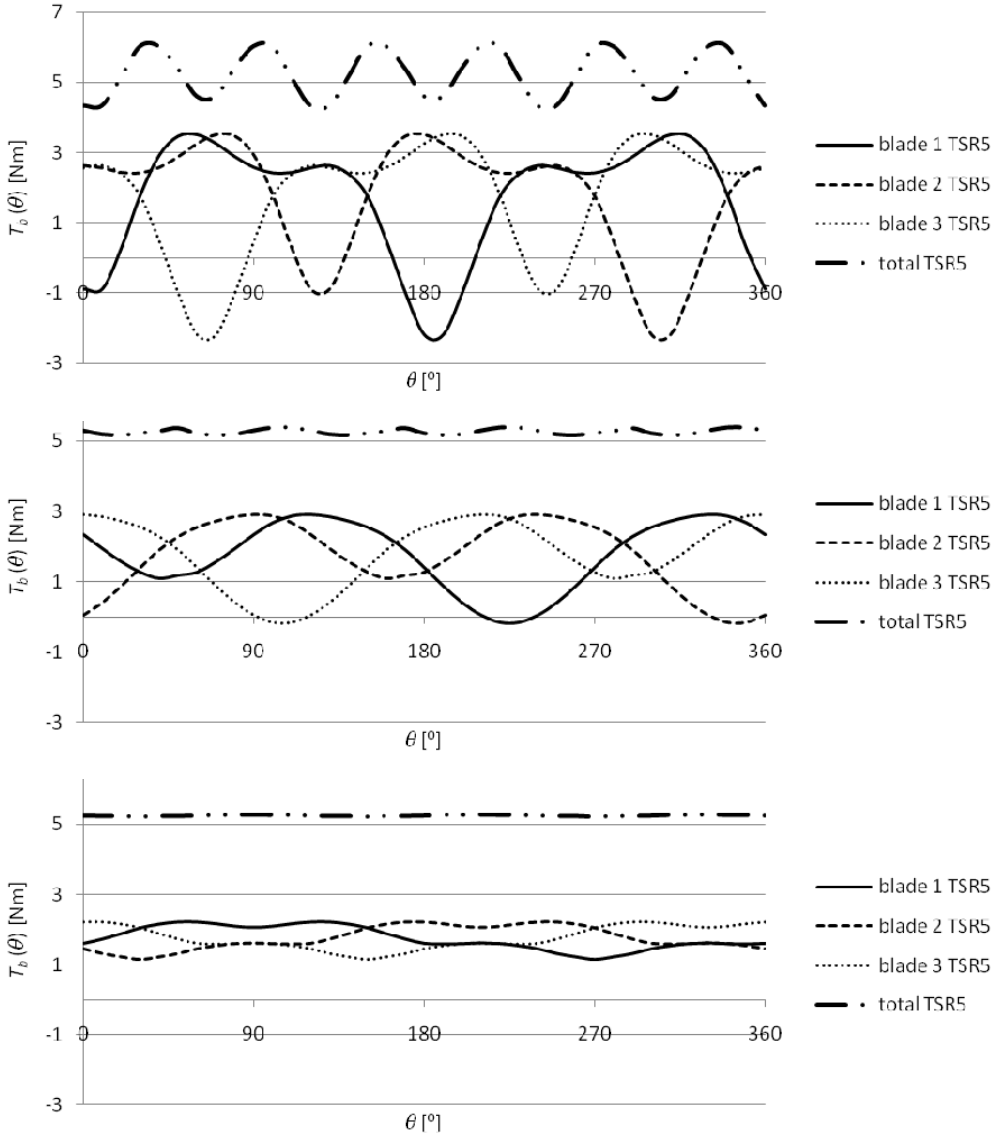

Fig. 57: Azimuthal torque delivered by the single blades for λ=5 with BAD=0.00; 0.75; 1.50 (top to bottom)

For all the three *BAD* cases the sum of the total torque is the same, but for the H-rotor without slope, the total torque is oscillating six times per rotation with amplitudes of about 1Nm. The more the blades are twisted, the lower gets the amplitude. With a reduction of this tower torque variation, vibrations induced to the tower are reduced as well. On the other hand bending moments in the blades are introduced, due to the uneven distribution of forces along the blade. This issue is not investigated.

Thinking of small vertical axis wind turbines which might be installed on building rooftops or façades, a major issue is the transmission of vibrations from the spinning device to the buildings structure. Taking the supporting arms into consideration, which connect the blades with the tower and transmit the torque, it can be seen that the higher the *BAD* factor is the lower the change in torque delivered by the single blades gets. In this way, alternating loads on the supporting structure can be lowered remarkably.

The graphs in Fig. 57 are only for the operation at λ=5. Operation at λ=5 means that the local wind velocity is manly dominated by the contribution of the rotational speed component and with that the angle of attack changes moderately over one revolution.

In Fig. 58 the torque delivered by one blade at different λ is plotted. For the case of the non-twisted blades it can be clearly seen that the torque contribution by a single blade varies significantly over one revolution, especially for low λs. If the rotor is operating at λ=3, the sum of the total torque is positive, but with considerable variations over one revolution. For some azimuth positions, the total tower torque reaches even negative values. With twisted blades the operations becomes smoother (see Fig. 59). Although the blade torque contribution at λ=3 varies vastly, the total torque on the tower does not bottom out at negative values for *BAD*=1.5.

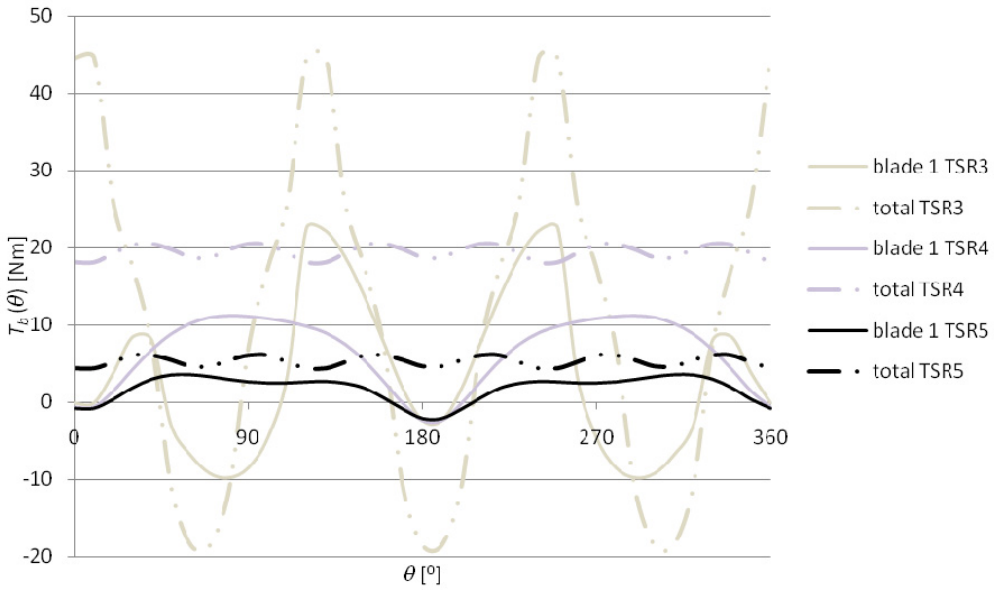

Fig. 58: Azimuthal torque delivered by one blade and total torque on tower at λ= 3; 4; 5 for BAD=0.00

Investigations on this topic are carried out by others as well. The work of [10] for example is conducted with a more advanced method including the deficiency in the rear rotor half for example, but the basic behavior is the same.

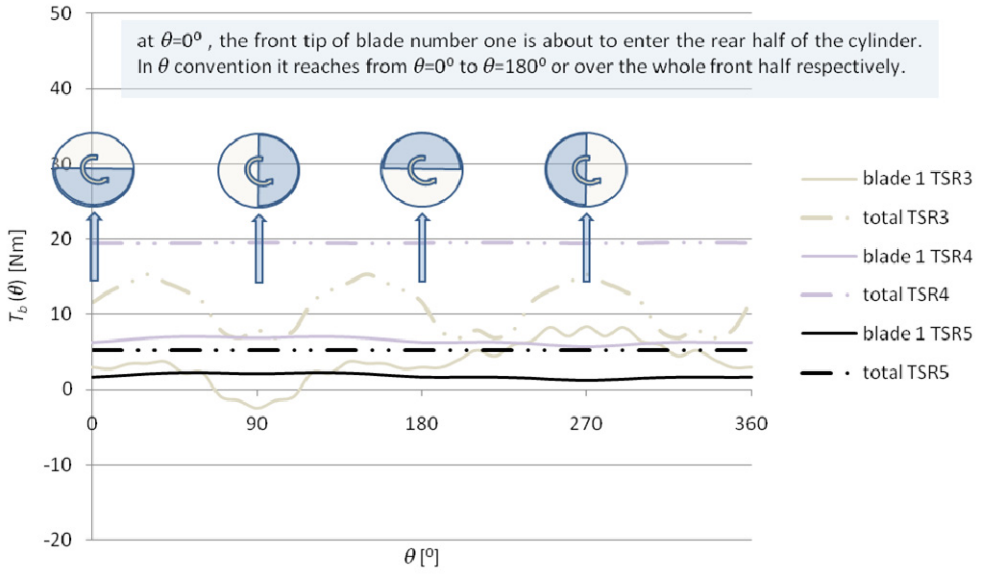

Fig. 59 Azimuthal torque delivered by one blade and total torque on tower at λ= 3; 4; 5 for BAD=1.50

4.3 VAWT Rotor Design Optimization

With the modified DART code implemented into HAWTopt capable of calculating tapered blades, instead of only constant chord distributions, one optimization option is the local elements' chord length. A vertical axis rotor can be optimized for a certain rotational speed at a certain inflow wind velocity. In the following the characteristics of a Darrieus rotor with constant chord length are shown. The working point for its peak performance is the design point for an optimization (*opti1*). HAWTopt with the modified DART code implemented is from this point called VAWTopt.

For the chosen initial design with H/R=2.4, R=0.83m and a constant chord of c=0.075m, rotational speed of 240rpm and a NACA0018 at Re=80'000, the C_{Pmax}=0.23 is found for an inflow velocity of 4.8m/s and λ=4.35, respectively. The rotor geometry, profile data and rotational speed are maintained for the first optimization. As design point the wind velocity of 4.8m/s is chosen. The design objective is maximum rotor efficiency, C_{Pdsg}, at that design wind speed, u_{dsg}. Constrain control points are distributed along the blade. The control points are connected to each other via linear interpolation to start with.

In Fig. 60 the initial design and corresponding C_P vs λ performance is shown.

The design optimized in 100 iteration steps for a λ=4.35 is shown in Fig. 61. How the layout performs for a range of λ is plotted in the same figure. Plotting among others the two graphs in Fig. 62 shows the shift of the C_P curve due to the improved chord distribution. The chosen C_l-C_d airfoil polar is a NACA0018 at Re=80'000. This decision is made, because 80'000 was closest to the average Reynolds number, Re_{ave}, read out from the initial design output file at λ=4.35. Optimizing at that point and then calculating on the resulting geometry through the range of λ=3.9-6.1 shows that the Reynolds number on the most effective parts of the blade is very close to Re=80'000. In this case it is suggested that it is acceptable to use the same profile polar for all wind velocities and λ's, respectively. To optimize for an incoming wind of 4.8m/s is reasonable too, considering the urban environment.

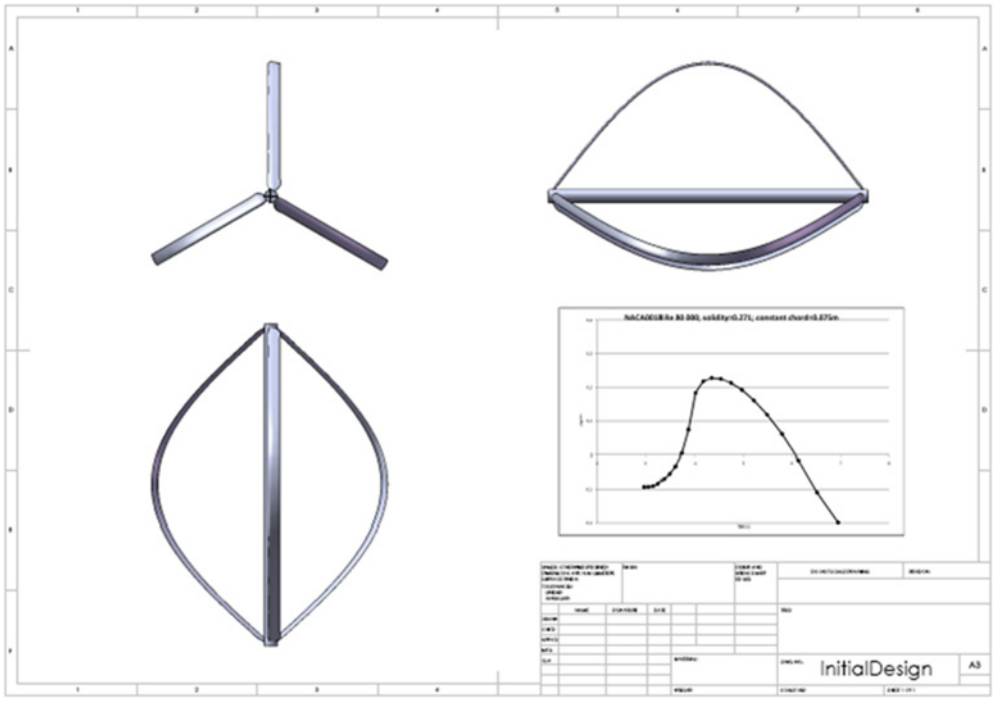

Fig. 60: Technical drawing of the initial rotor geometry

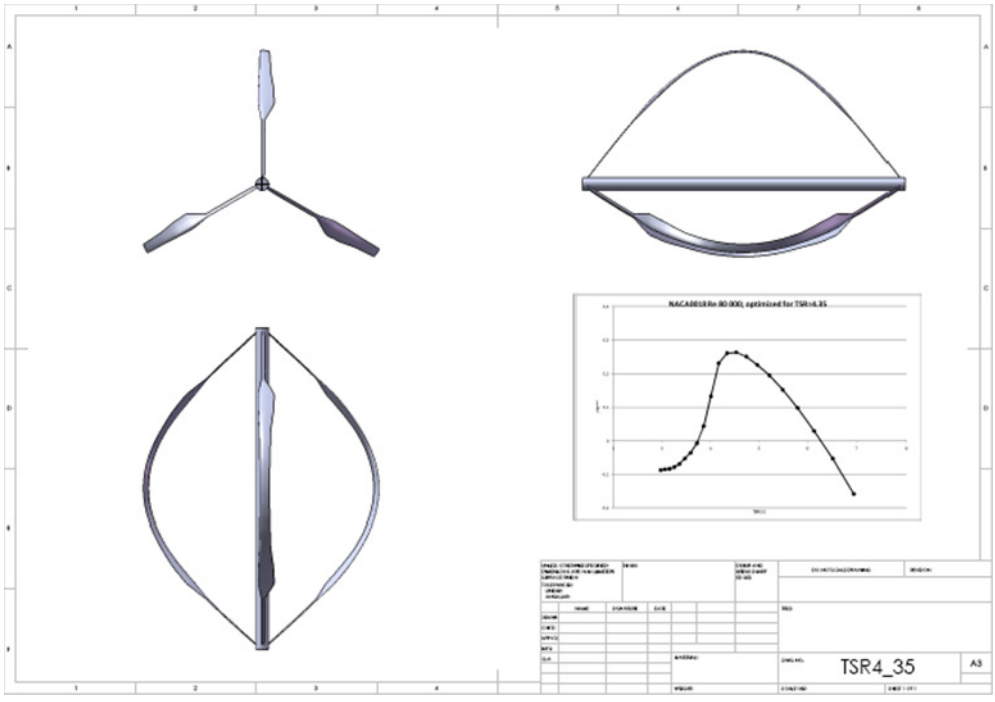

Fig. 61: Technical drawing of the rotor optimized for λ=4.35

Another option in the VAWTopt program structure is the optimization over a certain range of wind velocities, where the single wind velocities can be weighted (*opti2*). The wind range from u=4.2m/s-5.2m/s is subdivided in equal intervals weighted each with the factor 0.2. It actually does not lead to big changes in terms of C_P compared to one-point optimization (see Fig. 62).

Beyond that, another optimization strategy is to optimize the actual energy production for a defined wind velocity range where the Weibull distribution is taken into account (*opti3*). That actually is pretty interesting for wind turbine designs meant to be erected in the urban environment, since the wind potential is rather different from the one found on the open land. Wind data are collected at the rooftop of a building situated in the city of Copenhagen and Weibull parameters are found to be k=2.0 and A=4.3m/s for a certain period of the year. These values are used for the optimization for a wind range between u=3m/s-6m/s with 15 intervals.

The optimized design has a rather small chord length and directly connected to this is a decrease in Reynolds number, so that the polar for Re=80'000 is not appropriate anymore. Average Reynolds numbers are found to be about Re=50'000. Predicting the performance with the optimized geometry but with the C_l-C_d polar for Re=40'000 the performance shows rather poor quality (*opti3.2*). Changes in Reynolds numbers in such low Reynolds number areas are bonded to distinctive increase or decrease in lift and drag coefficients. In general, it looks like the design for the prescribed Weibull distribution pushed towards high λs, which is clear since high λs are connected to low wind velocities, when operating at constant rotational speed. High λs are again connected to low solidities. So, in another optimization shot, it is tried to run the same optimization, but at Re=40'000 (*opti4*). It does not change the C_P curve very much. In Table 9 the optimization cases are listed and the C_P vs λ can be seen Fig. 62. C_P vs u, chord distribution vs rotor height and actual power at the single wind speeds are plotted in Fig. 63.

Table 9: List of the design optimization parameters

	optimization	**design point**	**parameters**	***c***	***Re***	**rot. speed**
initial	-	-	-	const	80'000	const=240rpm
opti1	one-point	u =4.8m/s	-	var.	80'000	const=240rpm
opti2	range	u =4.2-5.2m/s	-	var.	80'000	const=240rpm
opti3	Weibull	u =3.0-6.0m/s	k=2.0; A=4.3m/s	var.	80'000	const=240rpm
opti3.2	-	-	-	var.	40'000	const=240rpm
opti4	Weibull	u =3.0-6.0m/s	k=2.0; A=4.3m/s	var.	40'000	const=240rpm

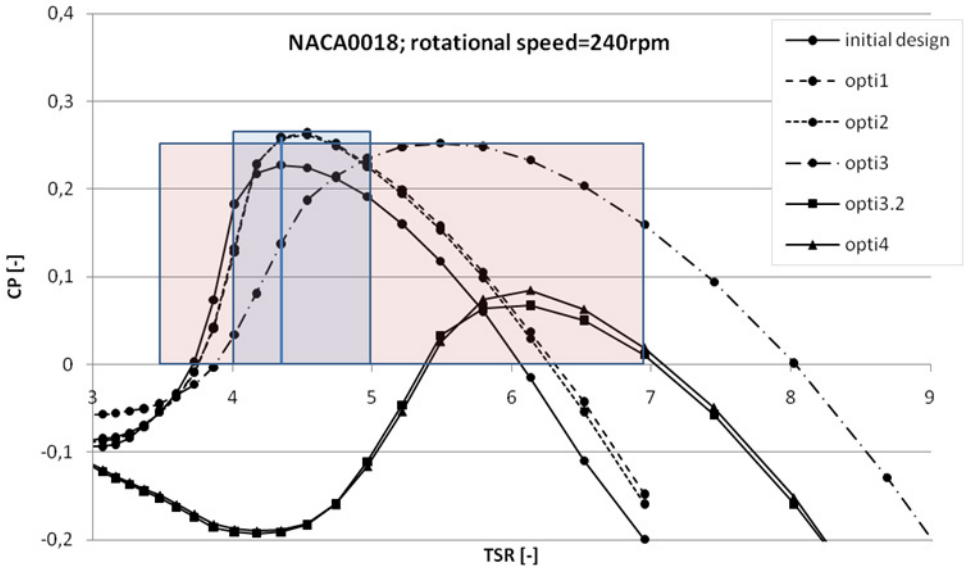

Fig. 62: Optimized designs graph; C_P vs λ curves

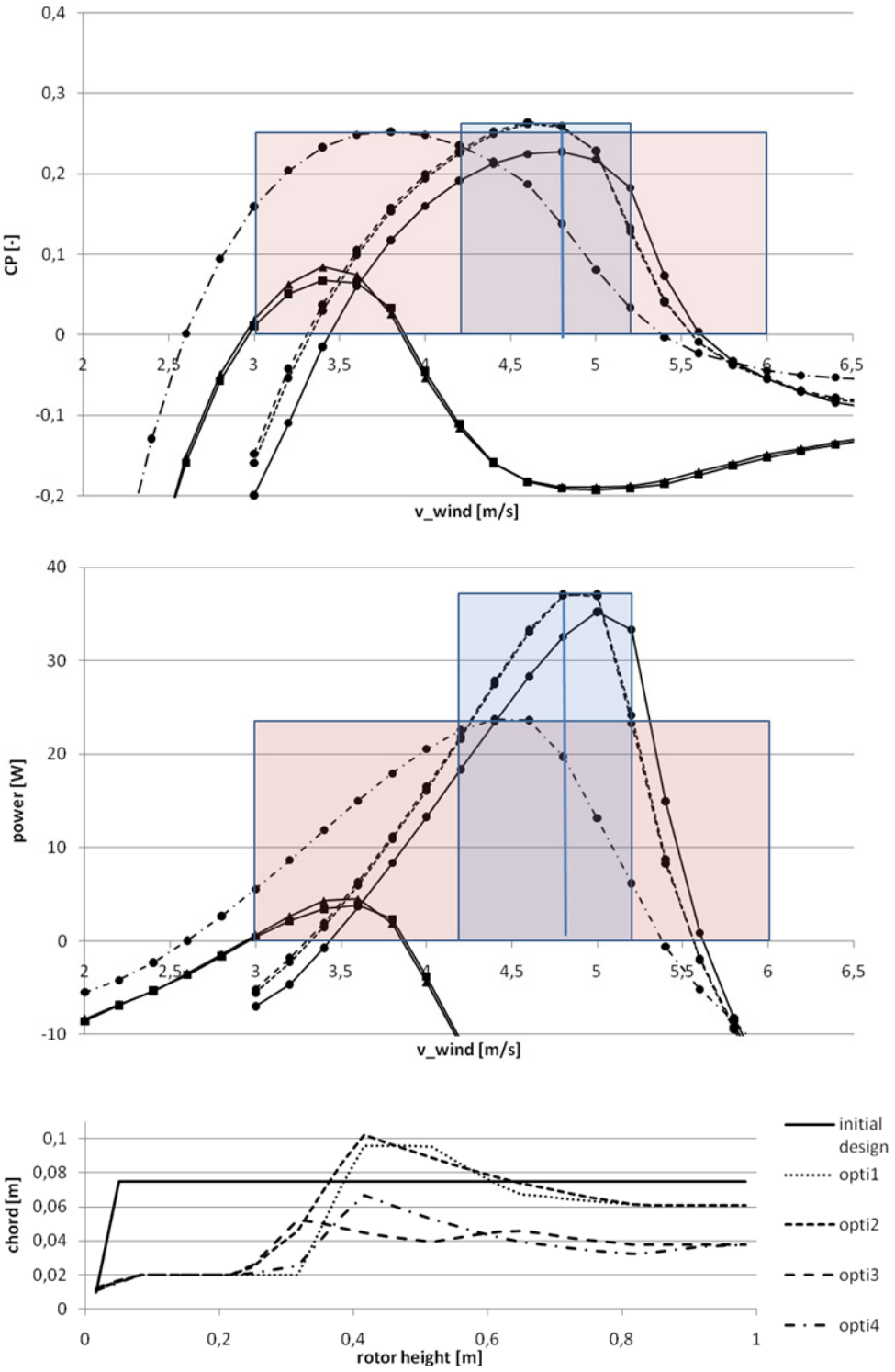

Fig. 63: Optimized designs graphs; top: C_P vs wind speed; middle: Power vs wind speed; bottom: chord vs rotor height

The power is not satisfying for a wind turbine with a swept area of about A_{rotor}=2.1m^2. Different design strategies can be followed to obtain a power output which is more meaningful. One strategy is to change the rotational speed to higher values. In this way the turbines performance curve is pushed towards higher wind velocities. Since the power is proportional to the wind speed cubed, higher power

output can be reached. On the other hand, the power curve then starts at higher wind speeds. These optimization cases are meant to demonstrate the design opportunities, but not to demonstrate a final design.

4.4 HAWT Design- An Autarkic Energy System

In this section a small-scale HAWT is investigated. Mounted on, e.g. a bike, the citizen is cycling and generating most of the wind. While the bike is parked and wind is blowing, energy is produced, meant to charge small electrical items. Different from the prior presented VAWT rotor design, the design is mainly driven by a given generator and its characteristics.

4.4.1 Design space

A pre-estimation of conditions is framed to create a base for the design of a small autarkic energy system. The requirements for such a system are shown in Table 10.

Table 10: Design space parameters and their initial guess

small rotor diameter	d~0.20m
number of blades	n=2 or 3
tip speed ratio	λ ~1.5-5
design wind speed	$u_{bicykle}$=u_{dsg}=25km/h=7m/s
C_P-curve	flat optimum
minimum C_P	~ 0.20
yaw angle	fixed or free
material	reinforced plastic, inflatable, wood…
manufacturing method:	RPT= rapid prototyping, moulds...
generator size:	geometric and energetic fitting
generator characteristics:	low torque for low velocities
usage of power:	charge MP3 player, mobile phone, generate light…

Compared to large-scale turbines other boundary conditions for the design of a mini-scale turbine must be considered. With a diameter of d=0.2m, 2 or 3 blades, respectively, a maximum rotational speed of 2000rpm corresponding to a tip speed of u_{tip}=21m/s, the design Reynolds number is in range of Re_{dsg}=30'000-50'000. Airfoils for this range are found in model aircraft applications (e.g. NACA0012). The twist and chord length distribution for the rotor design are obtained with the design tool developed by Risø DTU, HAWTopt [70], with a tip speed ratio in the order of λ=3. Furthermore, the efficiency of such a configuration is low and therefore the production costs must be kept at a reasonable level. Two rotor design approaches are considered; the one focused on a simple manufacturing process, but not necessarily aerodynamically shaped and the other focused on the aerodynamic design with less focus on the manufacturing process. For the first experiments, a 24V direct current motor is used as generator. The characteristics in the generator mode are obtained by connecting it to a motor of the same type, logging the rotational speed and the voltage of the generator circuit loaded in series with different resistances (0.47Ohm, 2.7Ohm, 5.6Ohm and 10Ohm). In this way the moment on the shaft versus rotational speed, current and power over the load resistor are derived.

Starting point for the rotor layout is a flat, slender plate to be twisted in a certain way and with that simple to produce (see Fig. 64). With the aim to reach power coefficients, C_P, able to deliver sufficient power to the generator shaft, variation on parameter constraints follow, like various twist distributions, chord distributions and rotor diameters, d, but also parameters like the design tip speed ratio, λ_{dsg}, and last but not least the design angle of attack, aoa_{dsg}, is investigated.

As airfoil the NACA0012 airfoil is selected, since it is symmetric and thick enough to be approached from a flat plate (f. e. chord length of 30mm corresponds to a thickness of 3.6mm). The airfoil characteristics predicted with xfoil6.96 [81] are plotted in the following section.

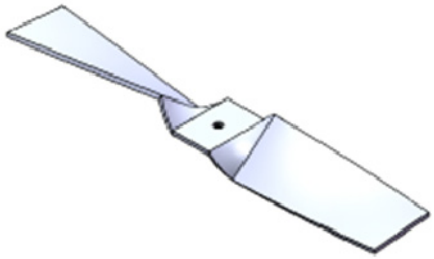

Fig. 64: Flat, twisted plate as design starting point

4.4.2 Design method

The restricting parameters are a maximum rotational speed of 2000rpm, a design wind speed of u_{dsg}=7m/s, corresponding to a bike speed of 25km/h without additional wind, and the generator shaft diameter with 4mm limiting the maximum rotor diameter with a rule of thumb to approximately 0.40m. In the following, the characteristics for the generator and airfoil are described and the way to find different rotor designs and their individual properties.

4.4.2.1 Airfoil

As airfoil a NACA0012 is chosen and aerodynamic data obtained with xfoil6.96 [81] for low Reynolds numbers, ranging between 20'000 and 80'000. Fig. 65 shows the predicted values.

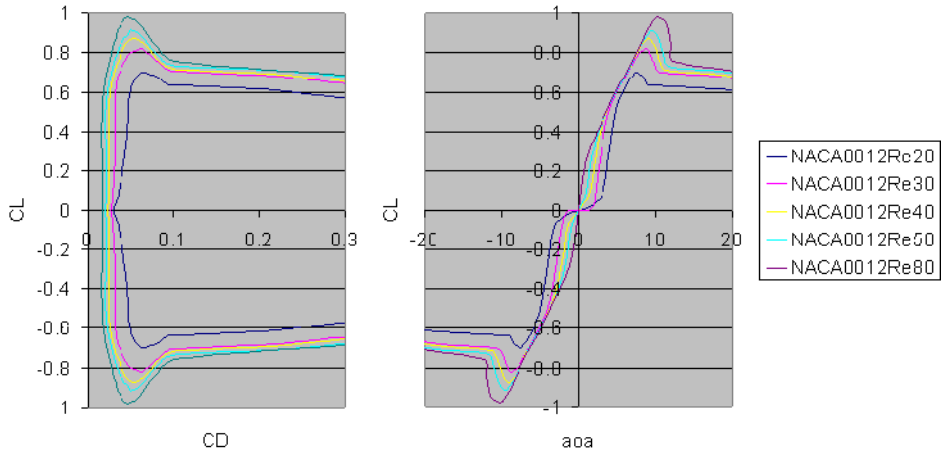

Fig. 65: NACA0012; left: C_l vs C_d; right: C_l vs aoa; both for Re=20'000 to 80'000

4.4.2.2 Generator

Two 24V direct current motors are connected stiffly at their axes, while one is operating in motor mode, driving the other in generator mode (see Fig. 66, top) and see the motor data sheet in Appendix F. In this way the input power for different rotational speed is measured. With different experimental set-ups the power used by the motor itself, the mechanical resistance of the generator and the additional electric resistance, depending on the connected resistor load, 10Ohm, 5.6Ohm, 2.7Ohm, 0.49Ohm, are ascertained and are plotted in Fig. 66, bottom. How the experimental set-ups are interconnected can be seen in the figure in Appendix G. In the next step a rotor design delivering the power to the generator shaft is investigated. Thereby the

rotor design is governed by the generators characteristics, since the rotor performance has to be fitted to the performance of the generator.

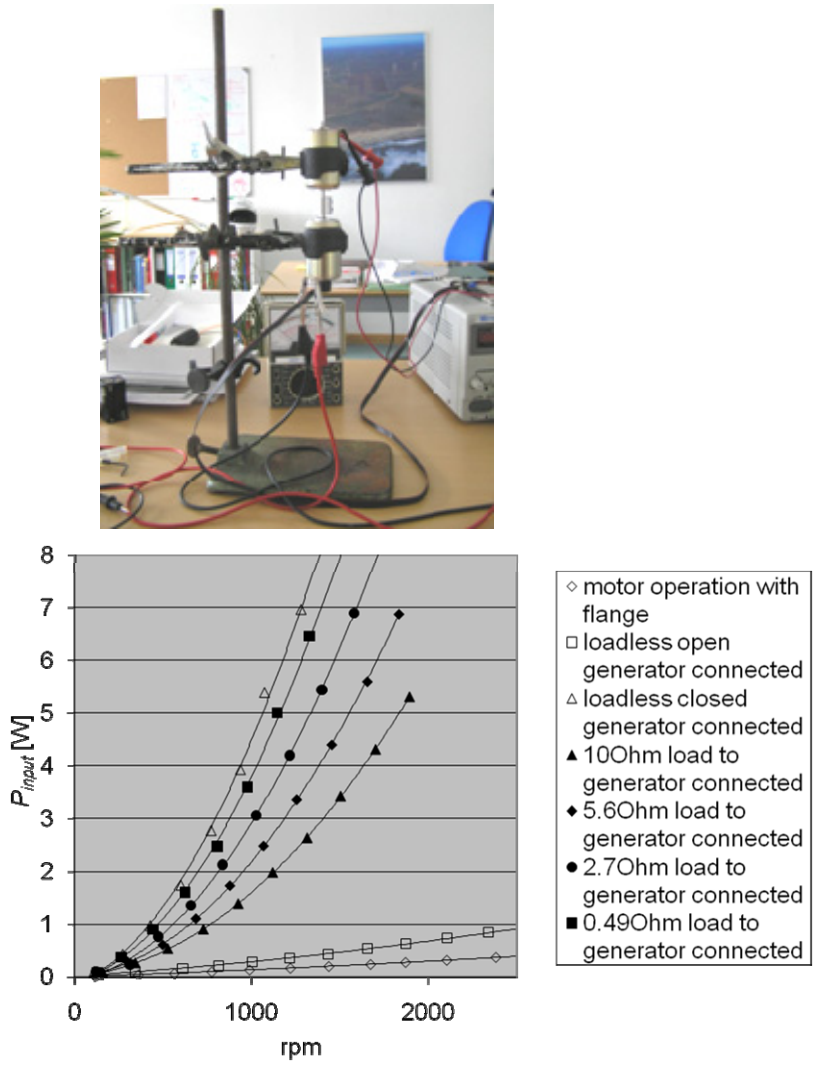

Fig. 66: Top: two motors stiffly connected on their axes; bottom: experimentally derived generator power curves

4.4.2.3 Rotor design

With the design tool HAWTopt developed by Risø DTU [70], and the airfoil data from xfoil6.96 [81] different constrained configurations are found and modified in order to approach the generator demand when a 10Ohm resistor is connected.
Design variables are

1. shape constraints
2. design tip speed ratio, λ_{dsg},
3. rotor diameter, d, and
4. design angle of attack, aoa_{dsg}.

The first settings are d=0.20m; λ_{dsg}=3.0; n=2,
with the modifications

1a) chord distribution: linear **1b**) chord distribution: Bezier
twist distribution: linear twist distribution: Bezier

The blade designed for a wind speed of 7m/s is then theoretically exposed to different rotational speeds at 7m/s and the same is done for various wind speeds. In Fig. 67 the results for the two modification cases are shown. The design point is marked with a big red circle. In general, the modification does not push the rotor power lines closer to the generator line.

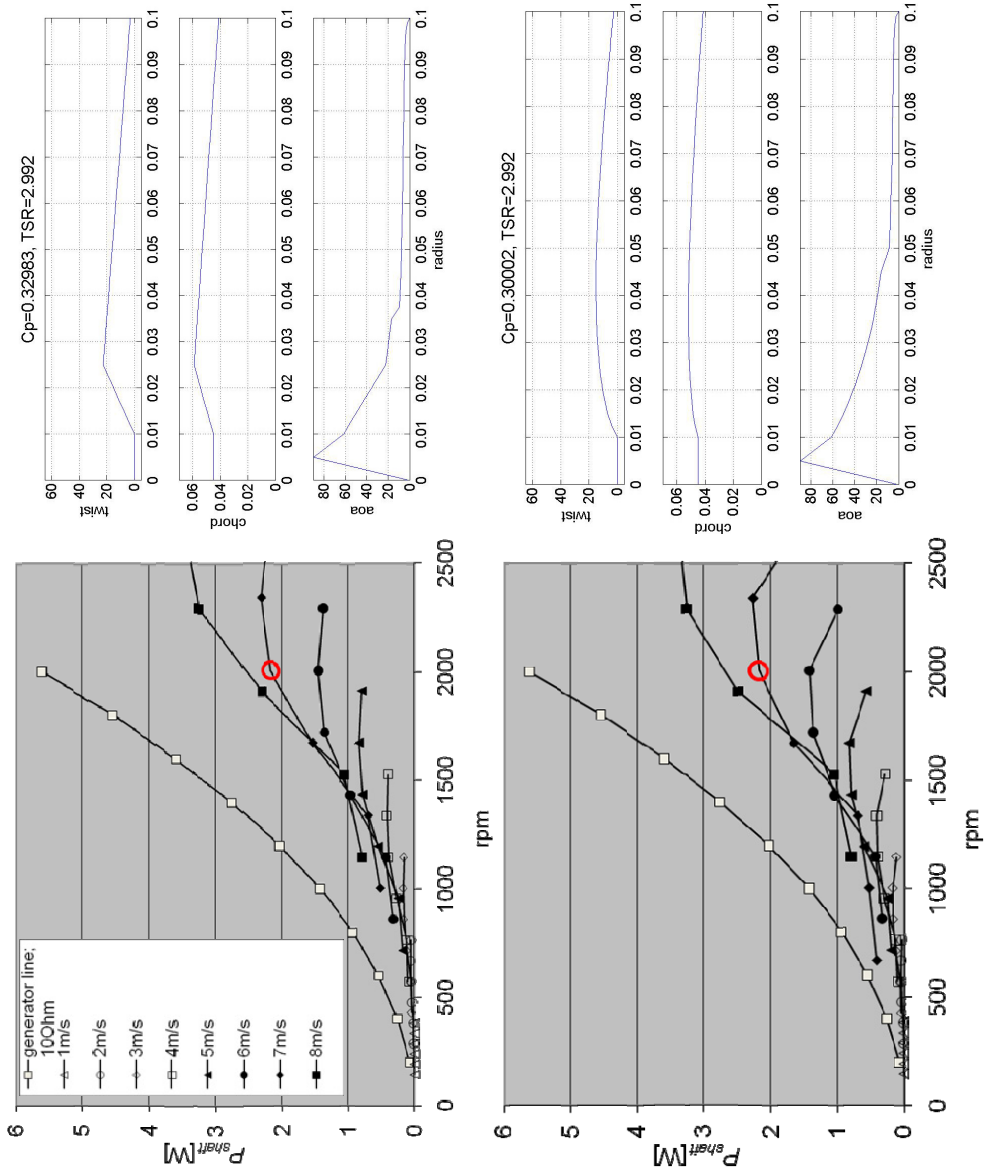

Fig. 67: Shape constraint modulation; left: case 1a); right: case 1b); top: twist, chord and aoa$_{dsg}$ distribution; bottom: P_{shaft} vs rpm

Second settings are as 1a) with modifications

1a) λ_{dsg}=3.0 **2b)** λ_{dsg}=2.0 **2c)** λ_{dsg}=1.5

By changing the design tip speed ratio settings the rotor power curves approach the generator line (see Fig. 68, bottom) while the C_P value at the design point, C_{Pdsg}, red circle, decreases significantly (C_{Pdsg}(2a)=0.33; C_{Pdsg}(2b)=0.25; C_{Pdsg}(2c)=0.19). When it comes to the twist distribution, it can be seen in Fig. 68, top, that the lower the λ_{dsg} is chosen the bigger the twist close to the root becomes, with an increasing

twist at the blade tip. The chord distribution does not change, since the maximum chord is limited to 0.06m and the chord distribution to linear. It has to be mentioned these designs are not optimized close to the root, but laid out with respect to a starting form of a flat plate, to be twisted simply and keeping a slender layout.

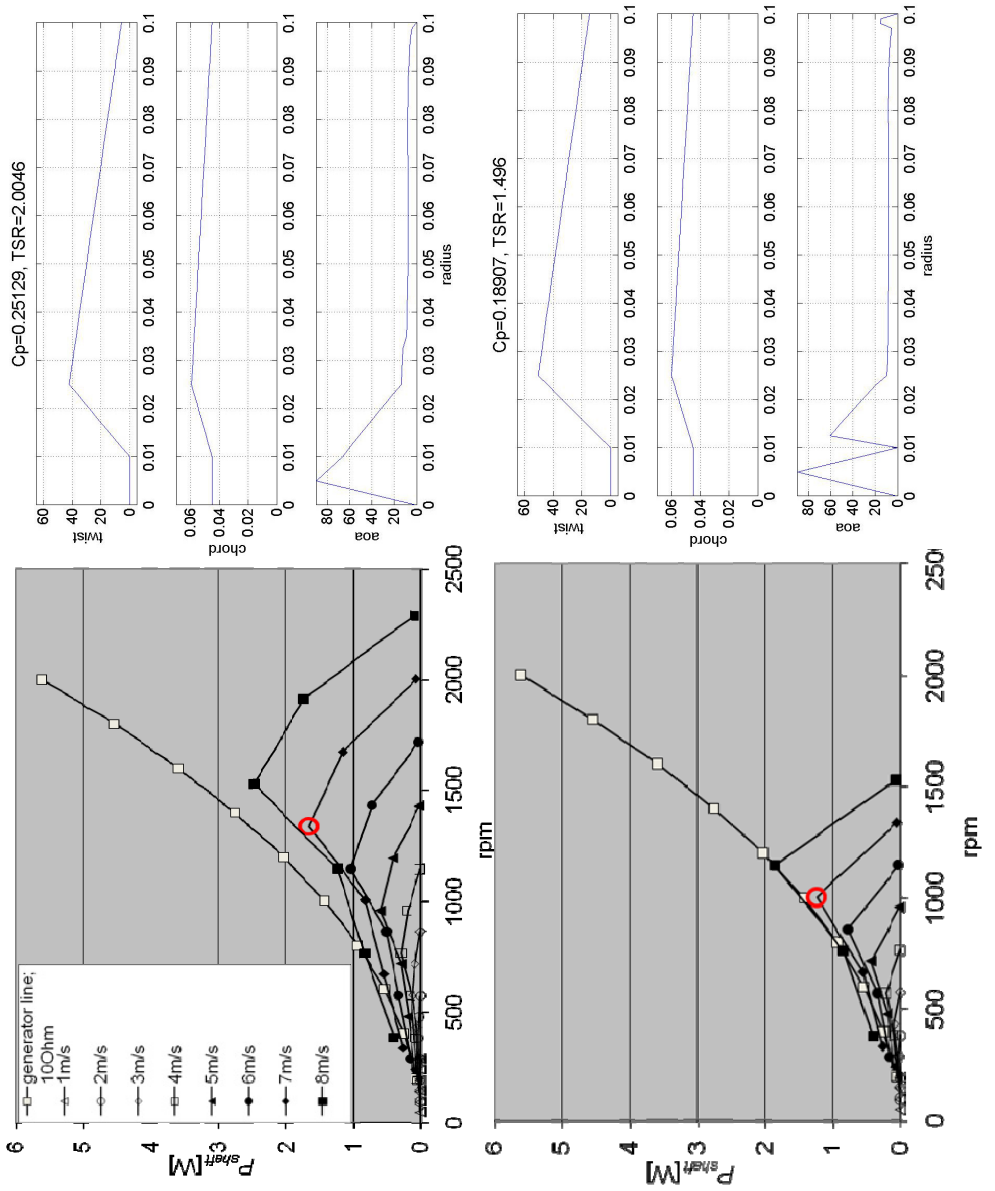

Fig. 68: λ_{dsg} modulation; left: case 2b); right: case 2c); top: twist, chord and aoa_{dsg} distribution; bottom: P_{shaft} vs rpm

Since uncertainties in measurements of the generator characteristics, in the ascertains of airfoil data from xfoil6.96 and uncertainties included in the manufacturing process as well as in the optimization algorithm should be considered, the calculated rotor performance should be higher than the measured generator demand. An easy way to increase the power is to increase the rotor diameter, d, ($d^2 \sim P_{shaft}$). And with that we proceed to case three. The settings are as 1a) with modifications

3a) d = 0.20m **3b**) d=0.25m **3c**) d=0.40m

The values for case 3b) and 3c) shown in Fig. 69 are obtained by using the C_P values

found for the tip speed ratios for case 3a) with the definition as in Eq. 37.

$$P_{shaft} = \tfrac{1}{2}\rho\, u^3 A_{rotor} C_P(\lambda) \qquad \text{(Eq. 37)}$$

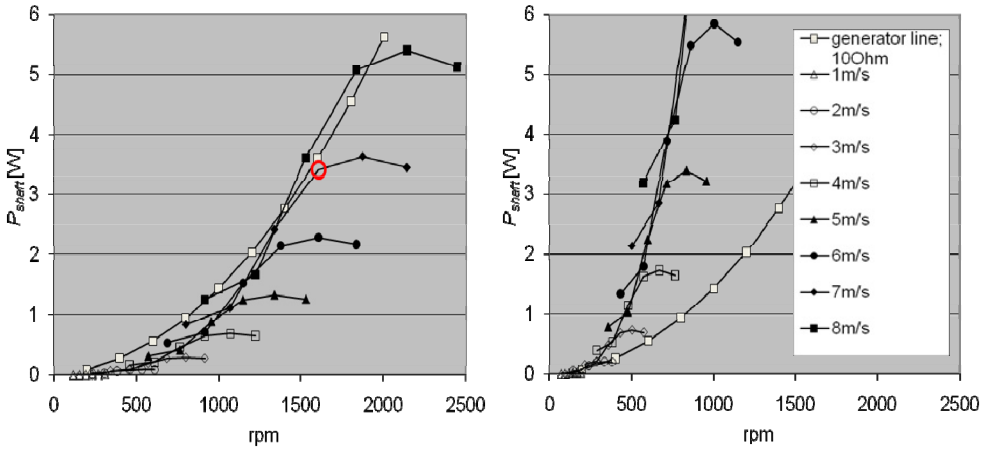

Fig. 69: d modulation; P_{shaft} vs rpm; left: case 3b); right: case 3c)

4.4.3 Results

To fit to a bicycle and to be printed with the help of "rapid prototyping" the diameter is set to 0.27m. In order to keep the efficiency in a tolerable range, the design tip speed is chosen to be λ=2.5. Additionally, bigger resistors connected to the generator circuit are considered and plotted in Fig. 70, left. The bigger the resistor is, the lower the necessary power on the shaft gets. These values are theoretical and not evaluated with measurements. In the next figures, wind speeds are indicated in the same way as in the foregoing figures.

Three various final designs are found named

1.BellAIRina,
2.BellAIR,
3.BellAIRphant.

For the first one the C_{Pdsg} is pushed to its maximum design lift and would thereby stall if it experiences wind gusts. The plot at the bottom, right, in Fig. 70 helps to clarify why. Here the aoa_{dsg} is around 9° over almost the whole blade. Going back to Fig. 65 and following the characteristic for a Reynolds number of 40'000, which is the design point Reynolds number for this geometry, it can be seen that this angle states the point of maximum C_l. As soon as a wind gust increases the angle of attack the blade stalls. That is why the design BellAIR is restricted in its angle of attack to 4.5° to the cost of C_{Pdsg} (see Fig. 70, middle).

Both designs are subjected to a maximum chord length of 0.06m. If the chord length is free to move the design comes to the third layout, BellAIRphant (see Fig. 70, top).

To compare the gain in rotor power in the design point, the C_{Pdsg} values are

C_{Pdsg}(BellAIRina) = 0.28;
C_{Pdsg}(BellAIR) = 0.26;
C_{Pdsg}(BellAIRphant) = 0.35.

In Fig. 70, middle, left, the tip speed ratio is indicated for u=7m/s.

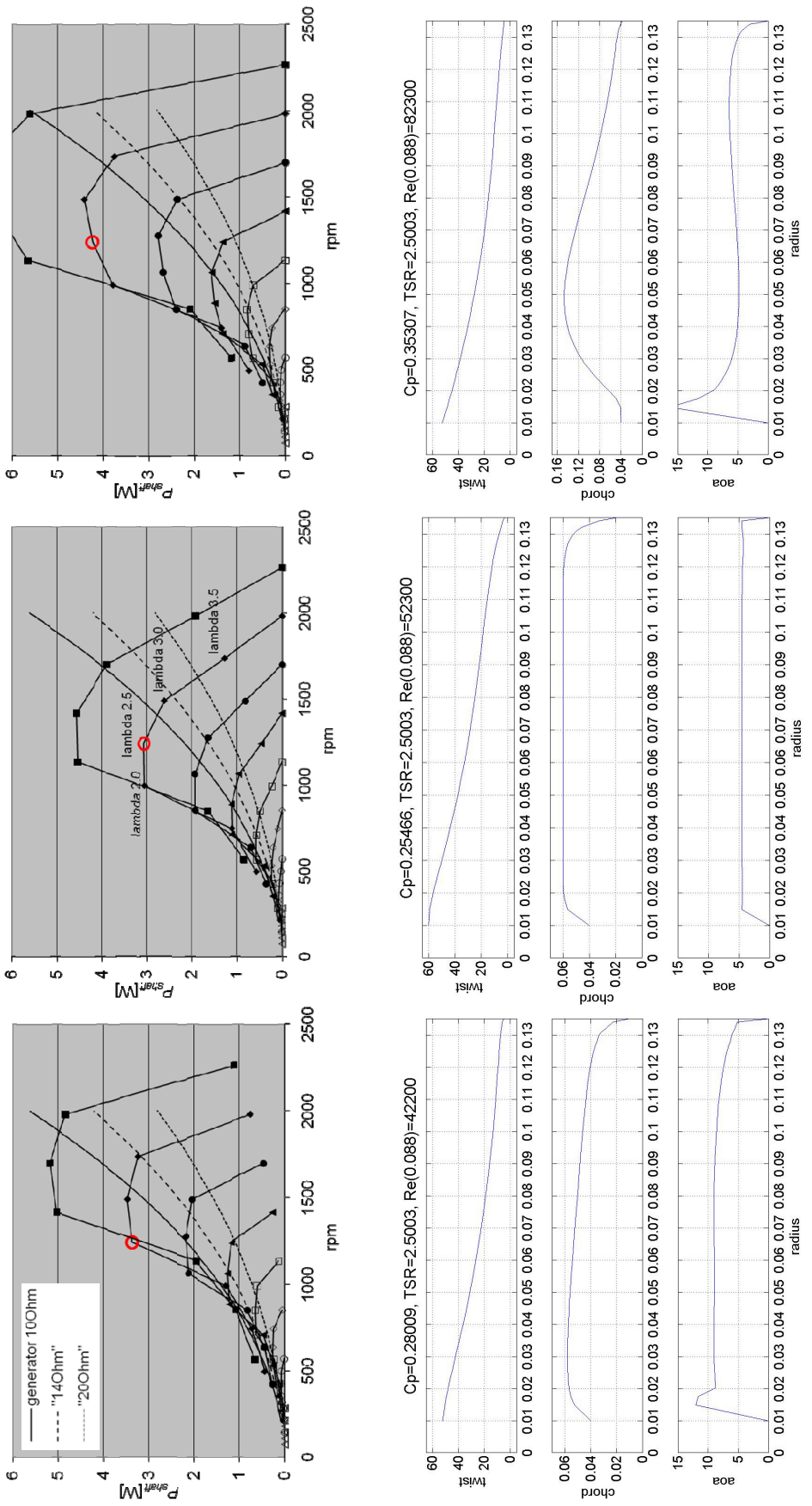

Fig. 70: Top: BellAIRphant; middle: BellAIR; bottom: BellAIRina. Left: P_{shaft} vs rpm with a red circle indicating the design point. Right: twist, chord, aoa_{dsg} distributions

Their properties and applicability are discussed in the next section. Fig. 71 is an illustration of the three rotors.

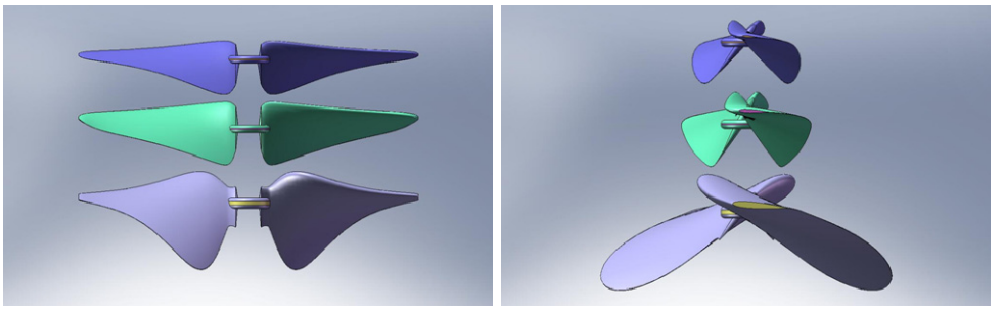

Fig. 71: Three dimensional models; BellAIRina, BellAIR, BellAIRphant

4.4.4 Discussion

In the method section was shown how different parameter variations influence the rotor performance. It turns out that a change of the chord distribution from linear to Bezier does not change the outcome significantly. More interesting is the variation of the design tip speed ratio, where the maximum power is shifted to lower rotational speeds and with that closer to the generator line. On the other hand this modification is paid by a less efficient rotor. Pronounced changes are obtained by increasing the rotor diameter, while not changing the power coefficient. These observations lead to a design tip speed ratio of 2.5 and a diameter of 0.27m.

In the results chapter three corresponding final designs were presented. For the first model the aerodynamic design is pushed towards maximum lift. With a design angle of attack of 9° corresponding to the maximum lift coefficient at a Reynolds number of 40'000, it reaches a design power coefficient of 0.28. The second model is designed for an angle of attack of 4.5° with a change of the power coefficient to 0.26. On the first glance model one seems to have the best performance, but seen on the performance in real wind conditions the second model has the advantage of its capability to take wind gusts better than model one. Both designs are restricted to a max chord length of 0.06m. This limit is chosen for aesthetic reasons. In the third design the chord length is almost free and results in a maximum chord of 0.15m and power coefficient of 0.35. Explanation for that is the higher induction in the rotor plane with the big rotor solidity. Examining Fig. 72 shows an approach of the induction to 0.1 for the second model, BellAIR, whereas the third model, BellAIRphant (Fig. 73) is close to 0.33, the value for an optimum design.

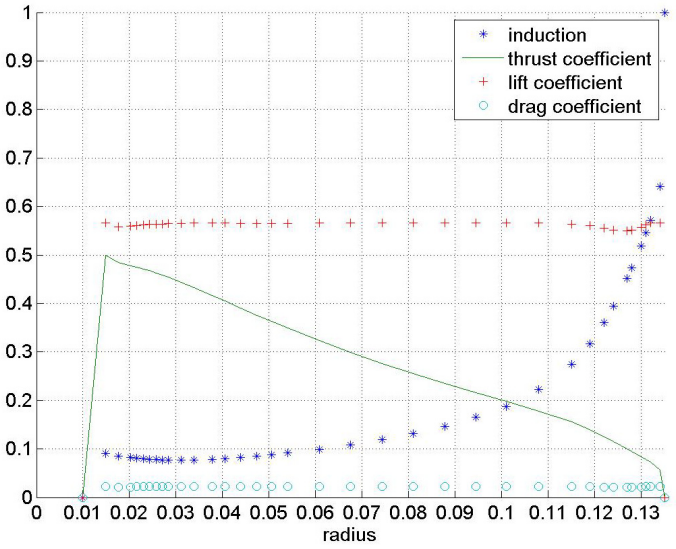

Fig. 72: BellAIR; induction (*), thrust coefficient (-), lift coefficient (+) and drag coefficient (o) vs radius

A higher solidity can be achieved with more blades as well. Whereas the design is restricted to a two-bladed rotor in order to fit into the diagonal of the three-dimensional printer's volume.

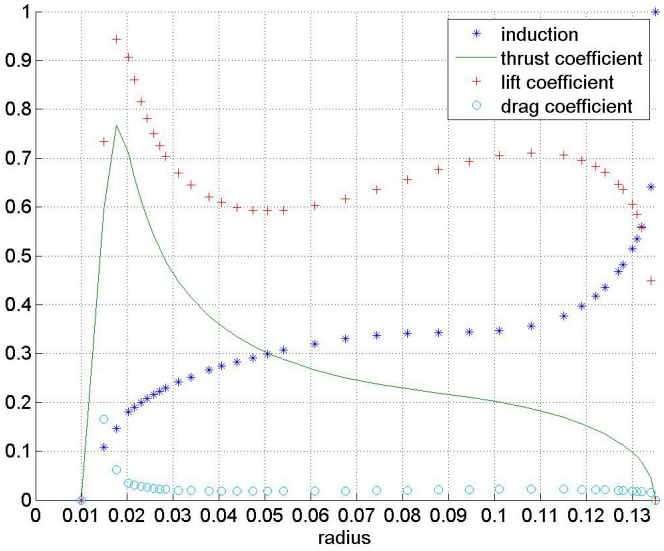

Fig. 73: BellAIRphant; induction (*), thrust coefficient (-), lift coefficient (+) and drag coefficient (o) vs radius

4.4.5 Conclusion

The optimum design with the given demands by the generator, safety limit to 2000rpm and dimension limit by the three dimensional printer is BellAIRphant. In the process of printing, though, it turns out that the blades are rather heavy due to the increasing thickness with increasing chord length. Furthermore, it takes more space, see Fig. 71. Alternative materials, for example inflatable structures, can make it more interesting. In general, the generator was over-dimensioned for the diameter limit given by the printer volume.

Anyway, for future work the findings shall be evaluated with the rotor models, connected to the generator, exposed to real wind. Investigations for rotors with more than two blades are reasonable and are promising to result in optimum designs with shorter chords. In Fig. 74, left, a rendering of two rotors for the attachment to a bicycle handle bar can be seen. To the right in the same figure the rapid prototype printed BellAIRina rotor is shown.

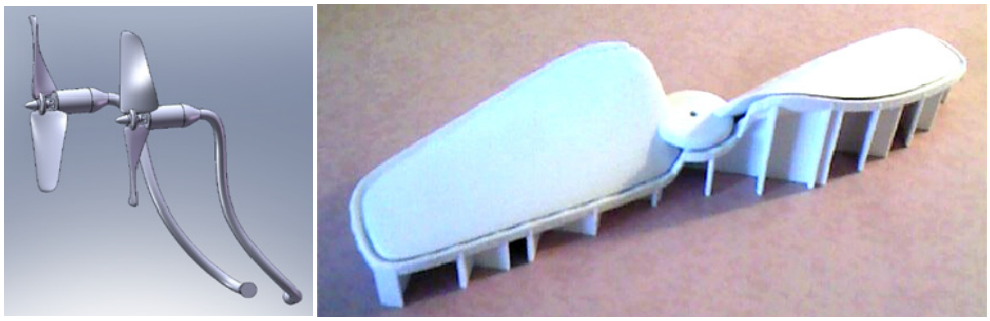

Fig. 74: Left: rendering of two BellAIR rotors attached to generator and arm to a bicycle handle bar; right: printed prototype BellAIRina

4.5 Summary and Conclusions

The content of this chapter is summarized below and the concluded findings, as well as facts, known on beforehand and found to be important, are imbedded as bullets into the continuous text.

To enter the urban environment with wind energy conversion systems, different strategies are conceivable. In general, small-scale rotors are the most eligible way to start with. The characteristics of each type of wind turbine, regardless of its size, have to fit to the conditions it is going to be exposed to. The following three statements concern aesthetic issues and are not scientifically proven.

- Wind turbines in an urban context shall be unintrusive and well integrated into the city appearance.
- In the inhabited area, a wind turbine is to be considered as a part of architecture.
- VAWTs in operation describe a constant volume and are therefore visually less disturbing than unducted HAWTs free to yaw.

Important design parameters for small-scale wind turbines, supposed to be implemented in the urban environment, are established with the help of parameter studies based on VAWT layouts. Thereby a simple multiple streamtube model, for Darrieus rotors with constant chord, is used to predict the aerodynamic performances. A small modification of the original code makes it capable to calculate on H-rotors as well.

The case study leads to design directives relevant for small VAWTs. Most of them hold for small HAWTs as well. Some of the following statements are based on the conducted case studies and are not necessarily new knowledge as such, but important issues and found worth to be mentioned highlighted as well.

- In contrast to large wind turbines, small wind turbines need high rotational speeds to obtain high tip speed ratios.

Small changes in the airfoil input data, especially at low Reynolds numbers, lead to significant differences of the rotor performance results.

- A reliable set of airfoil data is crucial.
- Reynolds numbers on the blade sections of small wind turbines are likely to be low.
- Increasing the Reynolds number in low Reynolds number ranges increases the rotor efficiency dramatically and the operational tip speed ratio bandwidth broadens.

The rotor solidity has an influence on the maximal power coefficient and the rotor's operational range.

- Designs with high solidities are more efficient for low tip speed ratios than designs with low solidities, while they only operate over a rather narrow tip speed ratio bandwidth.
- Designs with low solidities can operate over the same tip speed ratio bandwidth as rotors with high solidity, there mostly less efficient though, but can operate up to higher tip speed ratios.
- For low cut-in wind speeds low solidity designs are proposed.

Different from a HAWT rotor in unskewed flow, the angle of attack for a VAWT in the same flow is dependent on the azimuth position of the blade. The relative velocity vector on the airfoil is composed of the blade element velocity vector and the decelerated wind velocity vector, and the higher the tip speed ratio is, the greater the contribution of the blade element velocity becomes- for both concepts.

- VAWT operation at high tip speed ratios leads to more stable angles of attack over one rotor revolution.
- A lower rotational speed can lead to a lower cut-in wind speed, but also to lower Reynolds numbers and consequently to lower power coefficients.

HAWTs as well as VAWTs can induce alternating loads to the rotor tower in unskewed flow; HAWTs mostly due to the imbalance caused by the blades passing the tower and VAWTs mostly because of the changing angle of attack over one revolution of the rotor and with that changing aerodynamic loads. The shape of the VAWT blade has a tremendous effect on the alternating loads, but also on the power coefficient as a function of the tip speed ratio.

- With an H-rotor higher power coefficients are reached than with a Darrieus rotor with the same radius.
- The performance for an H-rotor with constant chord length drops drastically if it is not operating at its optimum tip speed ratio, whereas a Darrieus rotor with constant chord shows a more docile behavior.

This can be explained by the fact, that an H-rotor with a constant chord has the same solidity over the rotor height, since all blade elements have the same distance to the axis, whereas a Darrieus rotor with constant chord has a changing local solidity over the rotor height. That means that only a part of the bended blade actually is operating at an optimal ratio between solidity and tip speed ratio at $\lambda(C_{Pmax})$. Besides the energy production, another design issue is how the torque from the blades is transmitted to the tower over one rotation.

- The torque contribution by a single non-twisted H-rotor blade varies significantly over one rotor revolution, especially for low tip speed ratios.
- The more the H-rotor blades are twisted, the more the oscillating torque amplitude is reduced, for both, the single blade contribution and the total torque.
- Alternating loads on supporting structures can be reduced remarkably with twisted blades.
- Different from straight blades, additional bending moments in the twisted blades are introduced due to the uneven distribution of forces along the blade.

The VAWT aerodynamic code used for the parameter studies is then implemented into a more advanced optimization code. With further modifications of the implemented multiple streamtube model, chord distributions along the blade optimal for differently defined working points or ranges can be found and further design directives proposed.

- The performance of a Darrieus rotor can be enhanced by blade chord distributions different from constant chord distributions.
- Optimizing a Darrieus rotor's chord distribution for lower wind speeds, but for the same rotational speed, results in a rotor with generally lower solidity.

Small rotors tend to be less efficient than large-scale rotors, mostly due to operation in low Reynolds numbers. Scaling the dimensions can involve essential performance changes.

For a very small HAWT rotor design the same optimization code is used, but with an aerodynamics model based on blade element momentum (BEM) theory. The design is mostly driven by a given generator and its characteristics, but also by an economic manufacturing process and aesthetics. Very general and well known design parameters are investigated thereby and are listed below.

- Rotor design is an interaction between generator and rotor characteristics.
- Changing the design tip speed ratio has a relevant effect for the generator fitting process.
- It is advisable to dimension the rotor diameter according to the generator size or vice versa.
- An easy way to increase the rotor shaft power is to increase the rotor diameter.
- Generator characteristics can vary noticeable depending on electronic components connected to it.

Generally it can be said that rotor design and optimization is an iterative process and needs experience to a certain extent.

5 INSTALLATION CASES & SITING

After investigating the urban wind climate with onsite wind measurements unfolding an annual Weibull distribution and a more detailed view on the daily and annual variations, followed by CFD simulations to detect characteristic flow phenomena, and finally a presentation of turbine designs and general design directives for especially VAWTs, a broad spectra of tools and methods is acquired. For this chapter, the developed tools are used in combination with each other together with wind and energy production measurements of a wind turbine type actually installed at various sites within Copenhagen and its vicinity. In addition, power curve measurements taken at the Risø test field in Roskilde, DK, of this exemplary turbine type are compared to its power curve as given by the manufacturer.

First, the installation sites are inspected and characterized and subsequently annual energy productions (AEP) estimated on the basis of the onsite wind measurements in conjunction with the actual measured power curve. Actual energy production measurements at the sites are then compared with these estimations. Occurring discrepancies are analyzed and tried to be explained. In a second step, the installation sites' wind climates constituted the design ground for new VAWT system layouts originated from the possessed knowledge and tools on hand.

Similar works are carried out by others, where energy yields of small-scale wind turbines mounted on rooftops are estimated, derived with CFD tools and analytical approaches with regard to wind speed profiles [53], [54], [82]. Another interesting paper written by Kooiman and Tullis [83] handles the power curve deficiency of a VAWT installed on a flat rooftop in an urban context, compared to the turbine performance measured in a wind tunnel.

5.1 Turbines in Copenhagen

In 2010, a company located in Copenhagen took the initiative to import ten 1kW VAWTs of the same type to Denmark, got the model certified and installed them at different site within the urban area. In their choice of the positioning they were focused on installing them at sites of different character. They took wind measurements at the rooftops and measured the actual energy production. In Fig. 75 three of the sites can be seen where a closer look was taken at in the following.

Fig. 75: Installation of turbines at (from left to right) Fælledvej, Svanevej and Vallensbækvej (by Logik&Co)

5.1.1 Site description

The sites of installation got case numbers assigned where ***site one*** is at Fælledvej on the rooftop of an Andelsforening (in English: collective association) in Nørrebro, Copenhagen. ***Site two*** is at Svanevej on the rooftop of the company Natur-Energi (in English: Nature Energy) in Nordvest, Copenhagen and ***site three*** is at Vallensbækvej on the 'House of Dreams' rooftop, at the side of the highway E21. Furthermore, the

Risø test site (***site five***) is analyzed and the reference site at H.C. Ørsted Institute, examined in detail earlier, is included as well in manner of its wind climate (***site four***). All together five wind climates are looked at. Some googlemaps' screenshots show the vicinity of all the measurement sites. Fig. 76 [47] shows the Nørrebro district, Copenhagen, where *site one*, *site two* and *site four* are located. The figure shall help to give an overview of the sites' surroundings and their own character in terms of built-up density and buildings (obstacles) arrangements. In Appendix H closer views of the plots are accessible, including street views and marking of the buildings, where the wind turbines or measurement devices are attached to.

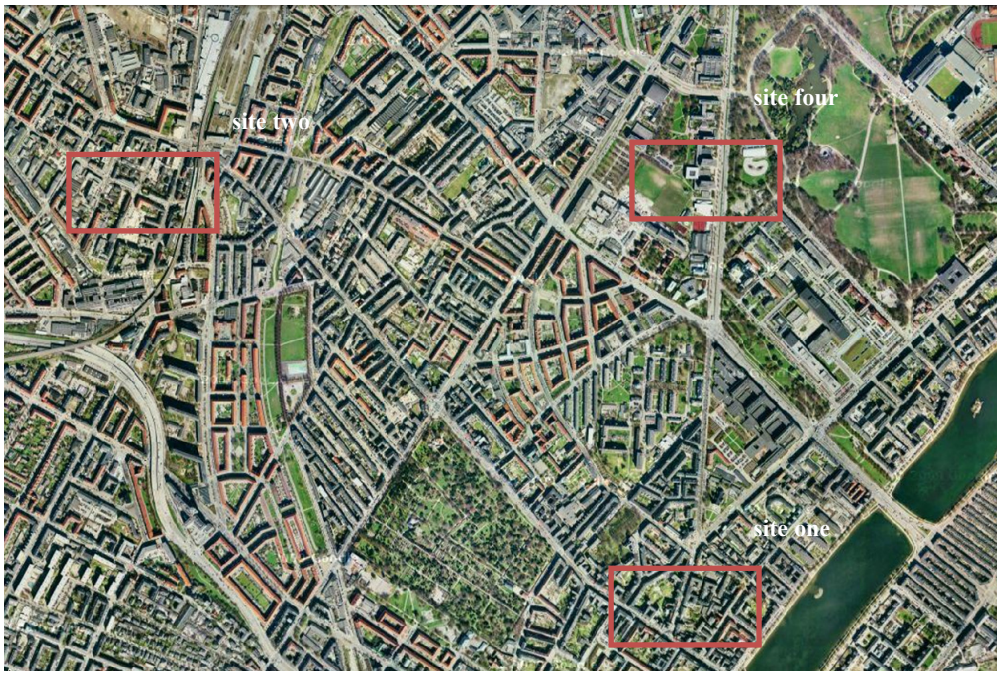

Fig. 76: Nørrebro, Copenhagen, DK, district with red squares indicating site one, site two and site four

Zooming in to the single site plots and using the methods introduced in chapter "Urban Wind Climate" the districts can be described in several terms. For this, it is necessary to ascertain the average mean height of the buildings in the districts, the built-up density, a reference mean wind speed at a known reference height, a fully described reference site outside the city and the downwind fetch for each site with reference to the outside reference site. For *site one* to *site four*, the Airport Kastrup site serves as reference site to employ the earlier introduced roughness step method (**method I**) as well as the geostrophic drag law method (**method II**).

So, to start off with the determination of the average wind speeds, examination of the single sites is required. *Site four*, H. C. Ørsted Institute, was studied throughout earlier and the same data are reused here. The urban sites where the turbines are installed got monitored by the company which imported and installed them. They logged the onsite wind speeds as well as the energy production of the turbines. Most of the measurement data for these sites are collected between January 2010 and June 2010. The monitored turbines are installed on flat rooftops with a 3m tower. Wind measurements are taken at the rooftops at the same time as the energy output is measured, that means the wind is measured somewhere set-off to the rotors, but mostly at hub height; 3m a.r.l. (above roof level).

Results obtained with the available wind data are shown in Fig. 77- Fig. 82, with the Weibull distribution, the wind directionality for the monitored periods, the wind profiles used as input and received as output with method I and method II, where in the same plot significant points are emphasized. Additionally, the defined site plots are shown with pink lines in them, marking the built-up areas and a table with input and output data is given. [47] is used to obtain the satellite pictures. The determined site descriptions for *site one* to *site four* are summarized in Table 11 as well. Generally, *dh* denotes the minimum height of a tower on the measurement's rooftop, where according to the displaced logarithmic wind profile derived with method I, a mean wind velocity of 3m/s is reached. Furthermore, the rectangles in the wind profile plots represent the buildings mean height and not necessarily the height of the building with the mounted equipment. The believed height of the individual building can easily be recalculated from the urban measurement height deducting the site-specific wind measurement mast height (*site one* and *site three: 3m*, *site two:* 2m, *site four:* 8m). It is recommended to insect the sites with buildings indication in Appendix H in combination with the graphs shown in the following.

Interesting in matter of energy production and energy consumption are the average wind velocities over a day. In Fig. 81 these are shown found for the different urban sites as well as for the open land site. A dashed line indicates the wind speed u=3m/s, which is marking the cut-in velocity for many turbines.

Table 11: Parameters describing site one to site four

site		**(1) Fælledvej**	**(2) Svanevej**	**(3) Vallensbækvej**	**(4) H. C. Ørsted**
u_{ave}	[m/s]	2.2	2.5	2.9	4.0
z	[m]	23	22	18	28
$\bar{H}$	[m]	20	20	15	15
λ_p	[-]	0.41	0.41	0.18	0.15
x	[m]	11510	13570	19180	12460
configuration [46]	#	6	7	9	4
z_0	[m]	3.23	0.64	0.71	1.39
d	[m]	11.8	18.4	12.5	10.0
$d/\bar{H}$	[-]	0.59	0.92	0.83	0.62
u^*	[m/s]	0.56	0.48	0.49	0.52

At *site one* (see Fig. 77), wind data are collected for 47 full days (February'10: 6days; March'10:30days; April'10: 11days). The wind turbines were taken down due to problems with reflections, as per Logik&Co. The Weibull coefficients are found to be k=2.0 and A=2.5m/s. At Svanevej, *site two* (see Fig. 78), wind data are collected for 57 full days (January'10: 14days; February'10: 24days; March'10: 8days; April'10: 11days). The wind measurements are taken at approximately 2m above roof level. For these days Weibull parameters are determined to be k=1.6 and A=2.7m/s. For *site three* (see Fig. 79) wind data are collected for 58 full days (February'10: 28days; March'10: 30days). The wind measurements are taken in between the two wind turbines at a height of about 3m above the rooftop. A Weibull distribution with k=1.8 and A=3.5m/s is detected.

In comparison to the three sites, results for *site four*, H. C. Ørsted Institute, are shown in Fig. 80. Here data are collected over a much longer period of time, but no turbine is installed and with that no energy production measured. As found earlier the Weibull parameters are k=2.4 and A=4.4m/s.

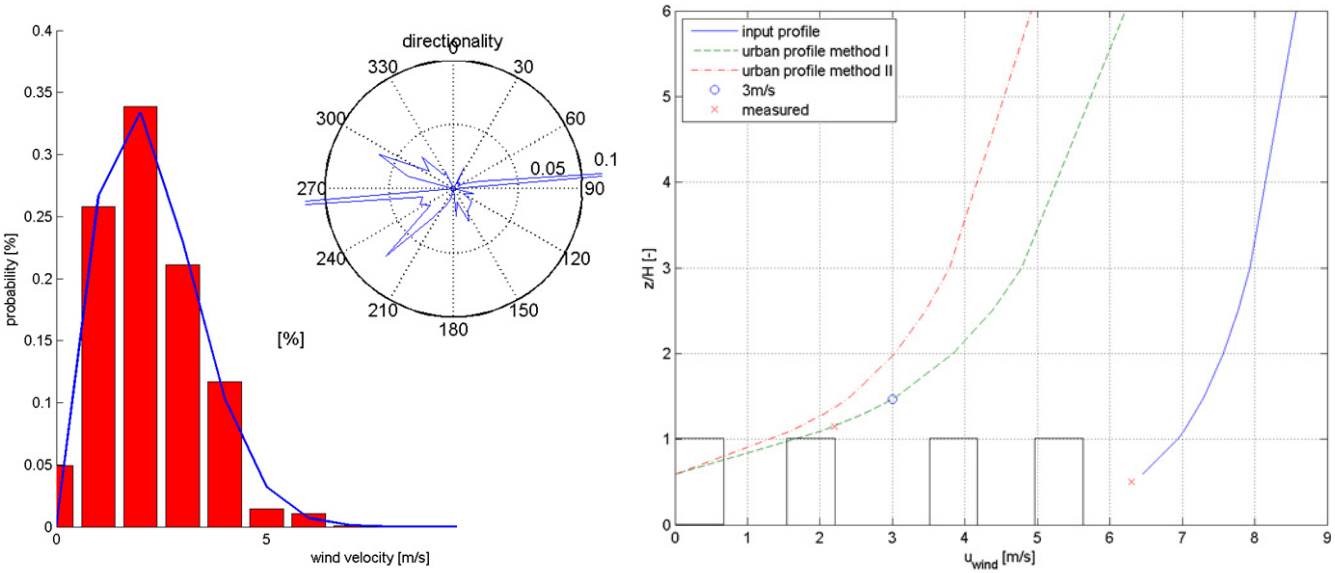

```
##INPUT########################################
  Reference Measurement:
  velocity   height   roughness length
  UA=6.3m/s  zA=10m   z0A=0.01m
  Urban Measurement:
  velocity   height   fetch      parameter
  U =2.2m/s  z =23m   x=11510m   m=0.75
  District Description:
  buildings mean height       occupation
  H= 20m                      lambda_p=0.41
##OUTPUT#######################################
  lifting height   roughness   length ratio
  d=11.8m          z0=3.23m    d/H=0.59
  IBL height       min hub a.r.l.
  delta=1682m      dh=9.4m for 3m/s
```

Fig. 77: Site one; top left: measured Weibull distribution and directionality rose; top right: wind profiles derived with method I and II; bottom left: site plot with built-up indication; bottom right: site description input and output

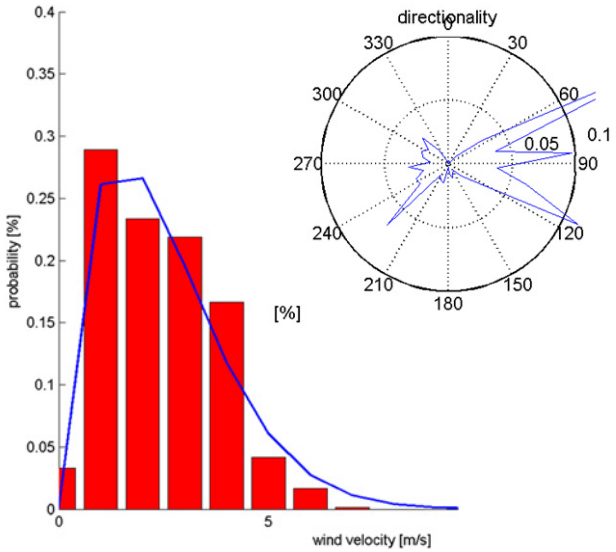

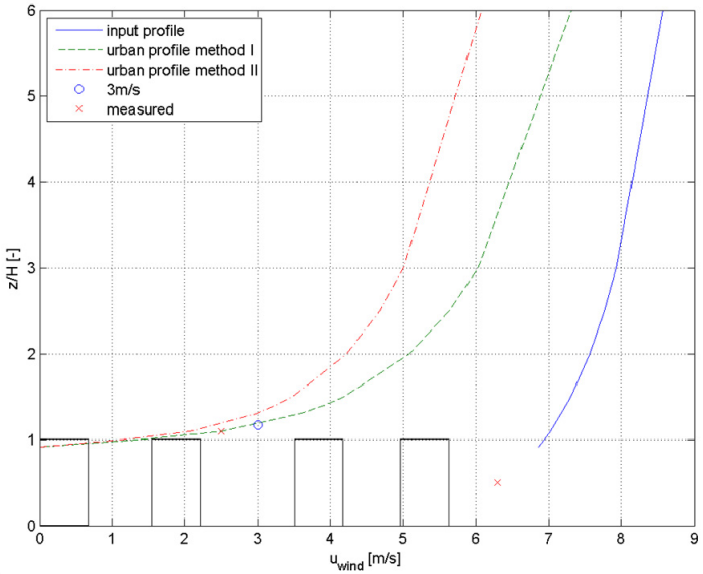

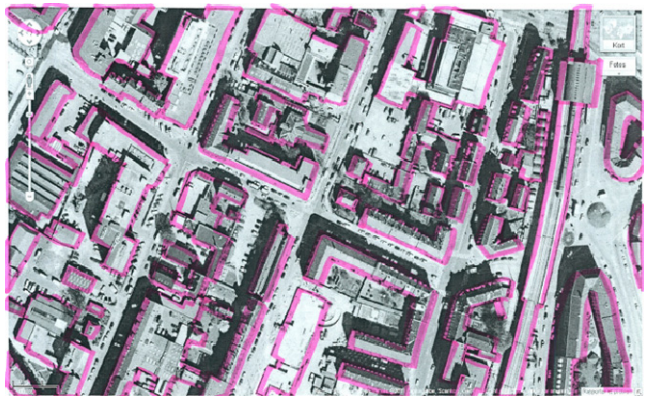

```
##INPUT########################################
  Reference Measurement:
  velocity   height   roughness length
  UA=6.3m/s  zA=10m   z0A=0.01m
  Urban Measurement:
  velocity   height   fetch      parameter
  U =2.5m/s  z =22m   x=13570m   m=0.75
  District Description:
  buildings mean height       occupation
  H= 20m                      lambda_p=0.41
##OUTPUT#######################################
  lifting height  roughness   length ratio
  d=18.4m         z0=0.64m    d/H=0.92
  IBL height      min hub a.r.l.
  delta=1390m     dh=3.5m for 3m/s
```

Fig. 78: Site two; top left: measured Weibull distribution and directionality rose; top right: wind profiles derived with method I and II; bottom left: site plot with built-up indication; bottom right: site description input and output

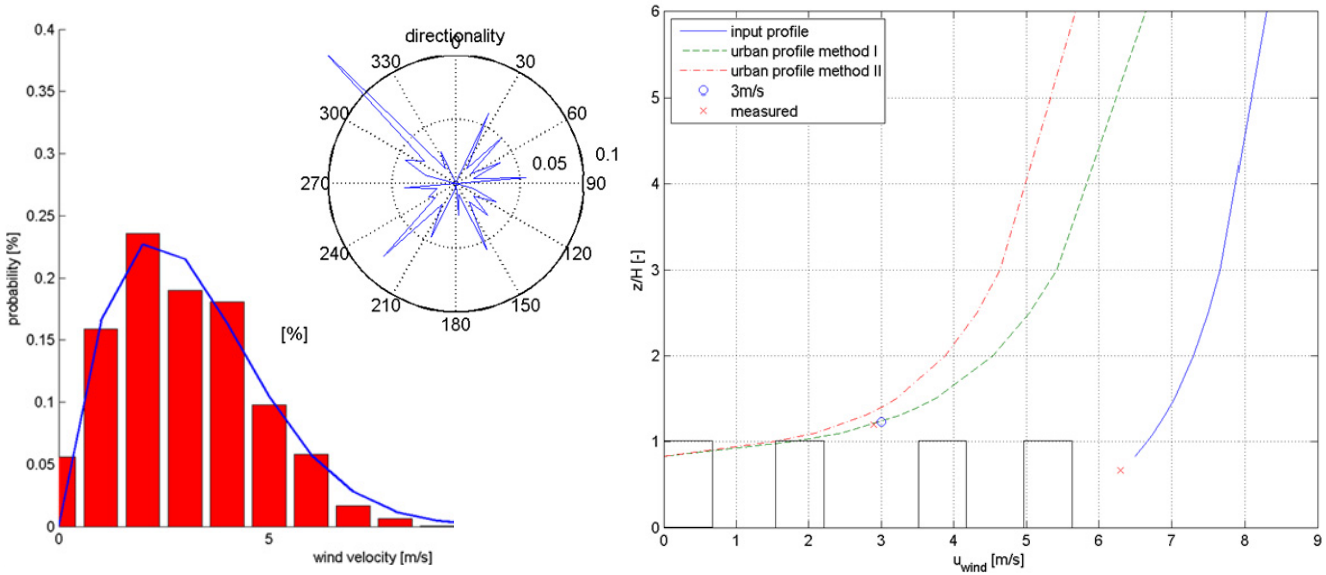

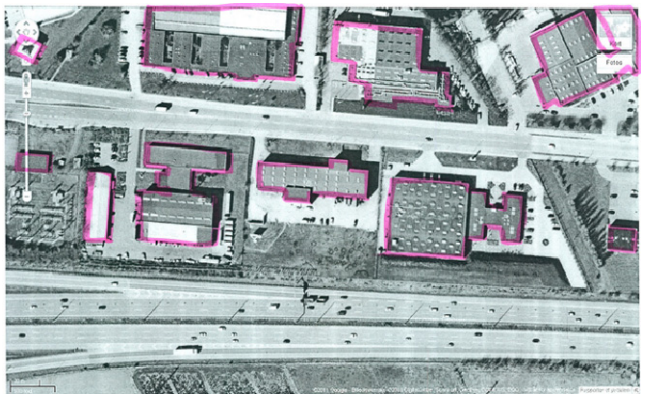

```
##INPUT########################################
  Reference Measurement:
  velocity   height   roughness length
  UA=6.3m/s  zA=10m   z0A=0.01m
  Urban Measurement:
  velocity   height   fetch      parameter
  U =2.9m/s  z =18m   x=19180m   m=0.75
  District Description:
  buildings mean height       occupation
  H= 15m                      lambda_p=0.18
##OUTPUT#######################################
  lifting height  roughness   length ratio
  d=12.5m         z0=0.71m    d/H=0.833
  IBL height      min hub a.r.l.
  delta=1870m     dh=3.4m for 3m/s
```

Fig. 79: Site three; top left: measured Weibull distribution and directionality rose; top right: wind profiles derived with method I and II; bottom left: site plot with built-up indication; bottom right: site description input and output

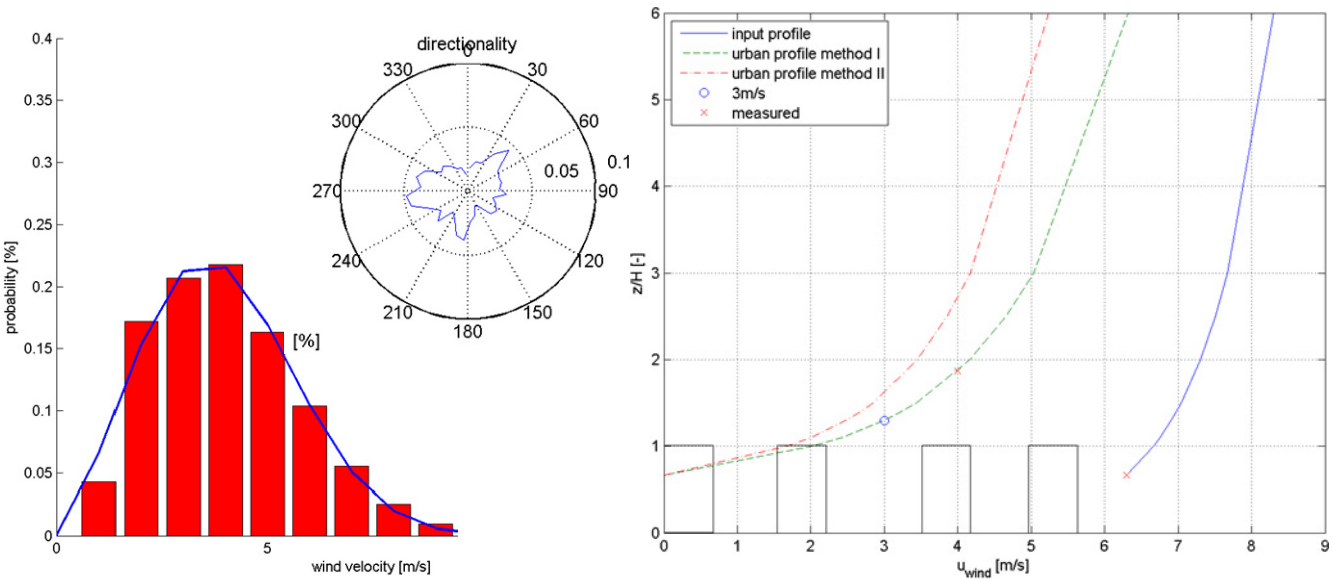

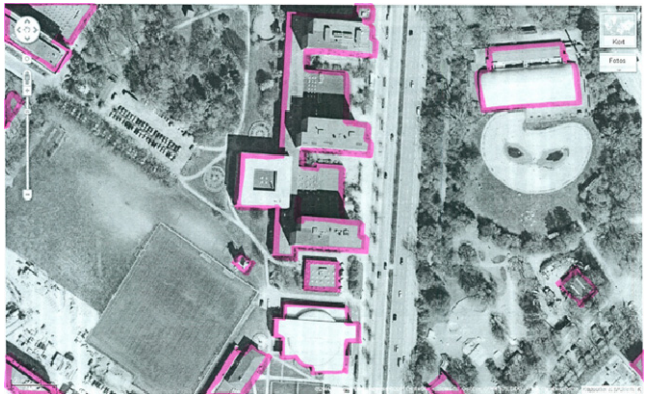

```
##INPUT########################################
  Reference Measurement:
  velocity   height   roughness length
  UA=6.3m/s  zA=10m   z0A=0.01m
  Urban Measurement:
  velocity   height   fetch      parameter
  U =4.0m/s  z =28m   x=12460m   m=0.75
  District Description:
  buildings mean height       occupation
  H= 15m                      lambda_p=0.15
##OUTPUT#######################################
  lifting height  roughness   length ratio
  d=9.93m         z0=1.39m    d/H=0.662
  IBL height      min hub a.r.l.
  delta=1513m     dh=-0.558m for 3m/s
```

Fig. 80: Site four; top left: measured Weibull distribution and directionality rose; top right: wind profiles derived with method I and II; bottom left: site plot with built-up indication; bottom right: site description input and output

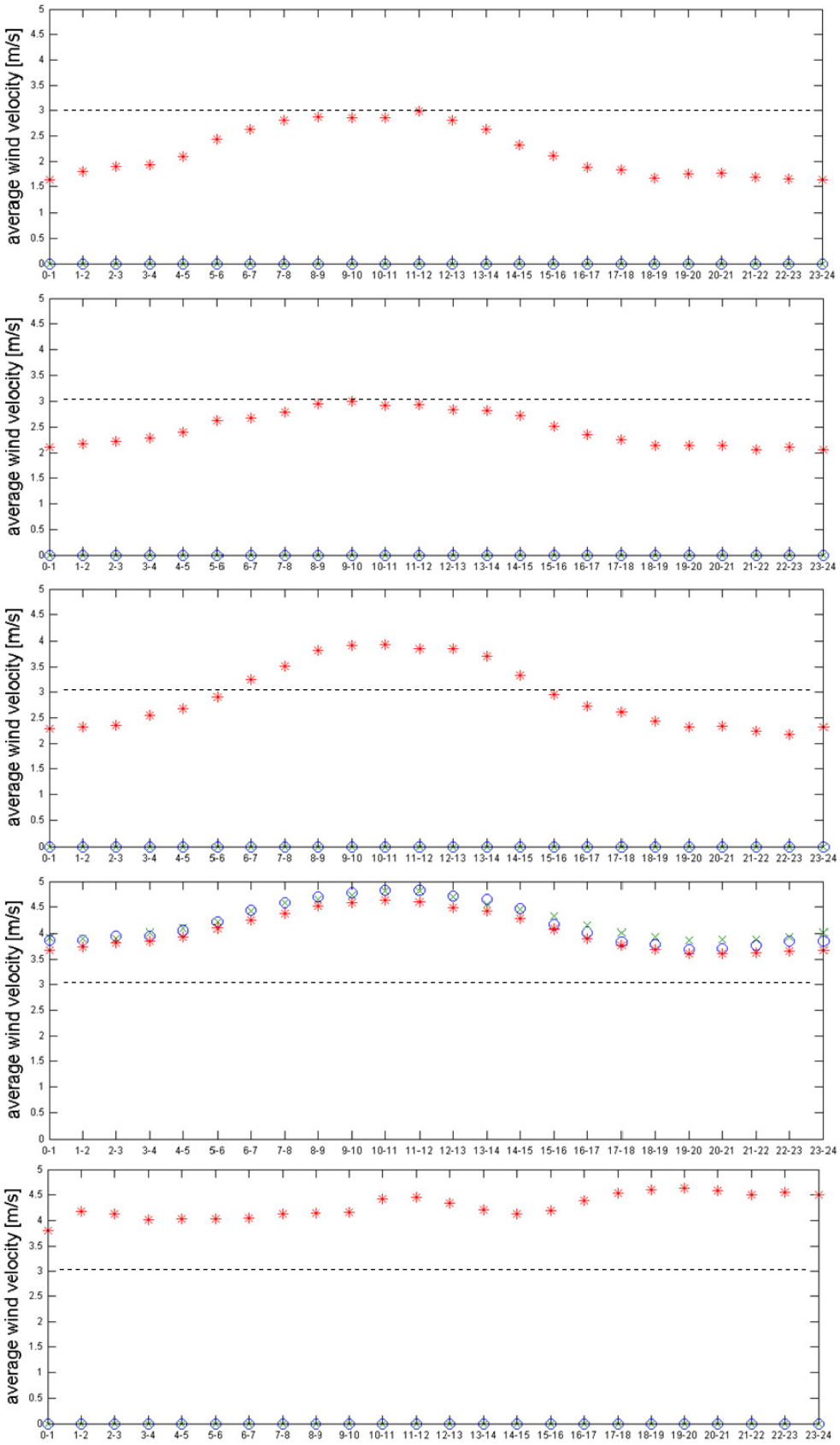

Fig. 81: Average wind velocity over a day with a dashed line indicating 3m/s wind velocity; top to bottom: site one, two, three, four, five

The Risø DTU test field in Roskilde, *site five*, is where data are collected to draw a measured power curve. Different from the four city sites, the surrounding can almost be considered as simple terrain. Only very few obstacles are located in the vicinity compared to the urban sites in a large distance. From one side the fjord constitutes a change in roughness class, if the wind comes in from its direction. A turbine of the type VENCO TL1000 is installed with 10m hub height. Wind measurements at the same height are taken at several points in such a way, that the incoming wind is least disturbed and could be considered as the same wind condition as the rotor is exposed to. Here, an average wind speed of 4.3m/s is measured and a fit with the Weibull distribution parameters k=1.8 and A=5.1m/s obtained (see Fig. 82). The wind profile is supposed to be not displaced in height. In the next section, the power curve is looked at more in detail.

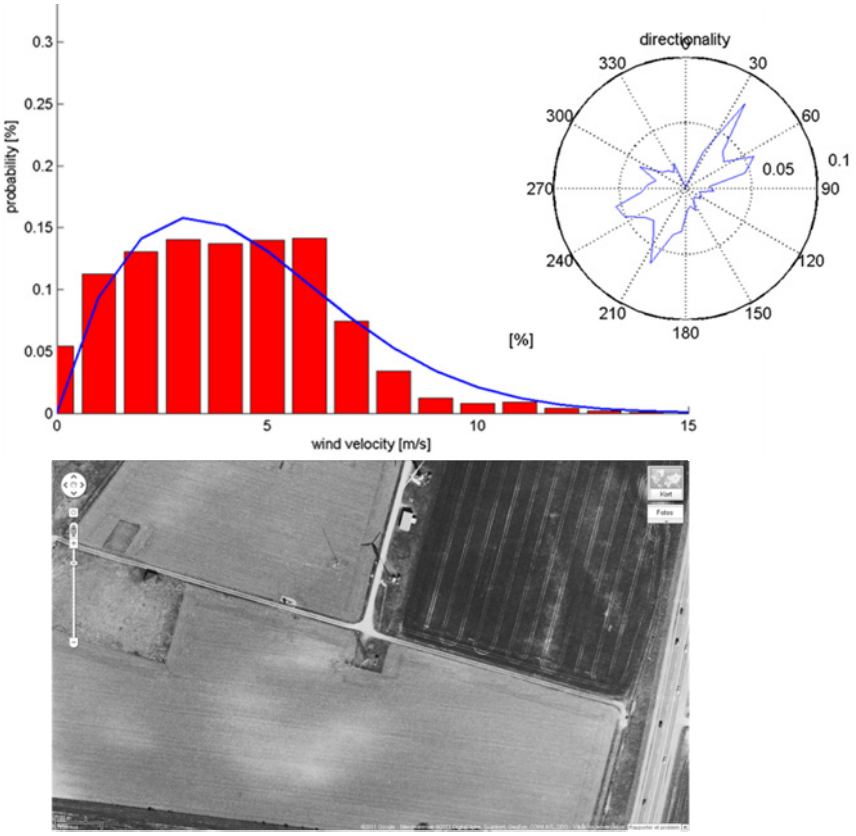

Fig. 82: Site five; top: measured Weibull distribution and directionality rose; bottom: site plot

5.1.2 Measured power curve

When the company Logik&Co imported and installed small-scale VAWTs of the type VENCO TL1000 at several sites around and in Copenhagen, their motivation was to strengthen ecologic housing in Denmark, and started with a study of the energy outcome depending on the installation site. To evaluate the location and the energy production, they took wind measurements at the same time. After a short while they had to realize, that the energy output was not satisfying according to the expectations coupled to the power curve given in the technical specifications. To restate, until now it is uncertain what the power curves for small wind turbines actually depict. It is possible that they are based on theoretical calculations, wind tunnel measurements where the power refers to the mechanical power on the shaft or the power is the value measured at the point where the electricity is fed into the grid.

The diagnosis of Logik&Co that the energy production is way lower than anticipated, can be constituted with a wind climate, not appropriate for the wind turbine and vice versa or a power curve referring to something else than the feed-in energy. So, they decided to provide one of their imported turbines to Risø DTU, where the certification group designed a measurement set-up for the rotor and since then energy output and wind measurements are logged continuously.

Based on an extraction of these data the plot in Fig. 83 was established. In the same plot the power curve as it is given by the manufacturer is inserted in form of the red circles. Besides that, a polynomial curve is fitted to the measurements and then used in the next section to calculate the AEP for the different observed sites.

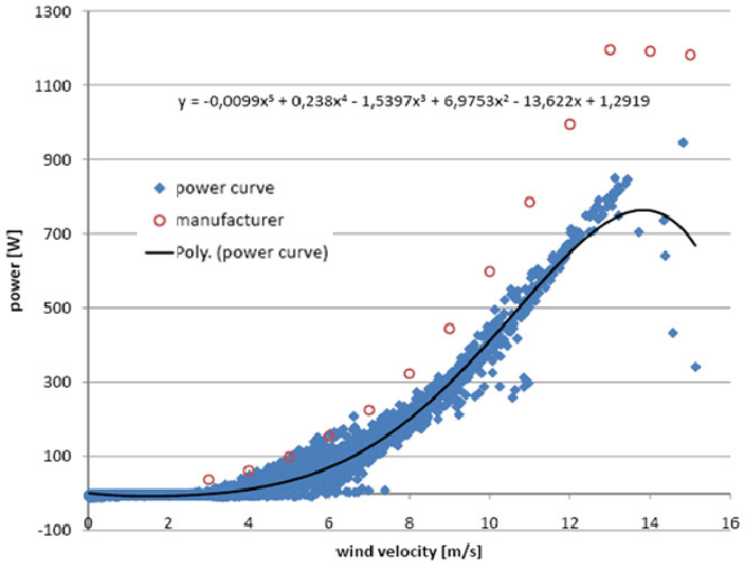

Fig. 83: VENCO TL1000 power curve given by manufacturer (red circles), power measurements taken at Risø test site (blue diamond) and a polynomial fitting line (solid black)

Judging the graph, it is obvious that the outcome has to be different from the expectations, despite the wind climate the turbines are exposed to. For the following calculations, the power curve values according to the polynomial fitting line listed in Table 12 are used.

Table 12: Power, P, and power coefficient, C_P, values corresponding to the polynomial fitting line

u	[m/s]	0-3	4	5	6	7	8	9	10	11	12	13	14	15
P	[W]	0	10.7	32.9	69.6	125	201	298	413	536	653	742	771	701
C_P	[-]	0	0.08	0.12	0.15	0.16	0.18	0.18	0.19	0.18	0.17	0.15	0.13	0.09

To evaluate the fitted wind turbine power curve, the energy production measured at the Risø site is compared with energy production estimations using the same wind data, meaning *site five*, together with the values in Table 12. The power measurements are negative for the periods where the wind was not blowing or was below the cut-in wind speed. These values are about 3W and in total negligible for this spot, since a high proportion of the time the wind velocities are adequately high and lead to positive energy production. Furthermore, at velocities right above the

cut-in the output is already 3 times higher than these 3W. For the observed 28days in November 2010 the energy output including the consumption was 33.8kWh, excluding the consumption would lead to an output of 34.9kWh. It has to be mentioned that actually only 51.2% of the time positive output was measured and the rest of the time the system was consuming energy, but as the numbers show at a fairly low fraction. Examining the wind climates just introduced, for some locations this energy consumption might become more significant though.

So, using a fifth grade polynomial to approximate the power curve and applying the wind measurements found at the Risø test stand leads to an AEP of 428.6kWh/year. The actual energy production, including the negative values leads to an AEP of 440.6kWh/year. That would mean the estimation is 2.7% too low. Excluding the measured negative values results in an AEP of 454.95kWh/year and with that the estimation with 428.6kWh/year is 5.8% too low. Anyway, the polynomial seems to deliver an acceptable approach. Applying the same power curve to the urban sites might be wrong due to a probable shift in power output with changing turbulence intensity. In the next section, a look is taken at the energy output estimated for the urban sites. Earlier estimations were done with three different small wind turbines exposed to the H. C. Ørsted Institute site, *site four*. Fig. 84 shows the C_P values of the used turbines at different wind velocities.

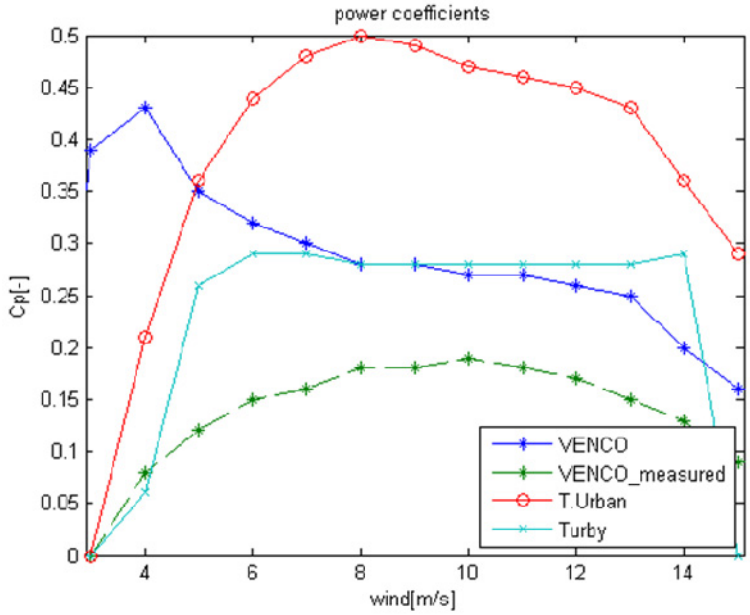

Fig. 84: C_P vs u for three different small wind turbines, based on manufacturer power curve and one based on measurements taken at Risø DTU test site (VENCO measured)

To be seen in this graph are also the C_P values determined with the power curve measurements. An earlier argument had been, to design a rotor-generator concept, which working range is optimized for lower wind speeds, since the wind climates, the turbines are most likely going to be exposed to, are characterized with Weibull distributions we saw earlier. A high proportion of the occurring winds are in the range of 1-6m/s.

5.1.3 Estimated AEP

Turbines of the type VENCO TL1000 were installed by the company Logik&Co among others on flat rooftops at Fælledvej, *site one*, Svanevej, *site two* and Vallensbækvej, *site three.* They had installed some wind measurement devices and

were monitoring the energy production for a certain period of time. Most of the data were collected between January 2010 and June 2010.

The wind measurements taken at the sites by the company are used to estimate an annual energy production (AEP) independent from the measured production. To do that, the wind measurements are analyzed in manner of the wind velocities probabilities and then multiplied with the power curve derived from measurements at the Risø DTU test field. Read more about the applied power curve in the prior section. Assuming the seasonal variability is low and the wind climate of the observed months is representative for the rest of the year, an AEP for the sites can be calculated, excluding maintenance or unscheduled production breaks.

Similar to the AEP estimation in chapter "Urban Wind Climate", the estimation are carried out here. The load factor is defined as in Eq. 9. C_E is again the parameter setting the AEP into relation with the annual wind energy potential and with that characterizes how efficient the rotor is performing in the given climate. When using different rotors in the same wind climate, this parameter seems to be somehow proportional to the site specific AEP per swept area, as shown in the foregoing estimations in chapter "Urban Wind Climate". But when it is used for different turbines in various wind climates, it gives another opportunity to rate the turbine performance, as shown in one of the following sections. In the earlier AEP estimations, among others, the same turbine as here was used as an example. Different though was the used power curve. In chapter "Urban Wind Climate" the VENCO TL1000 power curve was used as given in the technical description.

Although the VENCO turbine is rated as 1.0kW, for the load factor calculation a rated power of 0.77kW is used. This number is chosen based on the max power at 14m/s according to the approximated power curve. In Table 13 the estimated results are presented for the four sites. The rotors swept area is 3.6m^2.

Table 13: Annual energy production overview calculated with the measured power curve polynomial and onsite wind measurements for site one to site four

site	***k***	***A***	u_{ave}	**AEP**	**AEP/m^2**	**load factor**	**annual wind potential/m^2**	C_E
	[-]	[m/s]	[m/s]	[kWh]	[kWh/m^2]	[-]	[kWh/m^2]	[-]
one	2.0	2.5	2.2	22.21	6.15	0.003	108.58	0.057
two	1.6	2.7	2.5	39.38	10.91	0.006	150.23	0.073
three	1.8	3.5	2.9	99.35	27.52	0.015	265.07	0.100
four	2.4	4.5	4.0	275.52	**76.32**	**0.041**	572.43	**0.130**

The characteristic parameter for wind turbines, the load factor sets the actual energy production into relation with the fictive full-time energy production at rated power. For large offshore turbines this factor is about 30 to 40%. The load factors based on the measured power curve and the rated power of 0.77kW for these sites turns out to be only 0.3 to 4.1%. This result triggers the guess, that the generator is over-dimensioned. Also, a rated wind velocity of 14m/s is too high for a wind climate where barely a wind of 9m/s is seen.

In reality the energy productions were different from the numbers estimated. Referring to the evaluation of the power curve approximation, some explanation can be found there. Another explanation is the local variability of the wind velocities. The location where the wind was measured and the location where the actual production took place were not the same and different from the open land the wind field around obstacles is rather complex. With the help of flow phenomena around

obstacles, the local spots are analyzed more in detail in the following section. Satellite pictures of the sites are taken from [47].

5.1.4 Discrepancy

The AEP estimations for the urban sites, where wind turbines are installed, does deviate from the actual production numbers. Evaluating the approximated power curve in a flat terrain showed a discrepancy too where the estimation resulted in a more pessimistic AEP. But the estimations for the urban sites are for some cases too optimistic and for others too pessimistic. So it is decided to take a closer look on the local wind variability around obstacles in combination with the example sites. For *site one*, *site two* and *site three*, there are days where the energy production is measured, but not the wind speed and the other way around. The quality of the measurement data from these sites is not known. In some cases, it looks like the data logging somehow overwrites some other data, so that sometimes an identical block of data emerges again the next month, which is rather unlikely. Besides of this, the wind measurements do not necessarily represent the wind the turbines are facing. *Site three* for example, where two turbines are installed, one on the western end of the rooftop and one on the eastern end of the rooftop, is equipped with a wind measurement device, which is mounted in line with the turbines and approximately at the center height of the rotors, but in the middle of the rooftop (see Fig. 75, right, and Fig. 85).

5.1.4.1 Site three

To evaluate the estimations done before, wind measurements and energy production measurements from the months, where both are available, are taken to compare the measured onsite energy production with the calculated energy production based on the wind measurements. A first evaluation is done for *site three*. Energy production measurements at this site are given separately for the two turbines. Energy output data for the turbine positioned to the west are available over the time span March 2010 to June 2010. Unfortunately, useful data for the turbine located at the eastern end of the roof are only available for January 2010 (see Fig. 85 for positioning).

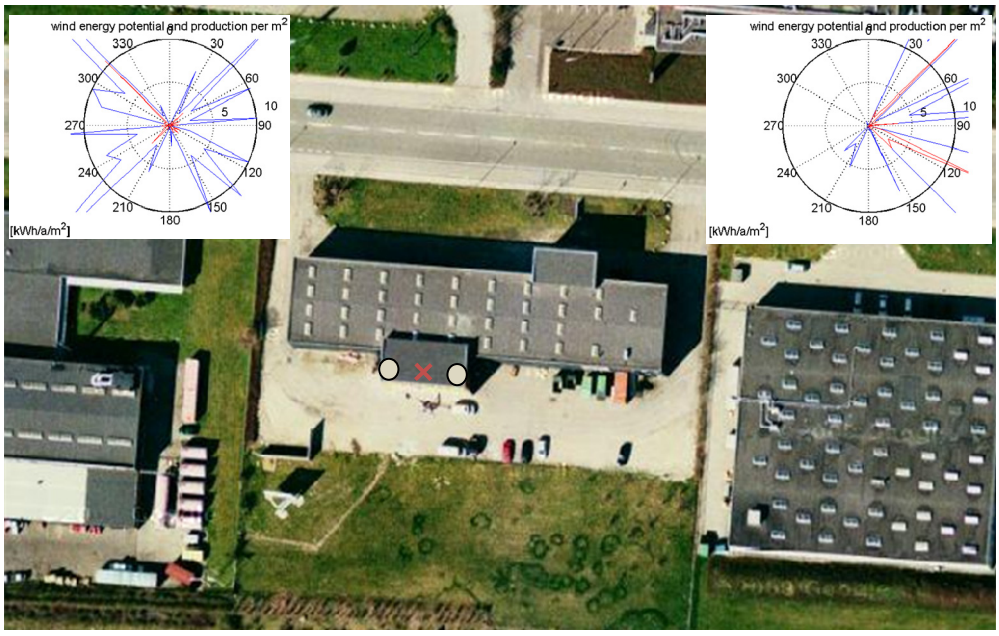

Fig. 85: Site three; close-up with circles at rotor locations, cross at wind measurements device and wind energy potential (blue) and according energy production potential roses (red). The roses are for the time where wind and energy measurements were available for the western and eastern turbine respectively.

Averaging the available energy production data for the four months and assuming that the conditions are the same for the rest of the year, the turbine to the west leads to an AEP of 154.8kWh/year. Using the wind data from exactly the same days combined with the approximated power curve concludes in an AEP of 105.9kWh/year. Hence, the estimation is 31.7% too low. With the data collected in January, the turbine to the east delivers an AEP of 162.79kWh/year, whereas the estimation results in 181.49kWh/year and with that an output 11.5% above the measured one.

For the western oriented turbine the estimation is 32% to low and for the turbine oriented towards the east it is 12% to high. It is obvious that the micro wind climate does play a role. Since the wind measurements are taken in between the two turbines, the estimation is more appropriate for this location rather than for the actual turbine positions. To come back to the micro climate issue. Examining the wind rose, based on the four months, directionality is visible (see Fig. 86, left).

Bringing this wind rose into relation with the building geometry explains the higher energy production for the western placed turbine. Because the wind is predominantly blowing from north-west over the according time span, the wind measurement device is positioned in an area, strongly influenced by the building. Whether the flow is separated at the northern edge of the small rooftop and with that the measurement device most likely positioned in the separation bubble or partly in the lifted wind profile. Or, in case of no separation and in case of reattachment before reaching the device respectively, the wind velocity is decreased. In opposition to that, the turbine to the west is more or less free from the small roof's decelerating influence, when the wind approaches from north-west. Quite the contrary, it could be exposed in the advantageous upwind region, found on the front edge of buildings higher than the surrounding buildings. Fig. 86, right, shows the development of the wind field over a flat rooftop, with the incoming wind perpendicular to the free-standing front face. Here it is observed that the wind velocity is decreasing over the rooftop's depth. In this case the flow keeps attached to the surface. Since this example simulation is a result of a wind field approaching the built-up area perpendicular, it does not tell the whole story, but is used to show the general behavior of flow over a flat roof of a first row rectangular box obstacle. Later, another example is shown, where a cube is exposed to a wind field approaching it in a 45° angle to the front face.

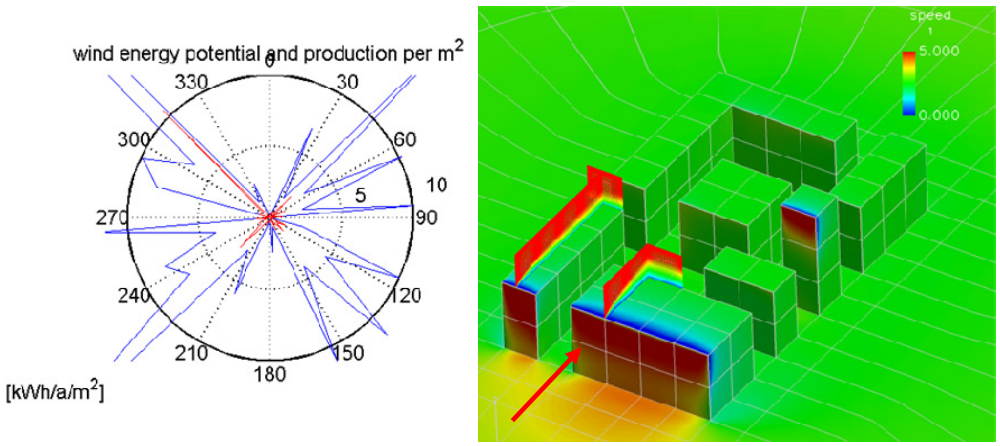

Fig. 86: Left: wind energy potential and production rose for site three (March to June 2010); right: simulation results for an obstacle cluster exposed to a wind approaching the façade perpendicularly.

The directed energy rose for January is shown in Fig. 87, left. With the phenomena in mind which might explain the underestimation for the turbine to the west, the directionality found in January can motivate the expectation that the energy output estimation for the turbine to the east is too low as well. Taking another effect into consideration helps explaining the actual overestimation. We are looking at Fig. 87, right.

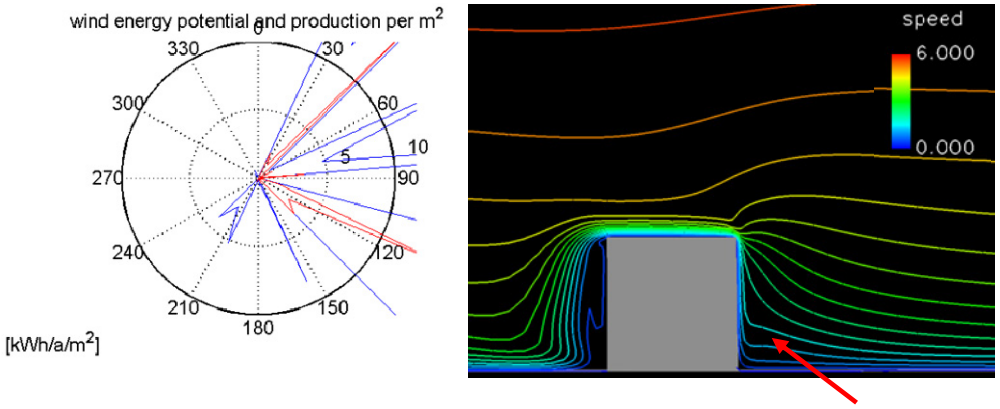

Fig. 87: Left: wind energy potential and production rose for site three (January 2010); right: simulation results for a cube exposed to a horizontal flow approaching the façade in a 45° angle.

In the figure the front face of a cube is shown, where the wind is approaching horizontally, but with a 45° angle between the wind vector and the cube façade. The contour lines are representing lines of the same speed in a plane parallel to the cube front face at 14% depths. Simplified, the eastern turbine would be on the right corner and the wind measurement device in the middle. It can be seen that at the right corner, beyond a certain height, the same velocities as in the middle are reached at greater heights. That means that at the wind turbine position the energy contained in the wind actually is lower than at the location of the wind measurement, when the wind approaches the cubic obstacle from 45°. Fig. 88 shows again iso-speed plots, one in the plane at 20% cube depth (top) and one at 80% depth (bottom).

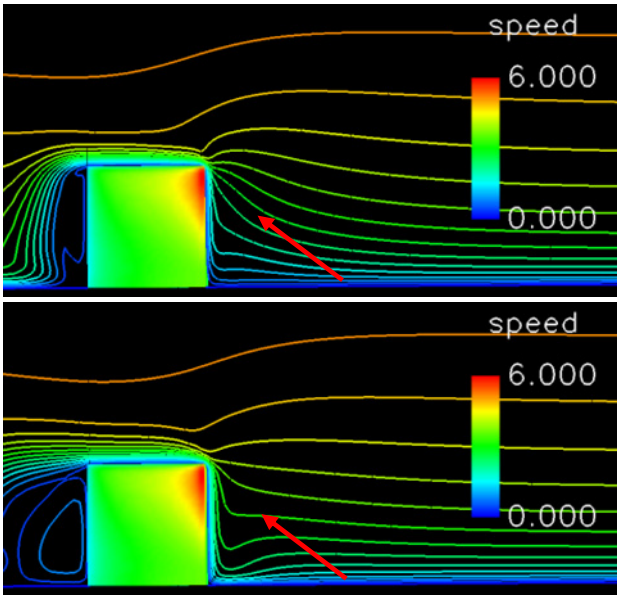

Fig. 88: Iso-speed lines for a cube exposed to a horizontal flow approaching the façade in a 45° angle. Top: plane parallel to front face at 20% cube depth and; bottom: at 80% cubes depth.

Furthermore, an iso-speed plot in a plane parallel to a cube top face is shown in Fig. 89. The contour lines show the iso-speed pattern above the cube top (30% cube height). The white lines indicate the planes at 20% and 80% depth. A slight asymmetry is present, which is most likely due to the rather short distance between the computational domain's inflow face and the cube. These simulations are not conducted with the PlayBox tool.

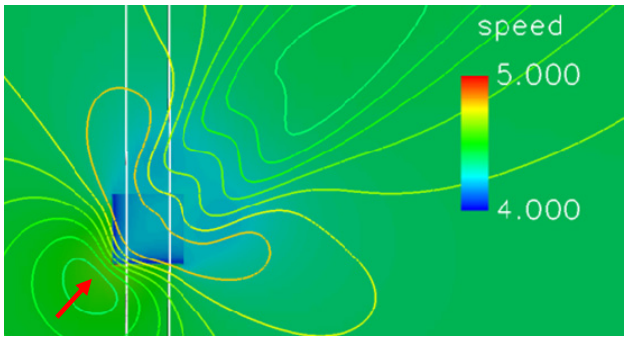

Fig. 89: Iso-speed lines in a plane parallel to top face of a cube exposed to a horizontal flow approaching the façade in a 45° angle

The plot above can also be used to understand the western oriented turbine situation. Since the greatest energy potential for the observed period is found in the 315° sector, the slice at 80% depth (Fig. 88, bottom) represents the most present flow field the turbine is exposed to. Again, the turbine would be standing on the right corner and the wind measurement taking place in the middle. Different from the flow field at 20% depth, the same velocities as in the middle are already reached at lower heights at the corner. Surely, the real onsite wind field is more complex, plus, the wind is also blowing from other directions than the ones richest in energy.

5.1.4.2 Site one

For the turbines at *site one* (see Fig. 90, left) only sparsely data are available. The energy production is not given separately for each of the turbines and it is not known where exactly the wind measurements device is installed. Data from February 2010 to April 2010 are the base for this evaluation.

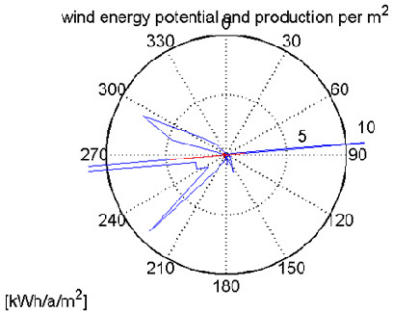

Fig. 90: Site one; left: close-up with circles at rotor locations and right: wind energy potential (blue) and according wind energy production potential roses (red). The rose is for the time where wind and energy measurements were available.

Again, an average is formed and an AEP found as for *site three*. This method leads to a measured energy production of 28.77kWh/year, where the estimation output is

with 27.19kWh/year 5.5% off. Looking at the turbines positions at the site and the found energy rose (Fig. 90, right), one may raise the guess that the southern positioned turbine performs slightly better than the one towards north. But it is too uncertain to say something about the performance over the year and seasonal directionality. Data of 34 days are used, most of them of the month February 2010.

5.1.4.3 Site two

For *site two* the month November 2010 delivers an interesting set of data to work with. The good thing is that data are available for both turbines for the same period. 15 days of energy production measurements lead to an AEP of 96.36kWh/year for the turbine to the west and 142.11kWh/year for the one to the east (see Fig. 91, left, for wind turbine orientation and local energy rose for the examined period). The AEP based on the wind measurements predicts an AEP of 67.58kWh/year. In this case the estimation is underestimating the energy production for both the turbines. For the one to the west it is underrating the production by 29.9% and for the one to the east severely by 52.5%. The wind measurement device is positioned somewhere south of the eastern turbine. As well as the turbine it is located on the small plateau, with a distance of about 2m from the VAWT axis and at approximately 2m a.r.l .

Despite the discrepancy between estimation and measurement, according to the directionality of the energy content for the observed period and the turbine positions in the built-up set-up, the turbine to the east is expected to have a greater energy outcome than the western located, as measured. For the eastern located turbine data of more than these 15days analyzed here are available. Estimations carried out with these other data sets results in AEP underestimations in the same order of about 50%.

Fig. 91: Site two; left: close-up with circles at rotor locations and right: wind energy potential (blue) and according wind energy production potential roses (red). The rose is for the time where wind and energy measurements were available.

Assuming the flow around the eastern plateau to be similar to the flow around a cube with a flow approaching in a 45° angle to the façade, the pictures in Fig. 88 illustrate the conditions again. The turbine would be positioned somewhere to the right and relatively to that the measurement device would be located to the left relative to the turbine. With a hub height of 3m a.r.l. for the turbine and a measurement height of 2m a.r.l. a remarkable speed difference can occur, actually for both the 20% and 80% depth.

5.2 Siting method

One way to evaluate the positioning of a turbine in the urban environment was shown in the prior section. Another approach is to evaluate a site and locate rotors accordingly to the most promising energy regime within the chosen site. A general

method is developed to do so and is presented exemplarily here with the help of *site two*.

The method is developed on base of

- wind measurements at an urban site (u_{ave}, $z(u_{ave})$)
- a fully described site outside but close to the city (u_{aveA}, $z(u_{aveA})$, z_{0A})
- graphical and geometrical information of the urban site (λ_P, $\overline{H}$, x)

Using then analytical equations determines the roughness length and displacement height present at the specific urban site (roughness step, method I in chapter "Urban Wind Climate"). Thereby the corresponding logarithmic wind speed profile is forced to go through the wind measurement point. Since the measurements are taken on a rooftop, the place where the local wind variability is known to be significant, the found roughness length and displacement height is employed as input for the geostrophic drag law, method II in chapter "Urban Wind Climate", resulting in a more general wind speed profile for the urban site.

In Fig. 92, right, the solid line pictures the wind profile based on the data from the site outside the city, here the Airport Kastrup weather station. The green dashed line is showing the logarithmic wind profile found with method I going through the point of measurement (little red x). For its generation, measurements and graphical information (see Fig. 92, left) are necessary as input. The dotted curve shall represent the possible local wind profile variation, going through the point of measurement as well. With the geostrophic drag law (method II) and the results from method I as input, the red dashed line can be drawn.

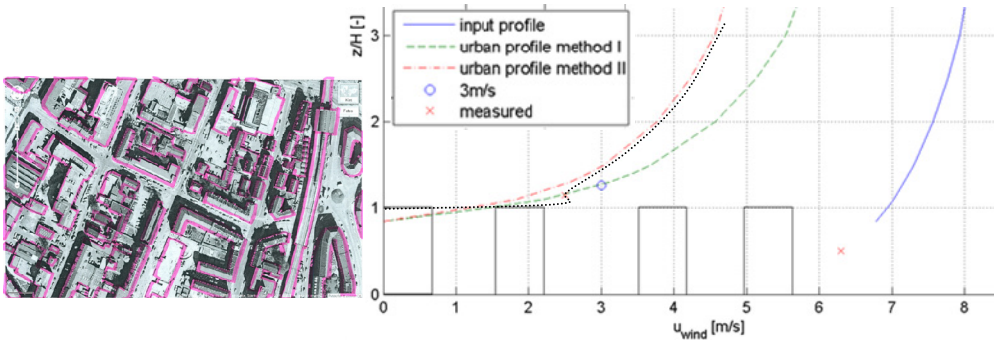

Fig. 92: Site two; left: site plot with built-up indication; right: wind profiles determined with method I and II and an example local variation profile (black dotted line)

This profile, assumed to be representative for the site, delivers a scaling factor for the CFD simulation results obtained with the tool Playbox. More details about the procedure are explained in the following. But first a summary of the necessary tools is given with

- roughness step method
- geostrophic drag law method
- CFD simulations (PlayBox).

With the help of CFD simulations flow patterns around building arrangements characteristic for the urban environment can be investigated. A tool like PlayBox introduced in chapter "Flow around Obstacles" can support the understanding of

flow behavior, but it can also detect areas with potentially higher wind energy content. The simulation examples in chapter "Flow around Obstacles" were orientated on the district descriptions Badde & Plate published in 1994 [46]. The roughness length on all surfaces was set to z_0=0.2m and the friction velocity for the approaching logarithmic wind profile not displaced in height was u^*=0.5m/s resulting in a wind velocity of 4.9m/s at 10m height above ground level. For many aerodynamic applications, the most important dimensionless number is the Reynolds number. In case of a streamline shaped profile for an airplane wing or blade of a wind turbine rotor for example, wind tunnel experiments can be conducted with a down-scaled model and results transferred to the original sized model, as long as the Reynolds number is maintained. Due to the aerodynamics of bluff bodies, here cubes with clear edges, Reynolds number independency is applicable (see Appendix C) and the most important similarity number is the Jensen number, assuming the flow is fully turbulent. So, the results obtained with the PlayBox CFD simulations can be transferred to another dimensional scale, as long as the relationship from Eq. 12 is met.

For *site one* to *site four,* roughness lengths, built-up densities, buildings mean heights and representative wind profiles were determined in one of the foregoing section. Comparing these results from the site descriptions with the PlayBox simulation cases, *site two* can be categorized as configuration 7 according to Badde and Plate's definition in terms of roughness length, built-up density and buildings mean height (see Table 14). Configuration 6 might be more appropriate, but simulations are not carried out for it and setting up such, requires time intensive work, which can be thought of as future work. For the moment, configuration 7 and *site two* are assumed to correspond to each other, explaining the method with the simulation case where the wind enters the plot from north.

Table 14: Measurement site, configuration and simulation description

	z_0 [m]	λ_p [-]	$\bar{H}$ [m]
site two	0.64	0.41	20
configuration 7 (Badde&Plate)	0.3-0.7	<0.5	>15
PlayBox model	0.2 (surface)	0.40	25.4

In order to transfer results from the simulation to the original site, *site two*, the similarity requirement has to be met by maintaining the Jensen number. That means the ratio between buildings height to roughness length has to be the same for the simulation and for the original site, when scaling. Therefore,

$$\bar{H}_{o\ scale} = \bar{H}_m \quad \text{and} \quad z_{0,o\ scale} = z_{0,o}\frac{\bar{H}_m}{\bar{H}_{o\ scale}} \qquad \text{(Eq. 38 \& Eq. 39)}$$

with indices *o* indicating the original, *site two*, and *m* indicating the PlayBox model.

Speed profiles are extracted from the simulation at locations of different character, as the approaching wind profile (***point one***), the wind profile on the rooftop of a building higher than the mean height (***point two***), on top of a building positioned in the wake of a higher building (***point three***), in a street canyon (***point four***) and behind a building (***point five***). The extraction locations in particular are indicated in Fig. 93.

The logarithmic wind profiles for the original urban sites calculated with method I and method II, are in general representing the average of all wind speed profile

variations in the district. That is why a collection of different variations in the simulation domain are collected. In Fig. 94, left, the extracted profiles and the calculated profiles are shown, without any scaling applied yet.

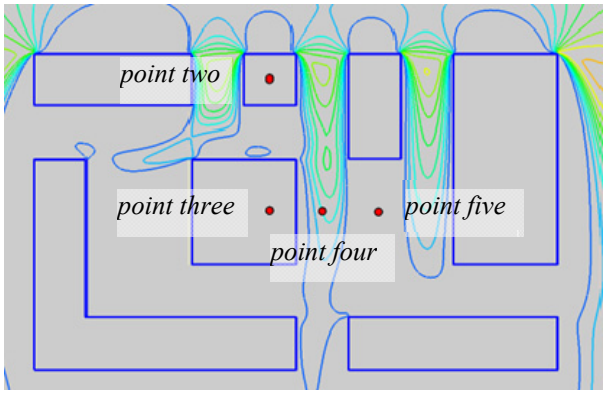

Fig. 93: Extraction points for local wind profiles

The ratio of the buildings mean height of the PlayBox model and the original site is $\overline{H}_m/\overline{H}_o$=1.27. Scaling the roughness lengths and displacement height found with method I with the factor 1.27 and feeding these values into method II, results in a friction velocity of u^*_{scaled}=0.491m/s. As mentioned earlier, the profile derived with method II is decided to be more appropriate to represent the average wind profile, since compared to the profile derived with method I, it is not forced to go through the point of measurement taken at a location expected to be subjected to a high variation. The two resulting profiles are plotted in Fig. 94, middle.

Examining the extracted local wind profiles, they seem to converge towards a common value in a certain height. A height of 200m is assumed to be the height where all the extraction profiles have reached a value of about 8.6m/s. Similar to the idea behind the geostrophic drag law, where the wind velocity of two wind profiles to compare are assumed to be the same at a certain height, the velocity at a height of 200m for the variation profiles, $u_{m\ scaled}$, and the averaged profile found with method II scaled according to the geometry, $u_{II\ scaled}$, have to be the same.

$$u_{II\ scaled}(200m) = u_{m\ scaled}(200m) \qquad \text{(Eq. 40)}$$

Comparing the wind speed of the scaled profile from method II at 200m, which is 6.60m/s, with the extracted profiles, the simulation speed results have to be scaled with a factor of 0.77. Doing so, results in local wind speed profile as they can be seen plotted in grey in Fig. 94, right. A closer look on the area of interest is given in Fig. 95 with all profiles scaled accordingly to the description of the method.

The first scaling provokes the method I profile to go through approximately 3.2m/s at 29m height, which is the scaled measurement at 23m height with 2.5m/s. In comparison to that, the scaled method II profile goes through 2.4m/s at 29m height. Averaging the four scaled profiles from the extraction points lying within the buildings cluster, results in a velocity of 1.85m/s at a height of 29m. With that the average velocity is 23% too low, compared to the 2.4m/s. Scaling the extracted profiles according to the wind speed at 200m found for the scaled profile with method I, results in an average velocity of 2.4m/s at 29m. This is 26% too low compared to the 3.2m/s. So, the wind speed scaling is orientated on the profile derived with method II, mainly justified with the earlier argument.

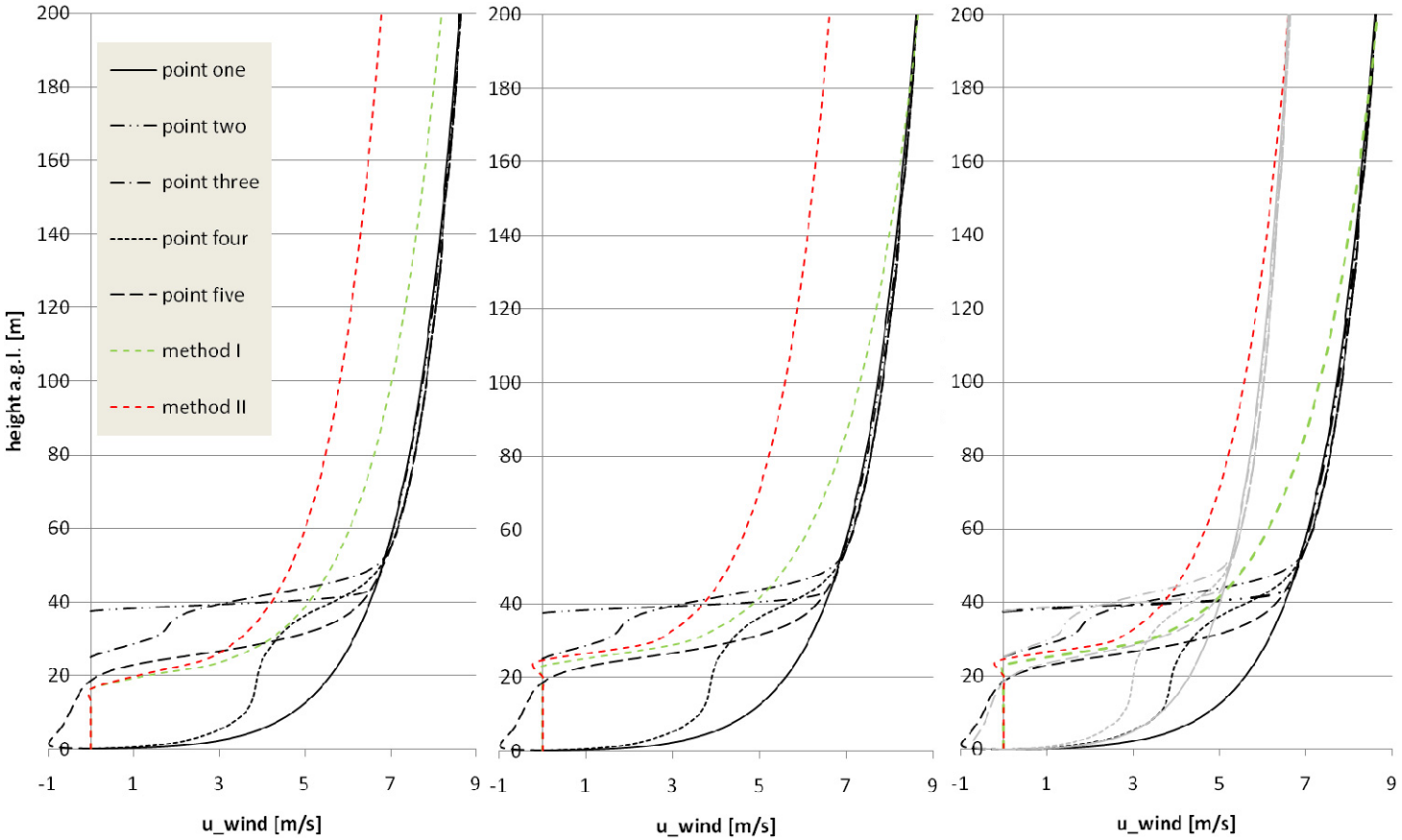

Fig. 94: Wind profiles from method I and II based on onsite measurements and simulation profiles locally extracted; left: not scaled at all; middle: scaled method I and II profiles; right: simulation profiles scaled to fit method II profile at 200m height

Only scaling the wind speeds found in the simulation is not enough though to make the climate comparable to the wind speeds found in the real urban areas, since the usual displacement height of the inflow wind profile is not considered in the simulations and the cube arrangement is directly exposed to the free stream wind profile, where in reality the site is surrounded by other similar rough districts. Surely, this method is connected to a row of assumptions and sources of inaccuracy, but at the same time it delivers an opportunity to draw a picture of orientation, based on the available data and the developed tools.

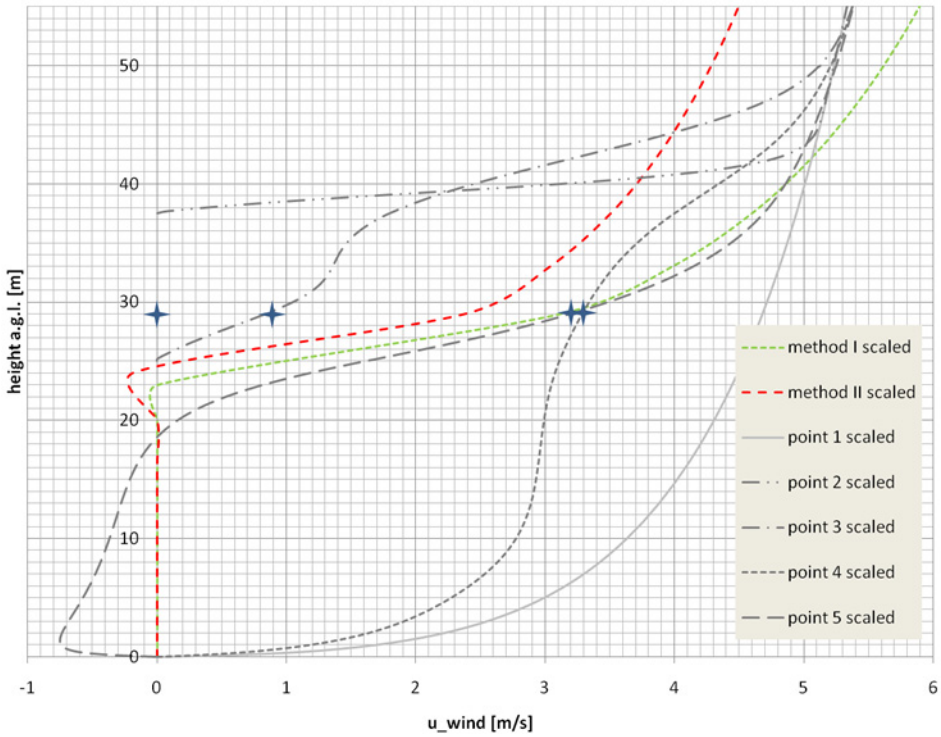

Fig. 95: Close-up of the scaled profiles with blue stars marking the scaled simulation wind speeds at the scaled height of the onsite wind measurement at site two

In the pictures in Fig. 96 iso-lines of the annual wind energy content per year are shown, based on a logarithmic non-displaced profile approaching the set-up from north. Only the wind components in the horizontal plane are considered and multiplied with the scaling factor 0.77. The colors indicate the annual wind energy content with a color scale from 0 to 100kWh/year.

Of course, it has to be taken into account that the wind would not only approach from one side and the annual wind energy content is calculated only with the local average velocity. A Weibull distribution is not considered. Furthermore, it does not picture the energy output of a wind energy conversion device. Both features can be desirable extensions.

Picture d) in Fig. 96 shows the plane 5m above most of the flat rooftops in this set-up. To transfer the result to *site two*, these 5m correspond to a height of 3.9m a.r.l. Actually the energy content has to be scaled back as well, because in these plots it is calculated based on the scaled wind velocities. Beyond the horizontal energy content various properties can be defined and plotted as well.

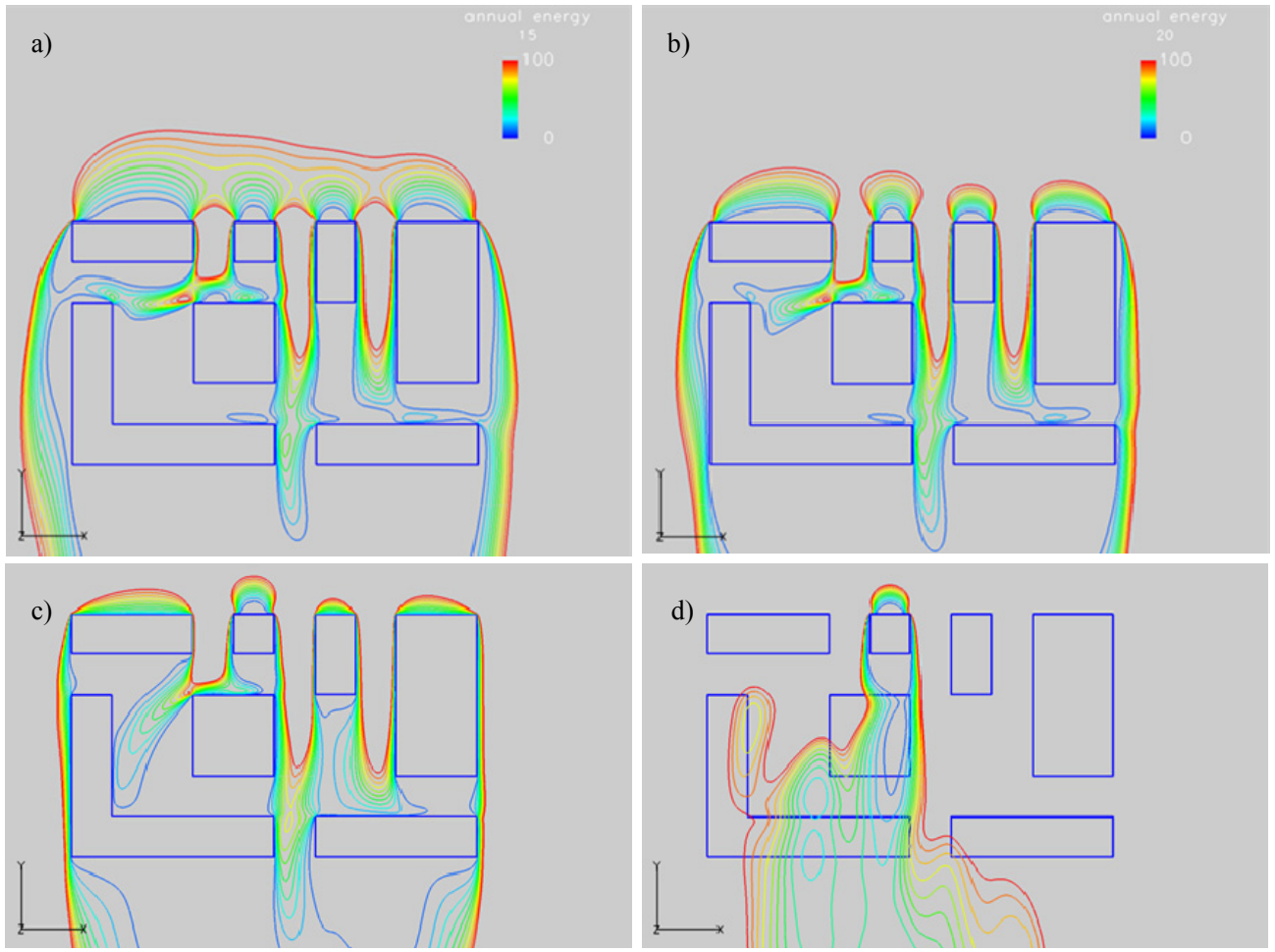

Fig. 96: Simulation results derived with the scaling method showing iso-annual-wind-energy-potential lines at a) – d) 15m, 20m, 25m and 30m. The heights are in the scale of the simulation dimension and wind energy potentials based on scaled wind speeds.

5.3 Conceptual Configurations

In this section different turbine concepts for small-scale VAWT (Vertical Axis Wind Turbine) are designed, their performances examined and compared with each other. The calculations are based on optimized designs which are found with the help of a multiple streamtube model for VAWTs implemented in the optimization code HAWTopt [70] introduced earlier, and is referred to as VAWTopt. This model has several restrictions and is subjected to simplifying assumptions. Nonetheless, this examination shows general qualities for different turbine concepts in various wind climates.

5.3.1 System parameter

For the configurations, the following design parameters and their variations are used:

Design parameter (1): (a) straight blades (H-rotor)
(b) bended blades (Darrieus rotor) with same rotor height and swept rotor area

Design parameter (2): (a) constant rotational speed (200rpm)
(b) constant tip speed ratio, λ

Given parameters: H=1.9m; A_{rotor}=3.61m^2; R_H=0.95m; $R_{Darrieus}$=1.50m

Design point: rotational speed=200rpm at u_{dsg}=5m/s

5.3.2 Geometric input

It is started with an initial design. Table 15 shows the geometric input as used for VAWTopt.

Table 15: Optimization input; left: H-rotor data; right: Darrieus rotor input

# VAWT H-rotor			
3	**Number of blades (-)**		
18	**NT**		
0.95	**R**		
1.9	**H**		
Radius	**Chord**	**Twist**	**Thick**
0.9490	0.10	0	18
0.9495	0.10	0	18
0.9500	0.10	0	18

# VAWT Darrieus-rotor			
3	**Number of blades (-)**		
18	**NT**		
1.5	**R**		
1.9	**H**		
Radius	**Chord**	**Twist**	**Thick**
0.118	0.10	0	18
0.35	0.10	0	18
0.574	0.10	0	18
0.784	0.10	0	18
0.974	0.10	0	18
1.141	0.10	0	18
1.279	0.10	0	18
1.386	0.10	0	18
1.459	0.10	0	18
1.495	0.10	0	18

The radius of the Darrieus shaped rotor, $R_{Darrieus}$, is chosen in such a way, that the swept area for both the rotor shapes is the same, A_{rotor}=3.61m^2. For the H-rotor the area is defined as in Eq. 41,

$$A_H = 2R_H H = 3.61m^2 \,, \qquad \text{(Eq. 41)}$$

with A_H as the swept H shaped rotor area, R_H as the rotor radius and H the height of the rotor. For the Darrieus shaped rotor the area is defined as

$$A_{Darrieus} = 2\int_0^H R_{Darrieus} \sin\left(\pi \frac{z}{H}\right) dz \,, \qquad \text{(Eq. 42)}$$

with $A_{Darrieus}$ as the swept area for the Darrieus shaped rotor, $R_{Darrieus}$ is the equatorial radius and z is the local height along H, the total rotor height. Integration leads to

$$A_{Darrieus} = \frac{4R_{Darrieus}H}{\pi} \qquad \text{(Eq. 43)}$$

and with $A_{Darrieus}=A_H$ the radius for the Darrieus rotor is then $R_{Darrieus}$=1.5m. Fig. 97 pictures the used rotor geometries.

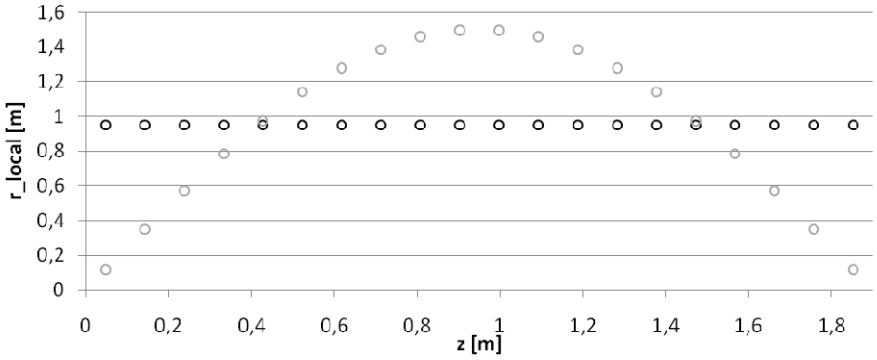

Fig. 97: Rotor elements arrangement for H- and Darrieus rotor; both $A_{rotor}=3.61m^2$

Another way to compare the two shapes is to say that the dimensions limits shall be the same (see Fig. 98). With an unchanged H-rotor, that corresponds to a Darrieus rotor with $R_{Darrieus}$=0.95m. Compared to the Darrieus layout with $R_{Darrieus}$=1.5m, this layout triggers changes due to a different blade slope, β, a different λ in case of constant rotational speed and probably most important, lower Reynolds numbers on the blade segments. This comparison option is interesting as well, but is not examined.

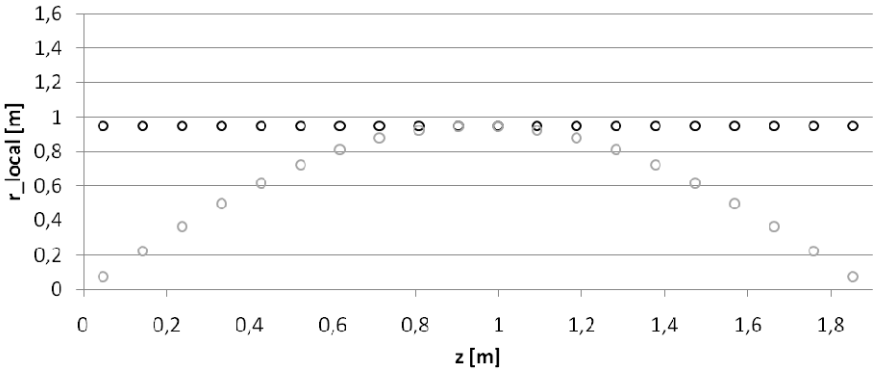

Fig. 98: Rotor elements arrangement for H- and Darrieus rotor; both R=0.95m

5.3.3 Aerodynamic input

In such geometrical dimensions and due to rotational speed limits, the operational Reynolds numbers are rather low. C_l and C_d values are changing significantly when the Reynolds number is changing in such low ranges. To be able to calculate a little

more accurate, values for a few Reynolds numbers are interpolated between the available ones. The following calculations are based on the values shown in Fig. 99.

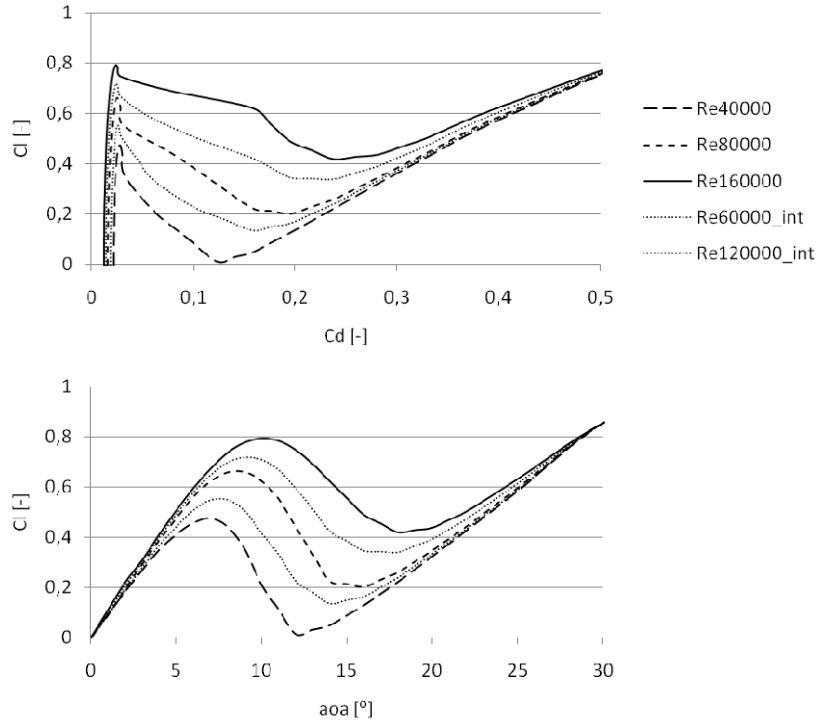

Fig. 99: Used NACA0018 airfoil data at Re=40'000 to 120'000 with interpolated values. Top: C_l vs C_d and bottom: C_l vs aoa

5.3.4 Optimizations

Earlier, in the chapter "Rotor Design", various optimization strategies were introduced. For the designs on hand, the strategy is chosen where the designs are optimized in one single design point, u_{dsg}=5m/s at a rotational speed of 200rpm. The aim is declared to be an optimal chord distribution along the blade to reach a max C_P in the design point. VAWTopt takes airfoil data passively, that means the airfoil data input is used regardless the actual Reynolds number. It is up to the user to decide which Reynolds number is appropriate. A quick calculation determines the design tip speed ratio as in Eq. 44 to be λ_{dsg}=6.3 for the Darrieus rotor and λ_{dsg}=4.0 for the H-rotor.

$$\lambda_{dsg} = \frac{u_{tip,dsg}}{u_{dsg}} = \frac{2\pi R rpm_{dsg}}{60 u_{dsg}} \qquad \text{(Eq. 44)}$$

With such a tip speed ratio, the rotational speed component is dominant on the blade elements and a fast local Reynolds number determination can be conducted with Eq. 45,

$$Re_{local} = \frac{u_{tip,dsg} c}{\nu}, \qquad \text{(Eq. 45)}$$

where c is the chord length and ν=1.5e^{-5}m^2/s the kinematic viscosity. The initial designs lead to Re_{local}= 132'600 for the H-rotor and Re_{local}= 210'000 for the Darrieus rotor. A first optimization is run for both initial designs with a NACA0018 profile at Re=160'000 as input. How the optimization limits are set can be seen in Appendix I.

In Fig. 100 the C_P vs λ is plotted for the initial designs calculated at *Re*=160'000 (solid line). Then, the performances of the optimized geometries are calculated with *Re*=160'000 (dashed line). It can be observed that the performances increase in the design point, but also that the curves flatten and C_{Pmax} moves to higher tip speed ratios, which is caused by decreased solidities. Actually, with the new chord lengths, both designs reach *Re*=80'000. Because of that, airfoil data for *Re*=80'000 needs to be considered. Calculating with the appropriate airfoil data, results in lower C_P values, even in the design points. These curves are shown as dotted lines in Fig. 100.

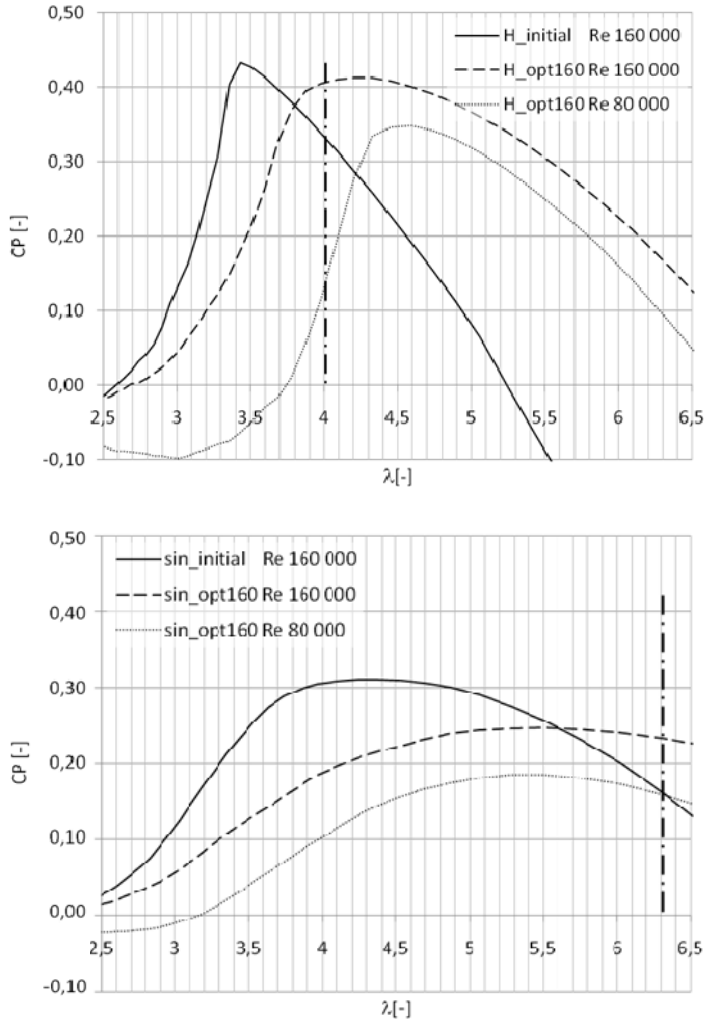

Fig. 100: C_P vs λ for the initial design with Re=160'000; the optimized design on base of Re=160'000 and optimized design performance with Re=80'000 input. Top: for the H-rotor; bottom: for the Darrieus rotor

In a second step, an optimization is run with the initial designs and the airfoil data at *Re*=80'000 instead of *Re*=160'000. In Fig. 101 the results are plotted (dotted lines). Because the optimization is based on the airfoil values with *Re*=80'000, the according curves for the initial design are drawn as well, to see the relative improvement (solid lines). Comparing the results of the new found optimized shapes with the one found with the optimization based on *Re*=160'000 (dash dotted lines) shows, the new optimization improves the performance in the design point for the H-rotor. In opposition to this, the performance for the Darrieus rotor actually gets not enhanced with this approach.

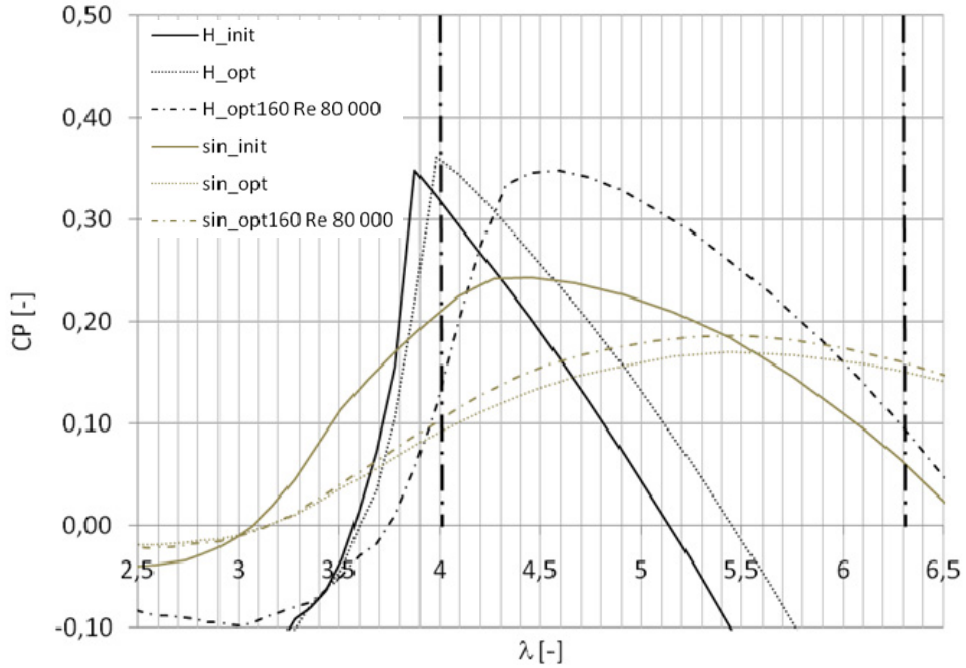

Fig. 101: C_P vs λ for the initial design with Re=80'000; the optimized design on base of Re=80'000 and optimized design on base of Re=160'000 input. H-rotor named H and Darrieus rotor named sin

That shows again that optimization is an iterative process. Nonetheless, the two designs based on the *Re*=80'000 input are considered to be the final designs.

5.3.5 Geometric output

The geometries found with the optimization process are listed in Table 16. Furthermore, three dimensional model renderings can be found in Appendix J.

Table 16: Geometric output for u_{dsg}=5m/s and 200rpm with a NACA0018 airfoil at Re=80'000; left: H-rotor; right: Darrieus rotor

# VAWT H-rotor			
3	**Number of blades (-)**		
18	**NT**		
0.95	**R**		
1.9	**H**		
Radius	**Chord**	**Twist**	**Thick**
0.9490	0.09	0	18
0.9495	0.09	0	18
0.9500	0.09	0	18

# VAWT Darrieus-rotor			
3	**Number of blades (-)**		
18	**NT**		
1.5	**R**		
1.9	**H**		
Radius	**Chord**	**Twist**	**Thick**
0.118	0.03	0	18
0.35	0.07	0	18
0.574	0.14	0	18
0.784	0.08	0	18
0.974	0.05	0	18
1.141	0.04	0	18
1.279	0.04	0	18
1.386	0.04	0	18
1.459	0.04	0	18
1.495	0.04	0	18

Most Darrieus rotor layouts do have a constant chord along the blade. Examining the geometric optimization output shows a changing chord distribution, in order to follow an optimal solidity distribution and with that to increase the rotor performance. In manner of manufacturing such blades might be more costly, though.

5.3.6 Aerodynamic output

Something very general can be said about the aerodynamics of an H and Darrieus rotor layout. The H-rotor reaches higher C_p values, but only for a very limited range of λs, whereas the Darrieus rotor layout has the ability to operate over a rather broad range of λs. Looking at the C_P vs λ curves for the rotor geometries at Re=80'000 (see Fig. 102), it can be seen that the new designs had improved the performances in the design point, compared to the initial designs. Because the equatorial radii are different for the H and Darrieus layout, the design points are located at different λs. For the H-rotor design the C_P value is enhanced from C_{PinitH}=0.32 to C_{PoptH}=0.36. And for the Darrieus layout the C_P value is enhanced from $C_{Pinitsin}$=0.07 to $C_{Poptsin}$=0.15.

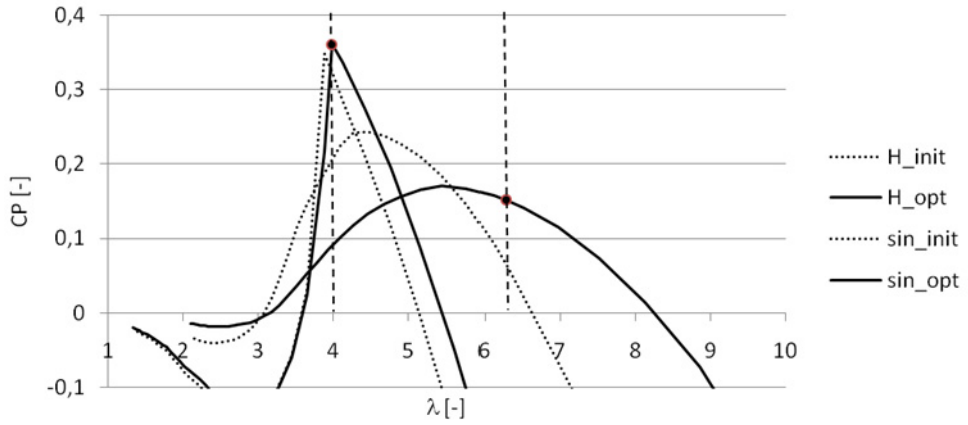

Fig. 102: C_P vs λ at Re=80'000 values for the two initial designs and the two optimized designs. $\lambda_{dsg,H}$=4.0 and $\lambda_{dsg,sin}$=6.3 are indicated with vertical dashed lines

The curves in Fig. 102 show only the values for Re=80'000. During operation different working points are passed through and other Reynolds numbers apply. A graph is drawn for that, on the basis of the two different generator principles, keeping either λ constant or the rotational speed (see Fig. 103).

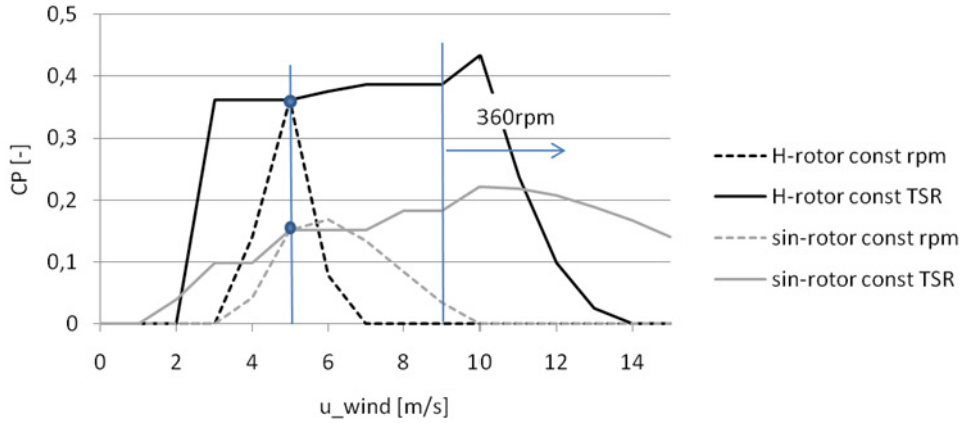

Fig. 103: C_p vs u for the four configurations with Reynolds number changes during operation

That is done by taking the designs found for the optimization at 5m/s with 200rpm at Re=80'000 and calculating the C_P values for the other working points while changing the airfoil data input according to the necessary Reynolds number. For the concepts with a constant λ a rotational speed of 360rpm is reached at a wind speed of 9m/s. It is decided to keep the rotational speed constant from this point on. The C_P curves look rather edged and not as smooth as one might be used to. This arises from the changing Reynolds number input. By using finer steps of Reynolds numbers the curves can be refined.

5.3.7 Distributions along the blades

The optimized Darrieus rotor design shows a high local solidity towards the shaft (see Fig. 104, top). At the equator the local λ is 6.3, whereas at the point with the highest local solidity, which in this case is the point with the highest local C_P value, the local λ is 2.4. C_P is dependent on λ, solidity and dependent on the airfoil data in terms of Reynolds numbers dependent C_l –C_d values. That means, by choosing a certain Reynolds number and rotational speed, an optimal solidity is found, corresponding to the local λ and actually also local blade slope, β. The found chords have to be examined, if the chosen Reynolds number is appropriate. So, it can be necessary to run several optimizations, where the designer changes the chord limits or the Reynolds number. Furthermore, another diameter, working point or working range can be chosen.

Fig. 104 illustrates the distribution of the local solidity and the corresponding local C_P before and after the optimization. The x-axis is thereby ranging to half the rotor height. With one of the restrictions of the DART code in mind, which was a moderate solidity, the rather high solidity present at the shaft for the Darrieus rotor has to be accepted with caution. On the other hand, the original code, before modification, is based on Darrieus shaped rotors with a constant chord along the blade only, corresponding to the initial design.

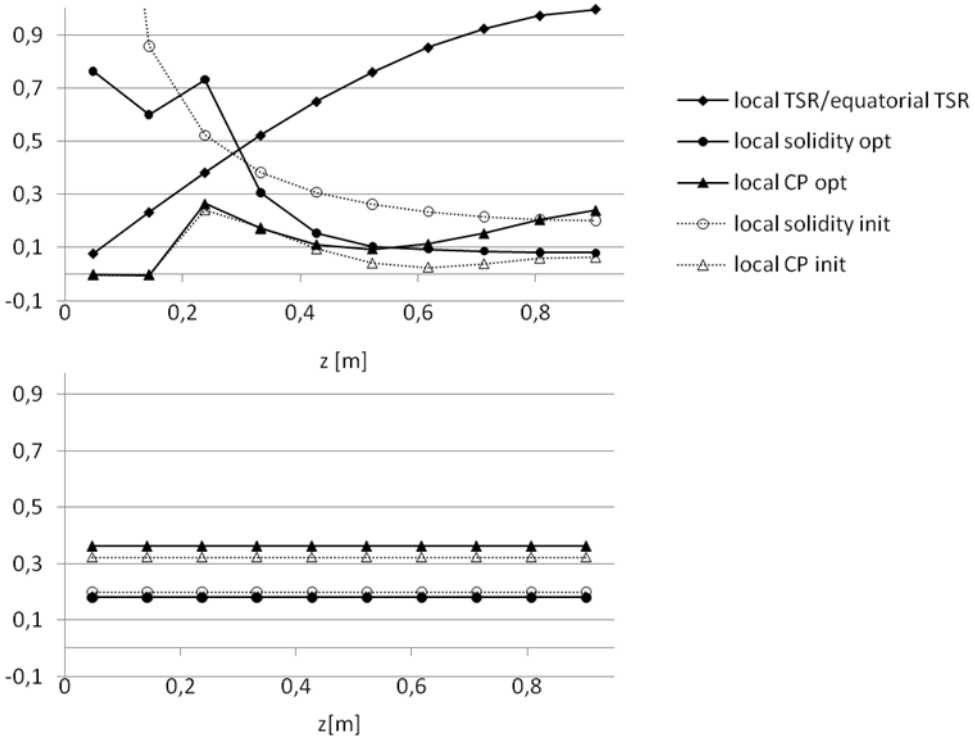

Fig. 104: Local blade characteristics for the initial and the optimized rotor at design point operation; top: Darrieus rotor; bottom: H- rotor

For the H-rotor design λ is constant along the blade and in the design point it is 4.0. An optimal constant chord length is found with 0.09m at exactly this working point (see Fig. 104, bottom). As soon as λ is changed, as it is the case for the constant rotational speed configuration, the solidity does not work ideally anymore and the performance decreases drastically, as it can be seen in Fig. 103.

5.3.8 Performance

The four designs, H-rotor operating with constant rotational speed (***conf one***), H-rotor operating at constant λ (***conf two***), Darrieus shaped rotor operating with constant rotational speed (***conf three***) and Darrieus shaped rotor operating at constant λ (***conf four***) are in this section exposed to four wind climates to evaluate their performances. In general, for operation at constant λ the H-rotor performs very well in terms of high C_P values (*conf two*). The Darrieus shaped rotor reaches less high power coefficients but in return operates over a broader range. The corresponding power curves, only based on aerodynamic properties, are shown in Fig. 105.

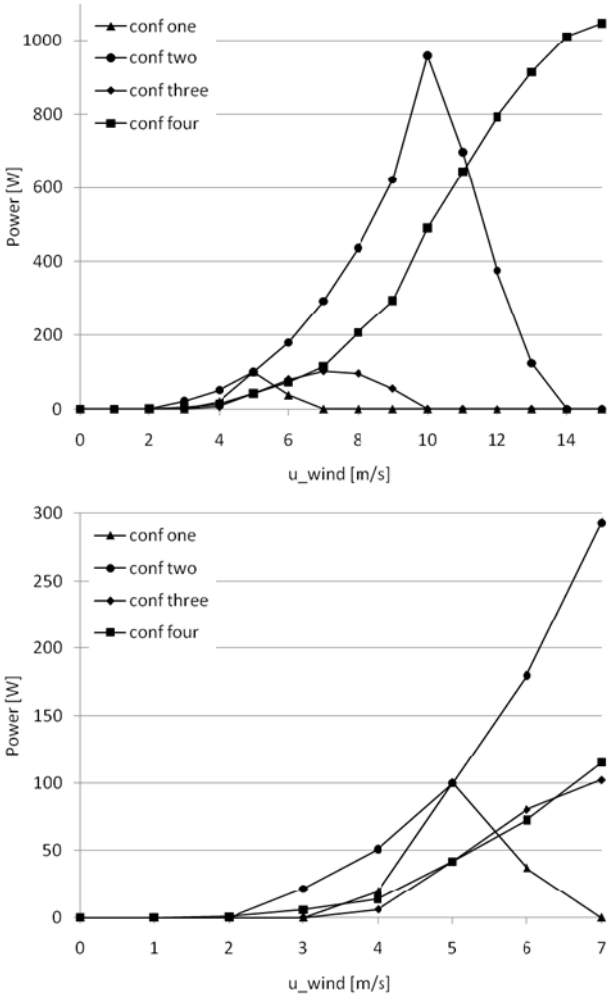

Fig. 105: Power curves for the four configurations. At the bottom a close-up of the low wind speed range performances.

These four designs are exposed to four wind climates of different character. The used climates are chosen from the ones described in detail earlier and are named ***A***, ***B***, ***C***, ***D*** as shown in Fig. 106.

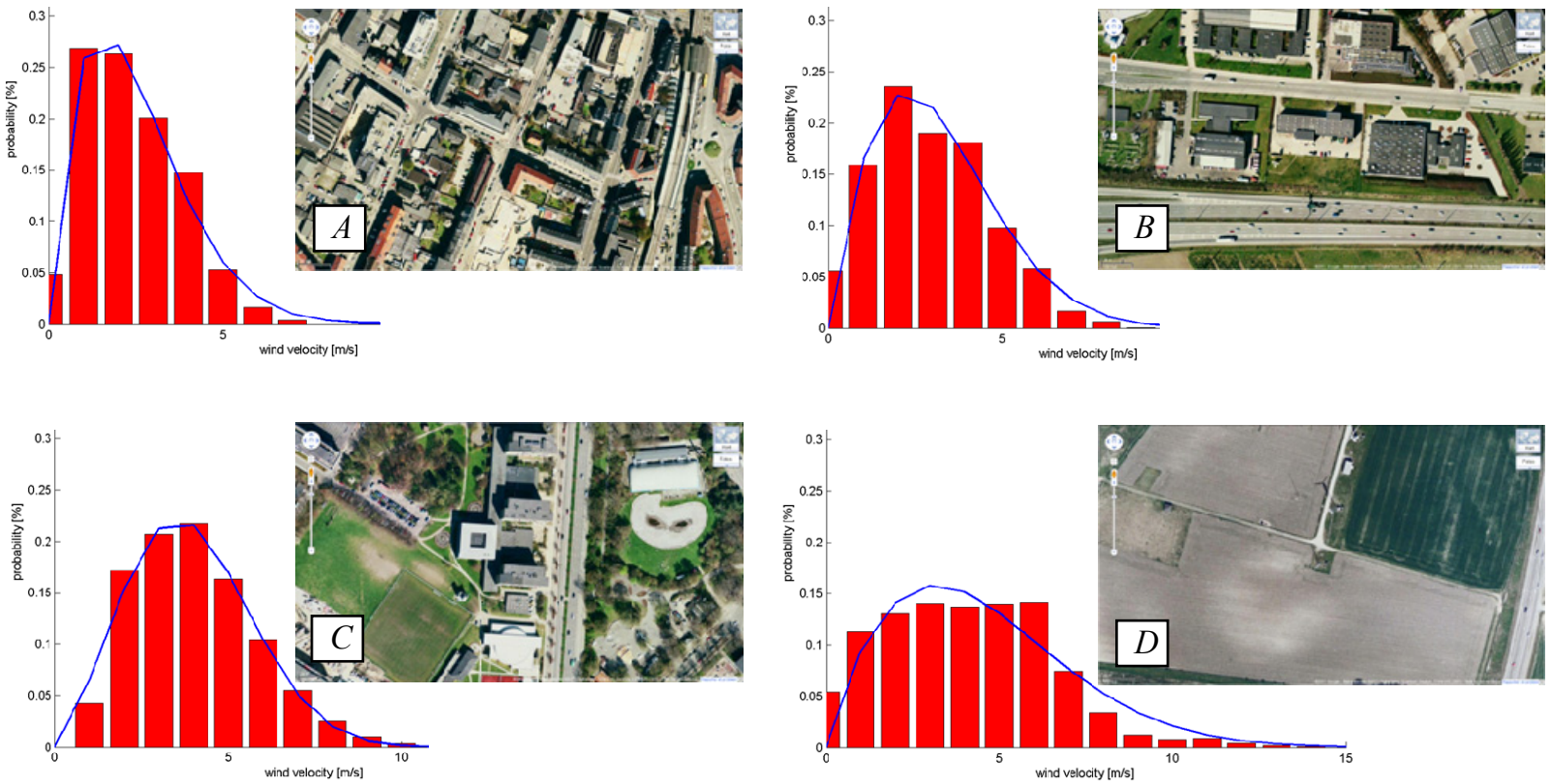

Fig. 106: Weibull distributions for different sites and satellite pictures of the sites

In Table 17 the results are summarized. All the turbines have a swept area of 3.61m^2 and each turbine configuration is rated at its max reached power. For *conf one* it is 0.1kW at 5m/s, *conf two* reaches its max power with 0.96kW at 10m/s, *conf three* has a rated power of 0.1kW at 7m/s and *conf four* has with 1.05kW the highest rated power, which however first is reached at 15m/s.

For this concept investigation special focus is taken on the load factor and the parameter C_E. The load factor reflects how well the generators capacity is used. Generators operate most likely less efficient in ranges below their design working point. So if generators are operating in a range far below their capacity they are suspected to introduce higher generator losses. Numbers obtained here do not include any losses at all. Besides the load factor the parameter C_E is believed to deliver a value to rate the operational efficiency of turbines. Different from the load factor it sets the AEP in a certain wind climate into relation with this certain wind climate instead of into relation with the optimal operation of the turbine concept. For both numbers counts, the higher value reached the better is the concept.

Table 17: Estimated annual rotor performances for the four configurations at four different sites

site	k	A	u_{ave}	AEP	AEP/m^2	load factor	annual wind potential/m^2	C_E
	[-]	[m/s]	[m/s]	[kWh]	[kWh/m^2]	[-]	[kWh/m^2]	[-]
A	1.7	2.7	2.5				153.27	
	conf one (100W)			76.92	21.31	**0.088**		0.14
	conf two (960W)			184.83	51.20	0.022		**0.33**
	conf three (100W)			41.63	11.53	0.048		0.08
	conf four (1050W)			63.21	17.51	0.007		0.11
B	1.8	3.5	2.9				284.44	
	conf one			130.24	36.10	**0.150**		0.13
	conf two			365.67	101.30	0.043		**0.36**
	conf three			106.98	29.63	0.120		0.10
	conf four			136.98	37.94	0.015		0.13
C	2.4	4.5	4.0				572.43	
	conf one			214.93	59.54	**0.250**		0.10
	conf two			763.84	211.60	0.091		**0.37**
	conf three			218.98	60.66	**0.250**		0.11
	conf four			307.30	85.12	0.033		0.15
D	1.8	5.1	4.3				787.13	
	conf one			192.24	53.25	0.22		0.07
	conf two			958.30	265.50	0.11		**0.34**
	conf three			258.58	71.63	**0.30**		0.09
	conf four			468.77	129.90	0.05		0.16

Fig. 107 contains numerous plots, illustrating the found numbers for the four concepts at the four example sites. First of all numbers, a user might be interested in the actual total AEP. That is shown in the plot, top left.

In the majority of cases, turbines with a high rated power are delivering a higher output. But, their generators operate at a low fraction of their full capacity, as seen in Fig. 107, top, second from left. Mentioned earlier, higher generator losses are suspected to be connected to operation with a low load factor. Losses are not

included in the results. Additional, prices for larger generators, e.g. 1kW, are higher than for small generators, e.g. 0.1kW, which settles in the investment costs and with that in the interest of the customer. On the other hand, the same plot reveals the flexibility of the concepts in terms of employing them in various wind climates. The load factor changes for the two high rated concepts are small. That means, they are rather flexible and can be employed in various wind climates, without changing their operational characteristics remarkably, whereas for example *conf one* shows a fairly site-dependent behavior. For *site D*, *conf three* reaches a load factor of 30%. That is a remarkable value in the order of large-scale offshore wind turbines.

Although *conf two* leads to generally low load factors, it shows a flexible behavior towards different wind climates. Furthermore, inspecting the plot in Fig. 107, top, third from left, it reaches clearly the highest C_E values among the four concepts. For all four sites it extracts a third or more of the available energy contained in the onsite winds. Compared to that, the other three concepts extracted approximately 10%.

To get a wholesome picture of the operation, in the last plot of Fig. 107, top, a dimensionless parameter is plotted called *Y*, defined as in Eq. 46.

$$Y = load\ factor * C_E \qquad \text{(Eq. 46)}$$

The load factor is considered important, but of significance is the extracted proportion of energy as well. A symbiosis of these two parameters shows that *conf one* actually is preferable for *site A* and *site B*. The applied weighting of these two parameters is equal but can be thought of being dependent on the investment costs on the load factor side and dependent on the production gain on the C_E side. Keeping the weighting equal, *conf four* is found to be least advisable for all four sites, which can be different with a changed weighting.

In the two graphs at the bottom of Fig. 107, a mapping of the concepts is shown. The one to the left indicates for each of the concepts the site where they operate most efficient, that means where they reach their max $C_{E.}$ (green dot) and with that for which site they are most appropriate. With the pink dots the sites are marked where the concepts reach their maximum AEP. *Site D* is the site with the highest average wind speed. That is why it is not surprising, that most of the concepts generate the most energy in this climate. On the contrary, it is surprising that *conf three* does not.

The last graph in Fig. 107, bottom, right, positions the C_E curves over the corresponding load factors. Here it clearly can be seen, that the load factor ranges of *conf two* and *conf four* are very narrow and located at low numbers. Furthermore, with the help of the two mapping graphs, assumptions can be drawn for *conf one* and *conf four*. The hand drawn curves describe the concepts' characteristics following wind climates with increasing average wind speeds. The maximum C_E values for *conf one* and *conf four* are not local maxima on the curves. So, *conf one* is suspected to be acceptably operating in wind climates with even lower average wind speeds and *conf four* is believed to operate most effective in wind climates with high average wind speeds, compared to the other concepts. Studying the concepts power curves (Fig. 105) and C_P values found for the single wind velocities (see Fig. 103) back up the stated guess.

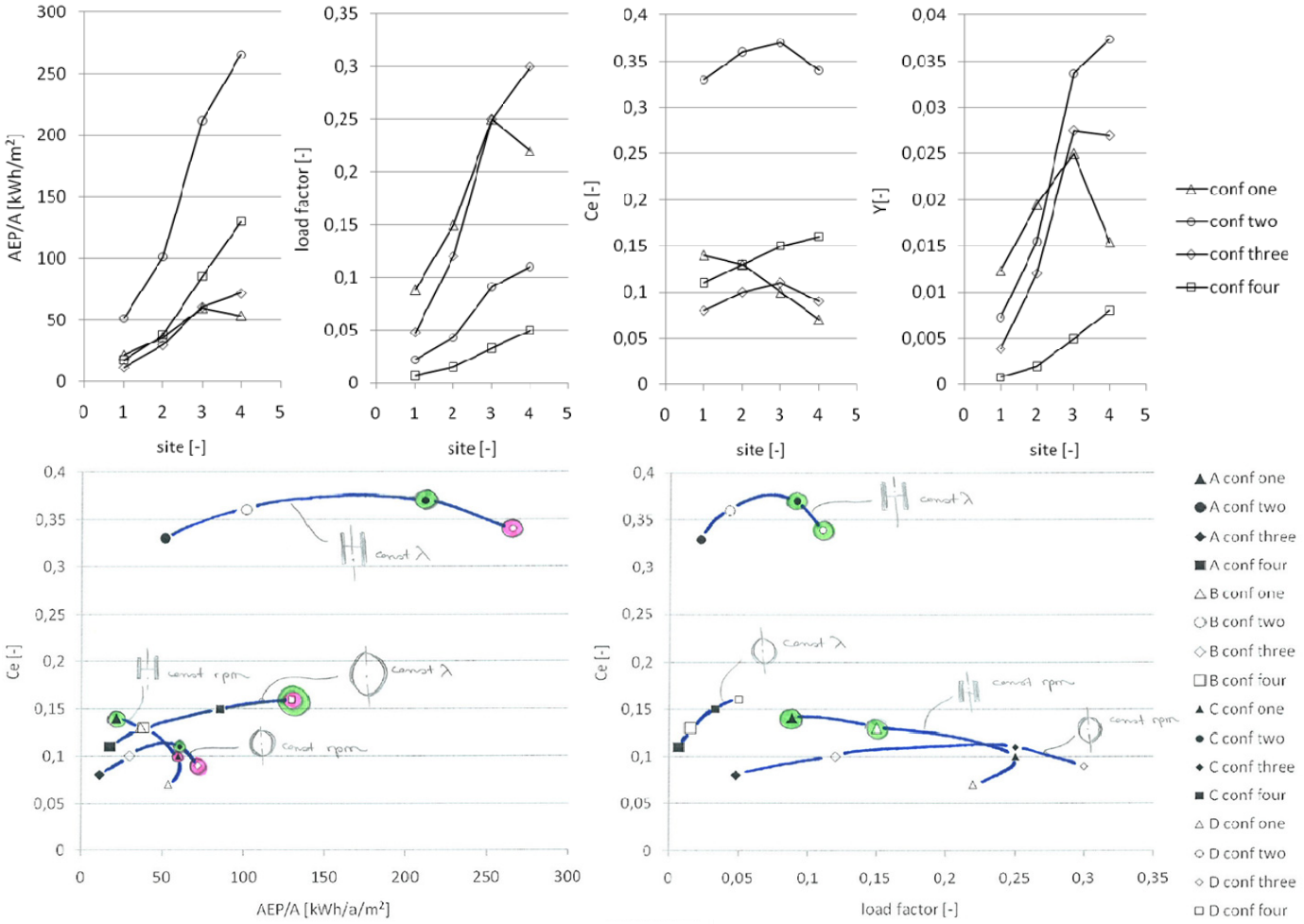

Fig. 107: Top row, left to right: Graphs for the four configurations of AEP/m^2; load factor; C_E and Y at the four sites. Bottom left: C_E vs AEP/m^2; right: C_E vs load factor

5.4 Summary and Conclusions

The content of this chapter is summarized below and the concluded findings, as well as facts, known on beforehand and found to be important, are imbedded as bullets into the continuous text.

With the actual installation of VAWTs on several rooftops within Copenhagen and its vicinity, energy production expectations based on manufacturer power curves and energy production predictions based on onsite wind measurements can be compared with actually measured energy productions. The installation sites chosen by the company Logik&Co are located in macro climates of different character. Within these macro climates the turbines are located at positions subjected to site-specific micro wind climates.

- The energy production of a wind turbine is depending on the local wind climate, the turbines positioning within the local wind climate and the turbines capability to operate under the conditions, it is exposed to.
- Certified power curves for small wind turbines are necessary to circumvent wrong expectations.
- Power curves may vary with site-dependent turbulence intensities.

Energy production estimations for the installed wind turbines, on the base of the measured power curve and wind measurements taken on the same rooftops, but aside the actual wind turbine positions, do vary significantly.

- If a specific installation position in a built-up area is chosen, performance estimations for a possible wind turbine model, based on wind measurements aside the actual rotor installation position, can vary seriously due to local wind variability.

The parameters describing the measurement sites are found to be different from each other, but for all measurement sites wind velocities in the range 1-6m/s are most represented. Calculating the load factor for the installed wind turbine type with the estimated energy production at these sites, results in very low generator capacity utilization.

- A low load factor is an indicator for an over-dimensioned generator.

A punctual wind measurement does not resolve the complex micro wind climate. Therefore a siting method is proposed, using the acquired knowledge, developed tools, methods and measurements.

- With punctual wind measurements and the proposed siting method, positions different from, but close by the measurement position can be evaluated.

Four rotor concepts, oriented on the installed wind turbine rotor dimensions, are designed and their performance investigated for the examined measurement sites. Thereby the resulting H-rotor and the Darrieus rotor, both with the same swept rotor area, are operated at constant rotational speed or constant tip speed ratio.

- For H-rotors operating with constant rotational speed decreases the performance drastically for wind speeds outside the optimal tip speed ratio.
- H-rotors operating with the optimal constant tip speed ratio perform very well in terms of high power coefficients.

Considerably high load factors are found. That does not mean that the energy production for a concept with a higher load factor is linked to higher energy production per square meter. In some estimation cases the energy production is highest for the concept with the lowest load factor. But here, the power curves calculated for the four concepts are referring to the shaft power delivered by the aerodynamics on the rotor, not taking any generator or transformer losses into account.

Two of the studied concepts show low load factors for all the four wind climates, whereas the load factors for the other two concepts change noticeably.

- Wind turbines with rather constant load factors, despite the wind climate, are fairly site-independent.

Besides the load factor another parameter, C_E, is introduced to evaluate site-specific rotor performances. It is the ratio of the actual site-specific energy production and the site-specific energy contained in the wind.

- With the parameter C_E it is possible to determine the wind climate which is most appropriate for a certain turbine in terms of energy extraction.

The analysis carried out is not complete, but highlights some very important issues in the design of rotors for urban sites.

6 SUMMARY

This work sketches the social, practical and physical conditions for wind energy applications in the inhabited environment. Emanating from the defined social aspects the focus is laid on small-scale wind turbines with a maximum rotor size of $5m^2$. The eligibility for a technology, merely seen with engineering eyes, less efficient in an urban context than in the well investigated and approved environment- the open countryside and the smooth sea- lies outside technical definitions.

Different from large-scale wind turbines located in e.g. offshore parks, small-scale wind turbines are affordable for private people. Decentralized energy production with a small wind conversion system at the location of consumption is bonded to enhanced awareness and responsibility of the consumer towards energy usage and with that the locally produced energy is not only based on renewable energy, but also anticipated to reduce the energy to cover. Such factors are not included in the efficiency determination for urban wind energy applications, but form the foundation and motivation of the work presented here. Furthermore, with an outlook into the future with decreasing fossil fuel, coal and gas resources, increasing pollution and consequently increasing energy prices, mostly controlled by the industry behind the centralized power plants, a decentralized privately owned power system is promising to become financially more and more viable.

With the topics investigated in this work, an attempt is fulfilled to deliver an insight into, and explanation of, the physical factors playing decisive rolls in urban wind energy. To recapitulate the elements important for the implementation of wind energy conversion systems, with:

- the macro wind climate
- the micro wind climate
- the siting within a micro wind climate and
- the choice of a wind turbine model most appropriate for the selected site.

This approach applies for common large wind turbines as well. Thereby, the micro wind climate at the common sites is not as complex and individual as in cities. For sites where large-scale wind turbines usually are erected, wind potential estimations tools are developed and already used for years. Consequently, well adapted wind turbines are designed and approved.

To do the same for the urban environment, methods, tools and rotor designs are proposed in the framework of the PhD thesis on hand. Results, conclusions and future work recommendations are summarized in this chapter.

6.1 Results

The results obtained with the studies conducted in this work are only a fraction of what can be done and what is worth to get investigated. First and foremost the conditions and expectations for wind energy applications in the urban environment are clarified to serve as a foundation and inspiration for further work.

In the following a short resume is given concerning wind conditions, siting and rotor design.

6.1.1 Wind Conditions

Most of the following conclusions are results from the chapter “Urban Wind Climate”.

Unlike the wind conditions on the countryside or offshore, the average wind velocities in built-up area are in the majority of cases low and turbulence intensities are high. The probability of the occurring wind speeds in a certain wind climate can be described with the help of the Weibull distribution and its parameters.

For offshore sites, exemplary Weibull parameters at 10m height can be k=1.73 and A=6.92m/s. For a site in the city of Copenhagen, wind measurements are taken at 8m above an approximately 20m high building. Weibull parameters based on data collected over one year are found with k=2.4 and A=4.4m/s. The wind speed probability distribution above the rooftop shows with that a rather low wind speed variance, whereas the offshore site is facing a broader bandwidth of wind velocities. Hence, the urban rooftop site requires a different turbine design concept than the offshore site does.

Furthermore, analyzing the wind data collected over two more years at the urban site, concludes in the same Weibull parameters, indicating a rather stable and predictable wind climate for the city, unless major changes in the surroundings are executed, e.g. cutting down a remarkable amount of trees in the neighboring park or erecting a huge building close by.

In terms of daily average wind velocity variability, the development over a day, for the observed sites, follows the trends common for rural sites in Denmark- low velocities in the night time, increasing with the heating of the air and earth induced by sunlight, and decreasing accordingly with the cooling in the evening hours. Depending on the utilization of the energy generated with decentralized energy systems, such variability might be of interest. This variability is observed for all urban sites investigated in this work. In other countries or at sites of very different character, this behavior can be different though.

At flat rural sites obstacles are rare and wind measurements taken at one point might be applicable for a wide periphery of the surroundings. In the built-environment this is not possible or rather said, areas of the same character are most likely narrow. Some of the exemplary urban sites in chapter “Installation Cases & Siting” are located fairly close to each other, but show very different wind potentials. On the one hand, the examined measurements are not taken at the same height and can therefore not directly be compared with each others. On the other hand, the characteristic of the measurement districts are different from each others in manner of the buildings (obstacles) dimensions and obstacles set-ups. Anyway, with the combination of method I and method II, presented in chapter “Urban Wind Climate”, an approach is delivered to determine macro wind climates for city districts.

6.1.2 Siting

Knowledge about the urban macro wind climate offers valuable clues to the general wind potential of a district. In a complex terrain, however, strong local variability is present and has to be considered for the siting of wind turbines within the micro climate.

That experience is made in chapter “Installation Cases & Siting”, where energy production estimations are based on wind measurements, taken aside the installed wind turbines. In Table 18 an overview is given of the estimated and measured energy productions. The estimation method is thereby validated with the help of the data found at the Risø DTU test stand. With the same method and same power curve, significant discrepancies occur for some of the urban installation sites. For one site, the estimation results in an underestimation of the actual energy production by 53%.

In this case it is assumed that the turbine is positioned at a more favorable spot within the micro climate than the wind measurement device.

Besides the micro wind climate, other reasons can cause or contribute to such a high discrepancy. Surely, the quality of the measurement data has an influence. It is also possible that power curves vary, dependent on the onsite turbulence intensity.

Table 18: Estimated and measured energy productions for the VENCO TL1000 installation cases

site	turbine	$AEP_{estimated}$	$AEP_{measured}$	discrepancy	load $factor_{measured}$
		[kWh]	[kWh]	[%]	[kWh/m^2]
Fælledvej		27.2	28.8	too low (5.5)	0.004
Svanevej	(west)	67.6	96.4	too low (29.9)	0.014
	(east)		142.1	too low (52.5)	0.021
Vallensbækvej	(west)	105.9	154.8	too low (31.7)	0.023
	(east)	181.5	162.8	too high (11.5)	0.024
Risø DTU test stand		428.6	440.6	too low (2.7)	0.065

Whether more experience is necessary or siting rules and tools are established, in order to detect appropriate locations in an urban set-up for a corresponding wind conversion system.

With the developed computational fluid dynamics (CFD) tool, PlayBox, presented in the chapter “Flow Around Obstacles”, it is possible to study typical flow phenomena around bluff body set-ups of different character. Some of the general rules, concluded on visual inspections of the conducted simulations, are listed in Table 19. In some cases one effect might dominate another effect. This has to be regarded in the application of the rules.

Flow around fairly simple bluff body shapes can already be rather complex, but typical. CFD simulations bear the potential to unfold and visualize flow patterns and various flow properties. The quality of the results is dependent on the simulation domain and condition set-up. The CFD tool, PlayBox, introduced in “Flow Around Obstacles” can capture the Reynolds number independency behavior, as observed in wind tunnel experiments. With that the chosen set-up and simulation results are also valid for different wind velocities and different geometrical dimensions, as long as the Jensen number is maintained.

Although it is not trivial to categorize individual urban sites, parameters exist to do so to a certain degree. The example sites used in the presented CFD simulations are representing typical set-ups for urban district categories like regularly aligned residential blocks, city center areas including parks, commercial and industrial areas. Since the presented simulations are about generalization and simulations commonly are connected to inaccuracies, it does not necessarily make sense to include balconies, blinds oriels or the like.

Interesting in terms of detecting areas advisable or the contrary areas to avoid for installation of wind conversion systems in a certain city district, is the proposed siting method in chapter “Installation Cases & Siting”. The presented siting method utilizes the Reynolds number independency and the macro climate determination method defined in chapter “Urban Wind Climate” to make a real urban district comparable to a simulated district, where both the districts, original and model,

belong to the same urban district category. With the proposed siting method it is not only possible to detect flow phenomena likely to occur in the district of interest, but also qualitative and quantitative wind energy potential can be located in the simulated district and then transferred to the original urban district.

Table 19: Summary of some general flow phenomena observed in CFD simulations of bluff body set-ups

in an area with a typical urban built-up density skimming flow is a matter of fact, and therefore are upwind accelerations of flow over the roof edges low	upwind
upwind effect is mostly present for first row obstacles and buildings higher than the buildings mean height	
the flow entering a street canyon is accelerated similar to the flow through a nozzle, while the acceleration effect decreases in the course of the canyon	street canyon
wind perpendicular to a street canyon causes recirculation structures and no acceleration as such	
buildings in the wake of a higher building and buildings below the mean height are facing increased turbulence and lowered wind speeds	wake
tower wakes evoke speed deficiencies in the downwind region at heights even above tower height	
the wake influence decreases with increasing downwind distance to the wake provoking obstacle	
at the center of a tower rooftop the local wind profiles are almost the same, despite the changing incoming wind direction	directionality
depending on the local wind rose, tower wake deficiencies can be compensated considerably	wake/directionality
positioning on a first row obstacle does not need to be of advantage, if e.g. a higher building is located close by	upwind/directionality

6.1.3 Rotor Layout and Performance

De facto energy production of a wind turbine is depending on the local wind climate, the turbine positioning within the local wind climate and the turbines capability to operate under the conditions, it is exposed to. Most small wind turbines on the market, some of them installed in the urban environment, seem to be designed for a different wind climate than the climates actually found in cities.

In chapter “Urban Wind Climate” three small wind turbines, all of them especially design for the urban environment, are introduced and the power curves as they are given in the manufactures turbine specifications are studied. Evaluating their performance in an exemplary urban wind climate shows that rotors shall be well designed for low wind velocities, rather than for a broad bandwidth of wind velocities, to achieve a reasonable energy output.

Furthermore, so far no strict standards exist about the method how power curves for small wind turbines are derived and what they refer to. Power curves for small wind turbines given by the manufacturer can be based on e.g. theoretical calculations, wind tunnel measurements, where the power refers to the mechanical power on the

shaft or the power refers to the value measured at the point where the generated electricity is fed into the grid including generator and transformer losses. Due to this, energy production expectations linked to given power curves can diverge severely from actual energy productions, despite the chosen site. In chapter “Installation Cases & Siting” the power curve given by the manufacturer is compared with the power curve measured at the Risø DTU test field. The power curve derived at the test stand is based on the measured electricity fed into the grid, whereas it is not known what the power curve given by the manufacturer is based on. The discrepancy between the two curves turns out to be remarkable.

A more wholesome international small wind turbine standard is on the way though. It is recommended to be attentive and under circumstances the vendor shall be asked about the power curve and the method it was obtained with, before purchasing a small wind turbine.

In the chapter “Rotor Design” an overview is given of decisive rotor design parameters and their interconnection. The most important fact for small wind turbines, horizontal and vertical axis concepts, is that Reynolds numbers on the blade sections are likely to be low. That is due to low relative velocities on the blade elements and the small chord lengths. Connected to low Reynolds numbers are low power coefficients. Small changes in low Reynolds number ranges influence the rotor power coefficients dramatically. It can be concluded that the geometrical size of a rotor limits its efficiency, irrespective a good wind climate, design or control. Below a certain geometrical size a drag-driven rotor might be even more efficient, easier to design and produce, than a lift-driven rotor.

Different optimization strategies are introduced in chapter “Rotor Design”. Thereby it is focused on what kinds of optimization methods are possible and how the earlier explained design parameters are influenced by the set design frames, rather than on presenting a final design. An exemplary small vertical axis wind turbine with bended blades (Darrieus), constant chord length distribution along the blade, operating at 240rpm shows an operational optimum at a tip speed ratio of 4.4 and a wind speed of 4.8m/s. These calculations can be conducted with a simple streamtube model, which is designed for exactly such rotors. In the frame of the present work, this model is modified to be able to calculate the performance of vertical axis wind turbines with chord distributions along the blade different from a constant distribution. Furthermore, shapes different from the Darrieus layout can be calculated with it. This modified code is then implemented into an optimization code, originally designed for the optimization of horizontal axis wind turbines. With that the optimization code, from that point on referred to as VAWTopt, is capable of finding a chord distribution for vertical axis wind turbines for a given design frame. Optimizing the chord distribution for the exemplary Darrieus turbine in its initial operational optimum, results in a performance enhancement by 13%. A disadvantage of a changing chord distribution is that the blades cannot be extruded as it is possible for the initial blade with constant chord distributions.

Among the ideas to enter the urban space with wind energy applications in the “Introduction” chapter is an autarkic wind energy system in form of a very small horizontal rotor, thought of e.g. to be mounted on a bicycle handle bar, generating electricity to charge small personal convenience items, while the person is cycling and while the bicycle is parked and wind is blowing. In the end of chapter “Rotor Design” various parameter studies are carried out for this purpose. A series of appropriate rotor layouts are found to be matched to the characteristics of a small generator and the printing dimensions of an available three dimensional printer. The three final designs do have distinct properties. BellAIRina is designed to keep a

slender shape and the highest power coefficients in the design point. BellAIR is as well laid out with a slender geometry, but the optimization leads to a design less prone to stall, on the cost of decreased maximum efficiency. The third model, BellAIRphant, is not restricted in its maximum chord length and results in the most efficient design among the three types of the series.

In the very last study of this work four vertical axis wind turbine concepts are designed and their theoretical performances in four different wind climates examined. By introducing a parameter, which sets the site-specific energy production into relation with the onsite wind energy potential, a form is found to determine the wind climate a turbine is most appropriate for in terms of energy extraction. Furthermore, studying the load factor for the different concepts in the four wind climates concludes in the statement that wind turbines with rather constant load factors, despite the wind climate, are fairly site-independent. One of the concepts reaches a load factor of 30%, a value common for offshore wind turbines. Thereby is the ratio between rated power and swept area with $28 W/m^2$ very different from large-scale turbines. For an all-over evaluation of wind turbine concepts, it is proposed to include both, the load factor, connected to generator efficiencies and generator costs, and the new introduced parameter, connected to energy prices.

6.2 Future Work and Perspectives

The present work frames issues important for urban wind energy applications. Practical information, methods, tools, parameters and their influences are given to form a well-grounded overview. The results cannot be understood as a guideline for the perfect urban wind turbine in the most favorable urban wind climate, but can serve as a guideline to find the right ingredients for a certain application. Although the chapters are interconnected, they can also be read independent from each other, according to the field of interest.

Since the work presents a foundation for a technology in a new context, several possibilities are supposable for future investigations and developments. To start with the methods and tools developed in the course of the work at hand, the CFD tool PlayBox and the rotor optimization program VAWTopt bears the potential for further improvements. The aerodynamic code implemented in VAWTopt is restricted in many ways and the source of many inaccuracies. To draw general design directives it is sufficient, but to design more accurately the following extensions, or implementation of more advanced models including them, are worth to be considered:

- distinction between upwind and downwind side of the rotor
- tip-loss correction
- dynamic stall model
- supporting structure influence
- automatic choice of the right Reynolds number
- chambered airfoils or blades with preset pitch

A routine for the PlayBox tool can be thought of, capable of merging simulation results of different inflow angles, according to wind direction incidences and inflow angle dependent Weibull distributions. Also, the idea with the tool is to be able to build different urban set-ups easily and fast, similar to Lego. Such a routine with a user-friendly interface, including the proposed scaling method and wind rose merging algorithm can be of interest and usage not only for the field of urban wind energy, but also for the field of pedestrian wind comfort and urban planning for example.

With respect to the designed BellAIR rotor series, the next step is to print the rotors in a more appropriate material and test their performances. Rapid Prototyping is a fast and inexpensive process. Various types of printers and printing materials exist. A flexible, rubberlike material is contemplated, stiff enough to maintain its shape under normal operation conditions and soft enough not to be hazardous in case of a hand crossing the course of the blades.

Besides the possibilities directly connected to the conducted work, a tool can be thought of, capable of combining geometric input and quality controlled scattered wind measurement from a specific city. Equipped with a form of quick CDF code city-specific wind energy potential shall be visualized. With an included data base of small wind turbines and their certified power curves an appropriate wind turbine type can then be found for a chosen site and vice versa. For the city of Copenhagen, for example, a database of all buildings is available.

But, in general, seeking for the optimal solution merely with calculations is not the way to go. Equations trying to describe the nature are always bond to assumptions and in the minority of cases all influencing factors are regarded or even known. Theory can set frames and some general rules to find a reasonable starting point for practical fielding to collect experience and to evaluate the applied theory. Results from field experiments then can deliver input for new methods or carry the development of more refined and advanced tools. It is recommended to alternate between theory and field experiments.

7 AKNOWLEDGEMENT

First and foremost many thanks to Risø DTU making the present work possible, with accessibility to valuable sources of knowledge and with financial funding. Great gratitude goes to my supervising tutor Christian Bak with his continuous feedback and salutary advice. Many thanks to Mads Døssing for constructive discussions and input in rotor design matters. For the support in CFD issues, I am very thankful to Niels N. Sørensen, Andreas Bechmann and Pierre-Elouan Rethore. Special thanks to Sven-Erik Gryning with his broad expertise in the field of meteorology and his willingness to share and advocate valuable knowledge. I am grateful for the reliable and prosaic support from my second supervising tutor Helge A. Madsen. Peggy Friis with her experiences and recent activities in the certification of small-scale wind turbines was encouraging and helpful. I appreciate that. Very special thanks to the company Logik&Co which took the initiative to import small wind turbines and installed them on their own expenses to bring urban wind energy forward and delivered the base for several investigations in this work. Thanks to the company Faulhaber, for assisting my research with free provided motors. And last but not least warm gratitude to my dear friends Morten Lindahl and Jonas Tesch Hallberg for their help and opinion in editorial concerns.

8 REFERENCES

[1] Christensen K (2008). *Catalogue of small wind turbines*. ISBN 87 7778 125 4, published by FC print

[2] Thorstensson E (2009). *Small- scale wind turbines- introductory market study for Swedish conditions*. Master thesis, Chalmers University of Technology, Sweden

[3] Encraft (2008). *Warwick Wind Trials Interim Report*- August 2008

[4] Best M et al (2008). *Small-scale wind energy- technical report.* Met Office report for Carbon Trust, UK. Crown Copyright

[5] Mertens S (2006). *Wind energy in the built environment*. PhD thesis, ISBN 0906522 35 8 published by Multi-Science

[6] Bussel van GJW, Mertens S, Polinder H, Sidler HFA (2004). *The development of Turby, a small VAWT for the built environment*. Presented at Global Wind Energy Conference 2004

[7] Merten S, Kuik van G, Bussel van GJW (2003). *Performance of an H-Darrieus in the skewed flow on a roof*. Journal of Solar Energy Engineering Vol. 125, pp. 433-440

[8] Simão Ferreira CJ, Zuijlen van A, Bijl H, Bussel van G, Kuik van G (2009). *Simulating dynamic stall in a two-dimensional vertical-axis wind turbine: verification and validation with particle image velocimetry data*. In: Wind Energy 2010; 13:1–17

[9] Watson SJ, Infield DG, Barton JP, Wylie SJ (2007). *Modelling of the performance of a building- mounted ducted wind turbine*. Presented at "The Science of Making Torque from Wind 2007"

[10] Scheurich F, Fletcher TM, Brown RE (2010). *The influence of blade curvature and helical blade twist on the performance of a vertical- axis wind turbine*. Presented at 48th AIAA Aerospace Sciences Meeting Including the New Horizons Forum and Aerospace Exposition 2010, Orlando, Florida

[11] Bertényi T, Wickins C, McIntosh S (2010). *Enhanced energy capture through gust-tracking in the urban wind environment*. Presented at 48th AIAA Aerospace Sciences Meeting Including the New Horizons Forum and Aerospace Exposition 2010, Orlando, Florida

[12] http://www.buch-der-synergie.de/c_neu_html/c_08_01_windenergie_ geschichte.htm; July 2011

[13] http://de.wikipedia.org/w/index.php?title=Bild:SKMBT_C55007120513590-2.JPG&filetimestamp=20071231174948; July 2011

[14] http://de.wikipedia.org/w/index.php?title=Bild:WindradKop.jpg&filetimestamp=20061015134710; July 2011

[15] http://trendwatching.com/trends/8trends2008.htm; July 2011

[16] http://www.warwickwindtrials.org.uk/resources/Helen+Brown+-+Encraft+-+Results+of+the+Warwick+Wind+Trial .pdf; July 2011

[17] Energy Saving Trust (2009). *Location, location, location- domestic small-scale wind trial report*. Microwind Report

[18] Beller C (2009). *Urban wind energy- state of the art 2009*. Risø-R-1668(EN), Risø DTU, Roskilde, Denmark

[19] http://geotypografika.com/2008/05/29/metropolis-reflecting-on-the-gulf/; July 2011

[20] http://www.wirefresh.com/london-razor-high-tech-skyscraper-with-built-in-turbines/; July 2011

[21] Beller C (2007). *Layout design for a Venturi to encase a wind turbine, integrated in a high rise*. Master thesis, University of Stuttgart, Germany

[22] Beller C (2011). *Energy output estimation for a small wind turbine positioned on a rooftop in the urban environment with and without a duct*. Risø-R-1669(EN), Risø DTU, Roskilde, Denmark

[23] http://www.urbanwind.net/downloads.html; July 2011

[24] http://www.quietrevolution.com/gallery.htm; July 2011

[25] http://www.turby.nl/99-downloads/Turby-EN-Application-V3.0.pdf; July 2011

[26] http://www.tecnico.co.nz/uploads/77935/files/Case_Study_-_Blackpool.pdf; July 2011

[27] http://eur-lex.europa.eu/LexUriServ/LexUriServ.do?uri=OJ:L:2010:153:0013:0035:EN:PDF; July 2011

[28] http://www.leed.net/; July 2011

[29] Pierce J (2009). *Energy Aware Campus Dwelling: Eco-Visualization and the IU Energy Challenge*. Indiana University, USA

[30] http://www.thescavenger.net/environment/eco-feedback-can-change-our-consuming-ways.html; July 2011

[31] http://www.dkvind.dk/fakta/pdf/P10.PDF; July 2011

[32] http://www.dkvind.dk/fakta/pdf/P7.pdf; July 2011

[33] http://www.dkvind.dk/fakta/pdf/P8.pdf; July 2011

[34] http://www.vindmoellegodkendelse.dk/; July 2011

[35] http://www.vindmoellegodkendelse.dk/DK/Godkendte_anmeldte_sm%C3%A5_m%C3%B8ller.htm; July 2011

[36] http://www.dkvind.dk/arrangementer/tidligere/170910_husstandsmoller/henrik_lawaetz.pdf; July 2011

[37] http://www.cafe-pavillonen.dk/; July 2011

[38] http://commons.wikimedia.org/wiki/Image:CphPlanetarium.jpg; July 2011

[39] http://www.jasonbruges.com/; July 2011

[40] Beller C (2010). *Development of a simulation tool to predict urban wind potential*. In: Sustainability in Energy and Buildings, SIST 7, pp. 111–120

[41] Troen I, Petersen EL (1989). *European Wind Atlas*. ISBN 87-550-1482-8. Risø National Laboratory, Roskilde, Denmark

[42] Mortensen NG, Heathfield DN, Myllerup L, Landberg L, Rathmann O (2007). *Getting started with WAsP 9*. Technical Report Risø-I-2571(EN), Risø National Laboratory, Roskilde, Denmark

[43] Xiaomin X, Zhen H, Jiasong W (2006). *The impact of urban street layout on local atmospheric environment.* Building and Environment 41, pp. 1352-1363

[44] Blocken B, Carmeliet J (2004). *Pedestrian wind environment around buildings: literature review and practical examples.* Journal of Thermal Envelope and Building Science 28(2), pp. 107-159

[45] Hanna SR et al (2006). *Detailed simulations of atmospheric flow and dispersion in downtown Manhattan- an application of five computational fluid dynamics models*. American Meteorological Society, pp. 1713-1726

[46] Badde O, Plate EJ (1994). *Einfluss verschiedener Bebauungsmuster auf die windinduzierte Gebäudebelastung*. In: Abschlusskolloquium Strömungsmechanische Bemessungsgrundlagen für Bauwerke, University of Karlsruhe, Germany

[47] www.googlemaps.com; July 2011

[48] http://www2.dmu.dk/atmosphericenvironment/mjk/mjkall_files/statmet.htm; July 2011

[49] Viuf P (2006). *Undersøgelse af metode til måling af partikelfluxe i et urbant område*. Master Thesis, University of Copenhagen, Denmark

[50] Theurer W, Bächlin W, Plate EJ (1992). *Model study of the development of boundary layers above urban areas*. Journal of Wind Engineering and Industrial Aerodynamics Vol. 41 (1992), pp. 437-448

[51] Yersel M, Goble R (1986). *Roughness effects on urban turbulence parameters*. Boundary Layer Meteorology 37, pp. 271-284

[52] Wieringa J, Davenport AG, Grimmond CSB, Oke TR (2001). *New revision of Davenport roughness classification*. 3rd European & African Conference on Wind Engineering, Eindhoven, Netherlands

[53] Mertens S (2003). *The energy yield of roof mounted wind turbines*. Wind Engineering 27, No. 6, pp. 507-518

[54] Heath MA, Walshe JD, Watson SJ (2007). *Estimating the potential yield of small building-mounted wind turbines*. Wind Energy 10, pp. 271-287

[55] Taylor PA, Lee RJ (1984). *Simple guidelines for estimating wind speed variations due to small scale topographical features*. Climatological Bulletin 18, pp. 3–32

[56] ESDU (1982). *Strong winds in the atmospheric boundary layer*. ESDU 82026, part 1: mean-hourly wind speeds. ISBN 978 0 85679 407 0

[57] Simiu S, Scanlan RH (1996). *Wind effects on structures*. John Wiley & Sons, New York

[58] http://www.turby.nl/; October 2009

[59] http://www.vencopower.com/; July 2011

[60] http://www.wind-works.org/articles/; 26th October 2009

[61] Oke TR (1988). *Street design and urban canopy layer climate*. Energy and Buildings, 11, pp. 103-113

[62] Michelsen JA (1992). *Basis3D- a platform for development of multiblock PDE solvers*. Technical report AFM 92-05, Technical University of Denmark

[63] Michelsen JA (1994). *Block structured multigrid solution of 2D and 3D elliptic PDE's*. Technical report AFM 94-06, Technical University of Denmark

[64] Sørensen NN (1995). *General purpose flow solver applied to flow over hills*. Risø-R-827-(EN), Risø National Laboratory, Roskilde, Denmark

[65] Sørensen NN, Bechmann A, Johansen J, Myllerup L, Botha P, Vinther S, Nielsen BS (2007). *Identification of severe wind conditions using Reynolds Averaged Navier-Stokes solver*. Presented at The Science of Making Torque from Wind

[66] Patankar SV, Spalding DB (1972). *A calculation procedure for heat, mass and momentum transfer in three-dimensional parabolic flows.* Int. J. Heat Transfer, 15:1787

[67] Khosla PK, Rubin SG (1974). *A diagonally dominant second-order accurate implicit scheme*. Computer fluids, 2:207-209

[68] Castro IP, Robins AG (1976). *The flow around a surface-mounted cube in uniform and turbulent streams*. In: J. Fluid Mech. 79 part2: 307-335

[69] Strickland JH (1975). The Darrieus turbine: a performance prediction model using multiple streamtubes. Sandia Laboratories Report SAND-75-0431

[70] Fuglsang P, Thomsen K (2001). Site specific design optimization of wind turbines. ASME J. Solar Engineering, Vol. 123, pp. 296-303

[71] Beller C (2011). *VAWTopt manual*. Risø-I-3189, Risø DTU, Roskilde, Denmark

[72] http://www.wind-energy-the-facts.org/en/environment/chapter-1-environmental-benefits/energy-balance-analysis.html; July 2011

[73] http://www.eoearth.org/article/Energy_return_on_investment_(EROI)_for_wind_energy; July 2011

[74] Gipe P (1993). *Wind power for home and business*. Chelsea Green Publishing Company Post Mills, Vermont

[75] http://the-goodlife.blogspot.com/2005/10/savonius.html#; July 2011

[76] http://en.wikipedia.org/wiki/Yaw_system; July 2011

[77] http://www.windturbine-analysis.netfirms.com/index-intro.htm; July 2011

[78] Templin RJ (1974). *Aerodynamic performance theory for the NRC vertical-axis wind turbine*. N.A.E Report LTR-LA-160

[79] Madsen HA (1983). On the ideal real energy conversion in a straight bladed vertical axis wind turbine. PhD thesis, Aalborg University Center, Denmark

[80] Paraschivoiu I (2002). *Vortex model*. In: Wind Turbine Design with Emphasis on Darrieus Concept, Polytechnic International Press, pp. 85-98

[81] Drela M (1989). *XFOIL, an analysis and design system for low Reynolds number airfoils*. Low Reynolds Number Aerodynamics, Volume 54. Springer- Verlag Lec. Notes in English

[82] Watson S, Infield D, Harding M (2007). *Predicting the performance of small wind turbines in the roof-top urban environment*. Presented at EWEC2007, Milan, Italy

[83] Kooiman SJ, Tullis SW (2010). *Response of a vertical axis wind turbine to time varying wind conditions found within the urban environment*. In: Wind Engineering Volume 34, No. 4, pp. 389-401

APPENDIX

A: Roughness Classification after Davenport

z_0 (m)	Landscape description
1: 0.0002 *"Sea"*	Open sea or lake (irrespective of wave size), tidal flat, snow-covered flat plain, featureless desert, tarmac and concrete, with a free fetch of several kilometers.
2: 0.005 *"Smooth"*	Featureless land surface without any noticeable obstacles and with negligible vegetation; e.g. beaches, pack ice without large ridges, marsh and snow-covered or fallow open country
3: 0.03 *"Open"*	Level country with low vegetation (e.g. grass) and isolated obstacles with separations of at least 50 obstacle heights; e.g. grazing land without windbreaks, heather, moor and tundra, runway area of airports. Ice with ridges across-wind.
4: 0.10 *"Roughly open"*	Cultivated or natural area with low crops or plant covers, or moderately open country with occasional obstacles (e.g. low hedges, isolated low buildings or trees) at relative horizontal distances of at least 20 obstacle heights.
5: 0.25 *"Rough"*	Cultivated or natural area with high crops or crops of varying height, and scattered obstacles at relative distances of 12 to 15 obstacle heights for porous objects (e.g. shelterbelts) or 8 to 12 obstacle heights for low solid objects (e.g. buildings). (*Analysis may need* z_d .)
6: 0.5 *"Very rough"*	Intensively cultivated landscape with many rather large obstacle groups (large farms, clumps of forest) separated by open spaces of about 8 obstacle heights. Low densely-planted major vegetation like bushland, orchards, young forest. Also, area moderately covered by low buildings with interspaces of 3 to 7 building heights and no high trees. (*Analysis requires* z_d .)
7: 1.0 *"Skimming"*	Landscape regularly covered with similar-size large obstacles, with open spaces of the same order of magnitude as obstacle heights; e.g. mature regular forests, densely built-up area without much building height variation. (*Analysis requires* z_d .)
8: ≥ 2 *"Chaotic"*	City centres with mixture of low-rise and high-rise buildings, or large forests of irregular height with many clearings. (*Analysis by windtunnel advised.*)

Fig. 108: Davenport classification of effective terrain roughness [51]

B: Typical Building Configurations defined after Badde & Plate

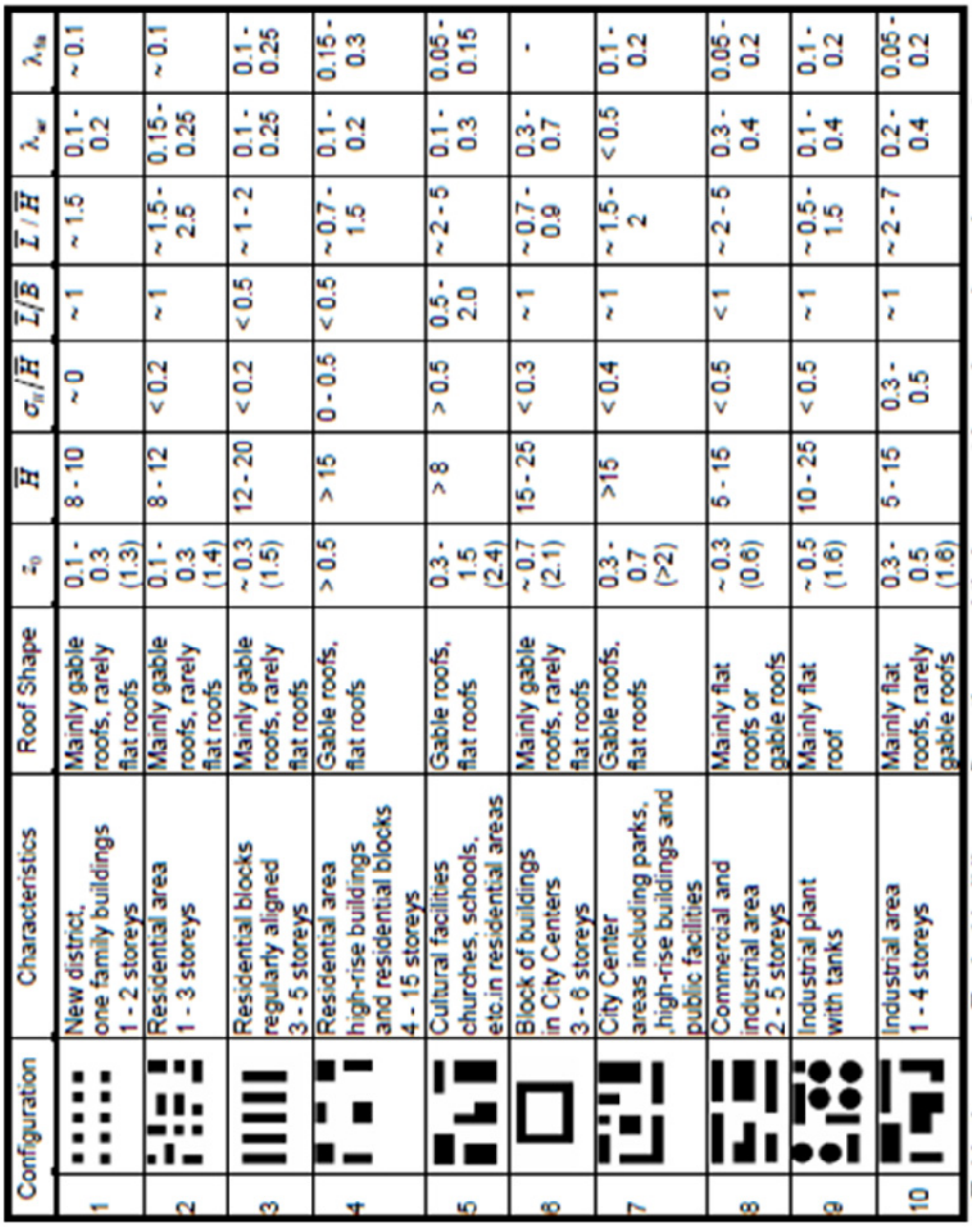

	Configuration	Characteristics	Roof Shape	z_0	$\overline{H}$	$\sigma_H/\overline{H}$	$\overline{L}/\overline{B}$	$\overline{L}/\overline{H}$	λ_w	λ_{fa}
1		New district, one family buildings 1 - 2 storeys	Mainly gable roofs, rarely flat roofs	0.1 - 0.3 (1.3)	8 - 10	~ 0	~ 1	~ 1.5	0.1 - 0.2	~ 0.1
2		Residential area 1 - 3 storeys	Mainly gable roofs, rarely flat roofs	0.1 - 0.3 (1.4)	8 - 12	< 0.2	~ 1	~ 1.5 - 2.5	0.15 - 0.25	~ 0.1
3		Residential blocks regularly aligned 3 - 5 storeys	Mainly gable roofs, rarely flat roofs	~ 0.3 (1.5)	12 - 20	< 0.2	< 0.5	~ 1 - 2	0.1 - 0.25	0.1 - 0.25
4		Residential area high-rise buildings and residential blocks 4 - 15 storeys	Gable roofs, flat roofs	> 0.5	> 15	0 - 0.5	< 0.5	~ 0.7 - 1.5	0.1 - 0.2	0.15 - 0.3
5		Cultural facilities churches, schools, etc.in residential areas	Gable roofs, flat roofs	0.3 - 1.5 (2.4)	> 8	> 0.5	0.5 - 2.0	~ 2 - 5	0.1 - 0.3	0.05 - 0.15
6		Block of buildings in City Centers 3 - 6 storeys	Mainly gable roofs, rarely flat roofs	~ 0.7 (2.1)	15 - 25	< 0.3	~ 1	~ 0.7 - 0.9	0.3 - 0.7	-
7		City Center areas including parks, ,high-rise buildings and public facilities	Gable roofs, flat roofs	0.3 - 0.7 (>2)	>15	< 0.4	~ 1	~ 1.5 - 2	< 0.5	0.1 - 0.2
8		Commercial and industrial area 2 - 5 storeys	Mainly flat roofs or gable roofs	~ 0.3 (0.6)	5 - 15	< 0.5	< 1	~ 2 - 5	0.3 - 0.4	0.05 - 0.2
9		Industrial plant with tanks	Mainly flat roof	~ 0.5 (1.6)	10 - 25	< 0.5	~ 1	~ 0.5 - 1.5	0.1 - 0.4	0.1 - 0.2
10		Industrial area 1 - 4 storeys	Mainly flat roofs, rarely gable roofs	0.3 - 0.5 (1.8)	5 - 15	0.3 - 0.5	~ 1	~ 2 - 7	0.2 - 0.4	0.05 - 0.2

Fig. 109: Typical building configurations and their geometric and aerodynamic parameters found in German cities. $\overline{H}$ is the mean building height, σ_H is the standard deviation of the building height. $\overline{L}, \overline{B}$ are mean length and mean width, resp. of buildings [45]

C: Reynolds Number Independency

In a CDF test domain for the PlayBox set-up, different cases for the flow around a cube mounted on a plate were conducted. Thereby the cube's height was h_c=2m and its surface roughness was in all following test cases the same as the surface roughness of the plate it was mounted on. First, the influence of changing inflow profiles was investigated. Three test cases were carried out, where the Reynolds number was changed, due to the changed inflow velocity. The surface roughness was the same throughout the three cases. In Table 20 the chosen values are summarized and the results, according to the Castro&Robins [68] experiment plotted in Fig. 110 and a close-up of it in Fig. 111. In chapter "Flow around Obstacles" more detailed information is given about the plots and the shown parameters.

Table 20: Parameter settings; independency study I

	z_0	u^*	u_h	*Re*	*Je*
	[m]	[m/s]	[m/s]	[-]	[-]
case 1.1	0.064	0.483	4.19	559'236	31.25
case 1.2	0.064	0.0518	0.45	59'918	31.25
case 1.3	0.064	0.0054	0.05	6'206	31.25

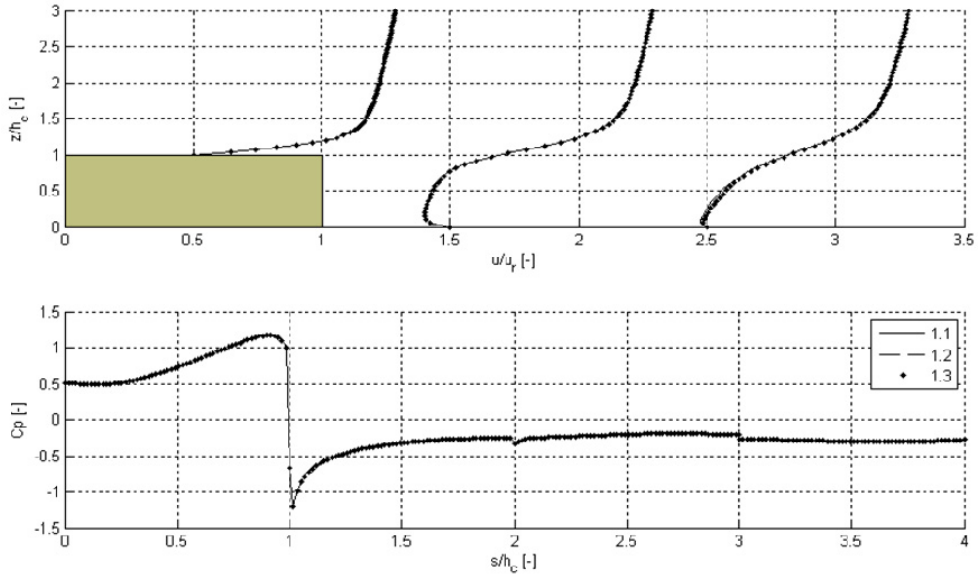

Fig. 110: Flow over a plate mounted cube at different wind speeds with constant Jensen number ($Je=z_0/h_c$)

In Fig. 110 it looks like the results are all the same, despite the different Reynolds numbers. Castro&Robins [68] observed a Reynolds number independency for their experiment for Reynolds numbers beyond approximately *Re*=3'000, in case of an approaching wind perpendicular to the cubes front face and a constant Jensen number. The CFD test cases were of another dimension then the experimental set-up of Castro&Robins. Also the Jensen number was different. In the experiment a Jensen number of *Je*=5 was present and here *Je*=31.25. Nonetheless, taking a closer look, Fig. 111 reveals a slight difference for case 1.3. The Reynolds number was only *Re*=6'000 and with that close to the limit, observed by Castro&Robins.

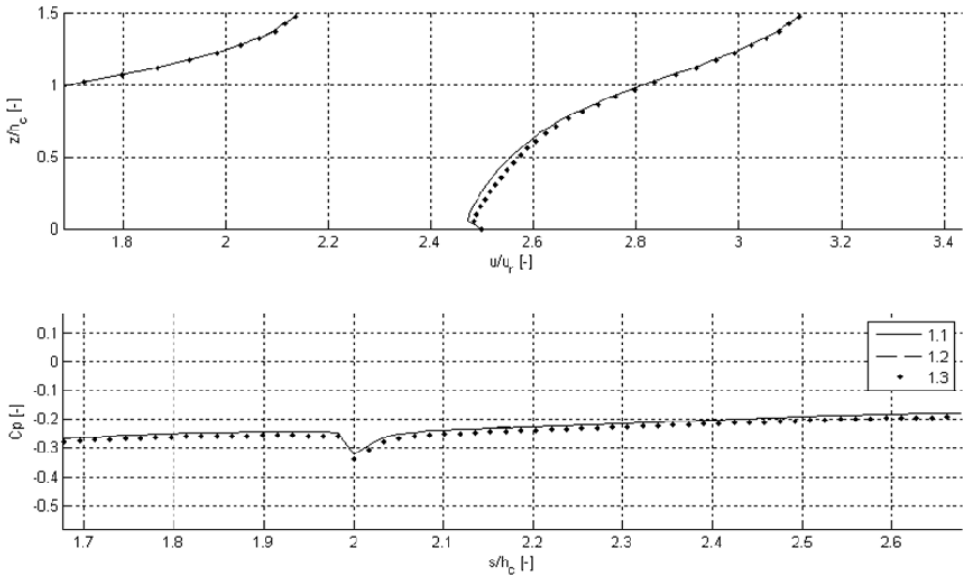

Fig. 111: Zoom in for flow over a plate mounted cube at different wind speeds with constant Jensen number ($Je=h_c/z_0$)

A clearer visualization of the agreement and slight disagreement of the flow patterns is given in Fig. 112.

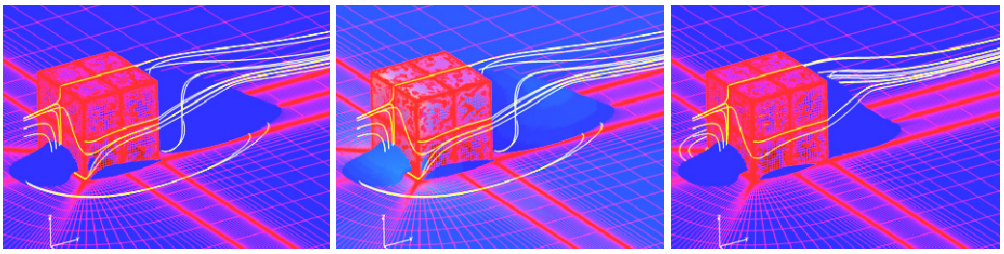

Fig. 112: Cube mounted on a plate at different Reynolds numbers with Je=const. Iso surfaces with zero speed are shown with the colour blue. Left: case 1.1; middle: case 1.2; right: case 1.3

To be sure of the ability of the CFD set-up to capture Reynolds number independency effects, a second test run was carried out. For this the Jensen number was changed by changing the surface roughness and keeping the cube dimensions with h_c=2m. The inflow velocity at cube height was different as well from case to case, while the friction velocity at the CFD domains inlet was kept constant. A summarization of the settings is given in Table 21.

Table 21: Parameter settings; independency study II

	z_0	u^*	u_h	*Re*	*Je*
	[m]	[m/s]	[m/s]	[-]	[-]
case 2.1	0.064	0.5	4.34	578’919	31.25
case 2.2	0.0064	0.5	7.19	957’966	312.50
case 2.3	0.64	0.5	1.77	236’177	3.125
case 2.4	6.4	0.5	0.34	45’322	0.3125

In the same manner as the plot for the constant Jensen number cases, Fig. 113 is plotted for the cases with changed Jensen number. It is obvious, that the results vary significantly. Also Fig. 114 shows distinct differences of the flow field around the cube. With that the CFD settings ability to capture Reynolds number independency effects was concluded.

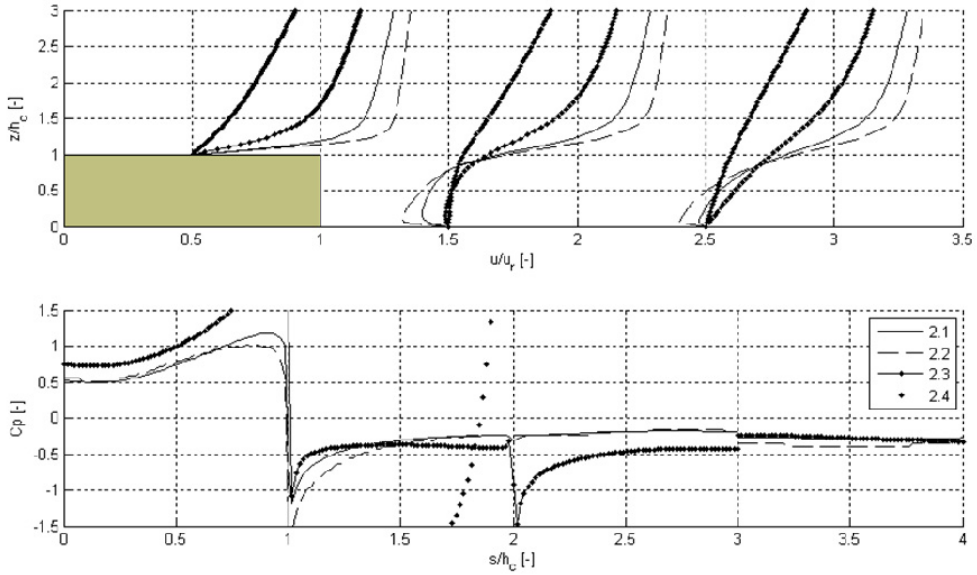

Fig. 113: Flow over a plate mounted cube at different wind speeds with varying Jensen number ($Je=h_c/z_0$)

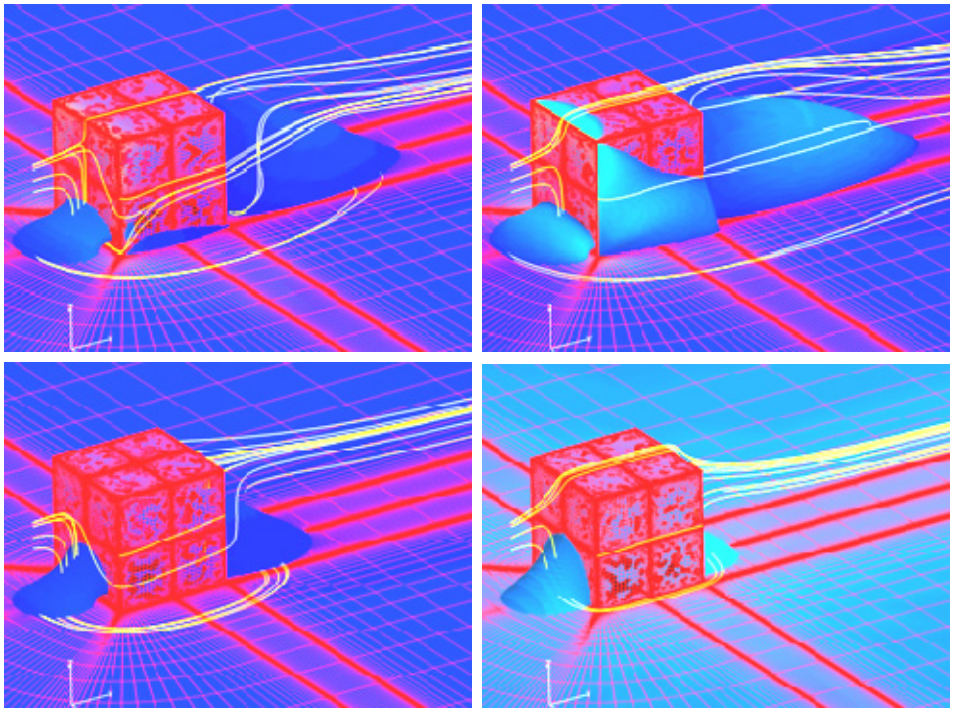

Fig. 114: Cube mounted on a plate at different Reynolds numbers with Je=variable. Iso surfaces with zero speed are shown with the colour blue. Top row: case 2.1, case 2.2; bottom row: case 2.3, case 2.4

D: Flow around Obstacles

Summarization of speed distributions on grid planes and streamlines to visualize and support the understanding in obstacle clusters, representing urban set-ups is plotted in Fig. 115

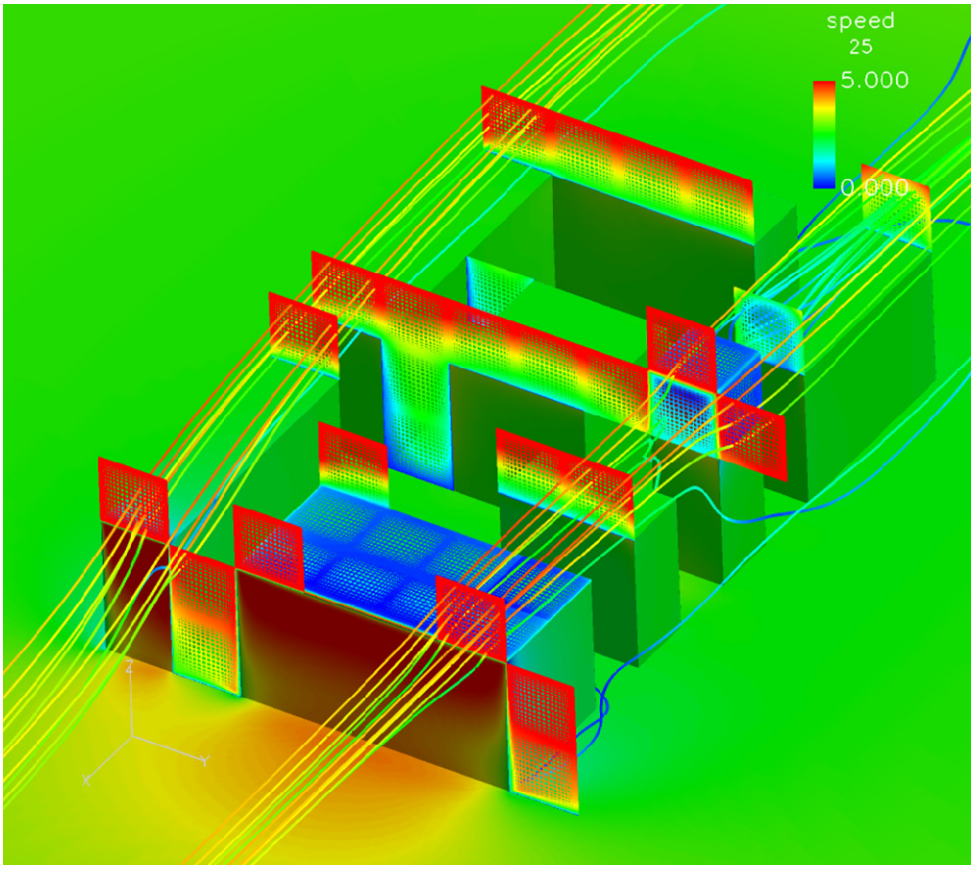

Fig. 115: CASE3: summary of grid plane and streamlines

E: Airfoil Data Used in the Calculations

Table 22: Airfoil data

	NACA0018					
	***Re*=40'000**		***Re*=80'000**		***Re*=160'000**	
α	C_l	C_d	C_l	C_d	C_l	C_d
0	0.0000	**0.0214**	0	**0.0162**	0	**0.0128**
1	0.0936	0.0215	0.0889	0.0163	0.11	0.0129
2	0.1833	0.0219	0.1935	0.0167	0.22	0.0131
3	0.2688	0.0225	0.2924	0.0172	0.3088	0.0137
4	0.3495	0.0235	0.388	0.0181	0.4114	0.0144
5	0.4117	0.0247	0.4753	0.0192	0.5068	0.0153
6	0.4573	0.0263	0.5615	0.0206	0.596	0.0166
7	0.4758	0.0282	0.6224	0.0223	0.6724	0.0181
8	0.4428	0.0303	0.6589	0.0242	0.7373	0.0198
9	0.3544	0.0327	0.6606	0.0264	0.7781	0.0217
10	0.2108	0.0620	0.6248	0.0288	0.7949	0.0238
11	0.1124	0.0925	0.5531	0.0315	0.7852	0.0262
12	0.0139	0.1230	0.4408	0.08	0.7488	0.0288
13	0.0314	0.1405	0.3332	0.119	0.6923	0.077
14	0.0489	0.1580	0.2256	0.158	0.6237	0.158
15	0.0889	0.1770	0.2142	0.177	0.5567	0.177
16	0.1287	0.1960	0.2027	0.196	0.4896	0.196
17	0.1758	0.2170	0.2315	0.217	0.4549	0.217
18	0.2228	0.2380	0.2603	0.238	0.4202	0.238
19	0.2732	0.2600	0.3038	0.26	0.4292	0.26
20	0.3236	0.2820	0.3472	0.282	0.4382	0.282
21	0.3751	0.3055	0.3951	0.3055	0.4704	0.3055
22	0.4265	0.3290	0.443	0.329	0.5026	0.329
25	0.5840	0.4050	0.5963	0.405	0.6321	0.405
30	0.8550	0.5700	0.855	0.57	0.855	0.57
35	0.9800	0.7450	0.98	0.745	0.98	0.745
40	1.0350	0.9200	1.035	0.92	1.035	0.92
45	1.0500	1.0750	1.05	1.075	1.05	1.075
50	1.0200	1.2150	1.02	1.215	1.02	1.215
55	0.9550	1.3450	0.955	1.345	0.955	1.345
60	0.8750	1.4700	0.875	1.47	0.875	1.47
65	0.7600	1.5750	0.76	1.575	0.76	1.575
70	0.6300	1.6650	0.63	1.665	0.63	1.665
75	0.5000	1.7350	0.5	1.735	0.5	1.735
80	0.3650	1.7800	0.365	1.78	0.365	1.78
85	0.2300	1.8000	0.23	1.8	0.23	1.8
90	0.0900	1.8000	0.09	1.8	0.09	1.8
95	-0.0500	1.7800	-0.05	1.78	-0.05	1.78
100	-0.1850	1.7500	-0.185	1.75	-0.185	1.75
105	-0.3200	1.7000	-0.32	1.7	-0.32	1.7
110	-0.4500	1.6350	-0.45	1.635	-0.45	1.635
115	-0.5750	1.5550	-0.575	1.555	-0.575	1.555

	NACA0018					
	***Re*=40'000**		***Re*=80'000**		***Re*=160'000**	
α	C_l	C_d	C_l	C_d	C_l	C_d
120	-0.6700	1.4650	-0.67	1.465	-0.67	1.465
125	-0.7600	1.3500	-0.76	1.35	-0.76	1.35
130	-0.8500	1.2250	-0.85	1.225	-0.85	1.225
135	-0.9300	1.0850	-0.93	1.085	-0.93	1.085
140	-0.9800	0.9250	-0.98	0.925	-0.98	0.925
145	-0.9000	0.7550	-0.9	0.755	-0.9	0.755
150	-0.7700	0.5750	-0.77	0.575	-0.77	0.575
155	-0.6700	0.4200	-0.67	0.42	-0.67	0.42
160	-0.6350	0.3200	-0.635	0.32	-0.635	0.32
165	-0.6800	0.2300	-0.68	0.23	-0.68	0.23
170	-0.8500	0.1400	-0.85	0.14	-0.85	0.14
175	-0.6600	0.0550	-0.66	0.055	-0.66	0.055
180	0.0000	0.0250	0	0.025	0	0.025

F: Motor Data Sheet

FAULHABER

DC-Kleinstmotoren 50 mNm

Graphitkommutierung

Kombinierbar mit (Übersicht Seiten 14-15)
Getriebe:
30/1, 32/3, 38/1, 38/2
Impulsgeber:
5500, 5540

Serie 3557 ... CS

		3557 K		009 CS	012 CS	020 CS	024 CS	048 CS	
1	Nennspannung	U_N		9	12	20	24	48	Volt
2	Anschlusswiderstand	R		0,70	1,34	4,0	5,5	23,0	Ω
3	Abgabeleistung	$P_{2\,max.}$		28,1	26,1	24,3	25,4	24,1	W
4	Wirkungsgrad	$\eta_{max.}$		78	79	79	78	76	%
5	Leerlaufdrehzahl	n_0		5 700	5 400	5 500	5 500	5 200	rpm
6	Leerlaufstrom (bei Wellen ø 4,0 mm)	I_0		0,190	0,125	0,070	0,065	0,040	A
7	Anhaltemoment	M_H		188	185	169	176	177	mNm
8	Reibungsdrehmoment	M_R		2,80	2,60	2,40	2,70	3,50	mNm
9	Drehzahlkonstante	k_n		643	456	279	233	110	rpm/V
10	Generator-Spannungskonstante	k_E		1,560	2,190	3,590	4,300	9,050	mV/rpm
11	Drehmomentkonstante	k_M		14,90	20,90	34,20	41,00	86,50	mNm/A
12	Stromkonstante	k_I		0,067	0,048	0,029	0,024	0,012	A/mNm
13	Steigung der n-M-Kennlinie	Δn/ΔM		30,3	29,2	32,5	31,3	29,4	rpm/mNm
14	Anschlussinduktivität	L		100	220	630	850	3 400	µH
15	Mechanische Anlaufzeitkonstante	τ_m		16	16	16	16	16	ms
16	Rotorträgheitsmoment	J		50	52	47	49	52	gcm²
17	Winkelbeschleunigung	$\alpha_{max.}$		37	35	36	36	34	10^3rad/s²
18	Wärmewiderstände	$R_{th\,1}$ / $R_{th\,2}$	1,5 / 9						K/W
19	Thermische Zeitkonstante	τ_{w1} / τ_{w2}	15 / 900						s
20	Betriebstemperaturbereich:								
	– Motor		– 30 ... + 125						°C
	– Rotor, max. zulässig		+ 125						°C
21	Wellenlagerung		Kugellager, vorgespannt						
22	Wellenbelastung, max. zulässig:								
	– für Wellerdurchmesser		4,0						mm
	– radial bei 3 000 rpm (3 mm vom Lager)		30						N
	– axial bei 3 000 rpm		5						N
	– axial im Stillstand		50						N
23	Wellenspiel:								
	– radial	≤	0,015						mm
	– axial	=	0						mm
24	Gehäusematerial		Stahl, galvanisch verzinkt, passiviert						
25	Gewicht		275						g
26	Drehrichtung		rechtsdrehend auf Abtriebswelle gesehen						
Empfohlene Werte - diese gelten unabhängig voneinander									
27	Drehzahl bis	$n_{e\,max.}$		5 000	5 000	5 000	5 000	5 000	rpm
28	Dauerdrehmoment bis [1]	$M_{e\,max.}$		50	50	50	50	50	mNm
29	Thermisch zulässiger Dauerstrom	$I_{e\,max.}$		3,150	2,260	1,300	1,100	0,540	A

[1] Wärmewiderstand $R_{th\,2}$ um 40% reduziert

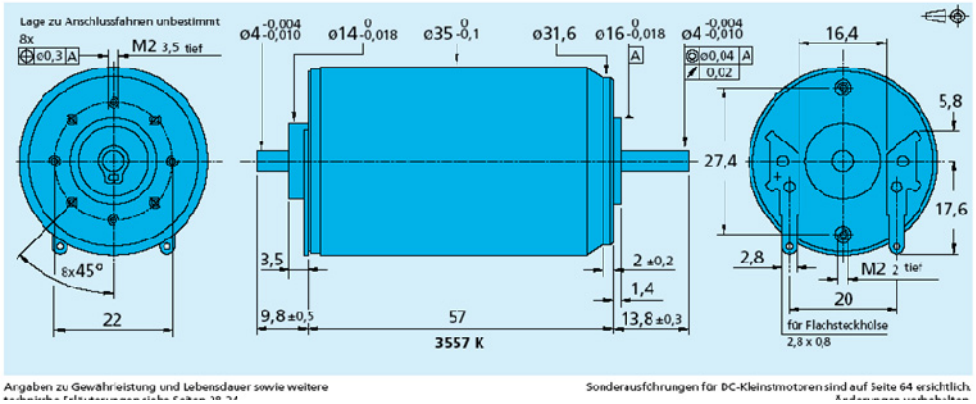

Angaben zu Gewährleistung und Lebensdauer sowie weitere

Sonderausführungen für DC-Kleinstmotoren sind auf Seite 64 ersichtlich.

Fig. 116: Data sheet of the used motors for BellAIR series, Faulhaber catalogue 2008-2009, p. 61

G: Experimental Set-Up

For the design of a very small scale HAWT rotor, a motor was used as a generator. To obtain its generator characteristics several measurements were carried out. The experimental set-ups are shown in Fig. 117.

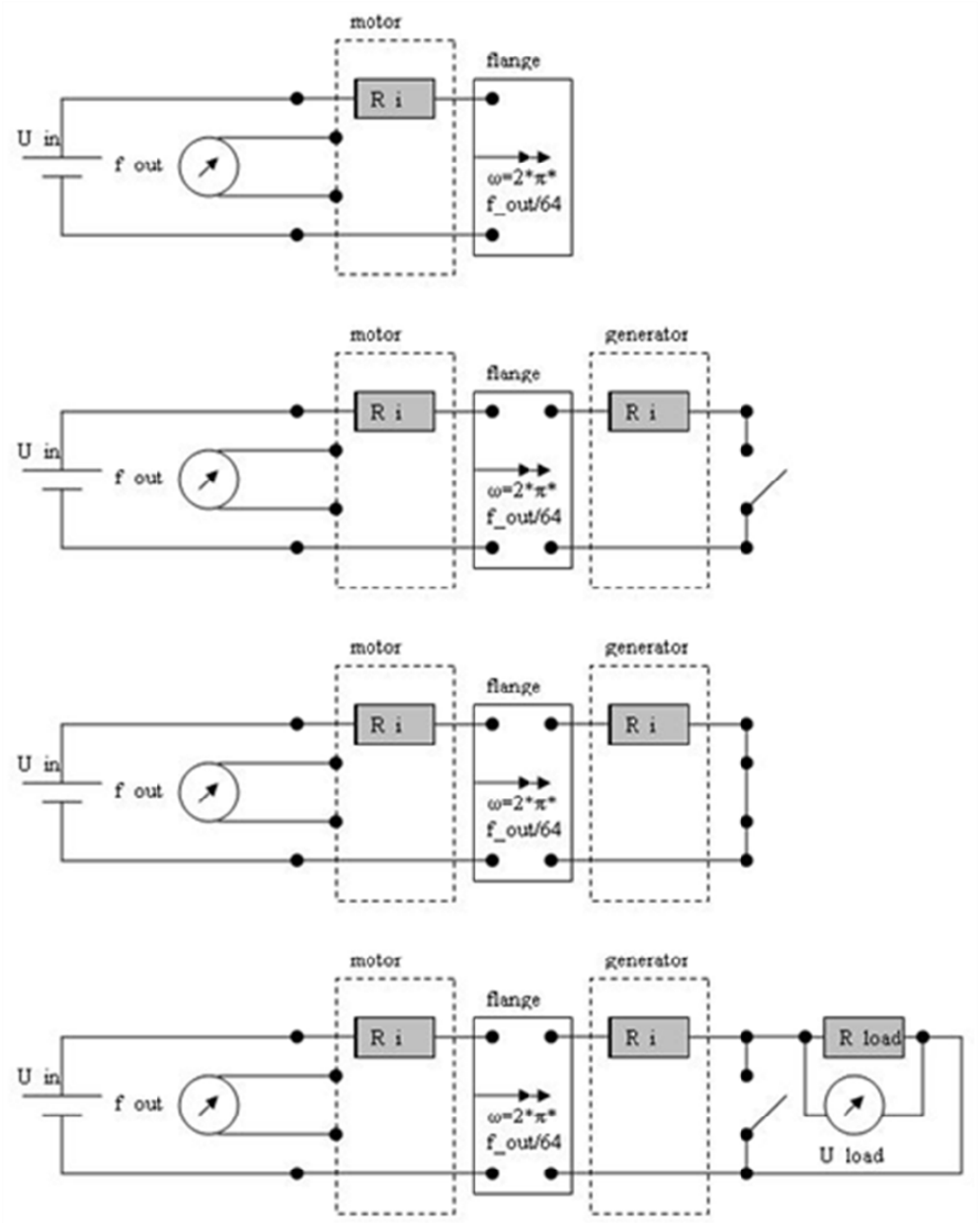

Fig. 117: Experimental set-up to determine generator characteristics

H: Site Views

site one

Fig. 118: Site one: satellite picture [[46]] with indication of the building, where turbines were mounted. The star is located at the spot the street views are taken at.

WEST

NORTH

EAST

SOUTH

Fig. 119: Site one: street views [46]

site two

Fig. 120: Site two: satellite picture [46] with indication of the building, where turbines were mounted. The star is located at the spot the street views are taken at.

WEST

NORTH

EAST

SOUTH

Fig. 121: Site two: street views [46]

site three

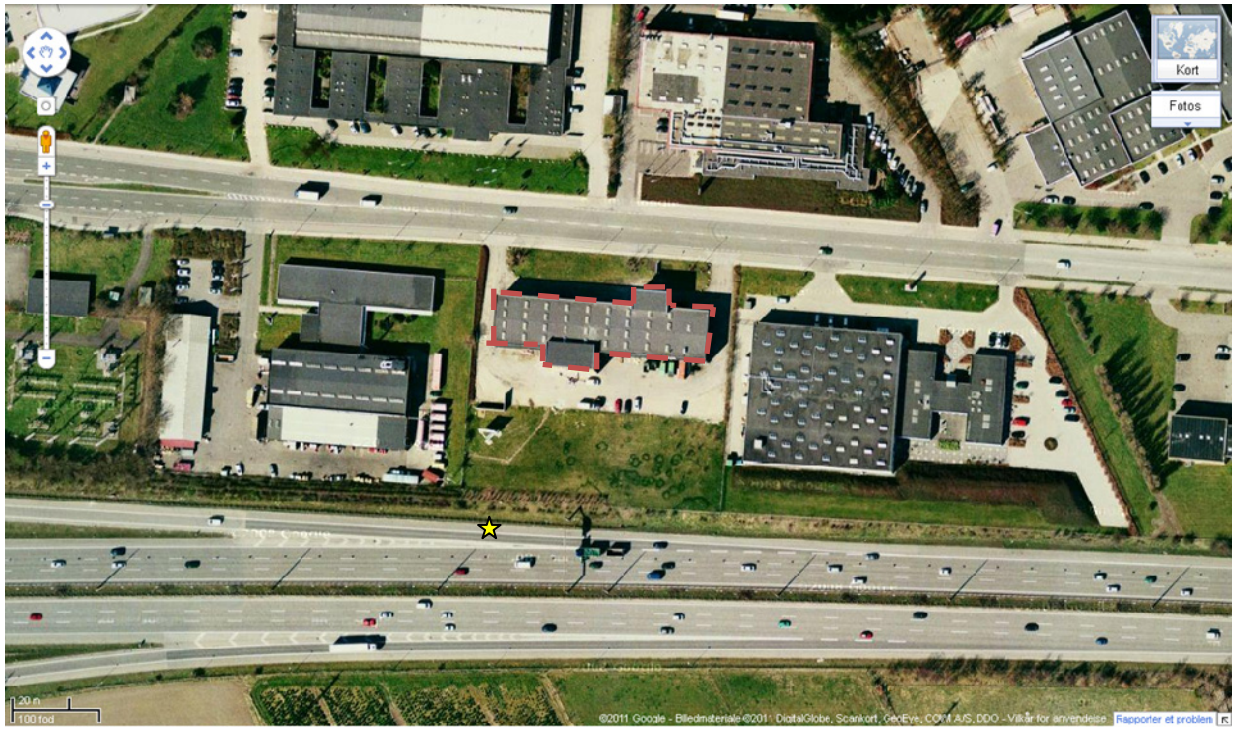

Fig. 122: Site three: satellite picture [46] with indication of the building, where turbines were mounted. The star is located at the spot the street views are taken at.

WEST

NORTH

EAST

SOUTH

Fig. 123: Site three: street views [46]

site four

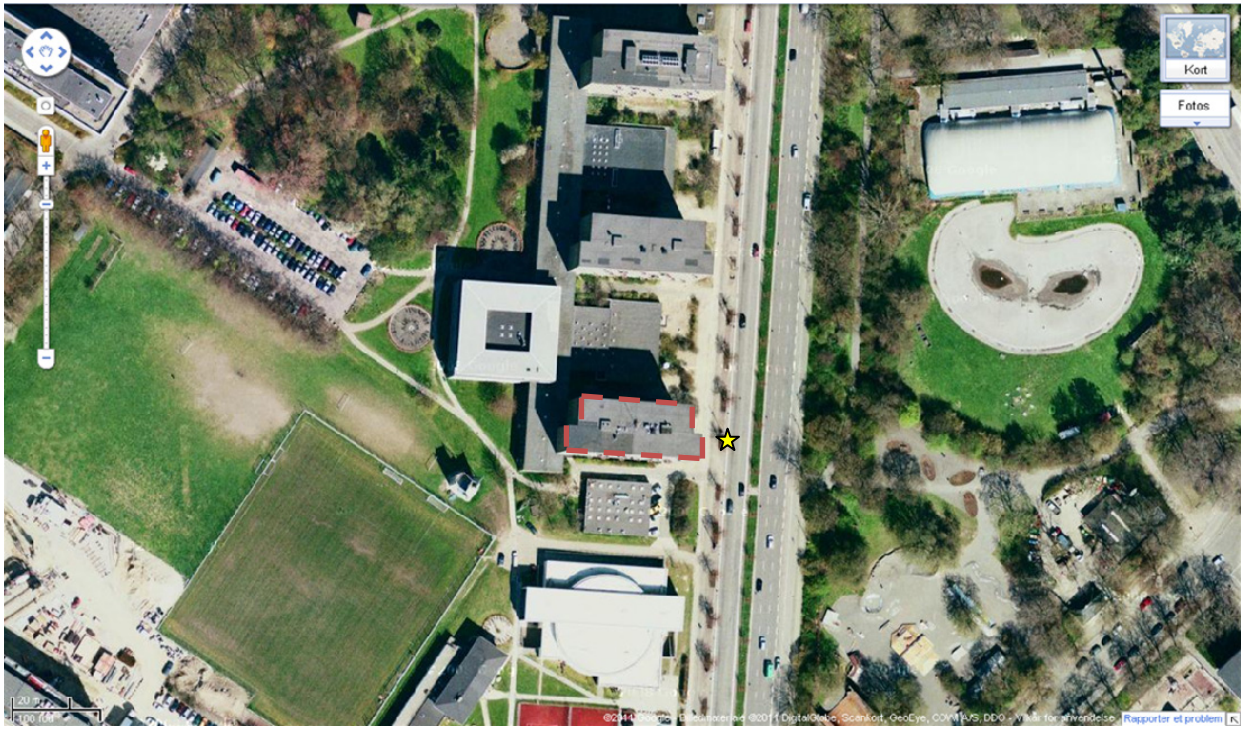

Fig. 124: Site four: satellite picture [46] with indication of the building, where wind measurements were taken. The star is located at the spot street views are taken at.

WEST

NORTH

EAST

SOUTH

Fig. 125: Site four: street views [46]

site five

Fig. 126: Site five: satellite picture [46] with indication of the spot of the test station (X). The star is located at the spot street views are taken at.

Fig. 127: Site five: street views [46]

I: Optimization Limits

Optimization for the H-rotor design in the design point:

```
###############################################################################
POWER_CONTROL (cutin=5, cutout=5, nwind=1, type=0; rpm=200; opt=0; pitch=0.0)
#
INTER_DVD  (module=WT_ROTOR, sensor=chord, ip=1, open=1, type=0,
            x = {0.9500,0.9595,0.9590}, y = {%,%,%} }
INTER_DV   (module=WT_ROTOR,sensor=chord,def={0,0},min=0.02,max=0.30,dx=1.e-1)
INTER_DV   (module=WT_ROTOR,sensor=chord,def={0,1},min=0.02,max=0.30,dx=1.e-1)
INTER_DV   (module=WT_ROTOR,sensor=chord,def={0,2},min=0.02,max=0.30,dx=1.e-1)
###############################################################################
```

Optimization for the Darrieus rotor in the design point:

```
###############################################################################
POWER_CONTROL (cutin=5, cutout=5, nwind=1, type=0; rpm=200; opt=0; pitch=0.0)
#
INTER_DVD  (module=WT_ROTOR, sensor=chord, ip=1, open=1, type=0,
            x = {0.118,0.35,0.574,0.784,0.974,1.141,1.279,1.286,1.459,1.495},
            y = {%,%,%,%,%,%,%,%,%,%} }
INTER_DV   (module=WT_ROTOR,sensor=chord,def={0,0},min=0.02,max=0.30,dx=1.e-1)
INTER_DV   (module=WT_ROTOR,sensor=chord,def={0,1},min=0.02,max=0.30,dx=1.e-1)
INTER_DV   (module=WT_ROTOR,sensor=chord,def={0,2},min=0.02,max=0.30,dx=1.e-1)
INTER_DV   (module=WT_ROTOR,sensor=chord,def={0,3},min=0.02,max=0.30,dx=1.e-1)
INTER_DV   (module=WT_ROTOR,sensor=chord,def={0,4},min=0.02,max=0.30,dx=1.e-1)
INTER_DV   (module=WT_ROTOR,sensor=chord,def={0,5},min=0.02,max=0.30,dx=1.e-1)
INTER_DV   (module=WT_ROTOR,sensor=chord,def={0,6},min=0.02,max=0.30,dx=1.e-1)
INTER_DV   (module=WT_ROTOR,sensor=chord,def={0,7},min=0.02,max=0.30,dx=1.e-1)
INTER_DV   (module=WT_ROTOR,sensor=chord,def={0,8},min=0.02,max=0.30,dx=1.e-1)
INTER_DV   (module=WT_ROTOR,sensor=chord,def={0,9},min=0.02,max=0.30,dx=1.e-1)
###############################################################################
```

J: Optimized Rotor Renderings

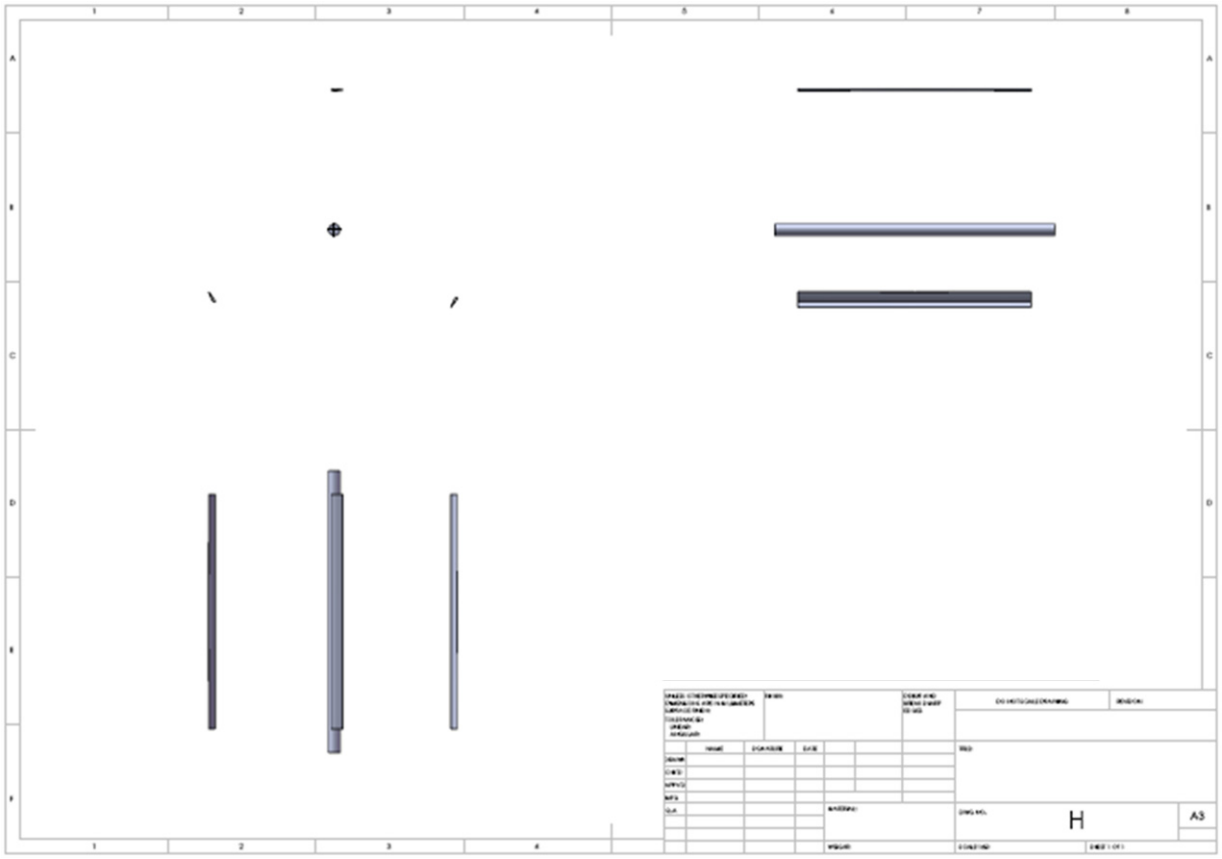

Fig. 128: Technical rendering of the optimized H-rotor

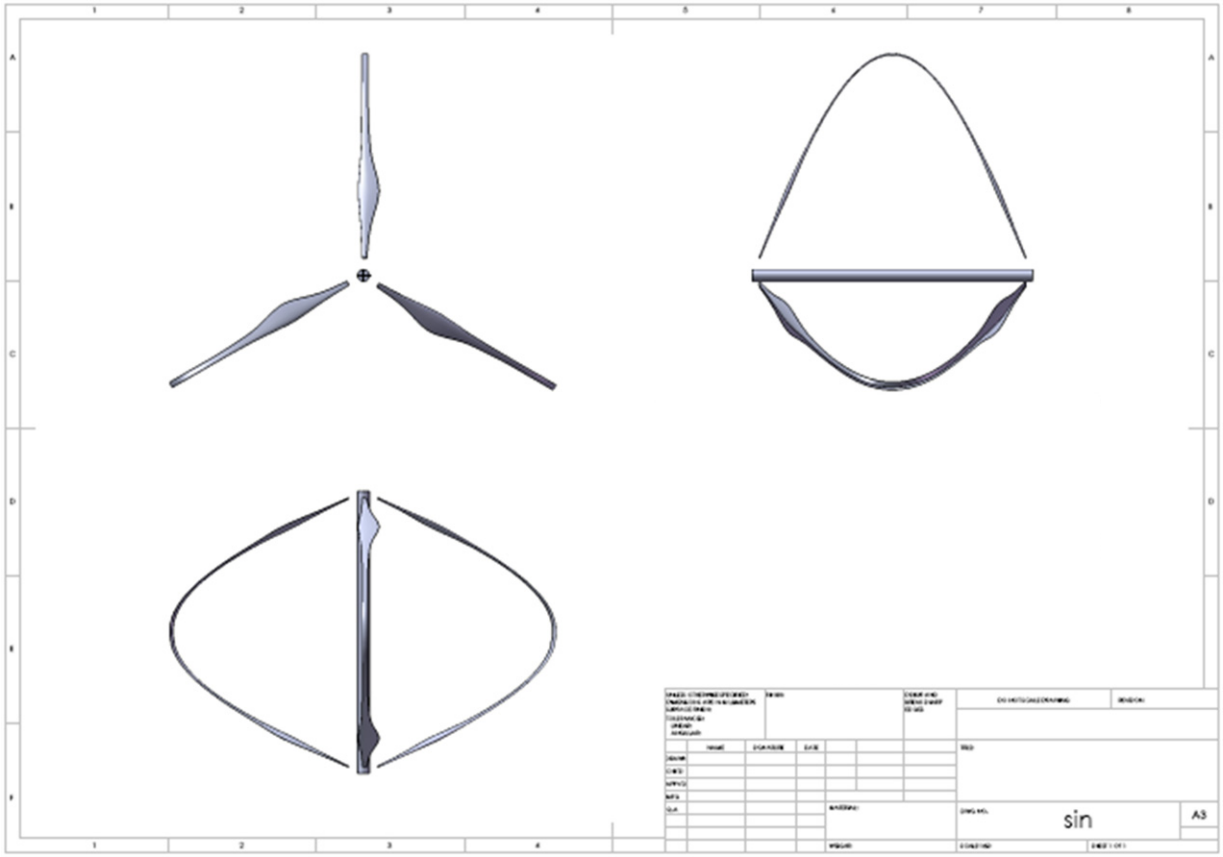

Fig. 129: Technical rendering of the optimized Darrieus- rotor

Risø DTU is the National Laboratory for Sustainable Energy. Our research focuses on development of energy technologies and systems with minimal effect on climate, and contributes to innovation, education and policy. Risø has large experimental facilities and interdisciplinary research environments, and includes the national centre for nuclear technologies.

Risø DTU
National Laboratory for Sustainable Energy
Technical University of Denmark

Frederiksborgvej 399
PO Box 49
DK-4000 Roskilde
Denmark
Phone +45 4677 4677
Fax +45 4677 5688

www.risoe.dtu.dk